Report Prepared by:
R.D. Granata
With:
F. Presuel-Moreno
M. Madani
B. Tran

Final Report

Environmental Suitability of Weathering Steel Structures Florida - Material Selection, Phase 2

BDV27-977-04

Submitted to
Florida Department of Transportation Research Center
605 Suwannee Street
Tallahassee, Florida 32399

Submitted by
Richard D. Granata
Principal Investigator
Department of Ocean and Mechanical Engineering
Center for Marine Materials
Florida Atlantic University
SeaTech
101 North Beach Road
Dania Beach, Florida 33004

August 2017

DISCLAIMER

The opinions, findings, and conclusions expressed in this publication are those of the author and not necessarily those of the State of Florida Department of Transportation.

CONVERSION FACTOR TABLE

SI* (MODERN METRIC) CONVERSION FACTORS

APPROXIMATE CONVERSIONS TO SI UNITS

Symbol	When You Know	Multiply By	To Find	Symbol
		LENGTH		
in	inches	25.4	millimeters	mm
ft	feet	0.305	meters	m
yd	yards	0.914	meters	m
mi	miles	1.61	kilometers	km
		AREA		
in^2	square inches	645.2	square millimeters	mm^2
ft^2	square feet	0.093	square meters	m^2
yd^2	square yard	0.836	square meters	m^2
ac	acres	0.405	hectares	ha
mi^2	square miles	2.59	square kilometers	km^2
		VOLUME		
fl oz	fluid ounces	29.57	milliliters	mL
gal	gallons	3.785	liters	L
ft^3	cubic feet	0.028	cubic meters	m^3
yd^3	cubic yards	0.765	cubic meters	m^3
	NOTE: volumes greater than 1000 L shall be shown in m^3			
		MASS		
oz	ounces	28.35	grams	g
lb	pounds	0.454	kilograms	kg
T	short tons (2000 lb)	0.907	megagrams (or "metric ton")	Mg (or "t")
		TEMPERATURE (exact degrees)		
^oF	Fahrenheit	5 (F-32)/9 or (F-32)/1.8	Celsius	^oC
		ILLUMINATION		
fc	foot-candles	10.76	lux	lx
fl	foot-Lamberts	3.426	$candela/m^2$	cd/m^2
		FORCE and PRESSURE or STRESS		
lbf	poundforce	4.45	newtons	N
lbf/in^2	poundforce per square inch	6.89	kilopascals	kPa

APPROXIMATE CONVERSIONS FROM SI UNITS

Symbol	When You Know	Multiply By	To Find	Symbol
		LENGTH		
mm	millimeters	0.039	inches	in
m	meters	3.28	feet	ft
m	meters	1.09	yards	yd
km	kilometers	0.621	miles	mi
		AREA		
mm^2	square millimeters	0.0016	square inches	in^2
m^2	square meters	10.764	square feet	ft^2
m^2	square meters	1.195	square yards	yd^2
ha	hectares	2.47	acres	ac
km^2	square kilometers	0.386	square miles	mi^2
		VOLUME		
mL	milliliters	0.034	fluid ounces	fl oz
L	liters	0.264	gallons	gal
m^3	cubic meters	35.314	cubic feet	ft^3
m^3	cubic meters	1.307	cubic yards	yd^3
		MASS		
g	grams	0.035	ounces	oz
kg	kilograms	2.202	pounds	lb
Mg (or "t")	megagrams (or "metric ton")	1.103	short tons (2000 lb)	T
		TEMPERATURE (exact degrees)		
^oC	Celsius	1.8C+32	Fahrenheit	^oF
		ILLUMINATION		
lx	lux	0.0929	foot-candles	fc
cd/m^2	$candela/m^2$	0.2919	foot-Lamberts	fl
		FORCE and PRESSURE or STRESS		
N	newtons	0.225	poundforce	lbf
kPa	kilopascals	0.145	poundforce per square inch	lbf/in^2

*SI is the symbol for the International System of Units. Appropriate rounding should be made to comply with Section 4 of ASTM E380.
(Revised March 2003)

TECHNICAL REPORT DOCUMENTATION PAGE

1. Report No.	2. Government Accession No.	3. Recipient's Catalog No.

4. Title and Subtitle	5. Report Date
Environmental Suitability of Weathering Steel Structures in Florida - Material Selection, Phase 2	August 2017
	6. Performing Organization Code FAU-OE-CMM-08-3
7. Author(s) Richard D. Granata, Francisco Presuel-Moreno, Mahmoud Madani, Bao Tran	8. Performing Organization Report No. BDV27-977-04
9. Performing Organization Name and Address Center for Marine Materials Florida Atlantic University – SeaTech 101 North Beach Road Dania Beach, Florida 33004	10. Work Unit No. (TRAIS)
	11. Contract or Grant No. BDV27-977-04
12. Sponsoring Agency Name and Address Florida Department of Transportation 605 Suwannee Street, MS 30 Tallahassee, FL 32399	13. Type of Report and Period Covered Final Report May 2014 – August 30, 2017
	14. Sponsoring Agency Code

15. Supplementary Notes

16. Abstract

For the purpose of establishing guidelines for selection of weathering steel material for bridges in Florida, data were collected to help establish appropriate guidelines. There were 30 monitoring stations set up for direct (weight loss) measurements and weather data. Data indicated that the corrosion rates in Florida are generally low for weathering steel. The use of weathering steel material for bridges in Florida in the context of adjusted guidelines is very favorable. Consideration should be given to increasing the allowable deposition rate of chloride to approximately 13 $mg \cdot m^{-2} \cdot d^{-1}$ corresponding to 4 miles from the shoreline. An alternative direct assessment at the site considered is recommended for determining the advisability for uncoated weathering steel in this manner: (1) Expose several plate specimens and collect monthly for a minimum of 4 months. (2) Directly compare the time series weight losses to known corrosion studies. ISO methods permit this alternative. Additionally, estimates of chloride and sulfur compound depositions can be obtained from the same exposed panels by analyses of panel wash water prior to oxide removal, if desired. The advantage of direct assessment is that no environmental factor will likely be neglected, such as pH, ammonia, fertilizer, ozone, exposure/sheltering, or unanticipated factors (positive or negative).

17. Key Word	18. Distribution Statement
weathering steel, corrosion, time of wetness, TOW, direct assessment, chloride, sulfur dioxide, bridge, unpainted, akaganeite, X-ray diffraction	

19. Security Classif. (of this report)	20. Security Classif. (of this page)	21. No. of Pages	22. Price
Unclassified	Unclassified	149	

Form DOT F 1700.7 (8-72) Reproduction of completed page authorized

ACKNOWLEDGMENTS

The authors are indebted to the FDOT Research Center and State Materials Office for their strong interest in this project and their willingness to move forward with the project in spite of unforeseeable delays. The Florida State Parks, Broward County Parks, Cities of Delray Beach and Weston, Sunshine Equestrian Center and the South Florida National Cemetery are thanked for permission and cooperation in establishing monitoring sites for this work.

EXECUTIVE SUMMARY

The Florida Department of Transportation is implementing a program to identify appropriate locations for use of unpainted weathering steel (UWS) for bridge structures where it should perform adequately. Weathering steels (WS) are low alloy steels formulated with small (total 3-5%) percentage additions, primarily, copper (Cu), chromium (Cr), nickel (Ni), phosphorus (P), silicon (Si), and/or manganese (Mn) and also molybdenum (Mo), vanadium (V), titanium (Ti), and zirconium (Zr), in some cases. The primary intent of the formulation is to promote the development of a protective oxidation (rust) layer; furthermore, an increase in strength results from the alloying and processing. The protective oxide or patina formed has been estimated to provide sufficient corrosion protection for more than 100 years without maintenance or painting in some cases. Significant cost savings are anticipated versus carbon steel (CS), primarily attributable to lower maintenance (little or no painting) and secondarily to design efficiencies of higher strength material. The primary focus is on establishing where weathering steel (WS) will perform adequately as unpainted weathering steel (UWS). In cases where an incorrect choice may be made to use WS, the structure can be modified by blast cleaning and painting. Current guidelines for determining advisability for using uncoated WS in Florida include:

- Anticipation of a slightly aggressive superstructure corrosive environment
- Yearly average time of wetness (TOW), as determined by ASTM Standard Method G84, not to exceed 60%
- Uncoated weathering steel shall not be used within 4.0 miles of the coast unless it is determined through testing that the proposed site conditions do not exceed the following thresholds:
    - The maximum airborne salt deposition rate, as determined by ASTM Standard Method G140, shall be less than 5 $mg \cdot m^{-2} \cdot d^{-1}$ (30-day average)
    - The maximum average concentration for SO_2, as determined by ASTM Standard Method G91, shall not exceed 60 $mg \cdot m^{-2} \cdot d^{-1}$ (30-day average)
- Do not use uncoated weathering steel over low crossings (12 feet or less vertical clearance over normal high water / mean high water).

The purpose of the project is to obtain data in support of Florida Department of Transportation guidelines on the appropriate use of weathering steel for bridges and other structures. The objectives selected to achieve this purpose are:

1. Collect pertinent information from literature review, consultations, databases, and other resources.
2. Identify and establish monitoring sites for data acquisition via sensors and corrosion specimens.
3. Develop monitoring methods that simplify site characterization and improve data quality.
4. Provide a basis for validation or refinement of FDOT guidelines for weathering steel use.

Major reports were identified from FHWA and NCHRP, as well as from individual researchers that documented its use under a wide range of environments. Unfortunately, WS was used too widely and encountered harsh responses, including complete bans on use by several state DOTs. WS has some sensitivity to the environment and its proper use was not generally understood. The details on how to best specify WS are still evolving. FDOT seeks to provide guidance for its use in Florida that has the advantage of not complicating the environmental issues with deicing salts required in more northerly states. Chlorides in Florida are derived from the natural environment, primarily, its ocean coastlines.

Thirty monitoring stations were established in south Florida for this study. The stations ranged from Key Biscayne in the south to Fort Pierce in the north and the coastline (beach) to the edge of the Everglades (21 miles, west). Each monitoring station included weather sensors for wind speed and direction, humidity, temperature, rainfall, wetness and rain conductivity, as well as specimens for direct corrosion measurements by weight loss. The findings for these studies are as follows:

1. There was no apparent relationship of %TOW to corrosion rates of plate corrosion specimens. The %TOW measurements may be problematic when correlated to surfaces laden with sea salt deposits because such surfaces can remain wet at 20% RH.

2. Few weathering steel bridge structures were located in south FL. Visual inspections showed well-developed dark oxide associated with protective WS patina.

3. For plate corrosion specimens, there was no significant correlation with %TOW or SO_2 . A strong correlation was observed for chloride where sites up to 2 mi from the shoreline were boldly exposed (no barriers).

4. Corrosion rates at sites more than 2 mi from the shoreline were generally very low.

5. The effect of chloride on corrosion rate diminishes rapidly with distance and shielding.

6. X-ray diffraction results determined that a problematic corrosion product, akaganeite, was present on many plate specimens. There was no strong correlation of akaganeite presence to chloride deposition or %TOW. Generally, the percentage akaganeite in the corrosion products decreased with distance from the shoreline.

7. Conductivity measurements (TDS) of the corrosion product water extracts showed four sites with relatively high or higher values that the other 26 sites. Most (>90%) of the conductivity was due to chloride and decreased with distance from the shoreline. The concentration of sulfate gradually increased with distance from the shoreline.

8. Deposition of SO_2 in Florida has been nearly eliminated except in ocean ports and perhaps at permitted sites. The reductions of sulfur in fuels are probably responsible for this change. It is likely that corrosion rates have decreased as a result.

9. The chloride deposition profile with increasing distance from the shoreline indicates the deposition rate is 13 $mg \cdot m^{-2} \cdot d^{-1}$ at 4 miles from the shoreline, decreasing to approximately 5 $mg \cdot m^{-2} \cdot d^{-1}$ at 30 mi from the shoreline. These rates are higher than the current guideline rates that are based upon a most conservative Japanese standard. Low corrosion rates were consistently observed at shoreline distances of 2 miles or more for WS plate specimens in this project, suggesting higher proposed rates should be strongly considered.

10. An alternative approach was proposed for rapid and simplified characterization of proposed WS construction sites based upon short-term exposures of direct measurement specimens. The approach that provides simple, fast, and cost-effective direct corrosion data and analysis should be given consideration.

TABLE OF CONTENTS

LIST OF FIGURES

LIST OF TABLES

1 BACKGROUND

1.1 Project Basis

The Florida Department of Transportation is implementing a program to identify appropriate locations for use of unpainted weathering steel (WS) for bridge structures where it should perform adequately. Weathering steels are low alloy steels formulated with small (total 3-5%) percentage additions, primarily of Cu, Cr, Ni, P, Si, and/or Mn and also Mo, V, Ti, and Zr, in some cases [1]. The primary intent of the formulation is to promote the development of a protective oxidation (rust) layer; furthermore, an increase in strength results from the alloying and processing. The protective oxide or patina formed has been estimated to provide sufficient corrosion protection for more than 100 years without maintenance or painting, in some cases. Significant cost savings are anticipated versus carbon steel (CS), primarily attributable to lower maintenance (little or no painting) and secondarily to design efficiencies of higher strength material. In other locations where uncoated WS is unsuitable, inorganic zinc coatings will be used and where severe environments are anticipated, the most robust paint systems (structural coating) will be specified, requiring special approvals. The primary focus is on establishing where WS will perform adequately. In cases where an incorrect choice may be made to use WS, the structure can be modified by blast cleaning and painting. Current guidelines for determining advisability for using uncoated WS in Florida include:

- Anticipation of a slightly aggressive superstructure corrosive environment
- Yearly average time of wetness (TOW), as determined by ASTM Standard Method G84, not to exceed 60%
- Uncoated weathering steel shall not be used within 4.0 miles of the coast unless it is determined through testing that the proposed site conditions do not exceed the following thresholds:
    - The maximum airborne salt deposition rate, as determined by ASTM Standard Method G140, shall be less than 5 $mg \cdot m^{-2} \cdot d^{-1}$ (30-day average)
    - The maximum average concentration for SO_2, as determined by ASTM Standard Method G91, shall not exceed 60 $mg \cdot m^{-2} \cdot d^{-1}$ (30-day average)
- Do not use uncoated weathering steel over low crossings (12 feet or less vertical clearance over normal high water / mean high water).

1.2 Project Objectives

The purpose of the project is to obtain data in support of Florida Department of Transportation guidelines on the appropriate use of weathering steel for bridges and other structures. The objectives selected to achieve this purpose are:

1. Collect pertinent information from literature review, consultations, databases, and other resources.
2. Identify and establish monitoring sites for data acquisition via sensors and corrosion specimens.
3. Develop monitoring methods that simplify site characterization and improve data quality.
4. Provide a basis for validation or refinement of FDOT guidelines for weathering steel use.

1.3 Approach

The selection of steel material for bridges and other structures requires consideration of materials properties and environmental conditions. Weathering steels offer both structural and maintenance benefits but have climatic environment issues [2] [3]. Moisture, wet conditions and pollutant presence must be considered when specifying bare WS versus inorganic Zn coated or painted steel surfaces. The issues related to good maintenance performance of the primary material choice, WS, are complex pertaining to the specific alloy, design details and environmental influences, and not yet fully understood [4] [5] [6]. However, excellent performance has been achieved in many cases. Guidelines offer a good approach to efficient use of these materials. The work described here was influenced by the author's more than 25 years association with WS issues including site inspections. The main standard methods accessed in this study were:

- ASTM Standard **G1** - *Standard Practice for Preparing, Cleaning, and Evaluating Corrosion Test Specimens*. This practice covers suggested procedures for preparing bare, solid metal specimens for tests, for removing corrosion products after the test has been completed, and for evaluating the corrosion damage that has occurred. Emphasis is placed on procedures related to the evaluation of corrosion by mass loss and pitting measurements [7].
- ASTM Standard **G33** - *Standard Practice for Recording Data from Atmospheric Corrosion Tests of Metallic-Coated Steel Specimens*. This practice outlines a procedure for recording data of atmospheric corrosion tests of metallic-coated steel specimens. Its objective is the assurance of (1) complete identification of materials before testing, (2) objective reporting of material appearance during visual inspections, and (3) adequate photographic, micrographic, and chemical laboratory examinations at specific stages of deterioration, and at the end of the tests [8].
- ASTM Standard **G50** - *Standard Practice for Conducting Atmospheric Corrosion Tests on Metals*. This practice defines conditions for exposure of metals and alloys to the weather. It sets forth the general procedures that should be followed in any atmospheric test. It is presented as an aid in conducting atmospheric corrosion tests so that some of the pitfalls of such testing may be avoided. As such, it is concerned mainly with panel exposures to obtain data for comparison purposes [9].
- ASTM Standard **G84** - *Standard Practice for Measurement of Time-of-Wetness on Surfaces Exposed to Wetting Conditions as in Atmospheric Corrosion Testing*. (1) This practice covers a technique for monitoring time-of-wetness (TOW) on surfaces exposed to cyclic atmospheric conditions which produce depositions of moisture. (2) The practice is also applicable for detecting and monitoring condensation within a wall or roof assembly and in a test apparatus. (3) Exposure site calibration or characterization can be significantly enhanced if TOW is measured for comparison with other sites, particularly if this data is used in conjunction with other site-specific instrumentation techniques [10].
- ASTM Standard **G91** - *Standard Practice for Monitoring Atmospheric SO_2 Using the Sulfation Plate Technique*. (1) This practice provides a weighted average effective SO_2 level for a 30-day interval through the use of the sulfation plate method, a technique for estimating the effective SO_2 content of the atmosphere, and especially with regard to the atmospheric corrosion of stationary structures or panels. This practice is aimed at determining SO_2 levels rather than sulfuric acid aerosol or acid precipitation. (2) The results of this practice correlate approximately with volumetric SO_2 concentrations, although the presence of dew or condensed moisture tends to enhance the capture of SO_2 into the plate [11].
- ASTM Standard **G92** - *Standard Practice for Characterization of Atmospheric Test Sites*. This practice gives suggested procedures for the characterization of atmospheric test sites. Continuous

characterization can provide corrosion data, environmental data, or both which will signal changes in corrosivity of the atmospheric environment. This practice can also provide guidance for classification of future test sites. (2) Two methods are defined in this practice for the characterization of atmospheric test sites. The methods are identified as characterization Methods A and B. The preferred characterization technique would require using both Method A and B for concurrent data collection. (2a) Method A is to be used when atmospheric corrosion is monitored on a continuing basis at a test site using specified materials and exposure configurations. (2b) Method B is specified when atmospheric factors are monitored on a continuing basis [12].

- ASTM Standard **G116** - *Standard Practice for Conducting Wire-on-Bolt Test for Atmospheric Galvanic Corrosion* **–** (1) This practice covers the evaluation of atmospheric galvanic corrosion of any anodic material that can be made into a wire when in contact with a cathodic material that can be made into a threaded rod. (2) When certain materials are used for the anode and cathode, this practice has been used to rate the corrosivity of atmospheres. (3) The wire-on-bolt test was first described in 1955 and has since been used extensively with standard materials to determine corrosivity of atmospheres under the names CLIMAT Test (CLassify Industrial and MarineATmospheres) and ATCORR (ATmospheric CORRosivity) [13].
- ASTM Standard **G140** - *Standard Test Method for Determining Atmospheric Chloride Deposition Rate by Wet Candle Method* **–** (1) This test method describes a wet candle device and its use in measuring atmospheric chloride deposition (amount of chloride salts deposited from the atmosphere on a given area per unit time). (2) Data on atmospheric chloride deposition can be useful in classifying the corrosivity of a specific area, such as an atmospheric test site. Caution must be exercised, however, to take into consideration the season because airborne chlorides vary widely between seasons [14].
- International Organization for Standardization, Standards ISO 8565 [15], ISO 9223 [16], ISO 9224 [17], ISO 9225 [18] and ISO 9226 [19] comprise a set of standards intended to estimate corrosion rates based upon four commercially pure metals and environmental parameters. The standards acknowledge that the estimations are complex, particularly when considering alloy materials and that direct measurements (weight loss) of corrosion are a valid alternative method when possible.

1.4 Literature

Literature and other resources were retrieved and reviewed. Background and more recent literature yielded a good basis for developing an analysis of data generated in this project. Reference [20] organized and focused understanding of differences among exposure sites and WS (weathering steel) versus CS (carbon steel) corrosion losses. Generally, comparisons to WS were for CS having less than 0.2% Cu. They used the classic approach observing the weight losses over a wide range of times for each material of interest. The ISO (International Standards Organization) approach, as explained by reference [21], combines the corrosion weight losses in one year with an atmospheric classification to estimate long-term corrosion weight losses. For example, ISO Class C3 corresponds to TOW (T4 = 2600–5200 h/y), chloride deposition (classes S0 and S1 = 0-60 $mg \cdot m^{-2} \cdot d^{-1}$), and sulfur dioxide deposition (class P0 = 0-10 $mg \cdot m^{-2} \cdot d^{-1}$). For WS, class C3 corresponds to corrosion rates, 2–8 $\mu m \cdot y^{-1}$, for the first ten years and 1-4 $\mu m \cdot y^{-1}$, for additional years. Reference [22] reviewed the background and performance of WS bridges based upon early issues that were observed. Reference [23] has compiled extensive data on corrosion rate studies with analyses of correlations aiding predictions for expected performance of WS in a wide range of environments. Reference [24] have updated their findings and

extended guidelines for WS use in various environments. More recently, Reference [25] has provided further updates and insight on protective strategies pertinent to WS. Other resources and collaborations have also been explored [26] [27] [28] with regard to more current technologies for addressing environmental data collection. Reference [26] addressed sensor methods for TOW measurements that demonstrated the caveats and difficulties involved with the task. Among other vendors, Reference [27] described development of a compact data logger for atmospheric monitoring initially focused on agricultural applications capable of supporting a wide variety of sensor including a dielectric-based wetness sensor [28]. There is still a need for methods that address the more damaging microenvironments within a bridge structure that impact WS applications as suggested in reference [29]. References [30] [31] developed analysis methods for steel corrosion products relative to WS corrosion performance in high humidity and chloride environments that indicate the akaganeite form of corrosion product is associated with poor corrosion resistance. Substantial work has gone into studies of WS and its interactions with the environment. However, there is still a strong need for development and implementation of guidelines and methodologies for specification of WS with reliably good performance.

The atmospheric corrosion of iron occurs in the presence of an adsorbed or thin layer of water through which oxygen diffused to oxidize elemental iron to ferrous and ferric ions. These ions combine with water to form iron hydroxides that upon drying form various iron oxides. Deposition of airborne materials such as chloride (salt particles), carbon dioxide or sulfur dioxide, promote conductivity of water layer which increases the corrosion rate. The corrosion rate decreases as corrosion products accumulate and block oxygen and water from contacting the metallic surface. The weathering steel alloy additions such as copper and nickel modify the properties of the oxides formed on the metal surface to enhance their barrier and corrosion resistance properties. These properties decrease the corrosion rate and distinguish weathering steel from carbon steel.

Water vapor, chloride and sulfur dioxide are the primary environmental components that enable atmospheric corrosion of steel. Weathering steel can tolerate limited exposures to these components while providing good service performance, i.e., resistance to corrosion. A review in reference [32] provides a deposition limit range of 6-300 $mg/m^2 \cdot d$ for salt and up to 200 $mg/m^2 \cdot d$ for SO_2 depending on which country, UK, Japan or USA, specifies the guidelines. Generally, the corrosion loss for weathering steel and other metals with growing protective films follows a power law, $C = At^B$, where C is the loss; t is time in years; A and B are constants. Corrosion studies have been conducted over two or more decades with data collection usually started at the end of the first year [22] [23]. Data at less than one year are limited. The power law can be modified to accommodate water vapor as time-of-wetness, chloride deposition, SO_2 deposition and temperature [32]:

$$C = At^B \left(\frac{TOW}{D}\right)^E \left(1 + \frac{SO_2}{F}\right)^G \left(1 + \frac{Cl}{H}\right)^I e^{J(T+T_0)},$$

where A, B, D, E, F, G, H, I, J and T_0 are empirical coefficients. Detailed and complete data are required to enable use of this equation. The methods used to acquire data on water vapor, TOW, chloride and SO_2 deposition may not be uniform across test sites. Author's note: The result of these modifications may skew rather that enhance the correlations in unexpected ways. For example, the temperature measurement may be in shade, partial shade or full daylight with temperate or tropical location. Wind speed is a major factor in assessing drying conditions, but it is not readily accommodated in these modifications. The simple power law equation is typically preferred and will be used to analyze data obtained in the current study.

2 EXPERIMENTAL

2.1 Generic Environmental Data

Basic environmental data were obtained from online websites acquired from personal and commercial weather stations for locations of interest. Archival data for several years was available and downloaded for selected locations. The areal density of weather stations was substantial, particularly in higher population density regions and agricultural areas. Generic weather information was available from many private and public sites. The specific sites were selected based upon data quality, completeness, ease of access and proximity to corrosion monitoring sites established during this project. Primary weather information interest was temperature and dew point for TOW and, secondarily, cloud cover, rain and winds (drying conditions). Note that direct measurement of surface wetness or condensation (for TOW) requires an existing structure or surrogate substrate (a lower temperature thermal mass) that is beyond the designed capabilities or intent of generic weather stations. Temperature and dew point data were used to estimate TOW as described in ASTM Standard G 84 [10].

2.2 Corrosion Product Collections from Existing Structures

Surveys were made along east-west roadways to collect data on chloride and sulfur depositions from existing steel and galvanized structures using spot testing and scrapings for off-site analyses. The depositions of Cl^- and SO_2 obtained from real structures provide information related to wet candle and sulfation plate data. Chloride and sulfate components of existing rust indicate their net concentrations, after wash-off or dissipation rather than their total cumulative depositions.

Table 1: Label designations for WOB specimens.

Site (01-30)	WOB Material Combinations: Bolt –Wire CS (bolt) WS (bolt) NY (bolt) AN (soft annealed CS wire) AL (soft Al wire)	Replicates (1-3)
01	A (WS – AL)	1, 2, 3
02	B (WS – AN)	1, 2, 3
03	C (NY – AL)	1, 2, 3
⋮	D (NY – AN)	1, 2, 3
29	E (CS – AL)	1, 2, 3
30	F (CS – AN)	1, 2, 3
Example: 2-C-3 specifies the 3rd replicate of a nylon bolt – Al wire specimen at site 02.		

2.3 Monitoring Sites at 30 South Florida Locations

Sites were established for direct corrosion measurements of CS, Al (aluminum) and WS using ASTM Methods G 50 [9], G 92 [12] and G 116 [13]. Specimens (six steel plates) were placed for the study (G50 & G92). The plates were labeled 1-30 for the site locations and A-F for the replicates at each site: For example, 02-B represents a plate specimen, B, at site 02. Use of modified ASTM G 116 (Wire-On-Bolt), ASTM G 50 (Atm. Corr. Tests on Panels) and ASTM G 92 (Atm. Site Characterizations) with CS, WS and Al give direct corrosion information versus indirect ASTM G 84 (TOW), ASTM G 91 (Sulfation Plate) [11] and ASTM G 140 (Wet Candle) [14] tests. ASTM G 116 specifies a cathodic or inert bolt material with an anode wire specimen, but WS is not available in wire form – Using commercially available WS, CS or NY (nylon) bolts with CS or Al anode wires were selected for direct corrosion information using ASTM G 92. Combinations include WS, CS and inert bolt materials with CS and Al wires. Table 1 gives the labelling designations and specimen codes. Comparisons of these material combinations with those obtained at benign versus aggressive sites should enable more direct assessment of WS suitability at specific sites with relatively short exposure times. Specifically, if a WS bolt is developing a protective patina, the weight loss of Al wires will be lower and decreasing with time versus the weight loss of Al wires on CS bolts or on WS bolts with no protective patina. ASTM G 50 tests provide direct corrosion data, but require longer exposure times (> 6 months). ASTM G 92 method provides corrosion site conditions and corrosion data, which enables correlation of the conditions with the corrosion observed. Correlations of these data sets across diverse sites should enable conclusions to be drawn. It is recognized that while fabrication operations on bolts and connection of Al to WS may alter quantitative data, the general trends and pass/fail conclusions should remain valid. The ASTM G 116 standard specifies aluminum as the wire material. Aluminum wire was used in this study.

A total of 30 sites have been established. Sites were solicited for use in this project at many locations and types of owners. The first sites were easily obtained at Florida Atlantic University campuses from the south at Dania Beach to the north at Harbor Branch Oceanographic Center and to the west at Davie, FL. Many potential site owners were difficult with which to communicate suggesting little interest in cooperating. Finally, Florida State Parks agreed to allow use of many sites and Broward County Parks agreed as well. Palm Beach County Parks considered the request but eventually denied placements. In addition, the City of Weston, City of Delray, South Florida National Cemetery and Sunshine Meadows Equestrian Center agreed to placements. Permits and agreements were obtained to enable the placements. Appendix A, Site Images, shows the monitoring stations at 30 sites.

Figure 1 and Figure 2 show the mounting of plate and WOB specimens on the monitoring station pole. Racks for the specimens were constructed as specified in standards ASTM G 50 and ASTM G 116. The typical setup for the monitoring station with corrosion specimen racks and data logger/sensors is shown in Figure 3. The data logger and weather station sensors were obtained from Decagon Devices, Pullman, WA, consisting of an Em50 Digital Data Logger or Em50G Remote Data Logger, a VP-3 Sensor (temp/RH) w/radiation Shield), an ECRN-100 high resolution rain gauge, a Davis cup anemometer (wind speed and direction), an ES-2 (electrical conductivity & temperature sensor) and a leaf wetness sensor. The plates were at 30 degree to horizontal and the WOBs were vertical. A map showing the locations of the 30 stations is provided in Figure 4 and an image of the east SeaTech site is provided in Figure 5.

For atmospheric corrosion studies, thin gauge materials are preferred for weight loss measurements for which sensitive balances used for measurements have limited capacity. Bridge steels are generally available in heavy gauges. In this study, A606-04 steel (light gauge) was used for the weight loss

measurements. The material composition closely matches that of A588 (COR-TEN B) and was obtained from Western States Decking, Inc., who agreed to cut and ship the materials as 0.6 m x 0.6 m plates. The material certifications are shown in Table 2. Based upon ASTM Standard G 101 [33], the calculated index for this material is 6.57 and falls within the range of indices (6.4-7.0) for compositions defined for weathering steels. The material was sheared to approximately 76 mm x 101 mm rectangular plates and a hole was drilled near the middle end of the narrow dimension for attachment of identification tag. WS is more difficult to shear, drill or abrade versus CS. Six plates were deployed at each site, for a total 180 plate samples (30 stations). The first set of 30 plates is referred to as 1st set or set 1. Set 2 or 2nd set consisted of two plates removed at the same time in which one plate was used for weight loss analyses and the duplicate plate used for XRD analyses.

Aluminum wire (0.9 mm, alloy 1100, meeting ASTM B211) and annealed carbon steel wire (0.9 mm, alloy 1006/1008) were used for the wire-on-bolt specimens. Nylon 6/6, CS and WS studs (1/2"-13) were used for the bolts. The steel studs and plates were cleaned by blasting with clean aluminum oxide grit, degreasing with mineral spirits, then alcohol rinse and warm air drying. The wires were more difficult to abrade and a winding rig (Figure 6) was assembled to repetitively pass the wire through silicon carbide abrasive papers positioned at 120 degree angles to the axis direction to abrade the entire wire circumference. The wires were degreased with mineral spirits, and then rinsed with alcohol and warm air dried. The nylon were degreased with mineral spirits and then rinsed with alcohol and warm air dried (no abrasion). The specimens were assembled following the ASTM G 116 for WOB specimens or ASTM G 50 plate specimens and deployed at monitoring sites.

Table 2: Material certification provided by the supplier.

Material:	A606-04							
	Element	%		Element	%		Element	%
	Carbon (C)	0.05		Nickel (Ni)	0.28		Niobium (Nb)	0.001
	Manganese (Mn)	0.86		Chromium (Cr)	0.56		Nitrogen (N)	0.008
	Phosphorus (P)	0.008		Molydenum (Mo)	0.01		Titanium (Ti)	0.005
	Sulfur (S)	0.001		Tin (Sn)	0.009		Boron (B)	0.000
	Silicon (Si)	0.037		Aluminum (Al)	0.04		Calcium (Ca)	0.002
	Copper (Cu)	0.29		Vanadium (V)	0.053		Antimony (Sb)	0.002
Product	Cold rolled full process: 0.0625 min x 48.0000 (inches)							
Direction	Test			KSI			Test	
L	Yield Strength			59.2			Elongation	32%
	Tensile Strength			68.0				

For this material composition, the ASTM Standard G 101 index was 6.57 as noted in Section 2.3, paragraph 4. The range specified for A588 steel is 6.1-7.0. This material satisfied the specified range. The index was calculated using the material certification data (Table 2) as follows:

$$I = 26.1(\%Cu) + 3.88(\%Ni) + 1.2(\%Cr) + 1.49(\%Si) + 17.28(\%P)$$

$$-7.29(\%Cu)(\%Ni) - 9.10(\%Ni)(\%P) -33.39(\%Cu)2 = 6.57$$

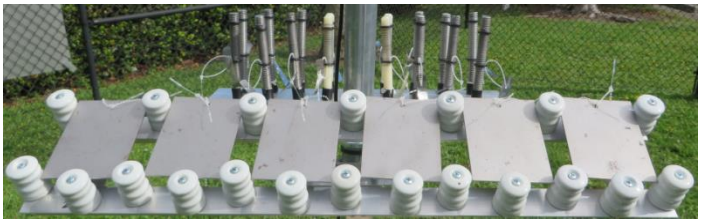

Figure 1: Plate specimens (G 50) mounted on 30-degree rack with WOB specimens in background.

Figure 2: WOB specimens (G 116) mounted on horizontal rack.

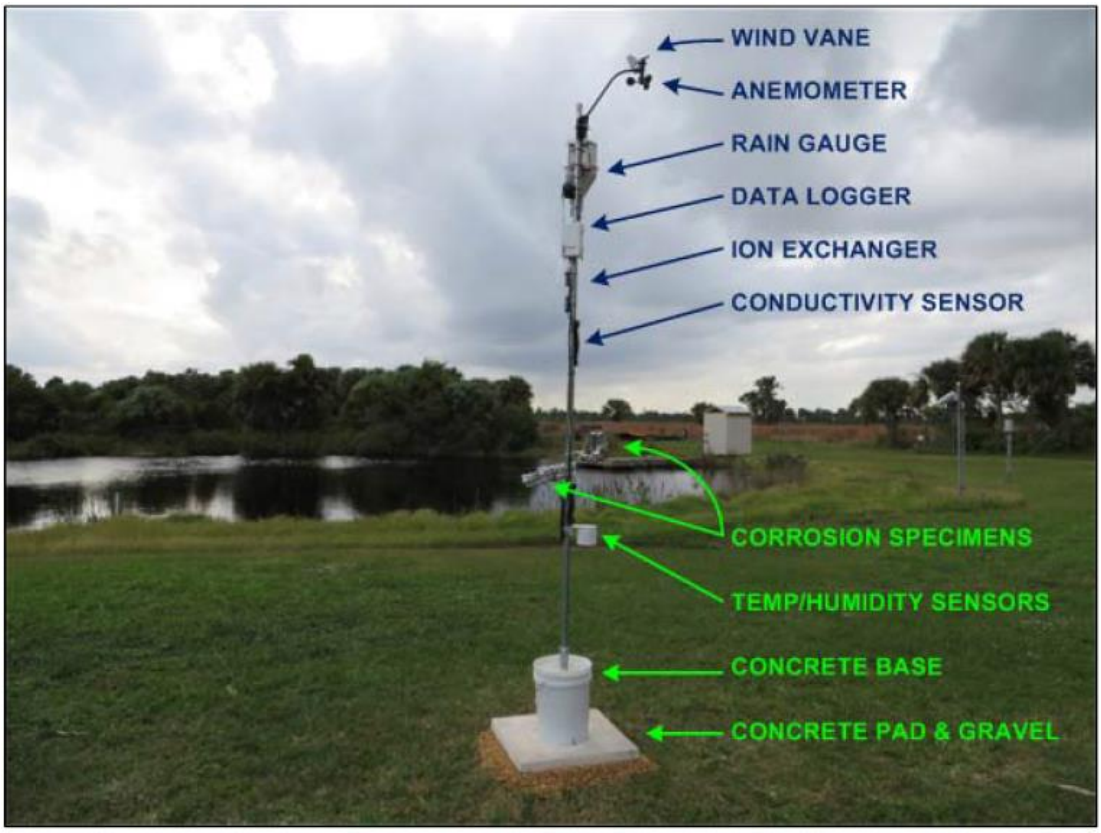

Figure 3: Monitoring station showing placement of corrosion specimens, weather monitoring components and mounting base.

Southeast Florida Locations of 30 sites.

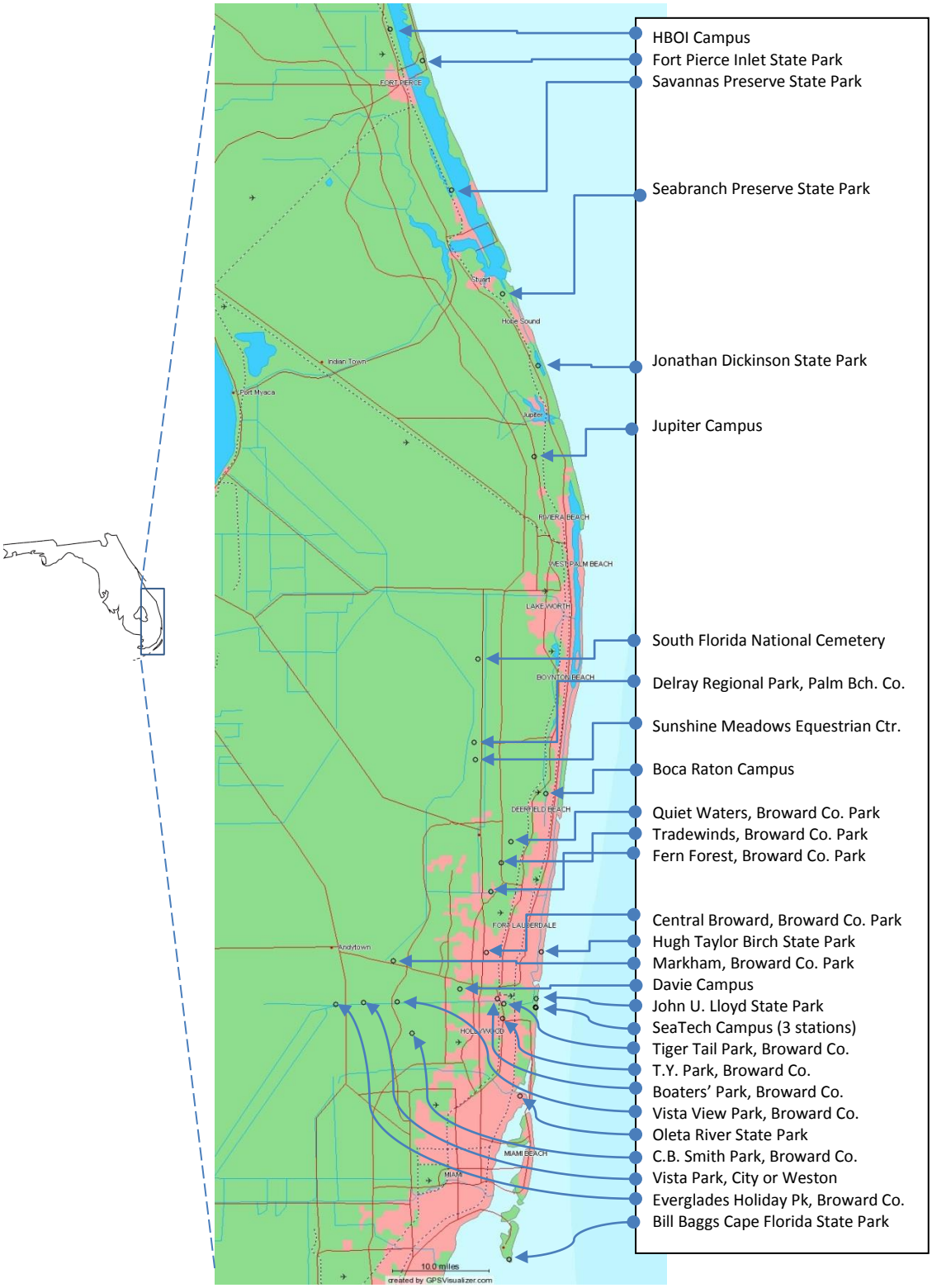

Map created by GPSVisualizer.com: US: Demis street-level map (uses TIGER data)

Figure 4: Map of site locations in south Florida.

Figure 5: SeaTech east, site 01.

Stations were set up following ASTM requirements [9] [13] and weather station recommendations [34]. Note, especially, that plate specimens are required to face south. Details of the additional components shown are given in the subsequent sections.

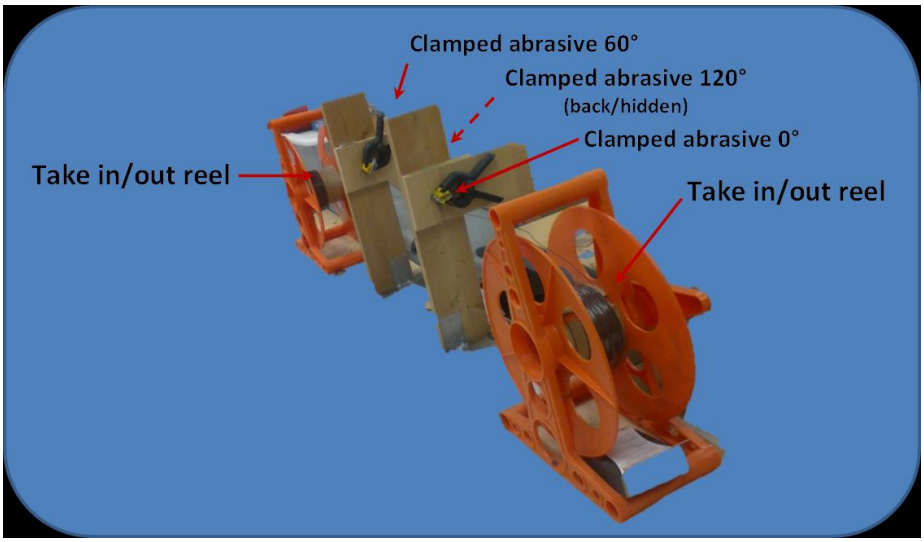

Figure 6: Wire abrasion rig.

2.4 Corrosion Product Removal Procedures

The WS specimens were exposed at the monitoring sites. The specimens were plate (G 50) and coil (G 116) shapes. To remove bulky corrosion product on panel specimens, a mechanical procedure was applied. Using a hand file as shown in Figure 7, the rust was scraped from each specimen surface. This step was carefully performed to ensure that the sample was not excessively scraped. In other words, only corrosion product was removed, not the base metal. Note that the rust from the front and the back of each specimen was collected and stored in separate bottles and labeled. For the first set of plate specimens, 25 mm x 25 mm square pieces were carefully cut from the plate using a heavy-duty hand shear. The cuts were made partially through the length and width of the specimen so that only the square piece was removed from the plate. The square piece was retained without cleaning for XRD measurements. The larger, remaining "L" shaped piece was cleaned and the area determined by image analysis using MatLab on a photocopied image of the "L" piece. The ratio of square piece to "L" piece was used to adjust the initial weight of the specimen for the weight loss determination.

Figure 7: Hand file used to remove corrosion products from plates.

With the coil specimens, the coil must be removed from the bolt before performing the electrolytic cleaning procedure. The coils were impacted in the corrosion products that filled the bolt threads and were very difficult to remove either because corrosion continued beyond the recommended exposure times or in the corrosion was severe. To facilitate removal of the coil from its bolt, a stainless steel wire loop (Figure 8) was used. One free end of the coil was placed through the stainless steel loop, and then the loop was pulled around the bolt, lifting the coil out of the bolt threads until the other end of the coil was reached. The coil was loosened which allowed the coil to be twisted in the counterclockwise direction to separate it from its base bolt. In this manner, the loose coil was unscrewed from the bolt. In some instances while removing the coil, some corrosion products fell off of the specimens. These corrosion products were saved in a glass bottle with designated label for later X-ray diffraction procedure.

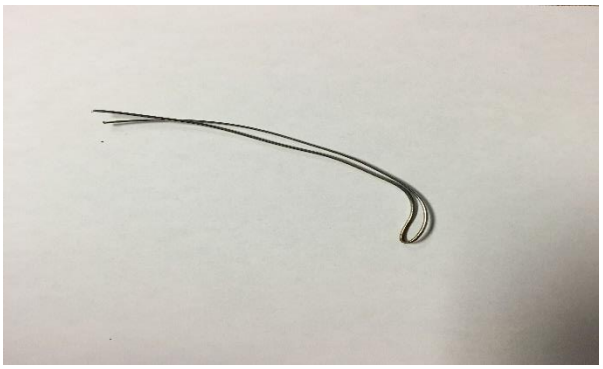

Figure 8: Stainless steel wire loop tool for loosening coil specimen from bolt.

After the mechanical procedure, specimens were cleaned cathodically by an electrochemical method (ASTM Standard G 1, A2, Table A2.1, E.1.1) consisting of NaOH, Na_2SO_4, and Na_2CO_3 at 25°C and 200 A/m^2 to remove the remaining corrosion product. Each specimen was basically cleaned in three cleaning cycles. In the first cleaning cycle, the specimen was placed in electrochemical cleaning cell for one hour. To simultaneously clean multiple specimens, the cleaning system was set up in series with constant currents of 2.3 A (L-shape specimens), 3.1 A (rectangle shape specimens) and 0.56 A for coils. The currents were calculated from their surface areas and the required 200 A/m^2. After electrochemical treatment, the specimen was rinsed with distilled water and then placed in the ultrasonic cleaner for 5 minutes to remove the loose corrosion product. Next, the specimen was sprayed with alcohol before exposing it to a warm, dry air flow to prevent condensation until dried. Alcohol helped the specimen to dry faster. After drying and before weighing, the specimen was tapped a few times on the hard table surface to ensure all loose corrosion products (smut) fell off of the specimen. Finally, the specimen was weighed to obtain the weight loss to complete one cleaning cycle. In the subsequent cleaning cycles, the specimen was cathodically electrolyzed for half hour increments. The specimen weights obtained were plotted versus cleaning time until consistent results were obtained as per the ASTM Standard G 1. An example plot is shown in Figure 9. After examining the data obtained using this method, it was determined that the specimens were not completely clean. Additional cleaning steps were performed using hydrochloric acid with corrosion inhibitor, hexamethylene tetramine (ASTM Standard G 1, A2, Table A1.1, C.3.5), with rinsing, drying and weighing as described above for electrolytic cleaning. Instead of a dull, dark gray surface with electrolytic cleaning, a bright, clean surface was obtained. These data were more consistent. A plot of the combined weight losses is shown in Figure 10. The aluminum wire specimens were cleaned with nitric acid (ASTM Standard G 1, A2, Table A1.1, C.1.1), with rinsing, drying and weighing as described above.

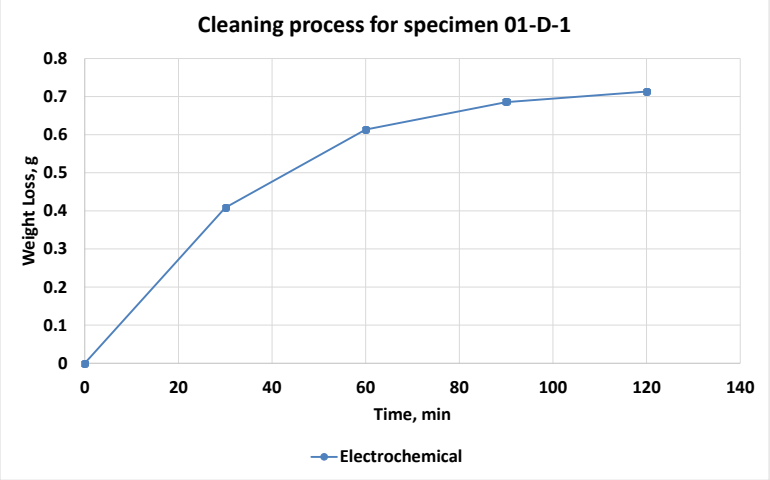

Figure 9: Weight loss versus electrolytic cleaning cycle.

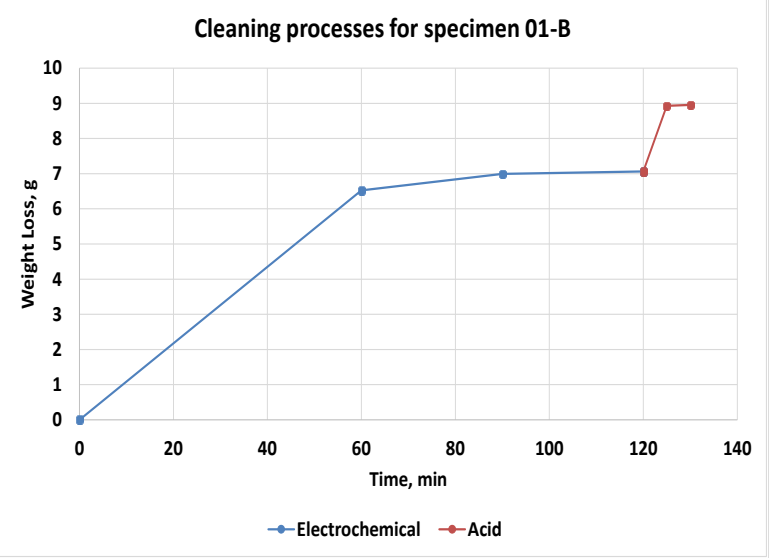

Figure 10: Weight loss versus combined cleaning methods.

2.5 Chloride, Sulfation and Time-Of-Wetness

Chloride depositions were obtained at sites 01 and 02 using the G 140 established methods [35]. Corrosion products were scraped from exposed and collected plate specimens (2nd set) and extracted with water. The conductivities of the extracts were measured with a total dissolved solids wand and the extracts were analyzed for chloride and sulfate with a SEAL AQ2 Discrete Analyzer and methods: Chloride, AQ2 Method No: EPA-105-A Rev. 5; and, sulfate, AQ2 Method No: EPA-123-A Rev. 5. Time-of-Wetness (percentage time above 80%RH) was determined from on-site logger data or using downloaded public weather station data.

Permit applications for establishing sites were denied based upon requirements provided in permit application guidelines or discussions to enable wet candle and sulfation testing. Applications were routed through environmental professionals that identify toxic materials with an end result of the permit being denied. Modifying the permit applications for site use without glycol and lead peroxide facilitated the application approvals. Alternative chloride and sulfation analysis methods were considered. Based

upon methods developed in the current project, rain gauge modifications (funnel) incorporating a conductivity sensor and a wet leaf sensor were installed at sites as alternatives to ASTM Methods G 140, G 91 and G 84 to include more suitable and detailed chloride and sulfate determination via rain gauge, conductivity sensor and ion exchange resins. The concept was to modify the rain gauge to allow the weather station to monitor the rainwater conductivity. This modification enabled rainwater ion exchange for collection of Cl^- and $SO_4^=$ via anion and cation polymers by passing the effluent from the rain gauge through a resin filter. The mixed bed resin selected was Dowex® Marathon™ MR-3 hydrogen and hydroxide form. The anion polymer was required for chloride and sulfate. However, cations Mg^{2+} and Ca^{2+} can be significant contributors to conductivity, hygroscopicity and pH modification and were possible to monitor via cation polymer. Most of the weather stations were modified to perform conductivity and ion exchange functions.

Weather station modifications consisted of bird deterrence and rainwater analysis. The bird deterrence was incorporated using stainless steel wire and hose clamp as shown in Figure 11. This arrangement was simple and was adopted from commercial products designed for straight edges of a wall or pipe. The perimeter and center of the round rain gauge was easily protected in this manner. Another detail (Figure 12) inserted into the rain gauge top was the crossed baffle designed to help collect passing airborne salt particles into the gauge opening. Continuing from the bottom of the rain gauge, a plastic funnel was attached to collect rainwater passing through the gauge (Figure 13) and to route the rainwater to the ion exchange filter shown in Figure 14. To prevent the conductivity detector and ion exchange filter from drying out, the water exits the conductivity gauge upward in a loop shown in Figure 14 that prevents complete drainage when the rainfall stops.

Figure 11: Rain gauge – bird deterrence and particle baffle.

Figure 12: Rain gauge – top view of particle baffle and bird deterrence.

Figure 13: Conductivity sensor (black bottom endcap) and ion exchange filter (upper tube with white endcap).

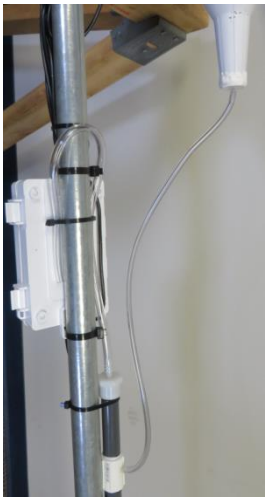

Figure 14: Rain water collection and routing. Rain water exits bottom of white funnel (top right), loops downward from right to conductivity sensor (bottom middle), then upward through ion exchange filter to overflow-drainage control loop (upper left).

2.6 Corrosion Products on Structures

Samples were collected from structures for off-site analyses or analyzed in-situ. Limited samples were collected when the opportunity presented while performing other activities for this project. These were stored for later analyses. XRD and XRF analyses were performed.

2.7 Analytical Methods

Scanning electron microscopy (SEM) with elemental analysis was performed on one plate specimen collected in the first set of site exposures. The FEI Quanta 200 system was used for this purpose. An Oxford X-Met 3000 TXV+ XRF instrument was used for elemental analyses in limited cases. The sensitivity of the instrument for elements less than Z=21 was poor (~5%). XRD was used to determine the corrosion products structure to determine the existence and percentage of the corrosion products formed from the samples. Each side of the plate specimens was subjected to XRD analysis before and after scraping off the surface oxides. The scrapings from each side were also analyzed. A Philips Model XRG3100/PW1710 system with DiffTech Visual XRD control software was used for the measurements. The X-ray source used for the analysis was a cobalt $K^{\alpha}1$ with a wavelength of 0.179 nm. The cobalt source reduced the fluorescence usually observed with Fe compounds such that much better XRD patterns are obtained with iron oxide samples. The operating parameters consisted of a range of 10-90 degrees 2-theta, step size of 0.05 degrees and dwell time of 2 seconds. Crystalline iron oxides such as akaganeite, goethite, lepidocrocite, hematite, magnetite and maghemite are identified and help determine the protective properties of the corrosion products formed on the steel surfaces. From the American Mineralogy Crystal Structure Database (AMCSD) [36], the Table 3 shows XRD data converted to Co-Kα for the corrosion products (minerals). The first, second and third major intensities with corresponding angles are shown in Table 3 to reference the relative intensities (%), location (degrees 2θ) and the type of corrosion product (mineral name or formula) that was formed in the sample.

The main steel corrosion products are shown in Table 3. Comparing the XRD pattern peaks and products with the table, the corrosion products in the sample can be identified and an estimate obtained for the percentage of the products for each sample. An example XRD pattern is provided for sample 01-A. The XRD pattern of the substrate is shown in the Figure 15. Several peaks related to the corrosion products are identified by reference to Table 3 and labeled in Figure 15. The peaks are easily distinguished. A strong set of peaks is clearly shown in the pattern near 41-42° and are recognized as hematite, magnetite or maghemite or match with additional peaks shown in Table 3. However, a peak of interest belongs to akaganeite which is known as a corrosion product that forms in the presence of chloride on steel substrates. There were other corrosion products also present.

The percentage of the corrosion products were calculated as follows: The 100% peaks (Table 3) for the following products were used:

- Akaganeite has a 100% peak at 13.95° and another peak at 66.2° with intensity of 51% (which was doubled to normalize the calculation). The peak at 66.2° was selected because there is no interference from other iron corrosion products at this position.
- Lepidocrocite has a peak at 16.6° and 100% intensity without any interference. The intensity of this peak was used for the lepidocrocite component.
- Goethite has a peak at 24.76° and 100% intensity and it is unique. The intensity at this angle was used for calculations.
- Hematite has a peak at 38.67° and 100% intensity and it is unique. The intensity at this angle was used for calculations.

The 100% peaks located in the range, 41.7° to 42.5°, belong to other iron corrosion product components that overlap with each other. Therefore, the intensity at this range was chosen for these remaining components: β-Fe_2O_3, γ-Fe_2O_3 (maghemite), Fe_3O_4 (magnetite), and FeO (wustite). The percentages of the main components of interest (akaganeite, lepidocrocite, goethite and hematite, were determined in this manner.The percentages of the components are normalized from the following formula for akaganeite:

$$Percentage = \frac{I_{Ak}}{I_{Ak} + I_{Le} + I_{Go} + I_{He} + I_{rest}} \times 100$$

Similarly, for each compound the percentage was calculated as in the above formula.

Table 3: XRD peak positions (CoKα) and intensities for corrosion products.

Name	Angle	Intensity
α-FeOOH Goethite	24.76° 42.93° 38.86° 62.85°	100% 77% 47% 40%
β-FeOOH Akaganeite	13.95° 66.20° 31.15°	100% 51% 90%
γ-FeOOH Lepidocrocite	16.60° 31.64° 40.37°	100% 64% 33%
α-Fe_2O_3 Hematite	38.67° 41.62° 63.67° 58.11°	100% 73% 45% 37%
β-Fe_2O_3	41.40° 74.17° 35.09° 50.48°	100% 42% 28% 20%
γ-Fe_2O_3 Maghemite	41.71° 42.17° 74.76° 35.37°	100% 64% 40% 34%
Fe_3O_4 Magnetite	41.43° 40.57° 55.84° 52.02°	100% 34% 27% 20%
FeO Wustite	49.10° 42.24° 48.86° 71.31° 41.55°	100% 51% 50% 27% 26%

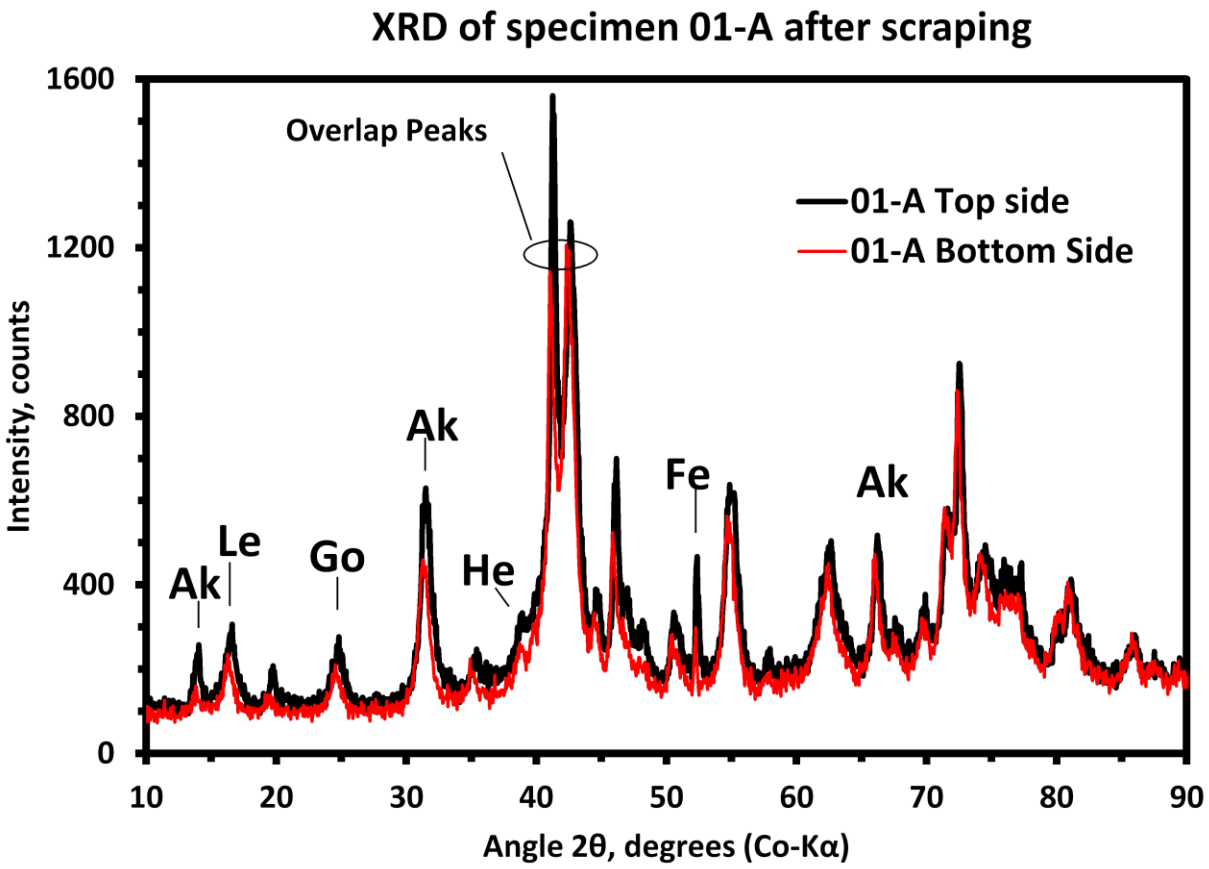

Figure 15: Corrosion products associated with peaks: Ak (akaganeite), Le (lepidocrocite), Go (goethite), He (hematite) and Fe (iron substrate). XRD pattern for top side of specimen (Black) and (Red) for the bottom side. The bottom side showed slightly lower intensities than the top side.

3 RESULTS

3.1 Environmental Data

The following website provides historical weather data recorded at hourly intervals.

http://www.wunderground.com/weatherstation/WXDailyHistory.asp?ID=KFLCORAL5&day=23&year=2009&month=1&graphspan=day

For example, there are more than 80 stations, most with websites serving data, in the vicinity of Fort Lauderdale Executive Airport. Figure 16 is a graphic representing weather stations proximal to the airport. Several websites have been accessed to download data obtained near the project monitoring sites. Data have been accessed from websites (via www.wunderground.com) for the following weather stations: KFLFORTP16, KFLJENSE9, KFLSTUAR31, KFLTEQUE5, KFXE, KFLLAKEW23, KFLDELRA29, KFLDELRA14 and KFLJUPIT18. Table 4 shows the weather station identifier, the monitor station, GPS locations and distances.

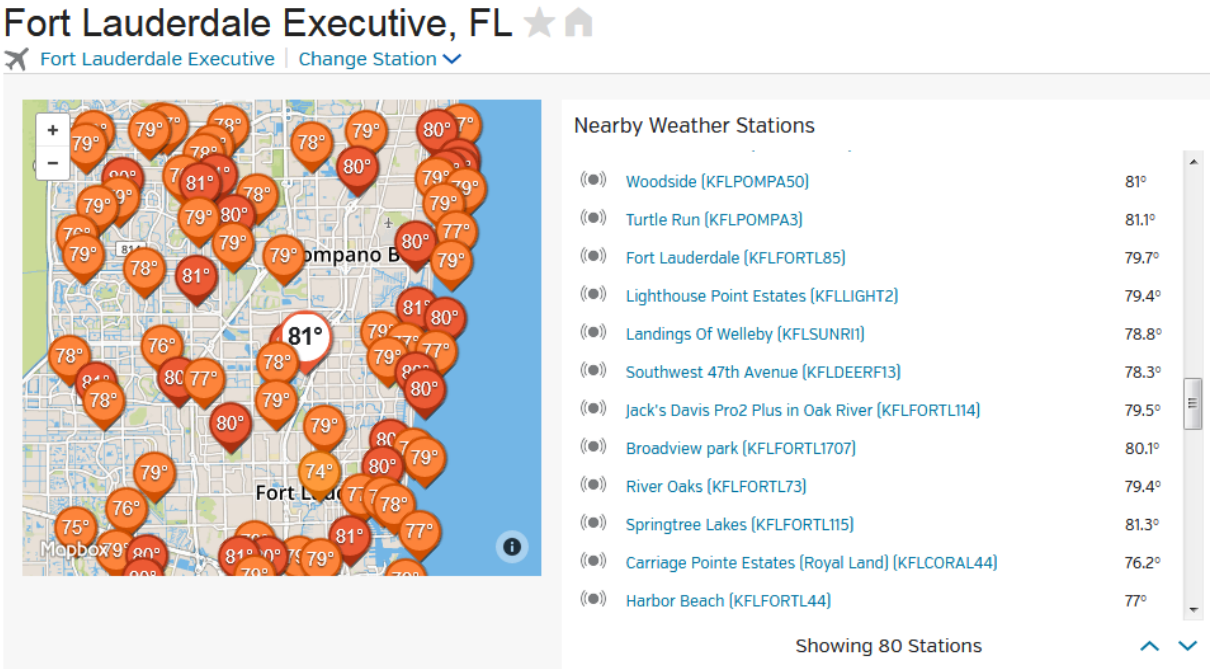

Figure 16: Example of weather station density in vicinity of Ft. Lauderdale Executive Airport.

Table 4: Station-to-site distances. Station data used for TOW calculation.

Weather Station	Station GPS	Station Proximal to Site	Site GPS	Proximal Distance, miles
KFLJUPIT18	26.905 -80.128	06-FAU Jupiter	26.887 -80.115	0.4
KFLTEQUE5	26.995 -80.094	12-Jonanthan D.	27.025 -80.109	0.9
KFLSTUAR31	27.154 -80.182	13-Seabranch	27.133 -80.169	1.6
KFLJENSE9	27.279 -80.246	14-Savannas	27.290 -80.253	2.3
KFLFORTP16	27.490 -80.298	15-Ft Pierce	27.485 -80.303	2.6
KFXE	26.196 -80.170	19-Fern Forest	26.230 -80.188	1.0
KFLLAKEW23	26.596 -80.210	24-SFNC	26.581 -80.209	2.5
KFLDELRA29	26.428 -80.175	25-Sunshine	26.429 -80.214	2.9
KFLDELRA14	26.434 -80.176	30-WDelrayRP	26.455 -80.216	1.4

In some cases, the data are available as hourly information while in others the data are averaged daily. For hourly data, the TOW is calculated by summing the number of hours above 80% RH, dividing by the total hours and expressing the result in percentage. If the data are available as daily averages, the following approach was taken:

> TOW per day was calculated in hours by observing if the High Humidity was less than 80%, then assign TOW a value of zero (0); and, if the High Humidity was not less than 80% and the Low Humidity less than or equal to 80%, then assign TOW a value 24 times the ratio of High Humidity minus 80% to High Humidity minus Low Humidity; if neither (both High and Low Humidity were above 80%), then TOW was assigned a value of 24. The hours above 80% were estimated assuming linear behavior by an Excel formula:
>
> =IF(HighHumidity<80,0,IF(AND(HighHumidity>80,LoHumidity<=80),((HighHumidity-80)*24/(HighHumidity-LoHumidity)),24)).
>
> Using these estimations, the percentage TOW was determined from the ratio of hours above 80% RH to total hours.

The %TOW for eight sites calculated from public archives is given in Table 5. The use of archived weather station data described here may be useful for characterizing the environment near a test or proposed test location. Furthermore, several sites can be characterized in the vicinity of the point of interest to develop greater confidence in the results. The information obtained will be used in later parts of this report.

Table 5: TOW from archive databases for eight sites.

Site Number/Name	Distance from Shoreline, miles	%TOW
06 Jupiter	3.8	40.5*
12 Jonathan Dickinson SP	0.75	33.9*
13 Seabranch SP	1.42	23.9*
14 Savannas SP	0.25	43.7*
15 Fort Pierce SP	0.52	51.6*
19 Fern Forest CP	6.2	36.4*
24 S. Florida Nat'l Cemetery	10.9	32.3*
30 W. Delray Regional Park	10	38.7*
*Calculations from proximal weather station online archived data.		

3.2 Corrosion Product Collections from Existing Structures

Most often, only very small sampling areas were accessible, making useful measurements very difficult. The reproducibility of the measurements would be difficult to gauge. Only small volumes of scraping specimens were possible.

Several surveys along east-west roadways were done. Very few unpainted steel structures were found. Most steel structures were painted and showed no significant rust. Damaged, painted surfaces were not deemed acceptable due to the significant differences in rust development on such surfaces versus unpainted steel. This method of acquiring samples had very low productivity. Consultation with a colleague from the National Steel Bridge Alliance, William McEleney, on October 19, 2016, suggested that very few weathering steel structures were in service in Florida and that developing documentation for the structures would be difficult. Subsequently, a presentation was located, authored by Mr. McEleney, presented at an FDOT conference showing images of three weathering steel bridges located approximately ten miles from the Gulf Coast (http://www.fdot.gov/structures/designconference2008/presentations/session35mceleney.pdf). The images show development of the typical protective patina color associated with well-performing weathering steel, including areas beneath the bridge decks. The bridges were constructed in 1999.

Two weathering steel pedestrian bridges, approximately 10 feet above water, were located in Margate, FL, approximately, 7.5 miles from the shoreline: 6030 Royal Palm Blvd, Margate, Florida, GPS: 26.254617, -80.204202. A visual inspection of the upper and lower areas of this bridge (Figure 17) showed excellent patina development.

The bridge crossing Whiskey Creek at the west end of the FAU Dania campus is primarily concrete construction. It is situated approximately 35 ft west of site 02 SeaTech and receives substantial chloride deposition. A steel fence beneath the bridge was well-corroded and yielded approximately 10% chlorine and no sulfur via X-ray fluorescence analysis (±5%), in situ, at the top surface of the fence where salt can accumulate without exposure to rainfall. It is expected that sheltered areas such as this may be problematic unless WS guidelines [25] are followed, enabling drainage of condensed moisture. Drainage of wind-driven and condensed water will wash surfaces while pooling concentrates salt deposits.

Figure 17: Weathering steel bridge in Margate, FL.

3.3 Monitoring Sites at 30 South Florida Locations

The monitoring sites were visited for corrosion specimen collections and data logger downloads. The corrosion specimens were cleaned and weight losses determined. Several data loggers suffered malfunctions that disabled them. For those data loggers, the most critical information desired was %TOW that was accommodated by accessing proximal weather station archived data. Table 6 provides the site, distance from shore, %TOW, specimen exposure times and weight loss data. Two plates were retrieved at the second collection, one for weight loss and the other for XRD analysis. Figure 18 shows that several sites exhibited TOW above the 60% level and TOW is weakly associated with an increase with distance from the shoreline. Figure 19 indicates that TOW above 60% does not yield the highest corrosion loss. It is likely that another parameter is responsible for high corrosion rates for these sites. The two highest corrosion losses occur at sites 01 and 02.

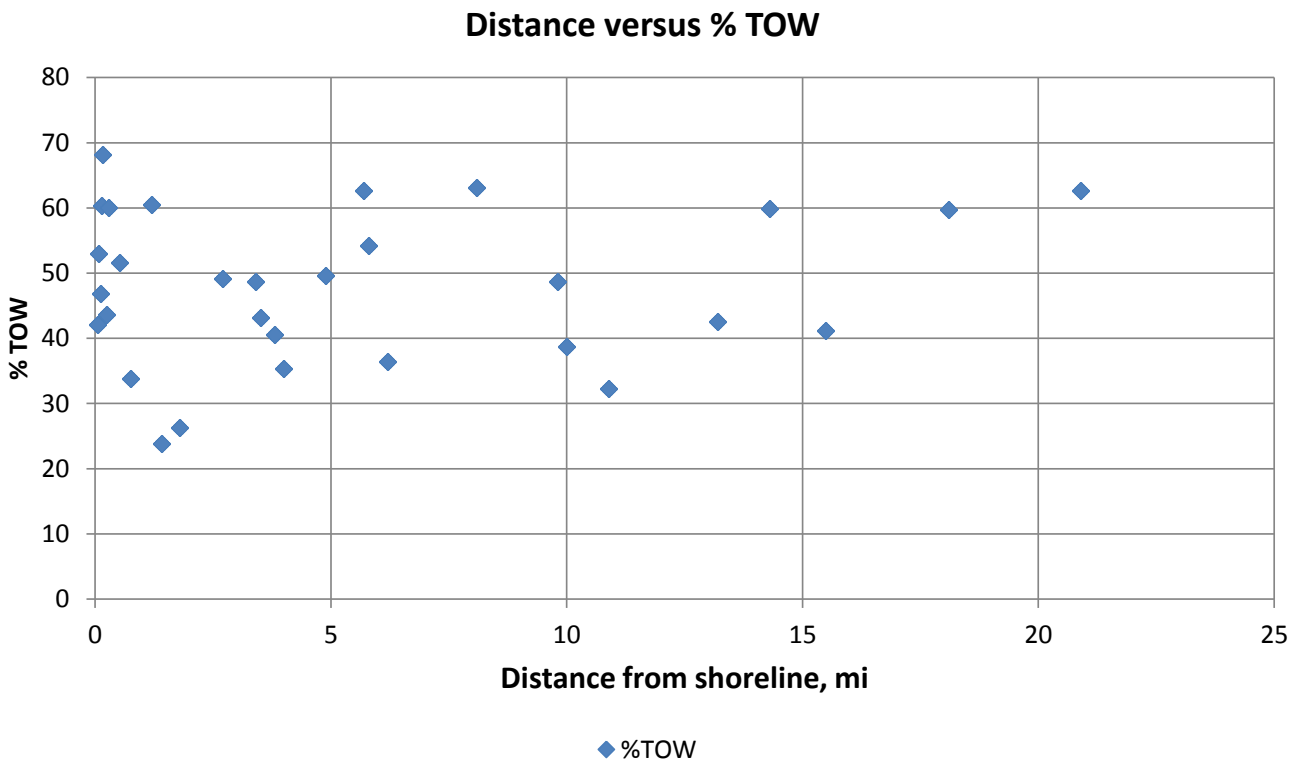

Figure 18: Time of wetness of all sites versus distance from shoreline.

Figure 20 is a plot of distance from shore versus weight loss for the first and second panels removed from the monitoring stations. For better readability the plot has three parts: 0-1 mile, 1-5 miles and 5-25 miles. The panels at SeaTech sites experienced the greatest weight losses. These panels were the most boldly exposed to flow of air from the shoreline and received considerably more salt deposition than shielded exposures. In some cases, the second panel showed smaller weight loss than the first panel collected at the site. This behavior can be attributed to the delayed start of the corrosion process. This delay is possibly due to the use of aluminum oxide blast grit on the plates that imparts some initial corrosion resistance. For future studies, garnet grit is suggested. The overall behavior of these data suggests that the corrosion decreases to a lower rate with increasing distance from the shoreline.

Figure 19: TOW versus weight losses for 2nd plate set.

Figure 21 is a plot of distance from the shore versus corrosion rate in weight loss per year. The trend line shows an initial decrease of corrosion rate as a function of distance from the shore followed by a trend to a constant rate. The highest corrosion rates are associated with the two SeaTech monitor stations closest to the shore. The third SeaTech monitor station furthest from the shore is somewhat shielded from direct ocean salt air and yielded a modest corrosion rate. The corrosion monitor station at Hugh Taylor Birch State Park is closer to the shore than one of the high rate SeaTech stations, yet yielded a low corrosion rate. This behavior is likely due to the protection afforded by the surrounding environment, trees and vegetation, at Hugh Taylor Birch Park.

Figure 22 is a plot of coil corrosion weight loss as a function of distance from the shore. The regression line suggests that there is a small increase with distance from the shore. More corrosion might be expected in a high chloride environment. The behavior of the carbon steel coils is different compared to the weathering steel plates. The steel wires are in a crevice configuration within the bolt threads that is

expected to have a higher corrosion rate than plate configuration. The coil corrosion rates appear to have no correlation to distance to the shoreline. A possible explanation is the coil corrodes rapidly in the crevice coating the remaining steel with a heavy oxide layer that compacts in the crevice and thereby providing protection from additional ingress of environmental aggressive agents (salt, water, oxygen) that results in decreased corrosion rate. This possible explanation is similar to the situation of tightly bolted plates whose corrosion products seal the crevices excluding the ingress of oxygen and water.

With regard to Table 6, specimens were not collected at equivalent exposure times. Data analyses among specimens can be difficult due to the nonlinear nature of the corrosion process. The corrosion rate for 2 years exposure is not simply the weight loss divided by 2 because the rate in the first year will be higher than in the second year. An approach was taken based on the known parabolic nature of atmospheric corrosion and protective oxide growth. The power law, $C = At^B$, can be used to assist comparisons of corrosion losses obtained for different times. For assumed identical or replicate specimens in the same environment, the values of A and B should be assumed identical. This point has been well-demonstrated for steel, weathering steel and most other metals by many researchers [2] [20] [22]. For example, data in reference [20] is replotted in Figure 23. The values of coefficients A and B vary by site, but the data plotted show good linearity with log-log scaling. Both carbon steel and weathering steel plots follow this behavior showing a higher slope for aggressive corrosion conditions and less material corrosion resistance. Comparing Kure Beach marine with Saylorsburg, PA, mild environments carbon and weathering steels is reasonably clear. Carbon steel corrodes faster than weathering steel and the Kure Beach environment is more harsh that Saylorsburg's.

Table 6: List of sites, distances, TOW, weight losses and exposure Times. Underlined TOW values calculated from archive weather sites.

Site Number & Name	Dist. Shore (km)	Dist. Shore (miles)	TOW (%)	1st Plate Weight Loss ($g \cdot cm^{-2}$)	1st Plate (days)	2nd Plate Weight Loss ($g \cdot cm^{-2}$)	2nd Plate (days)	Avg. D-Coil $_{Fe}$ Weight Loss ($g \cdot cm^{-2}$)	Coils (days)
01 Seatech	0.08	0.05	42.1	0.0503	847	0.0695	1210	0.0140	693
02 Seatech Wet Candle	0.21	0.13	60.3	0.0334	740	0.0490	1139	0.0234	622
03 Seatech West	0.26	0.16	68.2	0.0342	739	0.0284	1100	0.0325	583
04 Boca	2.90	1.80	26.3	0.0196	580	0.0130	1098	0.0259	580
05 Harbor Branch	4.34	2.70	49.1	0.0182	860	0.0200	1113	0.0143	860
06 Jupiter	6.11	3.80	40.5	0.0161	579	0.0185	1118	0.0182	579
07 Davie	13.03	8.10	63.1	0.0112	854	0.0277	1093	0.0148	854
08 Hugh Taylor SP	0.11	0.07	52.9	0.0219	938	0.0234	1111	0.0164	938
09 Oleta SP	1.95	1.21	60.5	0.0208	937	0.0223	1097	0.0211	937
10 John U Lloyd SP	0.18	0.11	46.8	0.0270	931	0.0283	1088	0.0200	931
11 Bill Baggs SP	0.47	0.29	60.1	0.0175	932	0.0129	1093	0.0127	932
12 Jonathan Dickinson SP	1.21	0.75	33.9	0.0230	567	0.0267	1099	0.0277	567
13 Seabranch SP	2.28	1.42	23.9	0.0036	567	0.0274	1099	0.0304	567
14 Savannas SP	0.40	0.25	43.7	0.0215	567	0.0282	1099	0.0306	567
15 Fort Pierce SP	0.84	0.52	51.6	0.0174	567	0.0205	1099	0.0243	567
16 Tiger Tail Lake CP	5.63	3.50	43.2	0.0094	536	0.0096	798	0.0199	536
17 Tradewinds CP	9.17	5.70	62.7	0.0174	630	0.0191	805	0.0298	630
18 Central Broward CP	9.33	5.80	54.1	0.0167	621	0.0249	806	0.0230	621
19 Fern Forest CP	9.98	6.20	36.4	0.0183	630	0.0200	776	0.0421	630
20 Quiet Waters CP	7.88	4.90	49.6	0.0161	615	0.0174	776	0.0259	615
21 Markham CP	24.94	15.50	41.1	0.0157	630	0.0160	793	0.0230	630
22 Everglades Holiday CP	33.63	20.90	62.6	0.0196	629	0.0215	803	0.0362	629
23 Vista Park Weston	29.12	18.10	59.7	0.0137	602	0.0145	772	0.0245	602
24 S. Florida Nat'l Cemetery	17.54	10.90	32.3	0.0159	271	0.0173	810	0.0383	271
25 Sun. Meadows Equest. Ctr.	15.77	9.80	48.7	0.0129	271	0.0185	813	0.0540	271
26 Vista View CP	23.01	14.30	59.9	0.0190	626	0.0208	800	0.0246	626
27 T. Y. CP	5.47	3.40	48.7	0.0162	599	0.0178	798	0.0212	599
28 Boaters CP	6.44	4.00	35.3	0.0146	612	0.0164	798	0.0191	612
29 C. B. Smith CP	21.24	13.20	42.6	0.0170	626	0.0182	796	0.0208	626
30 W. Delray Regional Park	16.09	10.00	38.7	0.0015	266	0.0199	795	0.0464	266

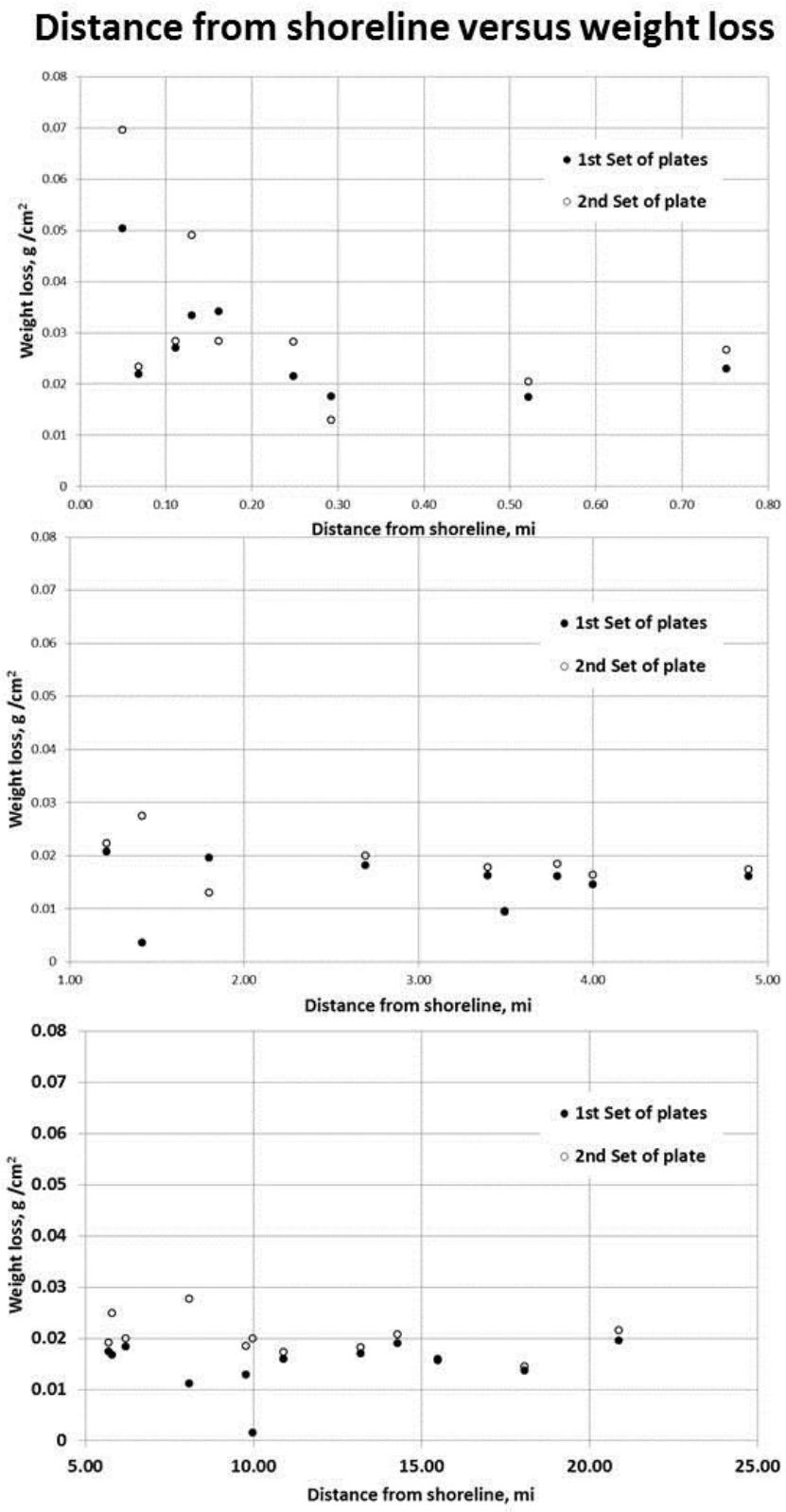

Figure 20: Distance from shoreline versus weight loss for the 1st and 2nd plate sets removed from the monitoring sites: Top, 0-1 mile; Middle, 1-5 miles, Bottom, 5-25 miles.

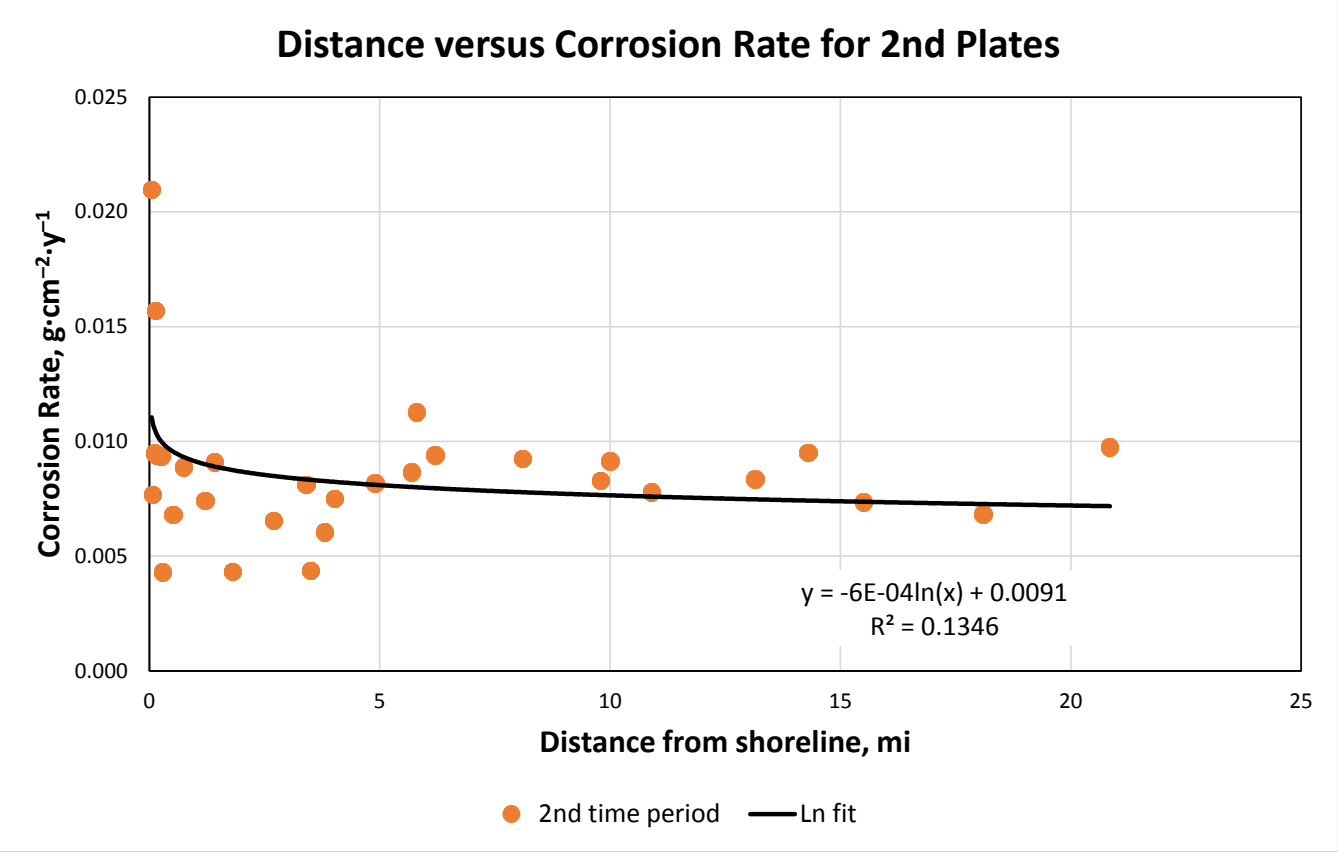

Figure 21: Distance from shoreline versus corrosion rate for 2nd plates.

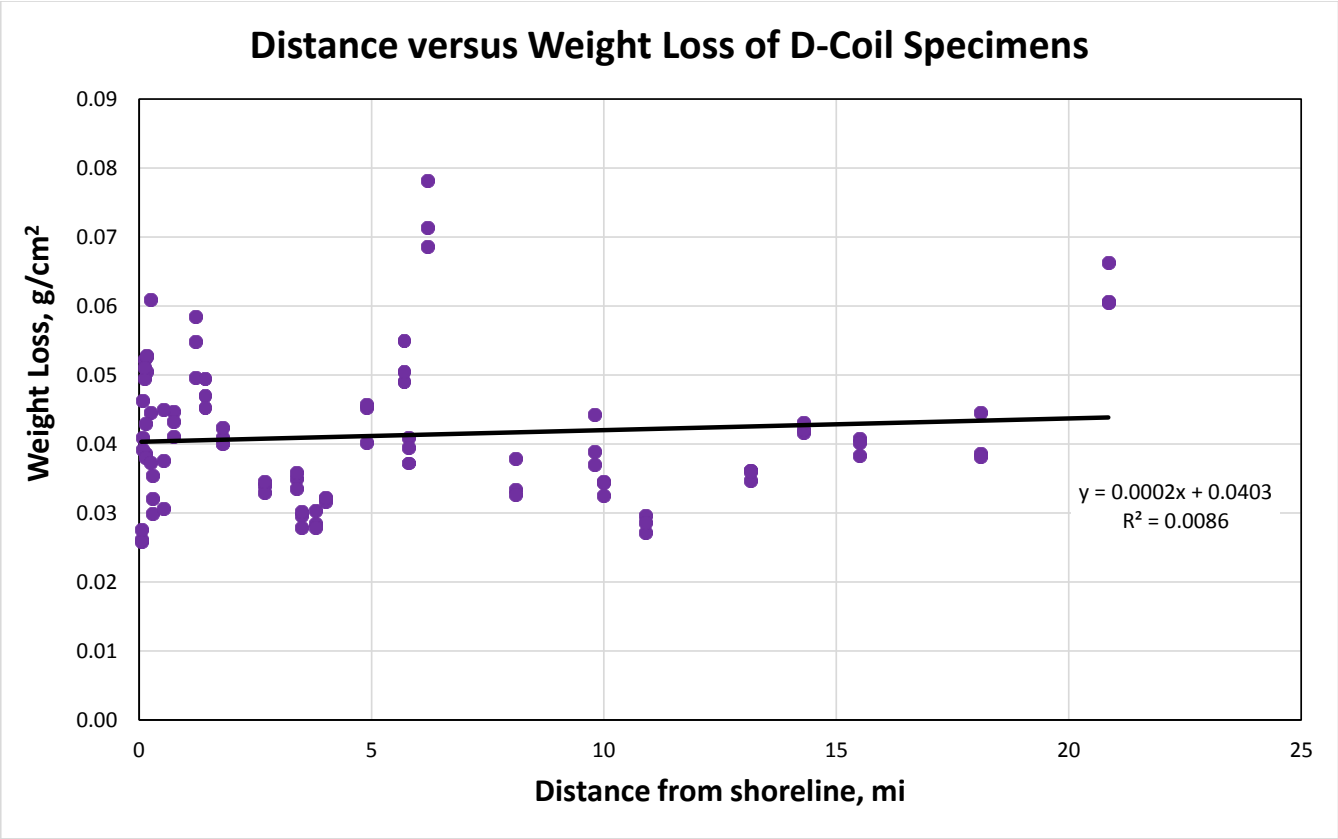

Figure 22: Distance from shoreline versus corrosion rate of CS coils on nylon bolts.

Figure 24 shows a plot of the corrosion losses for the 2nd set of panels. Two panels were in the aggressive region with losses greater than Kure Beach weathering steel. The uppermost point was corrosion loss at SeaTech 01, closest to the shoreline. The second highest point was from SeaTech 02. The remaining 28 panels were clearly lower losses than the most benign site in the Townsend study (Newark). This result suggests that corrosion rates for weathering steel in Florida are generally lower than locations that exhibit good performance in previous studies. This result implies that corrosion conditions are more benign in Florida than in those studies for one or more specific reasons, such as more regular rainfall, better drying conditions or lower SO_2 deposition rates. These possibilities will be discussed later in the report.

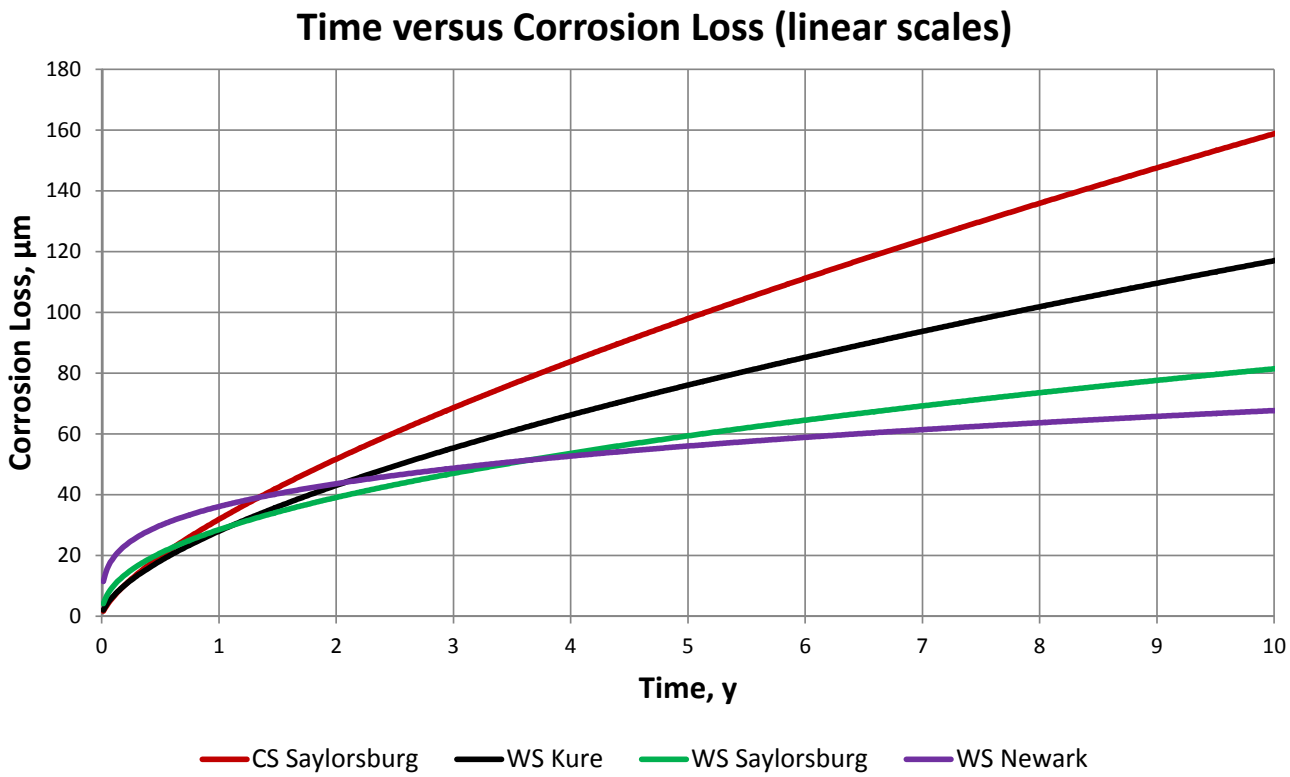

Figure 23: Replot of Townsend data (ASTM STP 767).

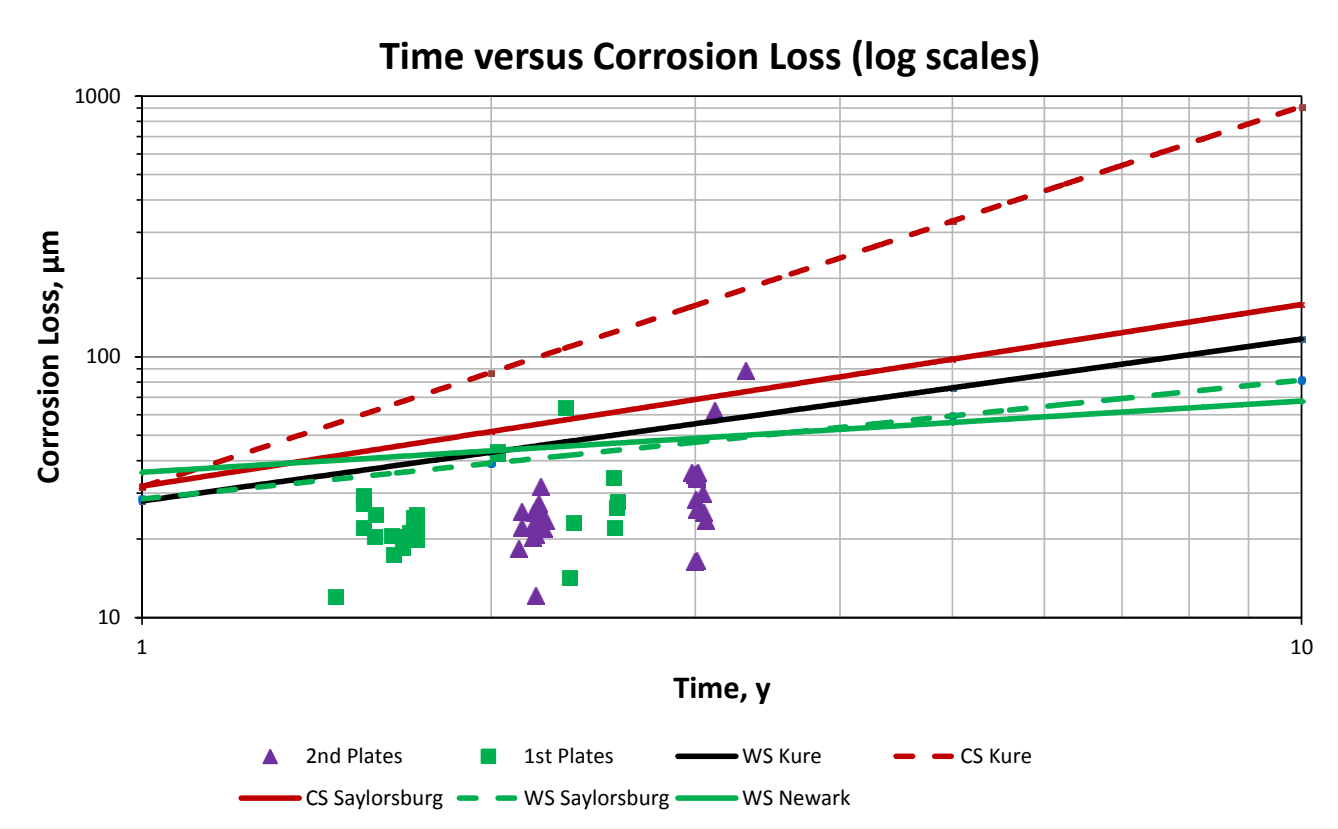

Figure 24: Townsend data with 30-site plate corrosion loss data.

3.4 Data Logger Results

Data loggers installed at all 30 sites provided information useful for determination of TOW listed in Table 6. In general, the completeness of the data sets was an issue. Work stoppage in Phase 1 resulted in expiration of the wireless subscriptions. The subscription restart required replacement of the SIM cards that would be difficult in the field. Manual downloads of data were performed instead of disassembling the stations in the field for SIM card replacement. Several data loggers ceased to operate due to water intrusion, insect damage or other causes. Generally, the battery life was outstanding, lasting well over a year in the case of units without wireless capability. The sensing of rainwater conductivity for assessment of ionic content was not generally successful due to algae growth in the tubing. No work-around for this was determined. Elimination of the ion exchange column is suggested.

Modification of wet leaf sensors was not immediately pursued due to issues with the data loggers. The intent was to develop a coating that could respond more effectively to humidity in the environment. This goal was considered to be marginally useful to the project and was transitioned to very low priority. A higher priority that would enable a more useful wet leaf sensor would be development of mounting system that could mimic moisture changes occurring in the highly corrosion susceptible areas sheltered by bridge deck, for example. This goal would not be readily addressable in the context of this project.

Large data files were obtained from the data loggers and were provided on CD or DVD for archiving.

3.5 X-Ray Diffraction of Corrosion Products

Diffraction patterns were obtained on the corrosion products of plate specimens. Six diffractograms were made from each panel: (1) Top side before scraping off oxide; (2) Top side after scraping off oxide; (3) Top side oxide powder; (4) Bottom side before scraping off oxide; (5) Bottom side after scraping off oxide; and, (6) Bottom side oxide powder. These patterns are provided in Appendix B, X-ray Diffraction Charts. Analyses of the patterns were made to determine the major iron oxide components. The results are shown in Table 7 and Table 8. Figure 25 and Figure 26 show the percentage oxide components for each side versus distance from shore. There is a modest trend for akaganeite to decrease with distance from the shore. The anticipated strong relationship between akaganeite and corrosion was not observed, possibly due to the low corrosion rates. Figures 27-29 plot corrosion losses, TOW, and average percentage of akaganeite observed on the second set of plate specimens (Top side before scraping + Top side powder + Bottom before scraping + Bottom powder)/4, which is an approximation of an average of the four measurements. No strong trends were observed. The result suggests that time of dryness may be a useful measurement for consideration. There does not appear to be much, if any, emphasis on drying conditions in the weathering steel literature. The presence of vegetation at the base of WS transmission towers is a known problem due to the prolonged drying times and moisture retention relative to ambient vegetation-free areas. It may be possible that drying conditions are important and are not simply the converse of TOW. Corrosion prevention designs for metal standards (pylons) appear to be evolving toward eliminating water retention and promotion of drying. It is known that drying conditions are important in cyclic corrosion testing.

Table 7: XRD results for plate top sides (%).

Sample Name	Akaganeite (β-FeOOH)	Lepidocrocite (γ-FeOOH)	Goethite (α-FeOOH)	Hematite (α-Fe_2O_3)	Maghemite & Magnetite
01-C Top Side	18.4	11.6	8.9	11.5	49.6
02-C Top Side	14.5	12.1	7.8	10.6	55
03-C Top Side	7.5	8.4	7.1	7.1	69.9
04-C Top Side	11.2	13.3	11.2	8.4	55.9
05-C Top Side	0	18.1	12.4	11.2	58.3
06-C Top Side	7.6	15.7	11.2	12.7	52.8
07-C Top Side	8.8	17.2	14.1	13.4	46.5
08-D Top Side	0	20	20	20	40
09-D Top Side	0	15.4	12.5	14.4	57.7
10-D Top Side	17.8	12.3	11	12.3	46.6
11-D Top Side	10.7	17.1	10.7	12.5	49
12-C Top Side	8.1	13.7	8.9	12.1	57.2
13-C Top Side	0	16.7	12.2	13.3	57.8
14-D Top Side	0	16.3	12.8	11.2	59.7
15-C Top Side	0	15.6	10.3	13.5	60.6
16-C Top Side	0	16	8.1	8.9	67
17-D Top Side	0	18.9	14.2	11.7	55.2
18-D Top Side	9.1	15.7	9.1	11.6	54.5
19-D Top Side	0	17.9	14.6	14.6	52.9
20-D Top Side	9.1	15.8	12.5	12.5	50.1
21-C Top Side	0	17.7	10.4	11.5	60.4
22-C Top Side	0	20	11.8	12.7	55.5
23-C Top Side	0	23.1	0	9.6	67.3
24-C Top Side	0	15.4	17.7	16.9	50
25-C Top Side	0	15.8	8.9	12	63.3
26-C Top Side	0	14.3	8.9	9.6	67.2
27-C Top Side	8.9	15.7	10.4	12.7	52.3
28-C Top Side	0	12	10	11	67
29-C Top Side	0	11.1	7.4	7.4	74.1
30-C Top Side	0	12.7	8.1	9.2	70

Table 8: XRD results for plate bottom sides (%).

Sample Name	Akaganeite (β-FeOOH)	Lepidocrocite (γ-FeOOH)	Goethite (α-FeOOH)	Hematite (α-Fe_2O_3)	Maghemite & Magnetite
01-C Bottom Side	21.3	6.1	11.5	8.4	52.7
02-C Bottom Side	21.2	8	7.4	10.1	53.3
03-C Bottom Side	21.4	7.9	5.6	8.4	56.7
04-C Bottom Side	15.3	8.3	5.9	8.4	62.1
05-C Bottom Side	0	13.1	5.7	7.4	73.8
06-C Bottom Side	0	13.2	5.9	7.3	73.6
07-C Bottom Side	0	15.7	8.5	10.5	65.3
08-D Bottom Side	0	12.1	7.8	9.2	70.9
09-D Bottom Side	0	11.3	5.3	7.8	75.6
10-D Bottom Side	18.4	8	6.9	9.1	57.6
11-D Bottom Side	6.2	9.3	4.3	6.2	74
12-C Bottom Side	7.2	9	3.9	5.8	74.1
13-C Bottom Side	0	11	4.7	5.5	78.8
14-D Bottom Side	10.6	7.7	3.6	5.3	72.8
15-C Bottom Side	0	8.1	4.8	6.5	80.6
16-C Bottom Side	10.1	9.6	4.6	6.4	69.3
17-D Bottom Side	0	10.8	6.6	7.2	75.4
18-D Bottom Side	13.9	8	3.7	5.4	69
19-D Bottom Side	0	13.6	4.9	6.2	75.3
20-D Bottom Side	11.6	8.1	4.1	5.8	70.4
21-C Bottom Side	0	14.4	6.5	7.2	71.9
22-C Bottom Side	0	12.9	6	6.7	74.4
23-C Bottom Side	0	14.4	5.6	0	80
24-C Bottom Side	0	19.9	7.7	8.3	64.1
25-C Bottom Side	0	13.4	5.4	14	67.2
26-C Bottom Side	0	11.5	5.3	6.8	76.4
27-C Bottom Side	13.4	8.6	4.3	5.8	67.9
28-C Bottom Side	0	10	7	7.1	75.9
29-C Bottom Side	8.9	9.4	3.9	5	72.8
30-C Bottom Side	0	12.2	4.7	6.1	77

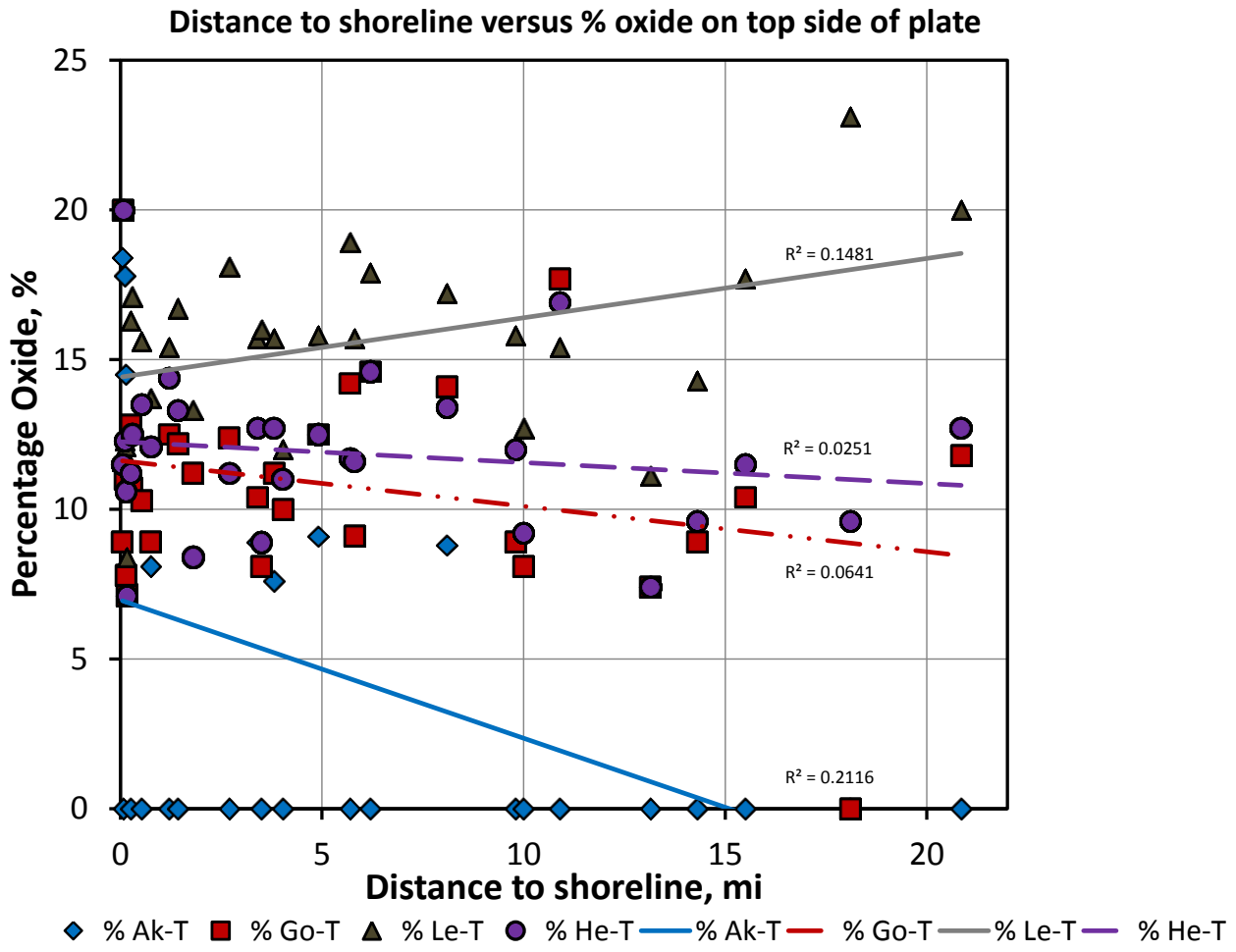

Figure 25: Percentage iron oxides on plate top sides: Ak (akaganeite), Go (goethite), Le (lepidocrocite), and He (hematite).

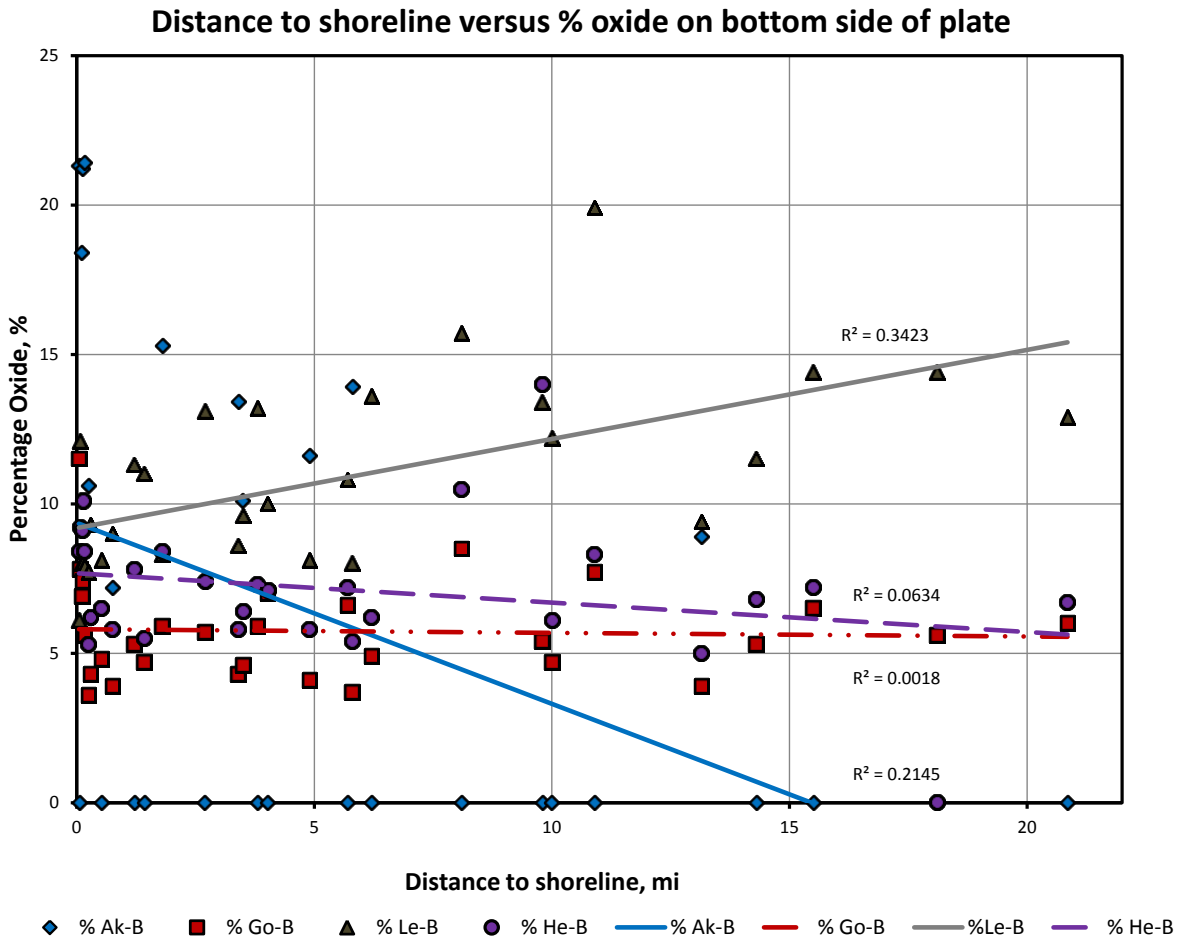

Figure 26: Percentage iron oxides on plate bottom sides: Ak (akaganeite), Go (goethite), Le (lepidocrocite), and He (hematite).

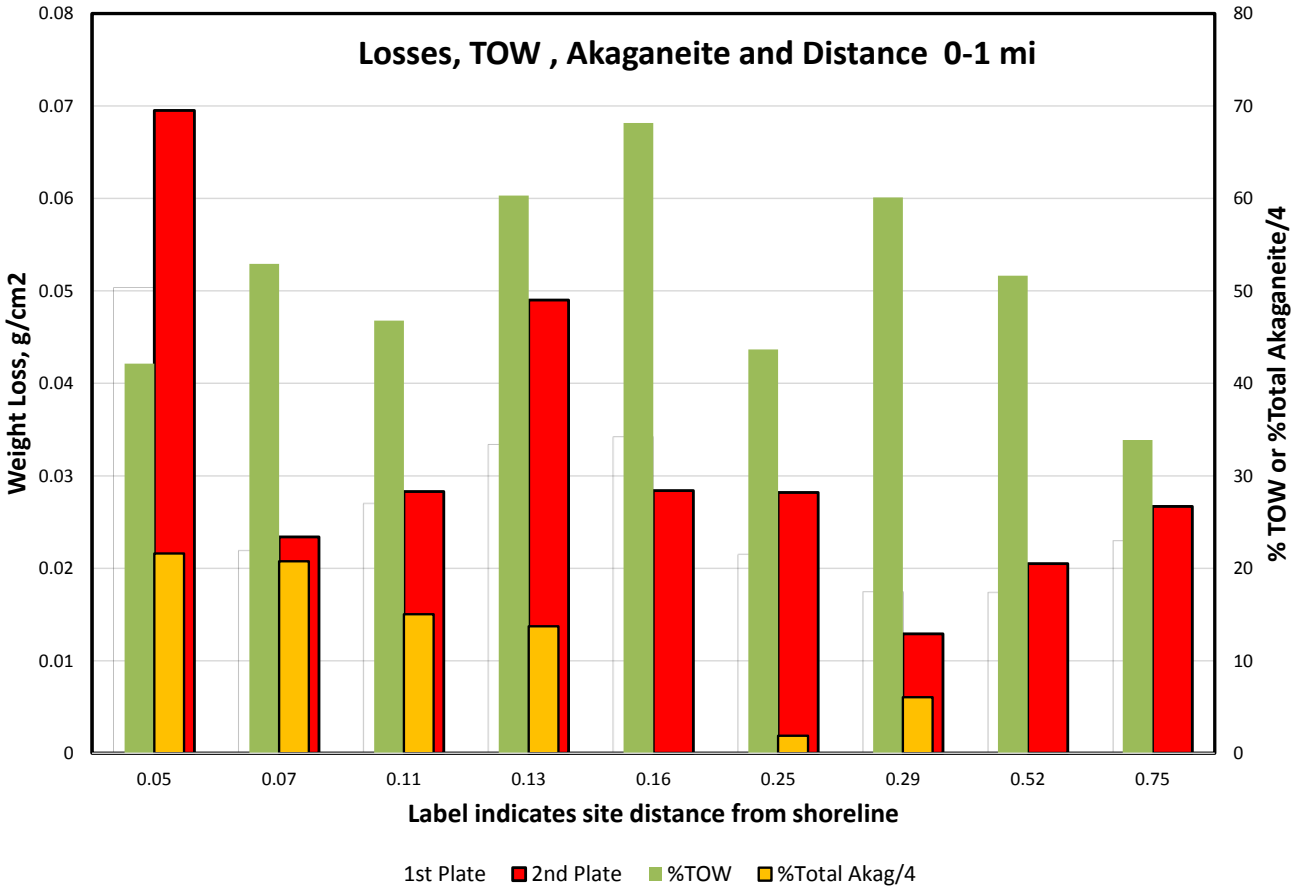

Figure 27: Graphic of corrosion loss, TOW and akaganeite for shoreline distances of 0-1 mi.

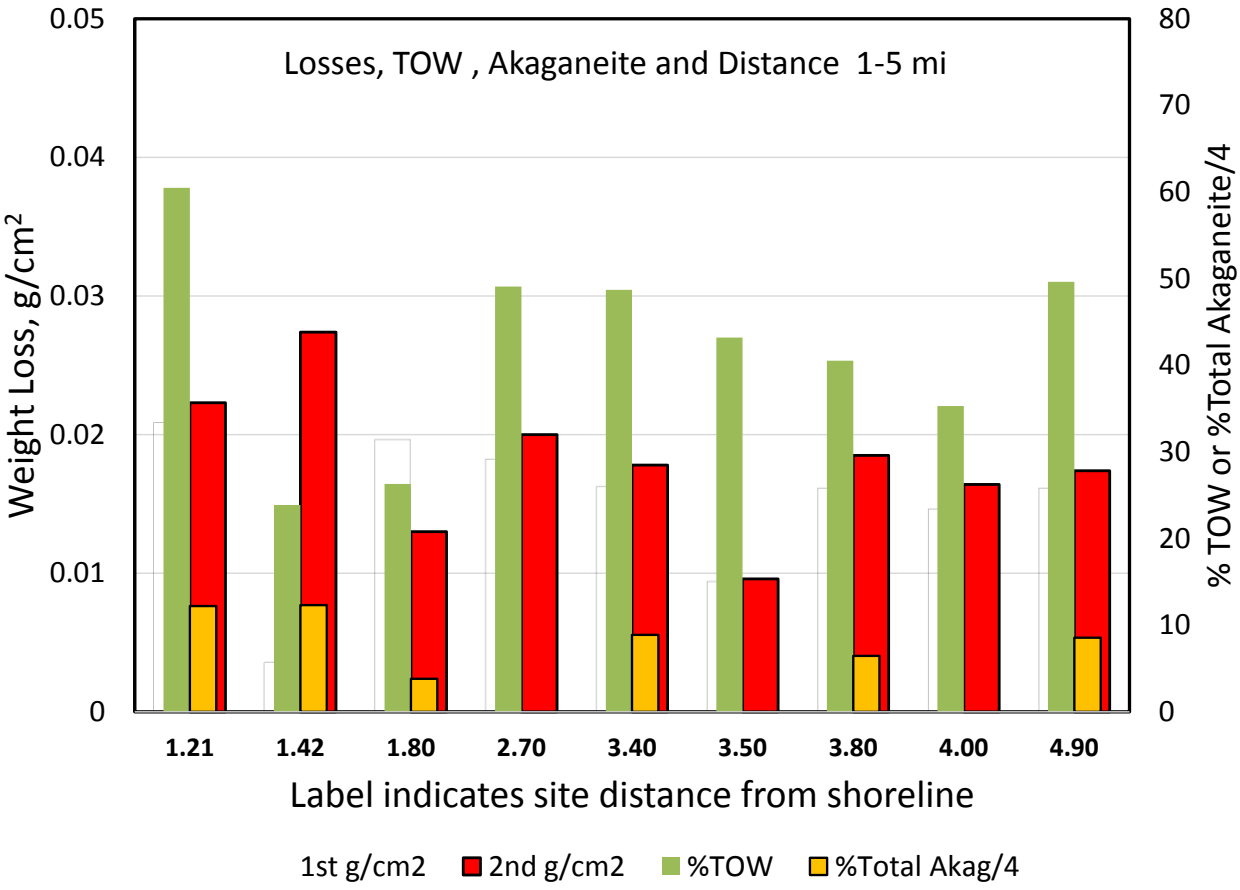

Figure 28: Graphic of corrosion loss, TOW and akaganeite for shoreline distances of 1-5 mi.

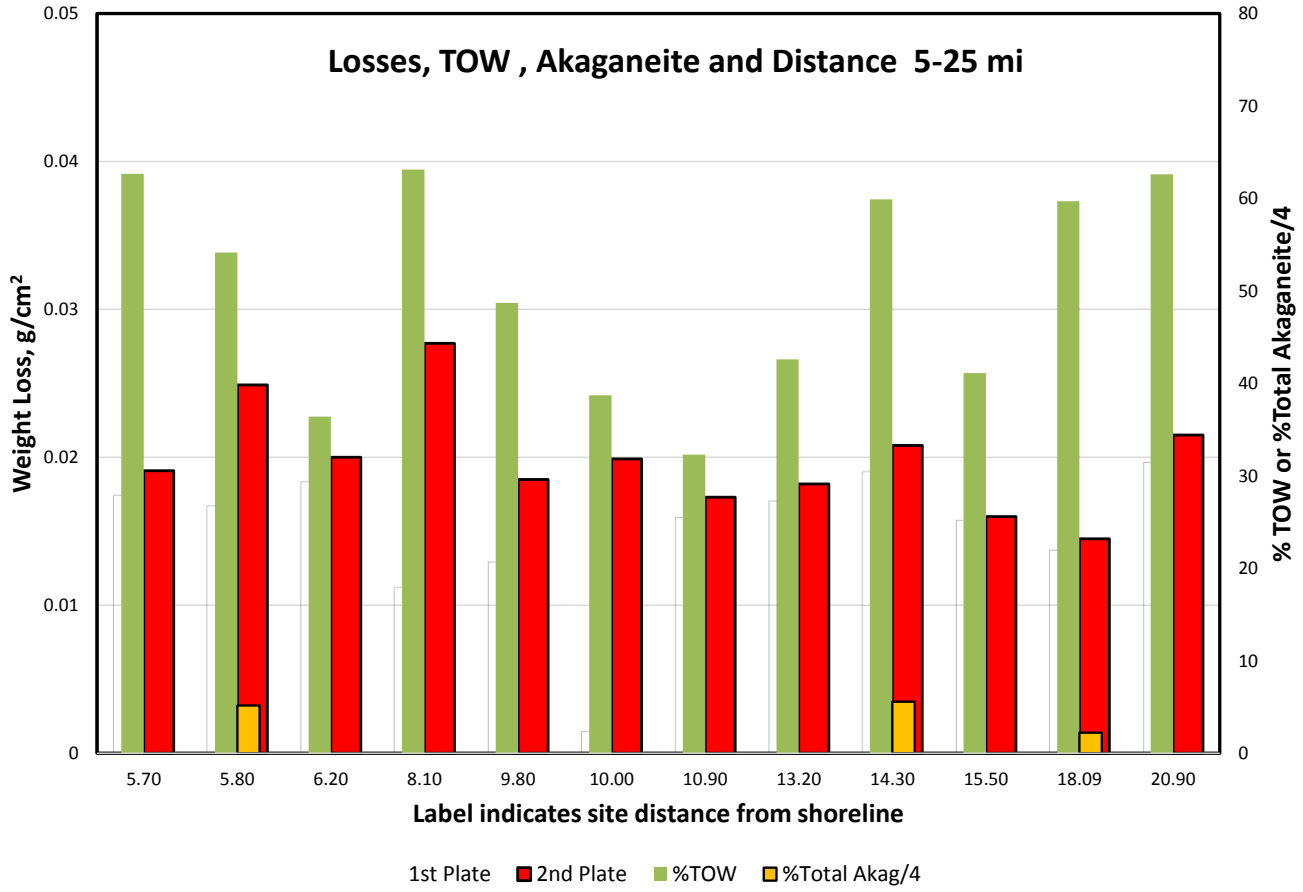

Figure 29: Graphic of corrosion loss, TOW and akaganeite for shoreline distances of 5-25 mi.

3.6 Chloride and Sulfate in Corrosion Products.

Corrosion products scraped from the 2nd set of plate specimens as described for XRD methods were analyzed for conductivity, chloride and sulfate. An estimate of chloride and sulfate deposition could be made from these measurements. The surface area of each side was 77.4 cm^2 .The powdered corrosion products were in 20 ml scintillation vials to which 20 ml of distilled water was added. The vials were shaken to disperse the powder and allowed to settle overnight. A 15 ml aliquot was aspirated from the vial into a second vial. A TDS (total dissolved solids) wand (Model TDS-3, TDS meter, HM Digital, Inc., Culver City, CA 90230) was inserted into the aliquot and the conductivity reading was obtained (Table 9). The vial was forwarded to the water analysis laboratory at the Davie campus for the chloride and sulfate analyses. Figure 30 shows the highest deposition rate occurs at short distances from the shoreline and bottom surfaces have higher salt retentions than top surfaces as expected due to less direct rainwater washing on the bottom surfaces. It also shows that distance may not be the only factor influencing deposition in that shielding by trees, hills or buildings is a likely factor. The chloride deposition appears to be related to shielding objects and parallels corrosion rates trend. Figure 31 provides the conversion of ppm solution to $mg \cdot m^{-2}$. Figure 32 is a plot of depositions of chloride and sulfate versus distance from the shoreline. The sulfate deposition starts low and trends slightly upward from the shoreline presumably due to increasing SO_2 from fuel combustion sources (cars, trucks, trains,

vessels in port, generators, etc.). There is a sharp downward trend for chloride from the shoreline. Comparing Figure 30 with Figure 32, the high conductivity values are primarily due to chloride deposition. Also shown on Figure 32 is the data from the KSC/SeaTech chloride profile (presented in next section) that parallels the corrosion product extract profile by a factor of about five lower – a reasonable qualitative expectation based upon incomplete sheltering of the plate backs by the specimen's 30° inclination.

Table 9: Solution conductivity of corrosion products on 2nd set of plates (C & D).

Sample	Conductivity	**Sample**	Conductivity
Front	µS/cm	**Back**	µS/cm
1C	215	1C	417
2C	74	2C	235
3C	30	3C	95
4C	18	4C	88
5C	12	5C	12
6C	8	6C	11
7C	15	7C	15
8D	9	8D	13
9D	9	9D	12
10D	17	10D	33
11D	16	11D	19
12C	14	12C	17
13C	11	13C	17
14D	12	14D	19
15C	10	15C	16
16C	26	16C	19
17D	15	17D	12
18D	13	18D	17
19D	8	19D	10
20D	12	20D	12
21C	9	21C	9
22C	11	22C	12
23C	9	23C	14
24C	8	24C	8
25C	21	25C	17
26C	10	26C	14
27C	13	27C	16
28C	10	28C	11
29C	8	29C	13
30C	8	30C	10

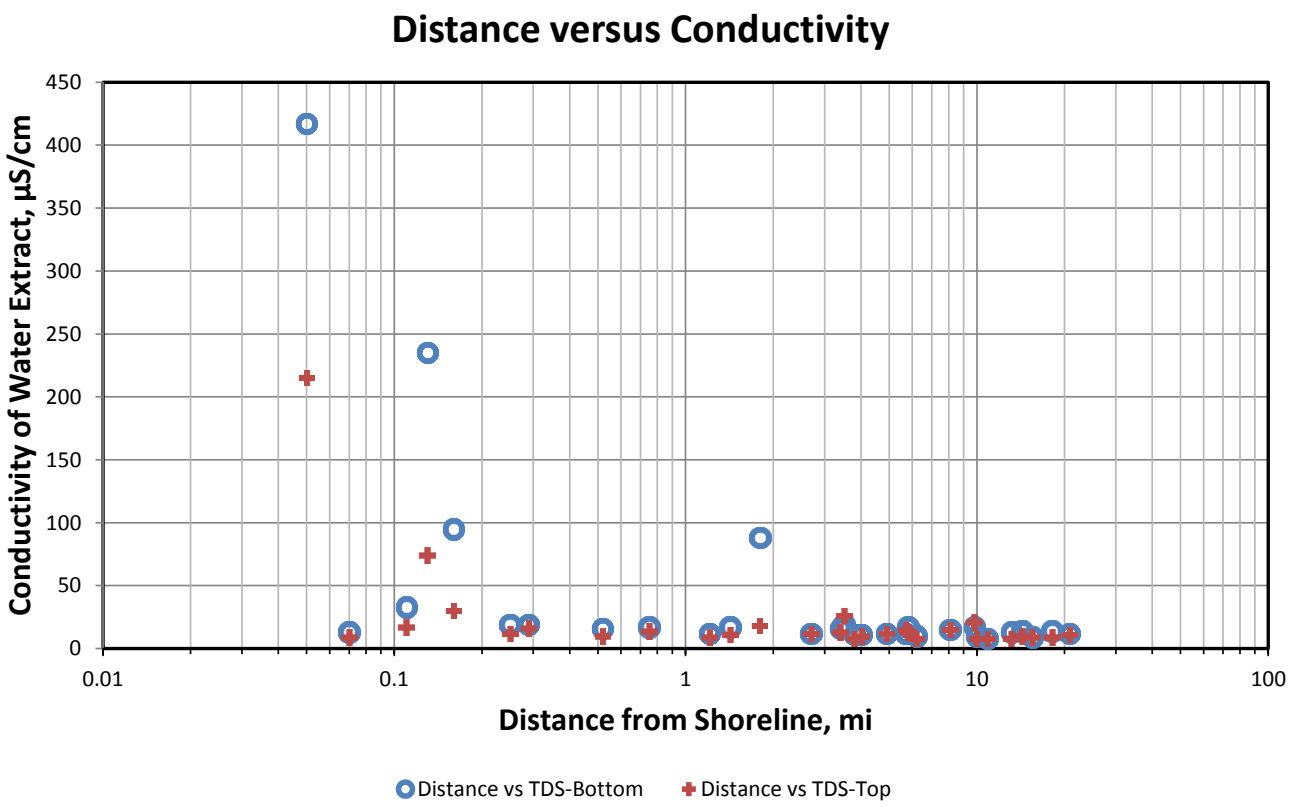

Figure 30: Distance from shoreline versus conductivity from top and bottom sides corrosion products.

Convert PPM result (A) to deposition rate (per month).

Time in (B) years.

Area of specimen is 77cm^2 area.

Sample volume is 20 ml (solution).

PPM = 1 µg/g.

Microgram - milligram: 1000 µg = 1 mg.

For dilute water solutions: 1 ml ~ 1 g.

$$\text{A ppm} = A\frac{\mu g}{ml} = A\frac{\mu g}{ml}\frac{mg}{1000\ \mu g} = A\frac{mg}{1000\ ml} = A\frac{mg}{1000\ ml}\ x\ 20\ ml = \frac{20\ mg}{1000}A$$

Convert mg to mg/m^2 :

$$A\frac{20\ mg}{1000}\ x\ \frac{1}{77\ cm^2}\ x\ \frac{100\ cm}{m}\ x\ \frac{100\ cm}{m} = A\frac{200\ mg}{77\ m^2}$$

Converting to rate for B years:

$$\frac{A}{B}\ \frac{200\ mg}{77\ m^{2\cdot}y}$$ = Deposition rate per year.

$$\frac{A}{B}\ \frac{200\ mg}{12\cdot 77\ m^{2\cdot}mont\ h} = 2.38\frac{A}{B}\ \frac{mg}{m^{2\cdot}mont\ h}$$ = Deposition rate per month.

Figure 31: Conversion of PPM solution concentration to deposition rate.

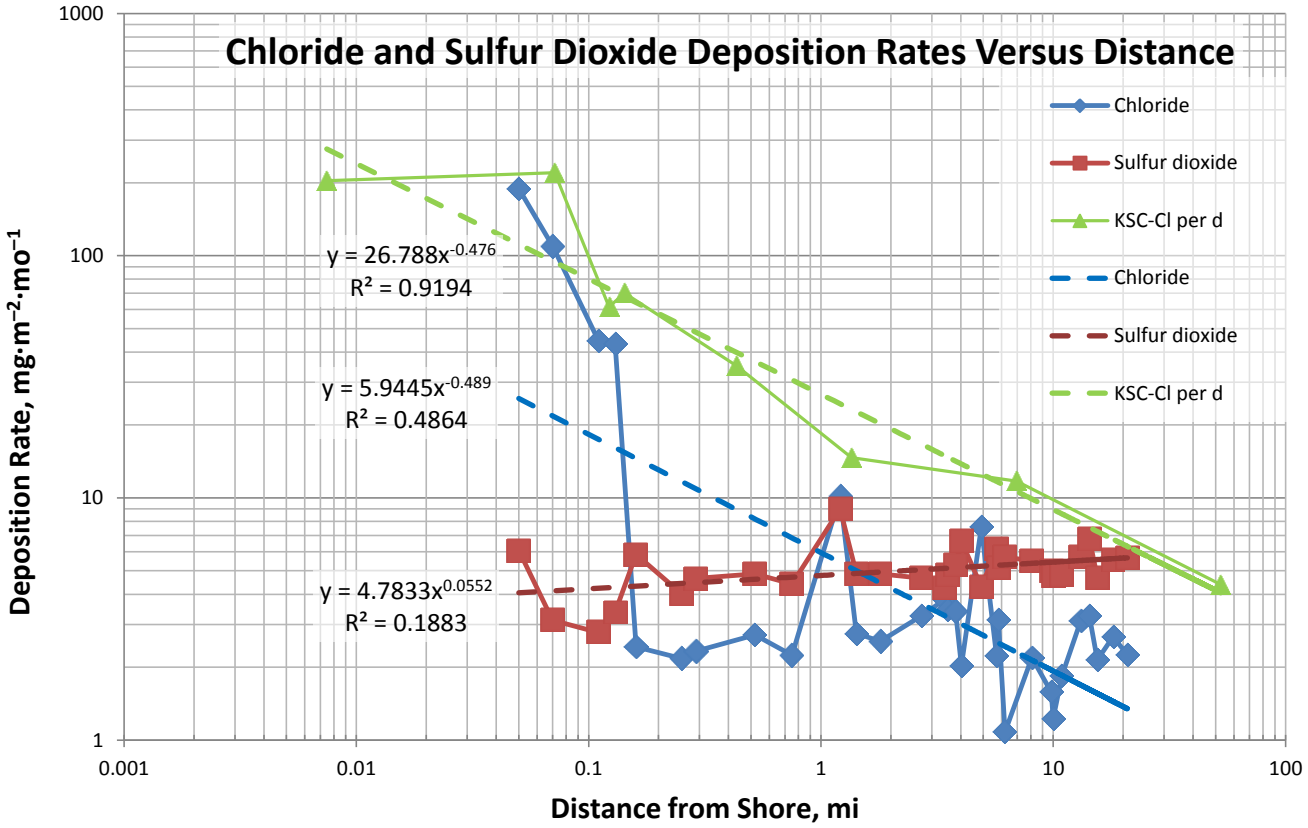

Figure 32: Deposition profiles of chloride and sulfate extracts and wet candle study.

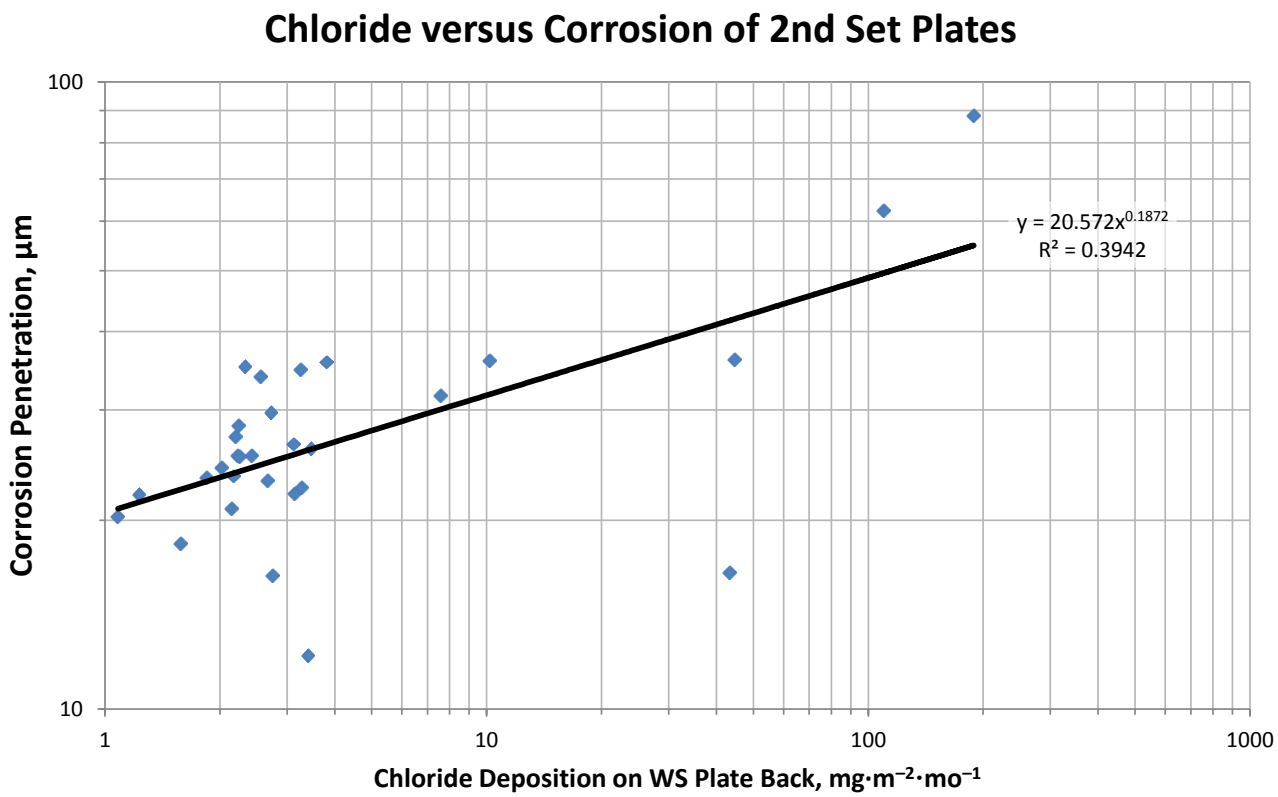

Figure 33: Chloride in corrosion product deposition versus penetration.

3.7 Atmospheric Chloride and Sulfur Dioxide.

An atmospheric chloride profile from the east Florida seacoast was studied in detail by NASA-KCS including parallel corrosion measurements on AISI 1008 and AISI 4130 steels [37]. Chloride deposition measurements were also made at several locations on the FAU Dania campus over a number of years. These data are plotted in Figure 34 yielding a regression analysis shown on the figure. The regression result was used to plot values shown in Table 10. The table indicates more than 30 miles is necessary for the calculated chloride deposition rates to decrease to the 5 $mg \cdot m^{-2} \cdot d^{-1}$ target maximum rate for acceptable corrosion rates for weathering steel. Referring to Figure 32, 0.2 miles may be adequate in specific situations and 4 miles may be a moderately conservative estimate for use of weathering steel based upon the corrosion rates determined in this project.

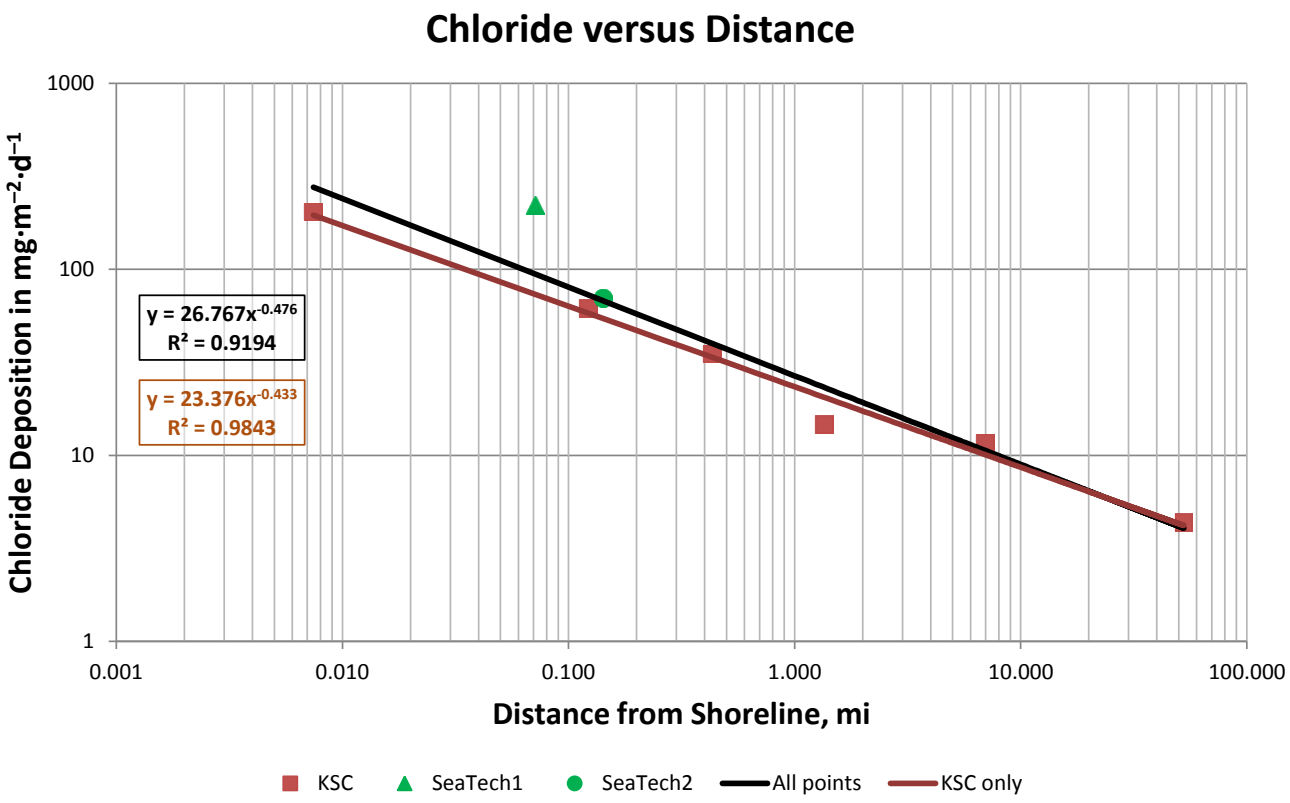

Figure 34: Chloride deposition versus distance from shore line.

Sulfur dioxide deposition data monitored continuously at AQS # L086-0019 PENNSUCO (DOT monitoring site in Miami) and published on the Florida Department of Environmental Protection website is given in Figure 35. The data are reported as 24 h max units pertaining to the highest observed values in a day for the year are indicated. The concentration units are ppbv or parts per billion by volume of air. The highest value per year was obtained plotted for the years indicated. In 2003, low-sulfur fuels were mandated among other regulations. A deep drop in SO_2 concentration is observed after 2003. The concentration drops to less than 1 ppbv that corresponds to less than 2.2 $mg \cdot m^{-2} \cdot d^{-1}$. Generally, SO_2 will not be a consideration except adjacent to specific generators such as ports with ocean-going vessels, oil and coal combustion equipment (power generation, etc.).

Table 10: Predicted regression-fit chloride depositions versus distance to shoreline.

Distance from Shoreline, miles	Chloride Deposition, $mg \cdot m^{-2} \cdot d^{-1}$
0.5	38.7
1	27.8
2	20.0
4	14.4
8	10.3
16	7.4
32	5.3
64	3.8

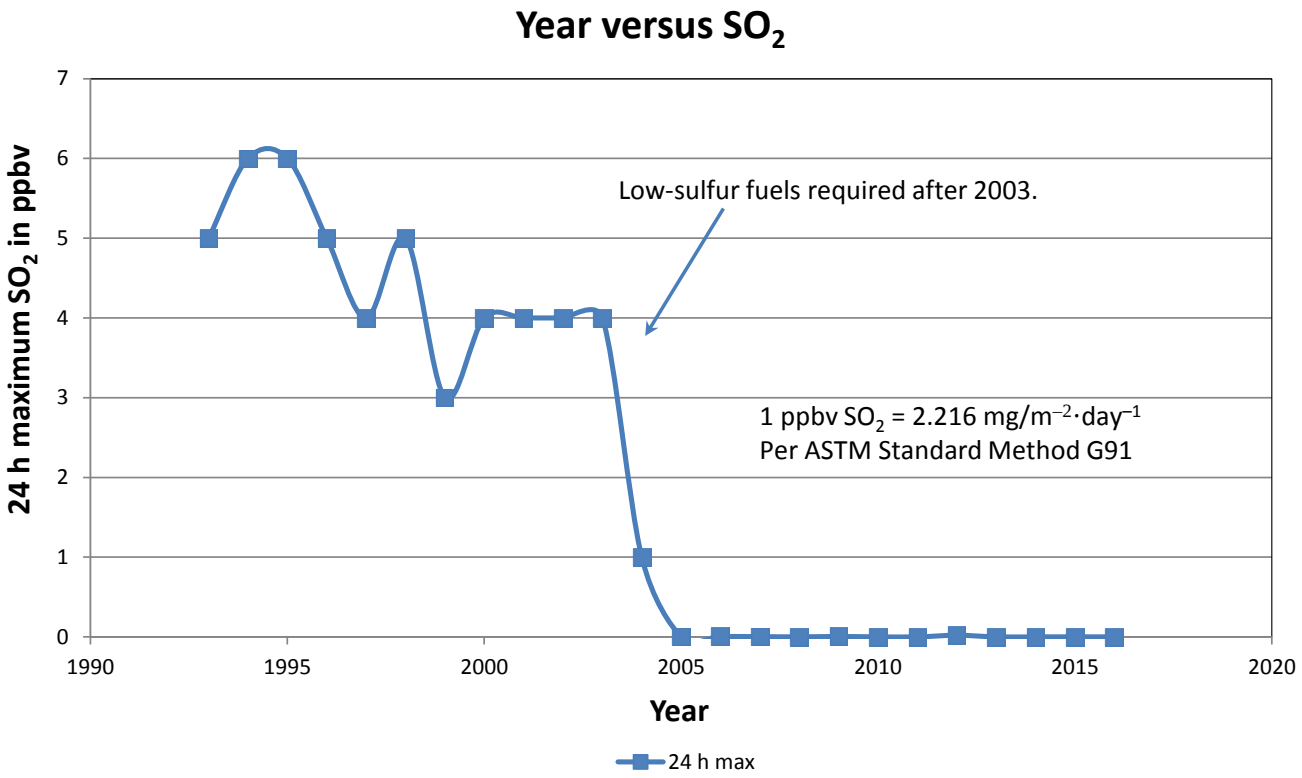

Figure 35: Plot of multiyear data from DOT Miami. FL data.

4 DISCUSSION

The primary focus of the project was on establishing where WS will perform adequately. Current guidelines for determining advisability for using uncoated WS in Florida were provided in the Executive Summary. These current guidelines served as an excellent starting point for this project and are addressed with regard to the findings obtained. The purpose of the project was to obtain data in support of Florida Department of Transportation guidelines on the appropriate use of weathering steel for bridges and other structures. The objectives were provided in the Executive Summary. The objectives were addressed with regard to the findings obtained. Emphasis was given to simplifying and improving site characterization.

4.1 Findings

TOW data was collected via data loggers and weather stations. The range was approximately, 25-70% TOW. There was no apparent relationship of TOW to corrosion rates of plate specimens. For example, the specimen experiencing the highest corrosion rate was subjected to 40% TOW, which is significantly below the 60% TOW expected for high corrosion rates. TOW measurements may be problematic when correlated to surfaces laden with sea salt deposits according to reference [26] who noted that such surfaces can remain wet at 20%RH.

Few weathering steel bridge structures were located in south FL. Corrosion products from the sheltered areas of the superstructure were most desirable for study but were rare. Visual inspections showed well-developed dark oxide associated with protective WS patina. These visual inspections were consistent with the additional findings presented below.

Plate and wire corrosion specimens were evaluated after exposures. There was no strong significant correlation with TOW or SO_2. A strong correlation was observed for chloride where sites were boldly exposed (no barriers) to winds from the shoreline. Shielding of sites by foliage, structures, and physical topography decreased the expected effect of proximity to the shoreline.

Corrosion rates of plate specimens were generally very low. Two sites with direct exposure to shoreline winds and within 0.2 mile of the shoreline exhibited high corrosion rates. Conversely, three sites within 0.3 mile of the shoreline with 30 feet high foliage or ground shielding exhibited 30-50% lower rates. The effect of chloride deposition on corrosion rate diminished rapidly with distance and shielding.

XRD results were obtained from corrosion specimens. Akaganeite was observed on many specimens but no strong correlation to chloride deposition or TOW was found. For those specimens whose corrosion products contained akaganeite, the percentage decreased with distance from the shoreline. Moreover, many specimens did not contain akaganeite.

Conductivity measurements (TDS) of the corrosion product water extracts showed four sites with relatively high or higher values than the other 26 sites. The analyses of the water extracts for chloride and sulfate indicated that most of the conductivity was due to chloride and decreased with distance from the shoreline. The sulfate was low and increased slowly with distance from the shoreline, suggesting the

origin of the sulfate was land-based, perhaps SO_2 from fuel combustion. This finding suggests that chloride measurements can be performed by simple conductivity measurements.

Deposition of SO_2 appears to have been all but eliminated in south Florida, except where high sulfur fuels are combusted, such as ocean ports, or possibly where special permits have been granted for sulfur fuel combustion or waste combustion. This circumstance may require reconsideration of the atmospheric corrosion of WS and other metals. Nearly all long-term corrosion studies were initiated when, historically, atmospheric levels of SO_2 were high. It is well known that initial exposure to SO_2 has a significant effect on the initial rate of corrosion. New corrosion studies may be required to better understand the effects of these new, very low SO_2 levels. However, it is likely that the benefits of low atmospheric SO_2 levels are greatly beneficial.

Chloride deposition profiles derived from data obtained at SeaTech and from a NASA-Kennedy Space Center study show deposition rates of approximately 13 $mg \cdot m^{-2} \cdot d^{-1}$ at 4 miles from the shoreline decreasing to approximately 5 $mg \cdot m^{-2} \cdot d^{-1}$ at 30 mi from the shoreline. These deposition/shoreline-distance values indicate that a large border from the shoreline would be excluded from use of WS. However, other considerations are possible. The Japanese guidance appears very conservative compared to UK and USA (6, 300, and 50 $mg \cdot m^{-2} \cdot d^{-1}$, respectively [32]), while 12 $mg \cdot m^{-2} \cdot d^{-1}$ is an alternative proposed guidance for Korean structures in reference [38]. Low corrosion rates were consistently observed at shoreline distances of 2 miles or more for WS plate specimens in this project.

4.2 Impact on Guidelines

The findings listed above indicate that there are no significant impediments to implementing weathering steel structures in Florida. The current guidelines serving as a starting point for this project might be reconsidered as follows:

- *Anticipation of a slightly aggressive superstructure corrosive environment* – WS should not be placed adjacent to a location, such as a chemical plant, generating a corrosive environment.
- *Yearly average Time of Wetness (TOW), as determined by ASTM Standard Method G84 not to exceed 60%* - The TOW parameter is not sufficiently understood to provide useful guidance [26]. The effect of a thermal mass approximating a WS superstructure seems critical to useful TOW measurements. TOW greater than 60% appeared to have no important impact on corrosion of WS in this project.
- *Uncoated weathering steel shall not be used within 4.0 miles of the coast unless it is determined through testing that the proposed site conditions do not exceed the following thresholds: The maximum airborne salt deposition rate, as determined by ASTM Standard Method G140, shall be less than 5 $mg \cdot m^{-2} \cdot d^{-1}$ (30-day average); The maximum average concentration for SO_2, as determined by ASTM Standard Method G91, shall not exceed 60 $mg \cdot m^{-2} \cdot d^{-1}$ (30-day average).* - The maximum airborne salt deposition rate could be changed to 14 $mg \cdot m^{-2} \cdot d^{-1}$ (30-day average) that corresponds to the predicted rate at 4 miles. No significant WS corrosion was observed in this project beyond 2 miles from the coast. The SO_2 deposition rate can be retained, but it may only be important in marine ports or permitted SO_2 generators.
- *Do not use uncoated weathering steel over low water crossings (12 feet or less vertical clearance over normal high water / mean high water)* – No experimental guidance was provided in this project regarding vertical clearance. The guideline seems reasonable and prudent. Although where steady low-level winds are prevalent, lower clearance may be proposed if it is determined through testing that the proposed site conditions merit. Testing will include direct measurement specimens sheltered and installed at the alternate clearance level and a compact, e.g.,USB fob, temperature/humidity recorder sheltered and installed two feet below specimens. The percentage TOW calculated from the recorder must be less than

60% over the period of at least one year. Adjustment downward of the threshold (80% RH) for the calculation should be considered.

4.3 Simplified Alternative Approach

In consideration of the objective to simplifying and improving site characterization, the following approach is proposed:

- Install direct measurement corrosion loss plates at the proposed bridge site.
- Collect specimens monthly at 1-4 months. If time is an issue, 3-week intervals are possible.
- Continue collections at 12 months, if time permits.
- Analyze specimens for weight loss and TDS/chloride. Soak in distilled water for 10 min in known water volume, determine TDS and, if desired, perform Cl^- analysis.
- Plot the weight losses versus results for known well-performing WS, e.g., Figure 36.
- Consider TDS/chloride data relative to distance from the shoreline.

The rationale and details are provided with Figure 36. Figure 36 is the data shown in Figure 24 plotted with axes having wider ranges. Additional data has been added, particularly, WS (A-588 steel) and CS (A-36 steel) for a study performed in Hawaii approximately 1 km from Pearl Harbor, HA. The study was guided by AISI, the steel industry representatives and the engineering research center, ATLSS (Lehigh University) [6]. Points and regression line (black) representing Albrecht's corrosion limit values for 35 μm, one-year thickness-loss and values to 100 years at 5 μm/y thickness-loss are included for reference. The data from the Hawaii study were generated at 1, 2, 3, 4 and 12 month time periods. Regression lines for HA-588 and HA-36 are consistent with good (green) and poor (red) performance, respectively. The regression lines for WS Kure and HA-588 were extrapolated to 100 years for comparison with the Albrecht model. This study demonstrated that short-term weight loss data can be quite useful in characterizing corrosion behavior at specific sites. Data points for the plates tested in this project are also included for comparisons. Except for SeaTech01 and SeaTech02 stations, low corrosion values were observed. To help bracket the range of possible corrosion performances, data for Toledo, Spain was added using ISO information for CS. The data collected in this project falls within expected performance ranges. The penetration values obtained at the Florida sites were low, but were not abnormally low compared to very low values obtained in Toledo, Spain. Only sites 01 and 02 demonstrated corrosion penetrations that should be considered too high for use of WS.

The key to being able to perform this study was the availability of thin-gauge WS that is now marketed as a roofing material. The thin gauge enables small weight losses to be measured on more sensitive balances than thick gauge plates – There is an adequate surface area-to-weight ratio. In this study, the typical plate specimen weight was less than 100 g with a total surface area of approximately 150 cm^2. The balance sensitivity required is 0.0001 g and such balances are now reasonably priced.

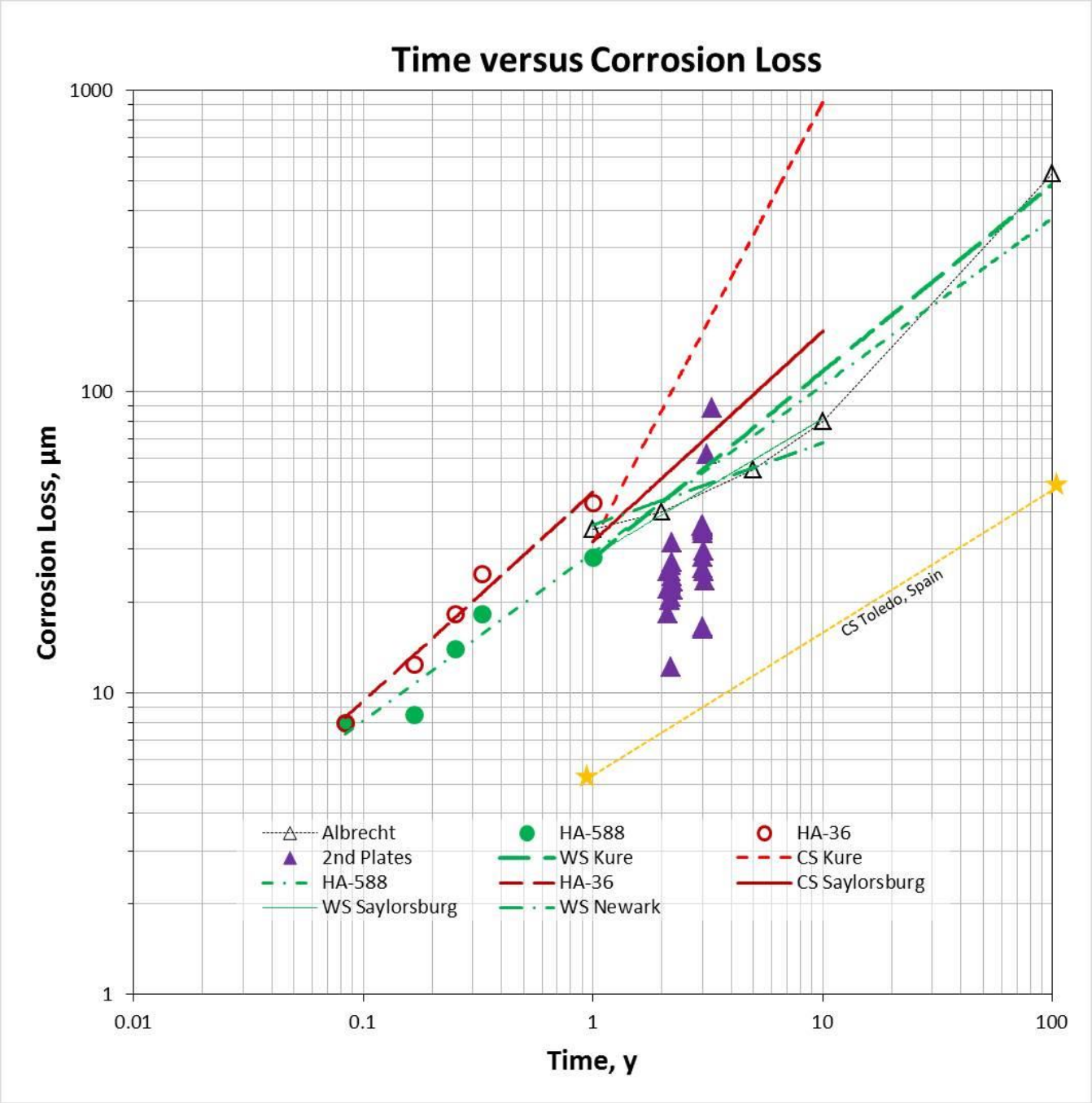

Figure 36: Plot of A36 and A588 steel plate corrosion losses in HA study with Townsend data. For comparison, low corrosion loss has been documented for Toledo, Spain.

The advantages of this alternative approach are:

- A direct measurement corrosion plate is the ultimate sensor because it does not neglect any parameter. It is likely the smallest sensor capable of addressing all parameters. It could be attached in confined and dead spaces of the bridge superstructure.
- Much simpler than on-site TOW sensors, wet candle and SO_2 tests.

- No environmental concerns of chemical contamination.
- Chloride and sulfur compounds retained on the surface can be analyzed from collected specimens. Soluble materials washed away by rain, fog or condensation no longer contribute to corrosion.
- Low cost materials and labor. Simple installation. No data logger required.
- Adaptable to many geometries for shielded, sheltered and other microenvironmental determinations (exterior flange & web, interior flange & web – magnetic clamp attachment possible for thermal contact with superstructure).
- Adaptable to other WS alloys.

5 CONCLUSIONS

This investigation presents the results of a study on material selection for the environmental suitability of weathering steel structures Florida. Based on the results and discussion presented in Chapters 3 and 4, the following conclusions are reached.

1. There was no apparent relationship of %TOW to corrosion rates of plate corrosion specimens. The %TOW measurements may be problematic when correlated to surfaces laden with sea salt deposits because such surfaces can remain wet at 20%RH.

2. Few weathering steel bridge structures were located in south FL. Visual inspections showed well-developed dark oxide associated with protective WS patina.

3. For plate corrosion specimens, there was no significant correlation with %TOW or SO2 . A strong correlation was observed for chloride where sites up to 2 mi from the shoreline were boldly exposed (no barriers).

4. Corrosion rates at sites more than 2 mi from the shoreline were generally very low.

5. The effect of chloride on corrosion rate diminishes rapidly with distance and shielding.

6. X-ray diffraction results determined that a problematic corrosion product, akaganeite, was present on many plate specimens. There was no strong correlation of akaganeite presence to chloride deposition or %TOW. Generally, the percentage akaganeite in the corrosion products decreased with distance from the shoreline.

7. Conductivity measurements (TDS) of the corrosion product water extracts showed four sites with relatively high or higher values that the other 26 sites. Most (>90%) of the conductivity was due to chloride and decreased with distance from the shoreline. The concentration of sulfate gradually increased from the shoreline.

8. Deposition of SO2 in Florida has been nearly eliminated except in ocean ports and perhaps at permitted sites. The reductions of sulfur in fuels are probably responsible for this change. It is likely that corrosion rates have decreased as a result.

9. The chloride deposition profile from the shoreline indicates the deposition rate is 13 $mg \cdot m^{-2} \cdot d^{-1}$ at 4 miles from the shoreline decreasing to approximately 5 $mg \cdot m^{-2} \cdot d^{-1}$ at 30 mi from the shoreline. These rates are higher than the current guideline rates that were based upon a most conservative Japanese standard. Low corrosion rates were consistently observed at shoreline distances of 2 miles or more for WS plate specimens in this project that suggests higher proposed rates should be strongly considered.

10. An alternative approach was proposed for rapid and simplified characterization of proposed WS construction sites based upon short-term exposures of direct measurement specimens. The approach provides direct corrosion data and analysis, simplicity, quickness, cost-effectiveness, adaptable to confined areas, and includes all environmental factors (whether identified or not) should be given strong consideration.

BIBLIOGRAPHY

[1] W. K. Boyd and F. W. Fink, ""Corrosion of Metals in the Atmosphere"," Metals and Ceramics Information Center, Battelles Columbus Laboratories, Columbus, OH, 1974.

[2] P. Albrecht and T. T. Hall Jr., "Atmospheric Corrosion Resistance of Structural Steels," *J. Mater. Civ. Eng.*, vol. 15, no. 1, pp. 2-24, 2003.

[3] T. Murata, "Weathering Steel," in *Uhlig's Corrosion Handbook*, 3rd ed., R. W. Revie, Ed., New York, J. Wiley & Sons, 2000, pp. 621-631.

[4] C. Leygraf and T. Graedel, "Atmospheric Corrosion, Electrochemical Society Series", New York: J. Wiley & Sons, 2000.

[5] R. Granata, J. Wilson and J. Fisher, "Assessing Corrosion on Steel Structures Using the Corrosion Coulometer," *ASCE Journal of Infrastructure Systems*, vol. 2, no. 3, pp. 139-44, 1996.

[6] R. Granata, J. Fisher and J. C. Wilson, "Update on Applications of Corrosion Coulometers, Paper 97307," in *CORROSION'97, NACE International*, Houston, 1997.

[7] ASTM Standard G1, 2003, Standard Practice for Preparing, Cleaning, and Evaluating Corrosion Test Specimens, West Conshohocken, PA: ASTM International, 2003.

[8] ASTM Standard G33, 1999, Standard Practice for Recording Data from Atmospheric Corrosion Tests of Metallic-Coated Steel Specimens, West Conshohocken, PA: ASTM International, 1999.

[9] ASTM Standard G50, 1976 (2003), Standard Practice for Conducting Atmospheric Corrosion Testing of Metals, West Conshohocken, PA: ASTM International, 2006.

[10] ASTM Standard G84, 1999 (2003e1), Standard Practice for Measurement of Time-of-Wetness on Surfaces Exposed to Wetting Conditions as in Atmospheric Corrosion Testing, West Conshohocken, PA: ASTM International, 1999.

[11] ASTM Standard G91, 1997, Standard Practice for Monitoring Atmospheric SO2 Using the Sulfation Plate Technique, West Conshohocken, PA: ASTM International, 1997.

[12] ASTM Standard G92, 2003, Standard Practice for Characterization of Atmospheric Test Sites, West Conshohocken, PA: ASTM International, 2003.

[13] ASTM Standard G116, 1999, Standard Practice for Conducting Wire-on-Bolt Test for Atmospheric

Galvanic Corrosion, West Conshohocken, PA: ASTM International, 1999.

[14] 2. ASTM Standard G140, Standard Test Method for Determining Atmospheric Chloride Deposition Rate by Wet Candle Method, West Conshohocken, PA: ASTM International, 2002.

[15] ISO, ISO 8565, Metals and alloys -- Atmospheric corrosion testing -- General requirements, Geneva, Switzerland: International Organization for Standardization, 2011.

[16] ISO, ISO 9223, Corrosion of metals and alloys — Corrosivity of atmospheres — Classification, determination and estimation, Geneva, Switzerland: International Organization For Standardization, 2012.

[17] ISO, ISO 9224, Corrosion of metals and alloys -- Corrosivity of atmospheres -- Guiding values for the corrosivity categories, Geneva, Switzerland: International Organization for Standardization, 2012.

[18] ISO, ISO 9225, Corrosion of metals and alloys -- Corrosivity of atmospheres -- Measurement of environmental parameters affecting corrosivity of atmospheres, Geneva, Switzerland: International Organization for Standardization, 2012.

[19] ISO, ISO 9226, Corrosion of metals and alloys -- Corrosivity of atmospheres -- Determination of corrosion rate of standard specimens for the evaluation of corrosivity, Geneva, Switzerland: International Organization for Standardization, 2012.

[20] H. E. Townsend and J. C. Zoccola, "Eight-Year Atmospheric Corrosion Performance or Weathering Steel in Industrial, Rural, and Marine Environment," in *Atmospheric Corrosion of Metals*, *STP 767*, S. D. Dean, Jr. and E. C. Rhea, Eds., West Conshohocken, PA, ASTM, 1982, pp. 45-59.

[21] S. D. Dean, Jr., "Atmospheric," in *Corrosion Tests and Standards: Application and Interpretation - Second Edition*, Philadelphia, PA, ASTM International, 2005, pp. 159-69.

[22] P. Albrecht and A. H. Naeemi, "Performance of Weathering Steel in Bridges, NCHRP Report 102," Transportation Research Board - National Research Council, Washington, D.C., 1984.

[23] M. Morcillo, B. Chico, I. Díaz and D. d. l. F. Cano, "Atmospheric corrosion data of weathering Steels. A review," *Corrosion Science*, vol. 77, pp. 6-24, 2013.

[24] P. Albrecht, S. K. Coburn, F. M. Wattar, G. L. Tinklenberg and W. P. Gallagher, "Guidelines for the use of weathering steel in bridges, NCHRP Report 314," Transportation Research Board - National Research Council, Washington, D.C., 1989.

[25] R. Kogler, "Steel Bridge Design Handbook: Corrosion Protection of Steel Bridges," Federal Highway Administration, Washington, D.C., 2015.

[26] E. Schindelholz, R. G. Kelly, I. S. Cole, W. D. Ganther and T. H. Muster, "Comparability and accuracy of time of wetness sensing methods relevant for atmospheric corrosion," *Corrosion Science,* vol. 67, pp. 233-241, 2013.

[27] Decagon Devices, Inc., Em50 Series Data Collection System, Pullman, WA: Decagon Devices, Inc., 2010-2016.

[28] Decagon Devices, Inc., Dielectric Leaf Wetness Sensor, Pullman, WA: Decagon Devices, Inc., 2006-2016.

[29] R. D. Granata, W. D. Michalerya, R. H. Wildt, H. Leidheiser, Jr. and B. W. O'Malley, Jr., "Quantitative Evaluation of Steel Corrosion in Microenvironments using the Corrosion Coulometer," in *Review of Progress in Quantitative Nondestructive Evaluation, Vol. 11, D.O. Thompson and D.E. Chimenti, Eds.*, New York, Plenum Press, 1992, pp. 1183-90.

[30] D. Cook, S. Oh, R. Balasubramanian and M. Yamashita, "The role of goethite in the formation of the protective corrosion layer on steels," *Hyperfine Interactions,* vol. 122, pp. 59-70, 1999.

[31] Cook, D.;, "Corrosion evaluation of weathering steel bridges along Interstate I-70, Maryland," Advanced Metal Coatings Incorporated, Virginia Beach, VA, 2015.

[32] I. Díaz, H. Cano, B. Chico, D. de la Fuente and M. Morcillo, "Some Clarifications Regarding Literature on Atmospheric Corrosion of Weathering Steels," *International Journal of Corrosion,* vol. 2012, no. Article ID 812192, 2012.

[33] 1. (. ASTM Standard G101, Standard Guide for Estimating the Atmospheric Corrosion Resistance of Low-Alloy Steels, West Conshohocken, PA: ASTM International, 2004.

[34] Campbell Scientific, Inc., Weather station siting and installation tools, Logan, UT: Campbell Scientific, Inc., 1997.

[35] S. T. Shill, "Chloride penetration into concrete structures exposed to the marine atmosphere," Florida Atlantic University, Boca Raton, Florida, 2014.

[36] R. Downs and M. Hall-Wallace, "The American Mineralogist Crystal Structure Database," *American Mineralogist,* vol. 88, pp. 247-250, 2003.

[37] NASA, Kennedy Space Center, "Report MTB 099-74, Relative Corrosivity of Atmospheres at Various Distances from the Seacoast," NASA, Kennedy Space Center, FL, 1980.

[38] S. S. Kim, "Appropriate environmental sphere of application for unpainted weathering steel," *Journal of Industrial and Engineering Chemistry,* vol. 9, no. 2, pp. 212-218, 2003.

[39] R. D. Granata and W. H. Hartt, "Integrity of Infrastructure Materials and Structures," U.S. Department of Transportation, Federal Highway Administration, McLean, VA, 2009.

[40] A. A. Bragard and H. E. Bonnarens, "Prediction at Long Terms of Atmospheric Corrosion of Structural Steels from Short-Term Experimental Data," in *Atmospheric Corrosion of Metals, STP 767*, West Conshohocken, PA, ASTM, 1982, pp. 339-358.

APPENDIX A: Site Images

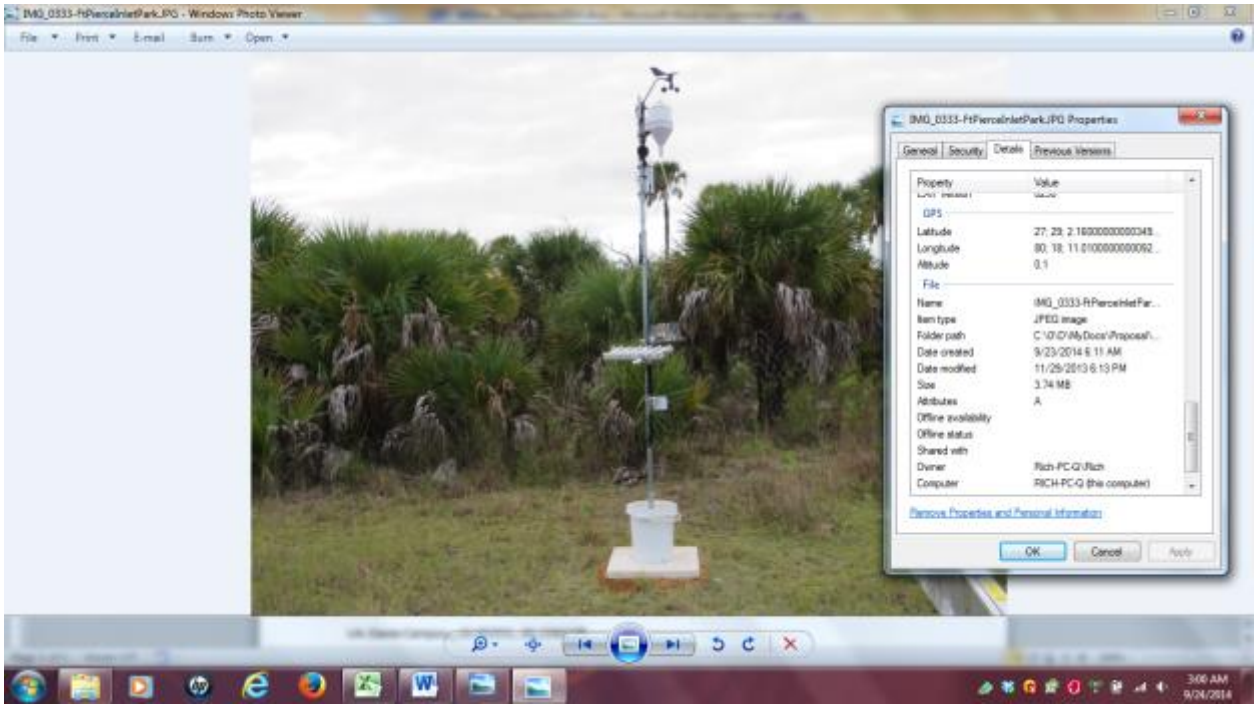

Figure A-1: Monitoring site 15 at Fort Pierce State Park, Lat./Long.: 27.485926, -80.303174.

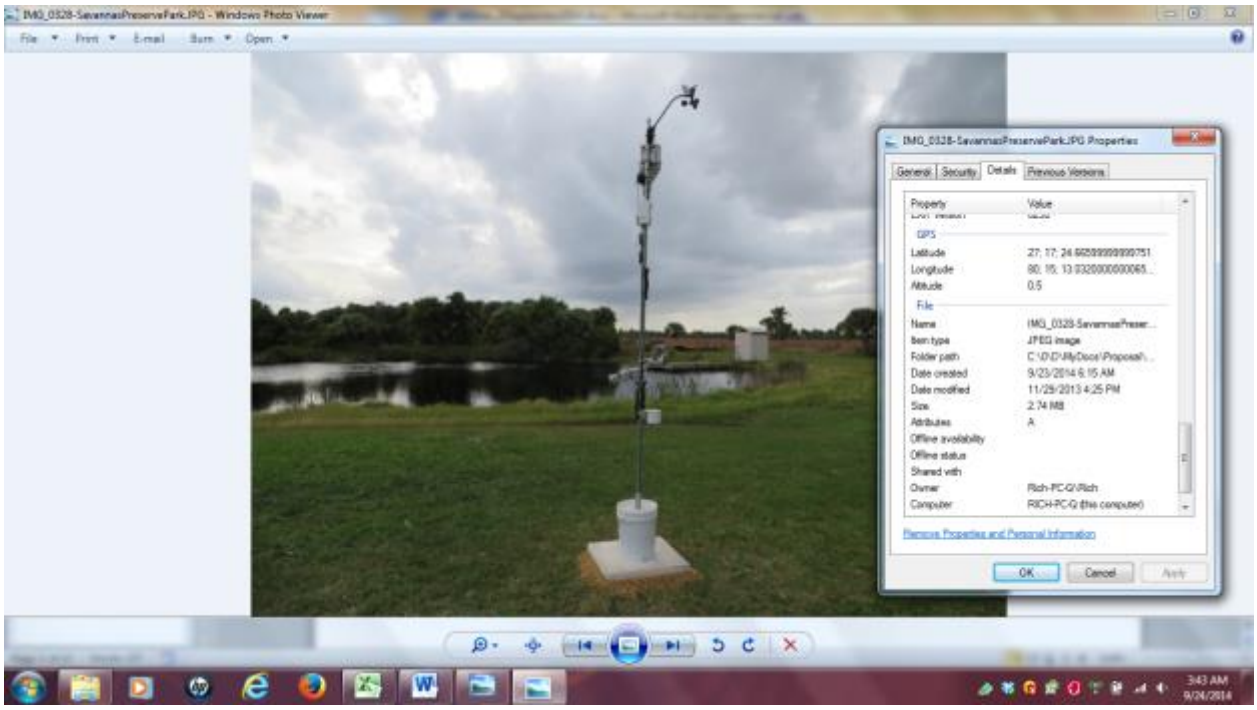

Figure A-2: Monitoring site 14 at Savannas Preserve State Park, Lat./Long.: 27.290184,-80.253711

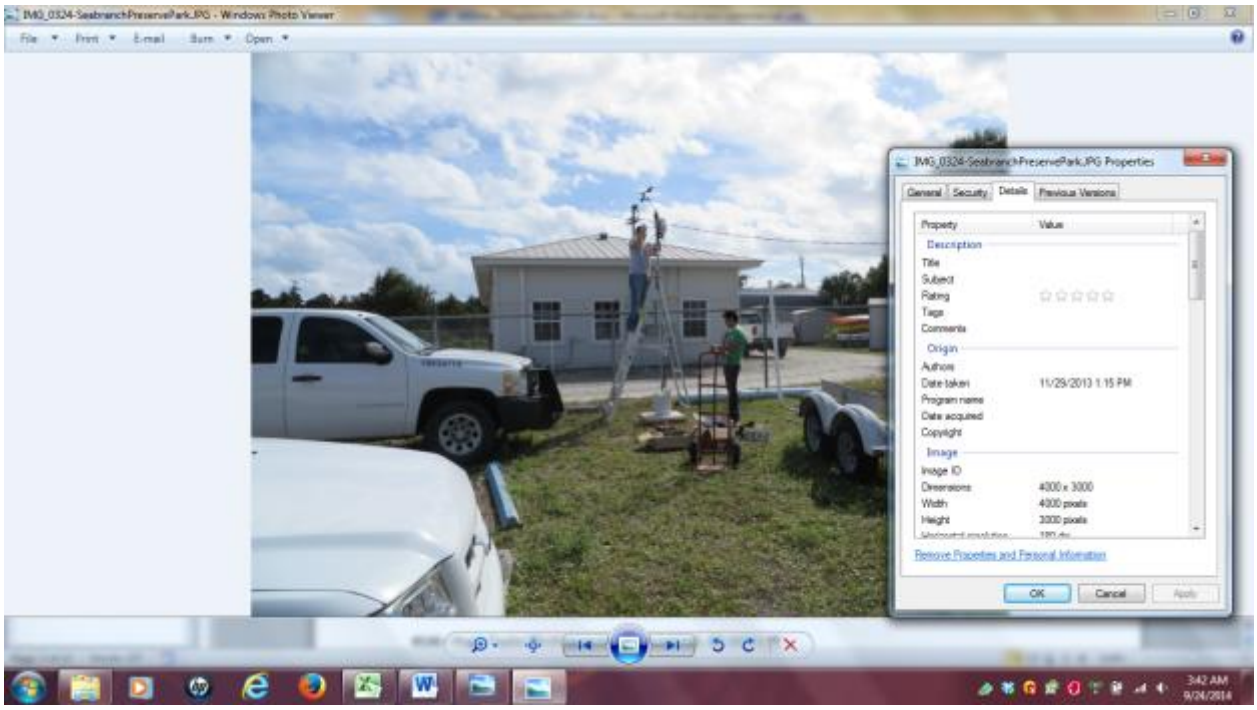

Figure A-3: Monitoring site 13 at Seabranch Preserve State Park, Lat./Long.: 27.133167,-80.169225

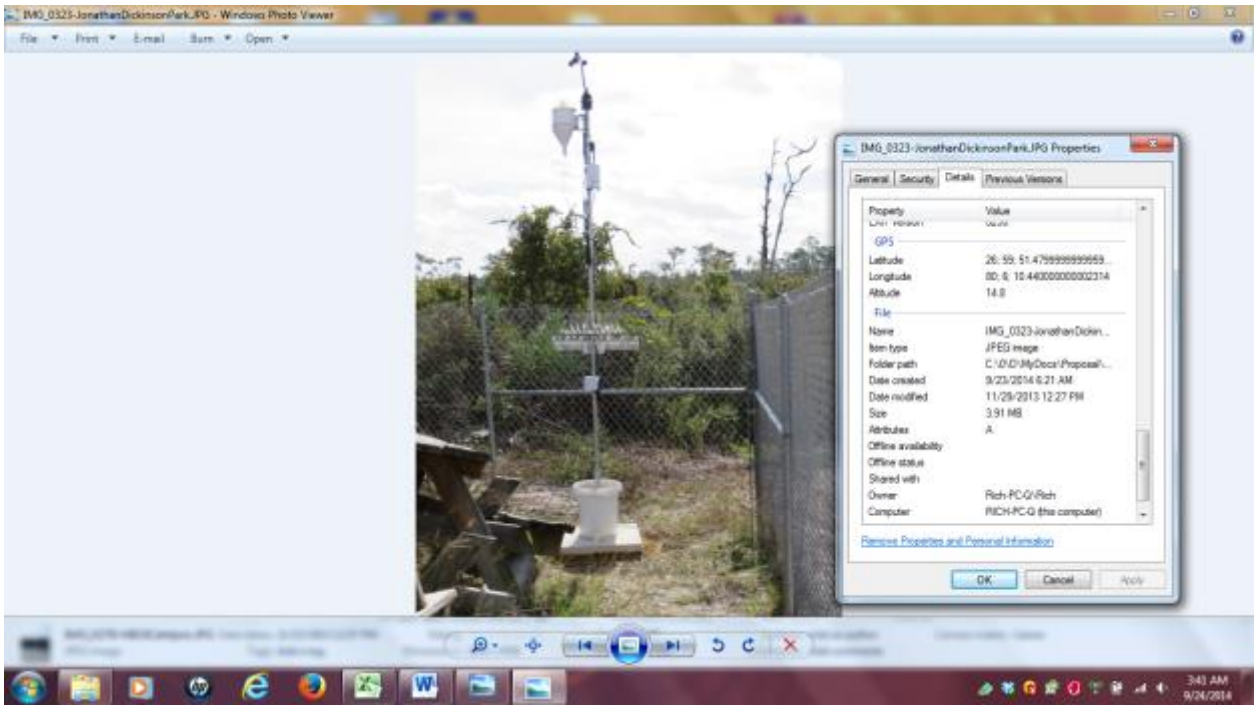

Figure A-4: Monitoring site 12 at Jonathan Dickinson State Park, Lat./Long.: 27.025088,-80.109068

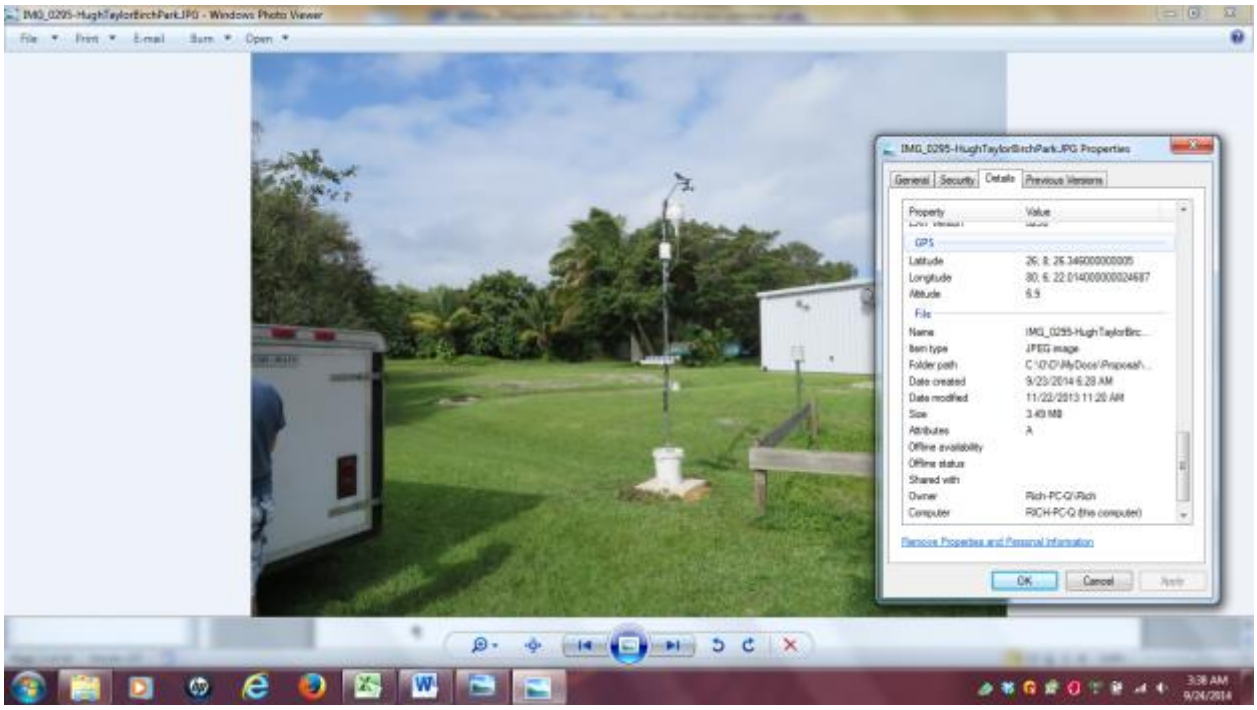

Figure A-5: Monitoring site 08 at Hugh Taylor Birch State Park, Lat./Long.: 26.138796,-80.103511

Figure A-6: Monitoring site 10 at John U. Lloyd Beach State Park, Lat./Long.: 26.06852,-80.11250

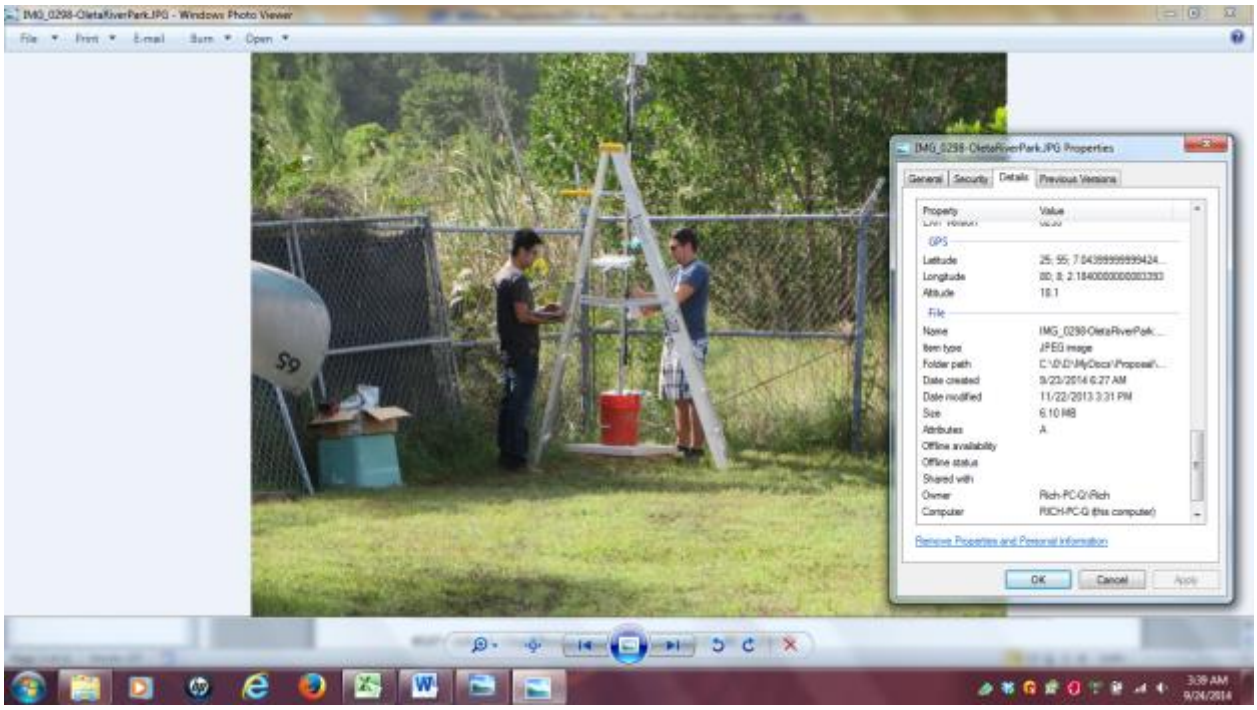

Figure A-7: Monitoring site 09 at Oleta River State Park, Lat./Long.: 25.920996,-80.140096.

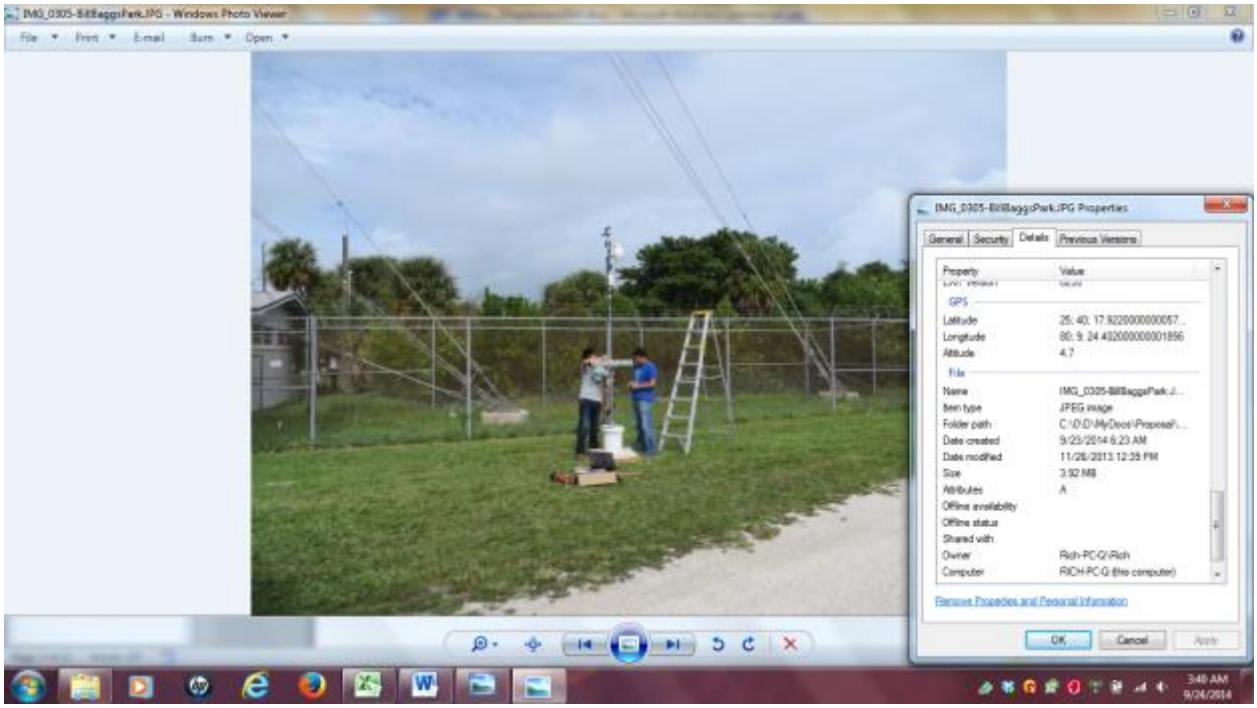

Figure A-8: Monitoring site 11 at Bill Baggs Cape FL State Park, Lat./Long.: 25.674833,-80.158099

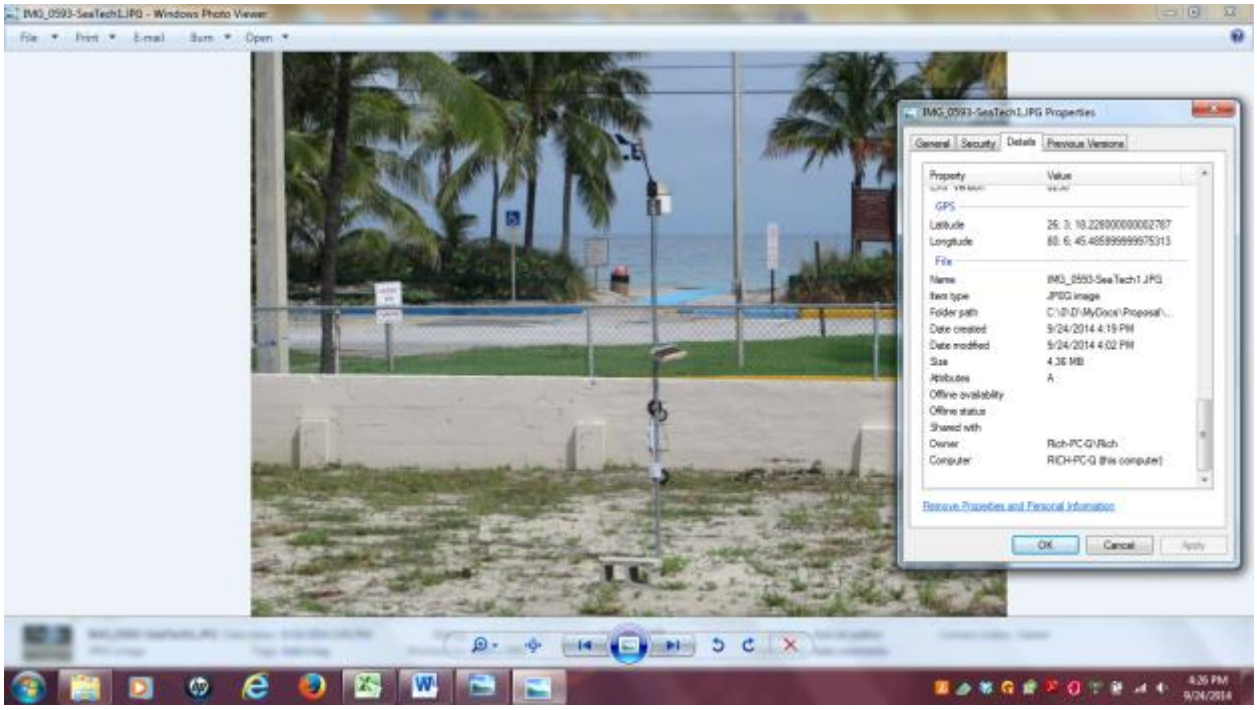

Figure A-9: Monitoring site 01 at SeaTech Station 1, Lat./Long.:26.055029,-80.112499

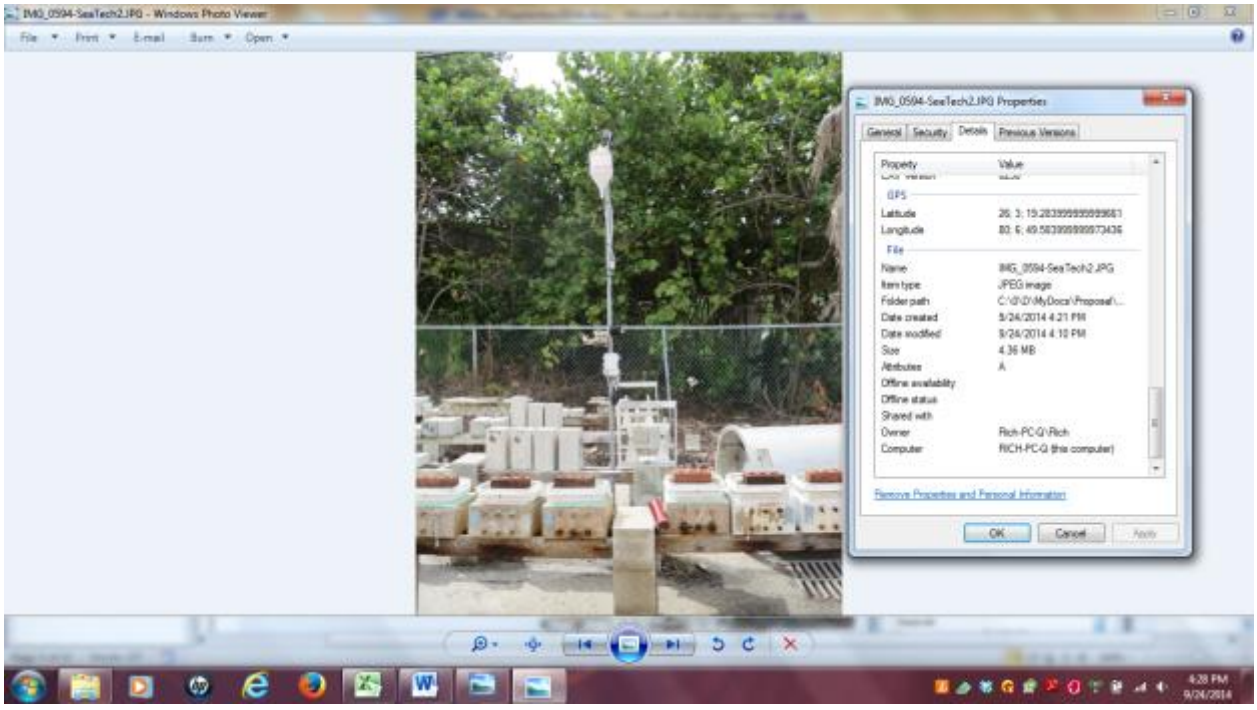

Figure A-10: Monitoring site 02 at SeaTech, Lat./Long.: 26.05525,-80.113802

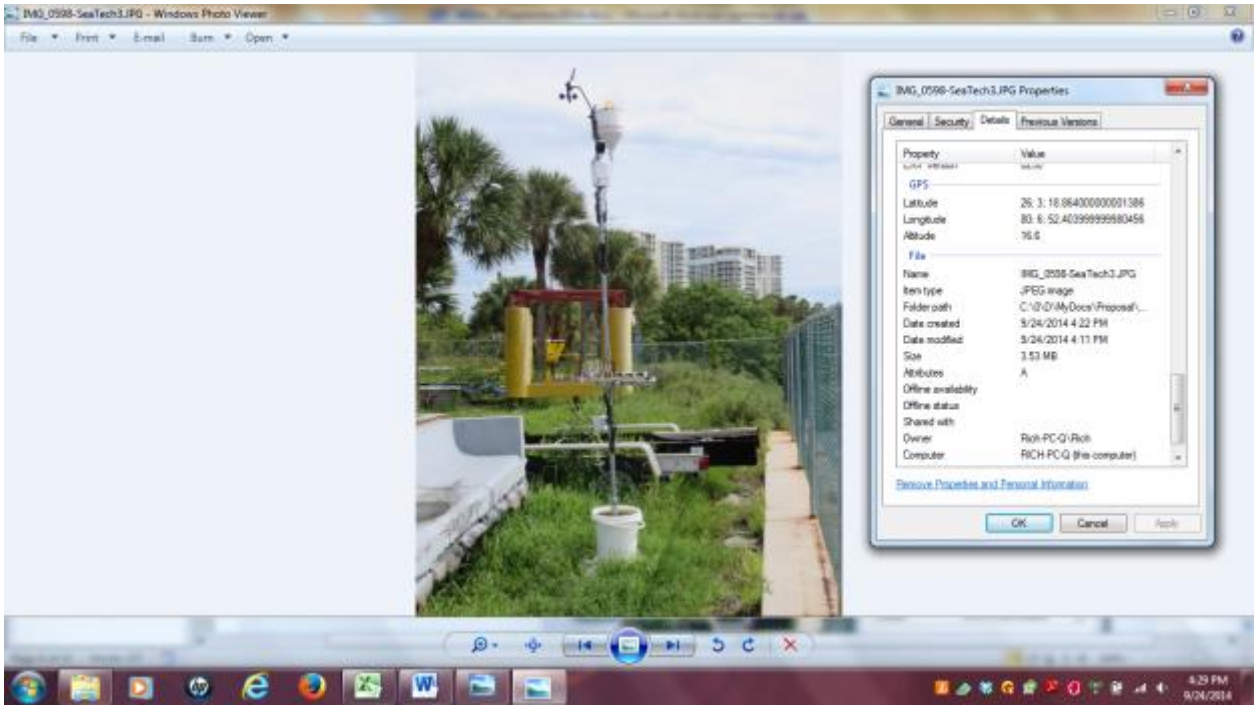

Figure A-11: Monitoring site 03 at SeaTech, Lat./Long.: 26.055202,-80.114178

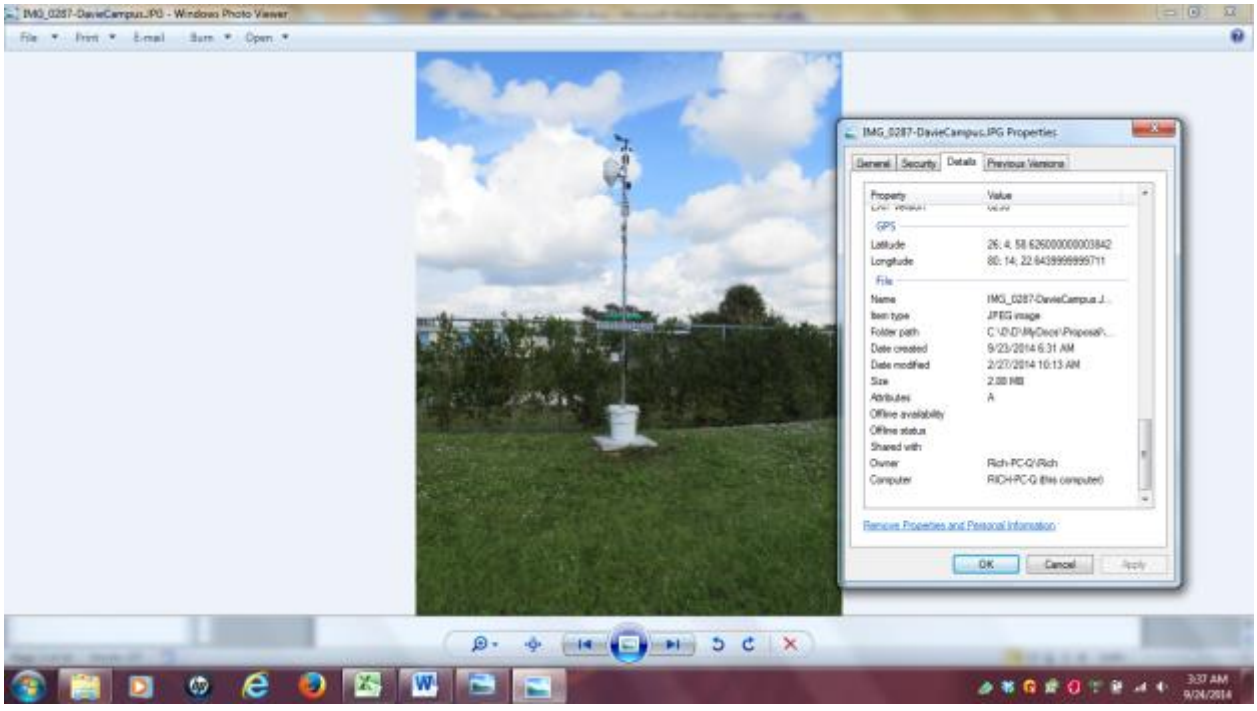

Figure A-12: Monitoring site 07 at Davie Campus, Lat./Long.: 26.082931,-80.239635.

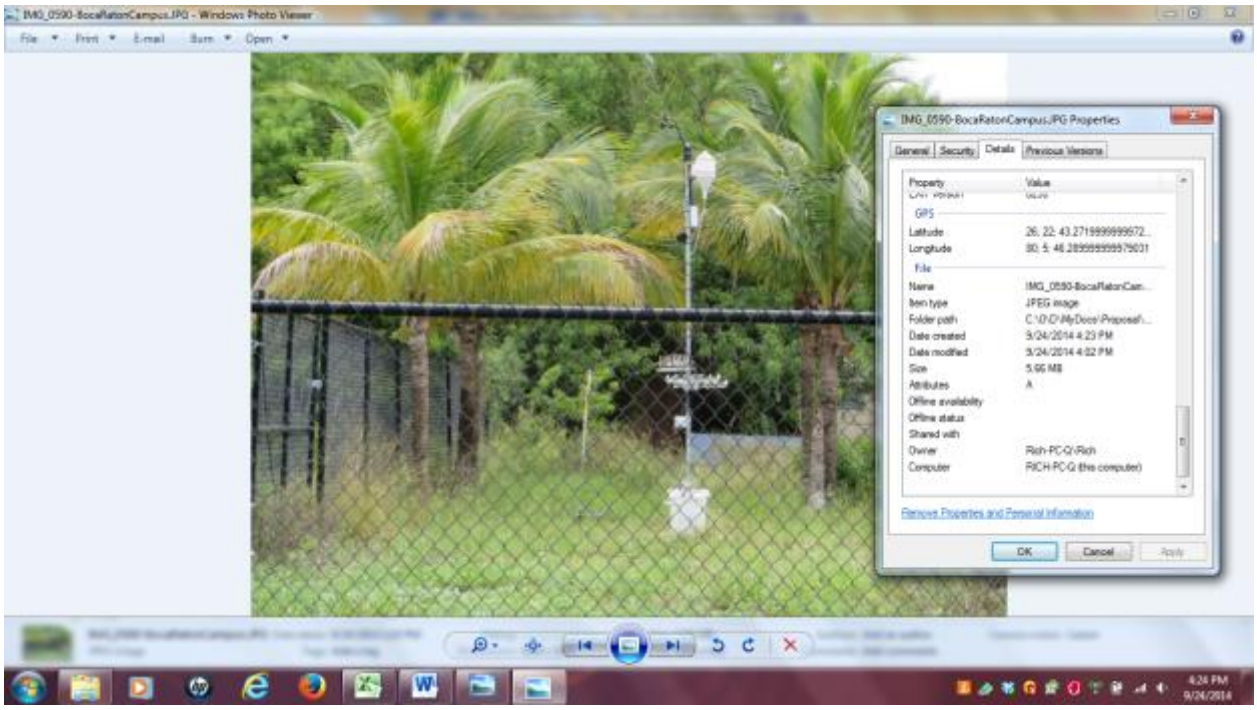

Figure A-13: Monitoring site 04 at Boca campus, Lat.Long.: 26.378469,-80.096263

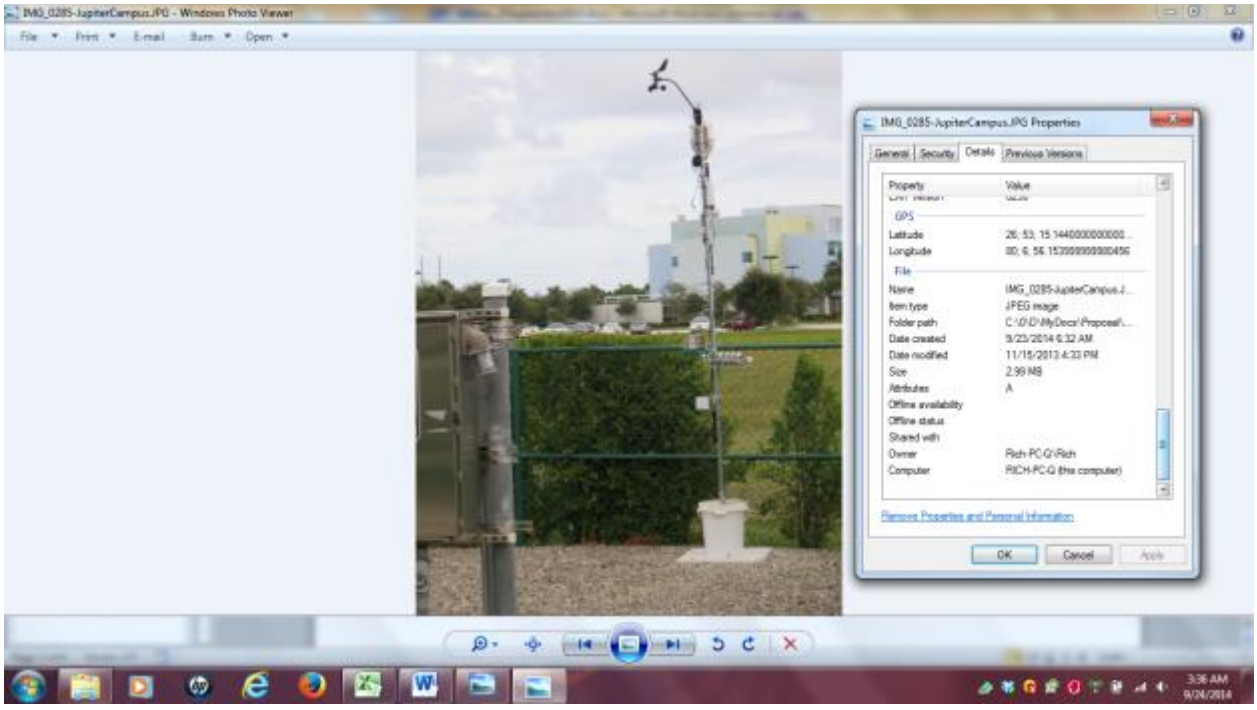

Figure A-14: Monitoring site 06 at Jupiter campus, Lat./Long.: 26.887445,-80.115444

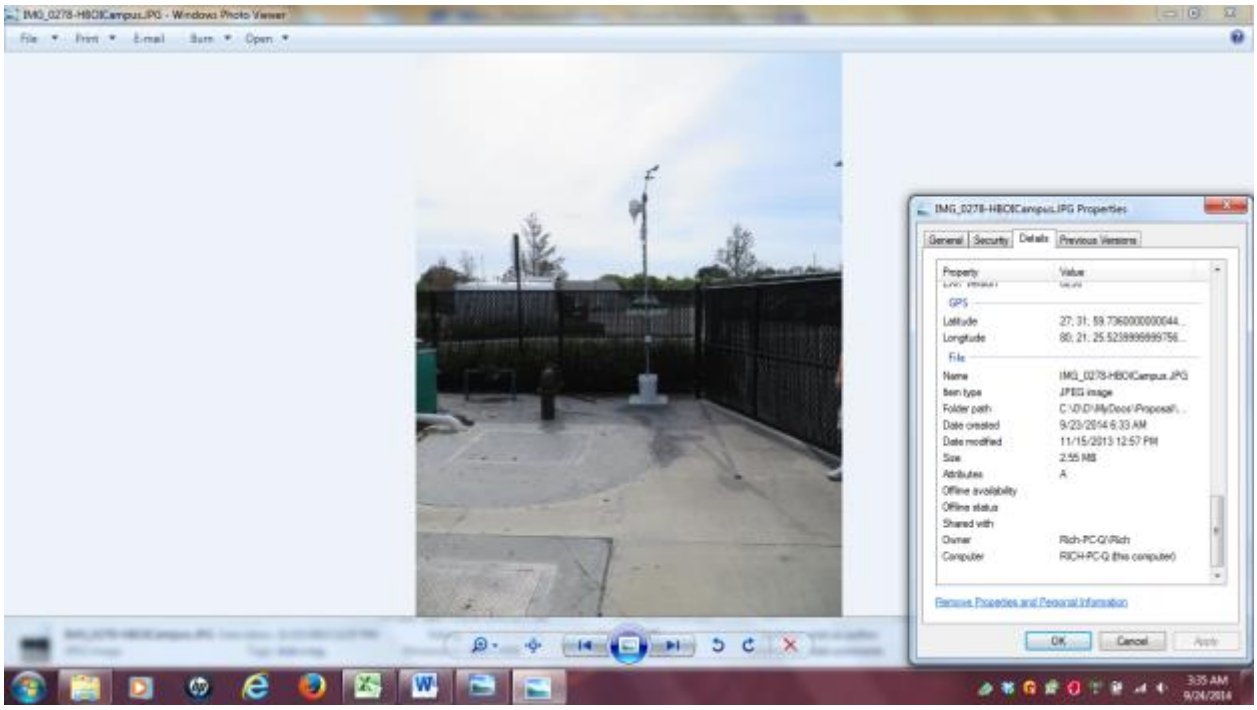

Figure A-15: Monitoring site 05 at Harbor Branch campus, Lat./Long.: 27.533358,-80.357295

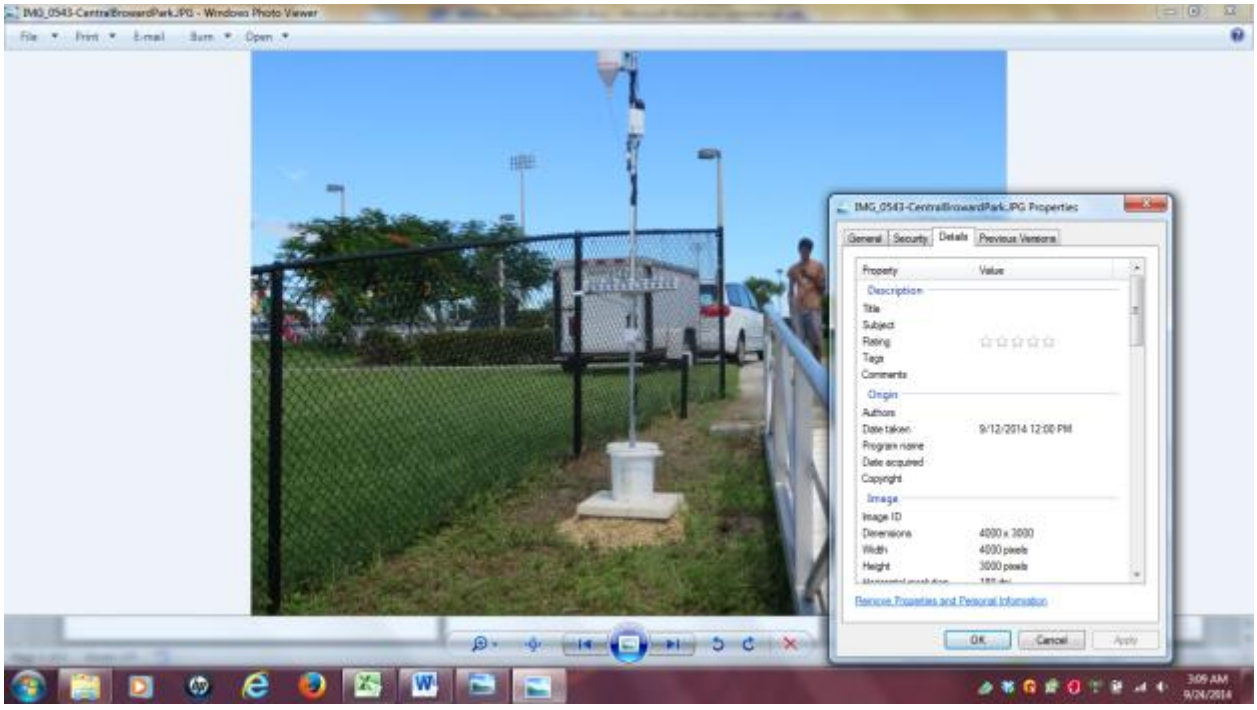

Figure A-16: Monitoring site 18 at Central Broward park, Lat./Long.: 26.138442,-80.196105

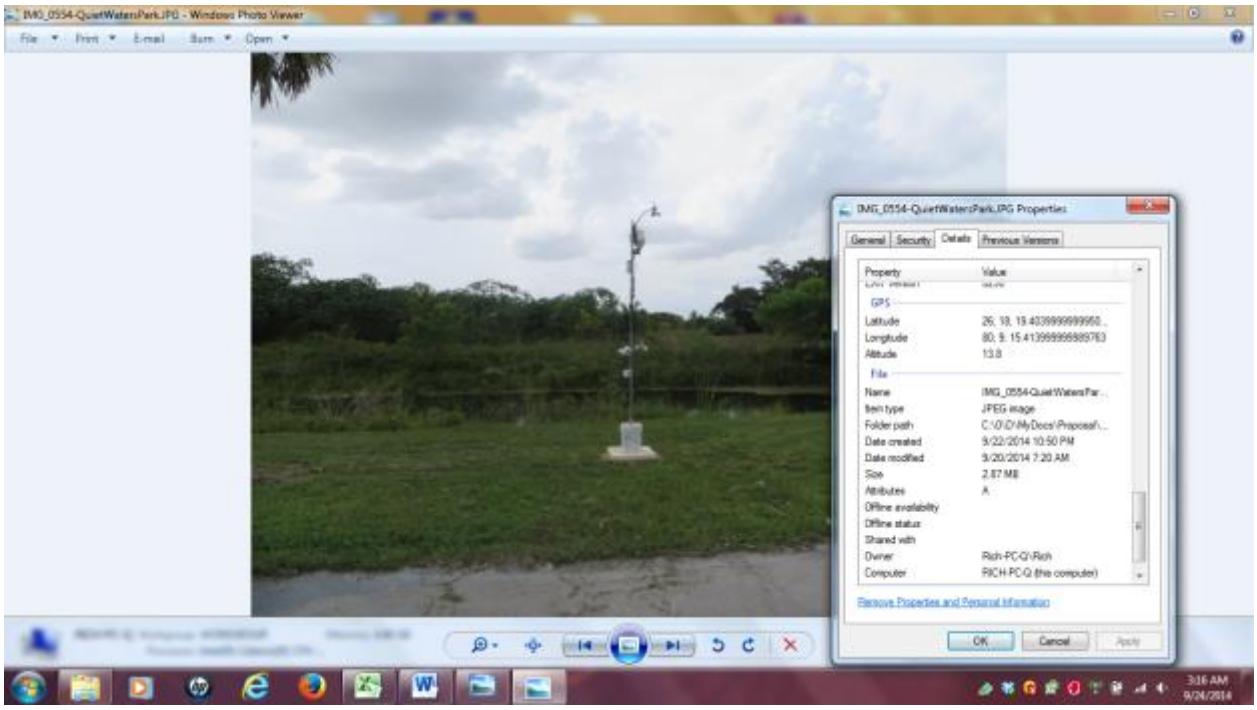

Figure A-17: Monitoring site 20 at Quiet Waters park, Lat./Long.: 26.305363,-80.154395

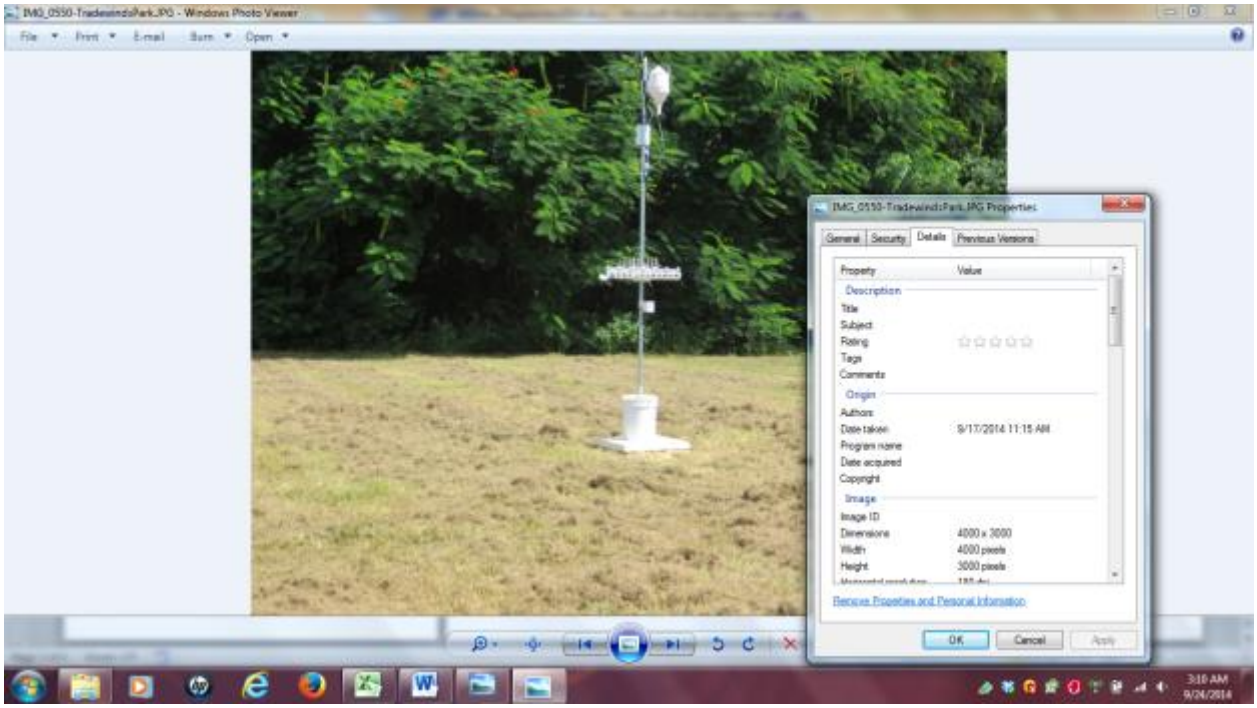

Figure A-18: Monitoring site 17 at Trade Winds park, Lat./Long.: 26.273256,-80.171086

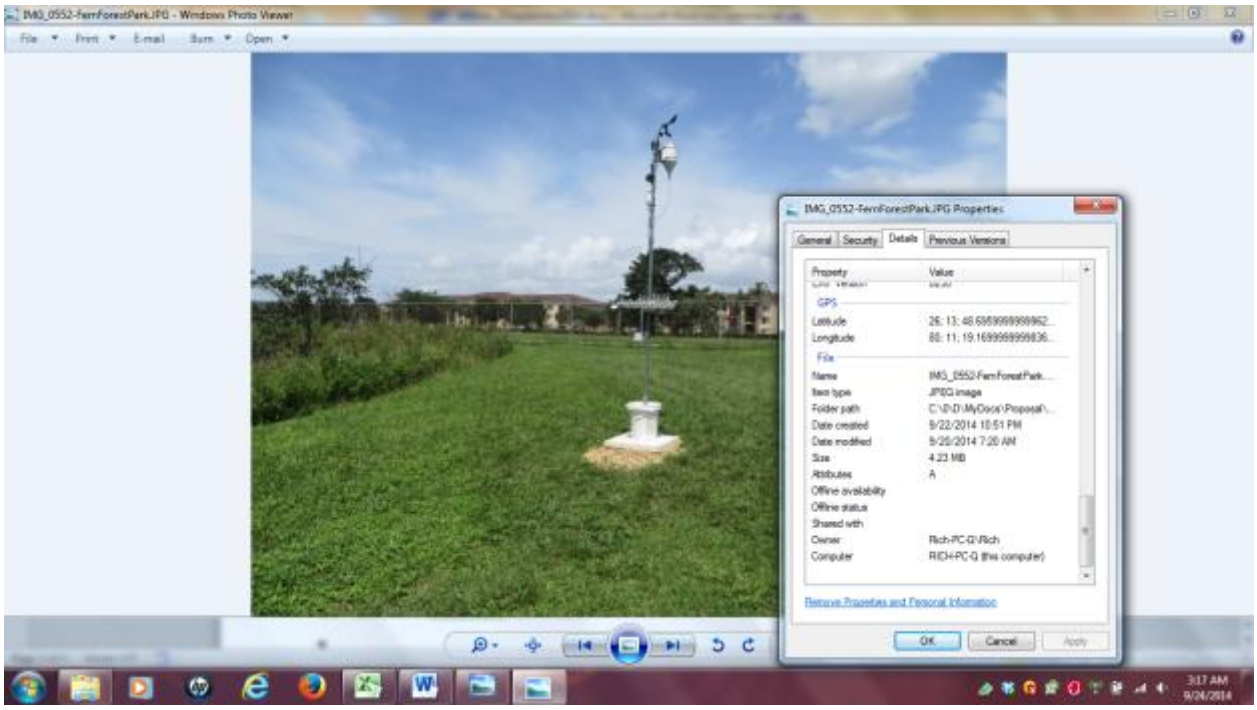

Figure A-19: Monitoring site 19 at Fern Forest park, Lat./Long.: 26.230159, -80.188709

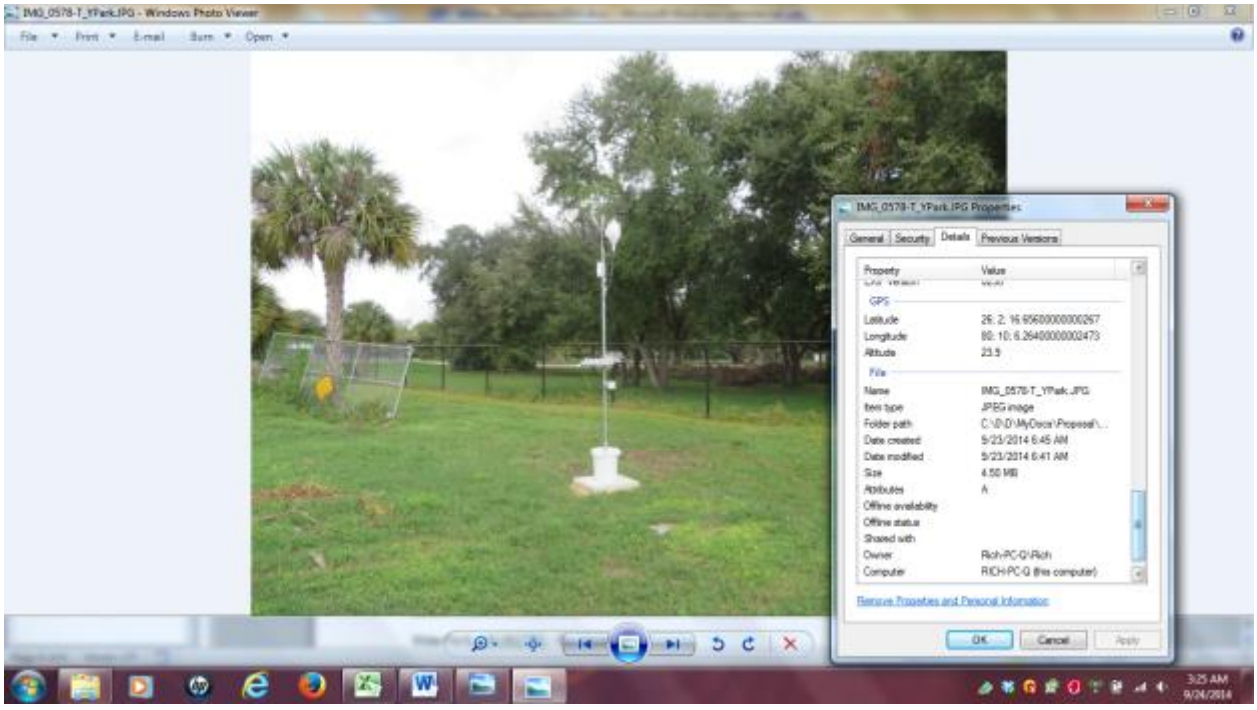

Figure A-20: Monitoring site 27 at T.Y. park, Lat./Long.: 26.03792,-8016848

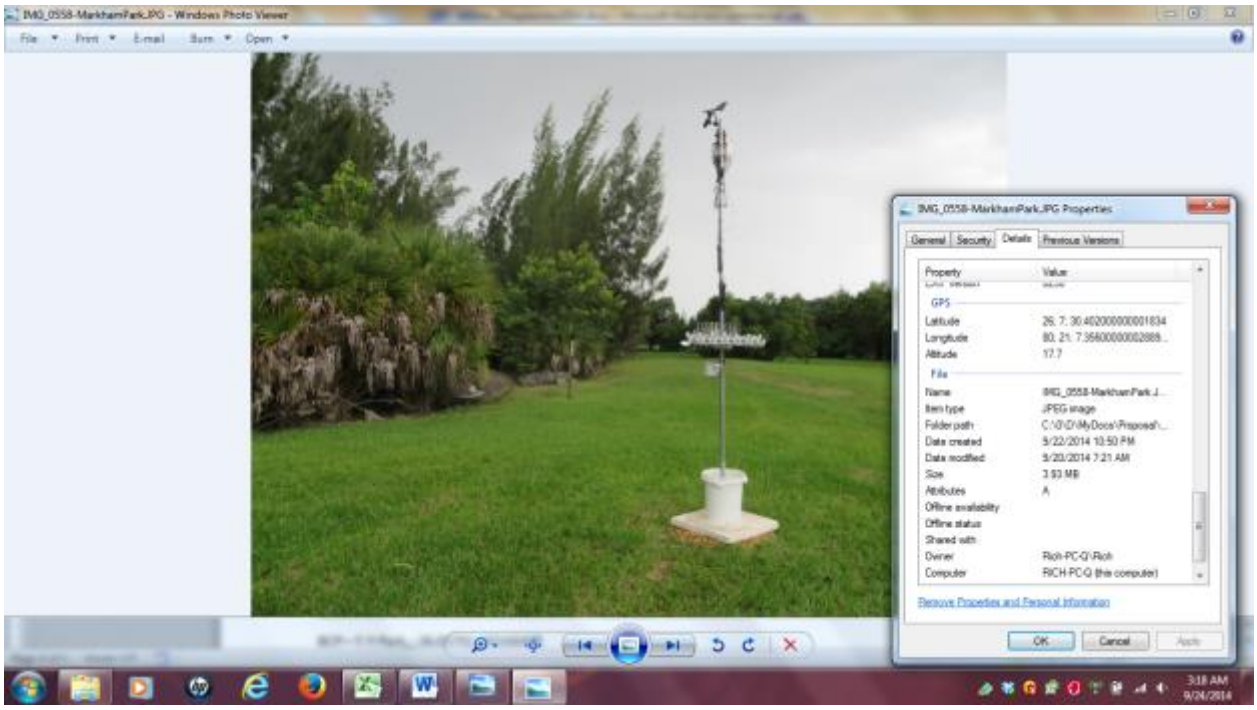

Figure A-21: Monitoring site 21 at Markham park, Lat./Long.: 26.125302,-80.351968

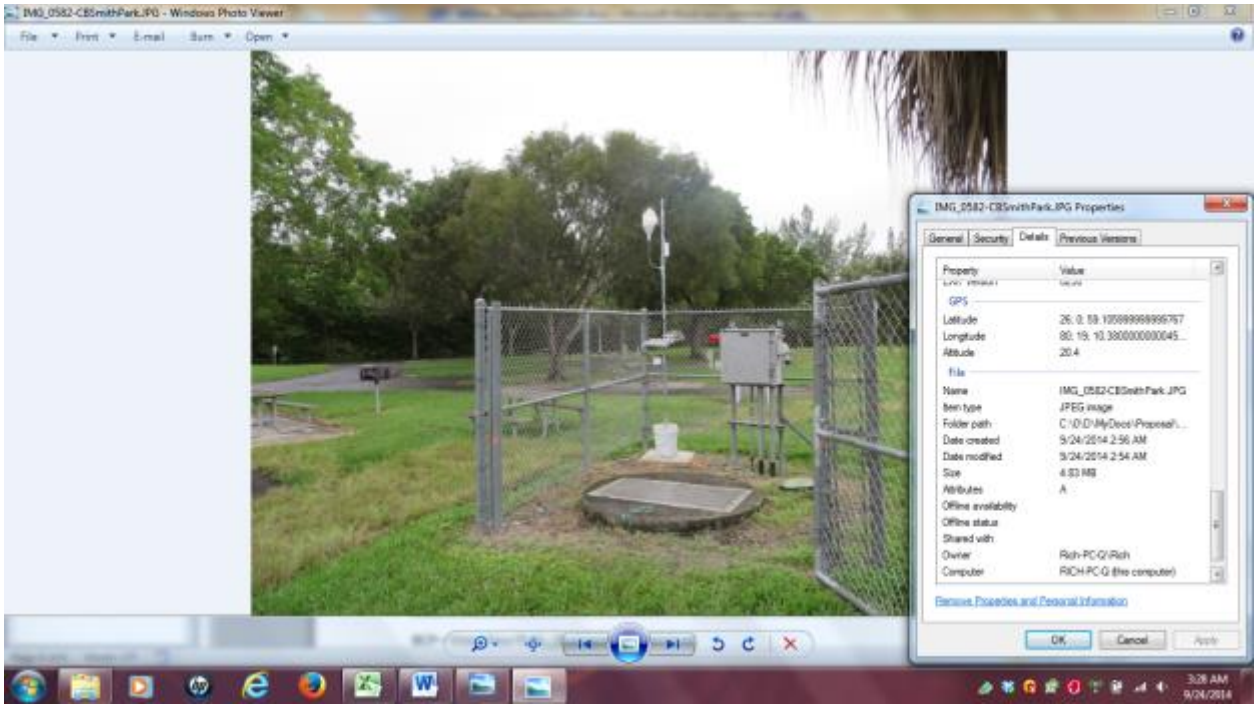

Figure A-22: Monitoring site 29 at C.B. Smith park, Lat./Long.: 26.016423,-80.319646

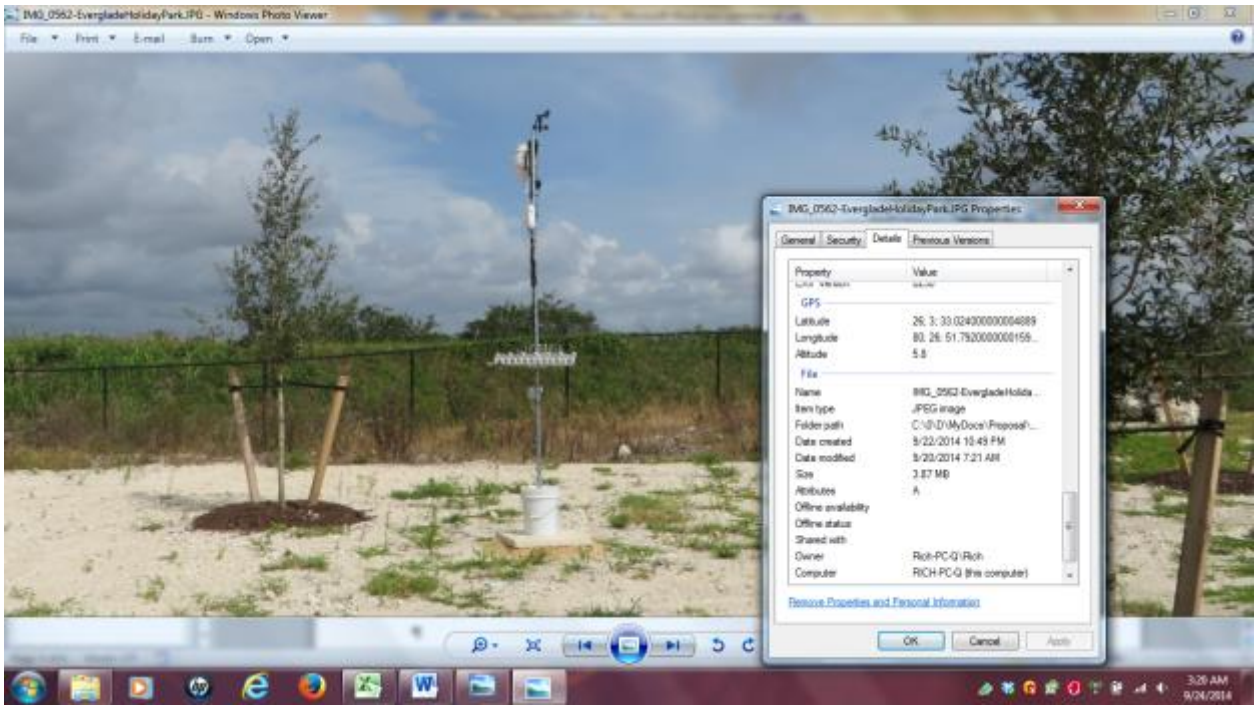

Figure A-23: Monitoring site 22 at Everglades Holiday park, Lat./Long.: 26.059264,-80.447751

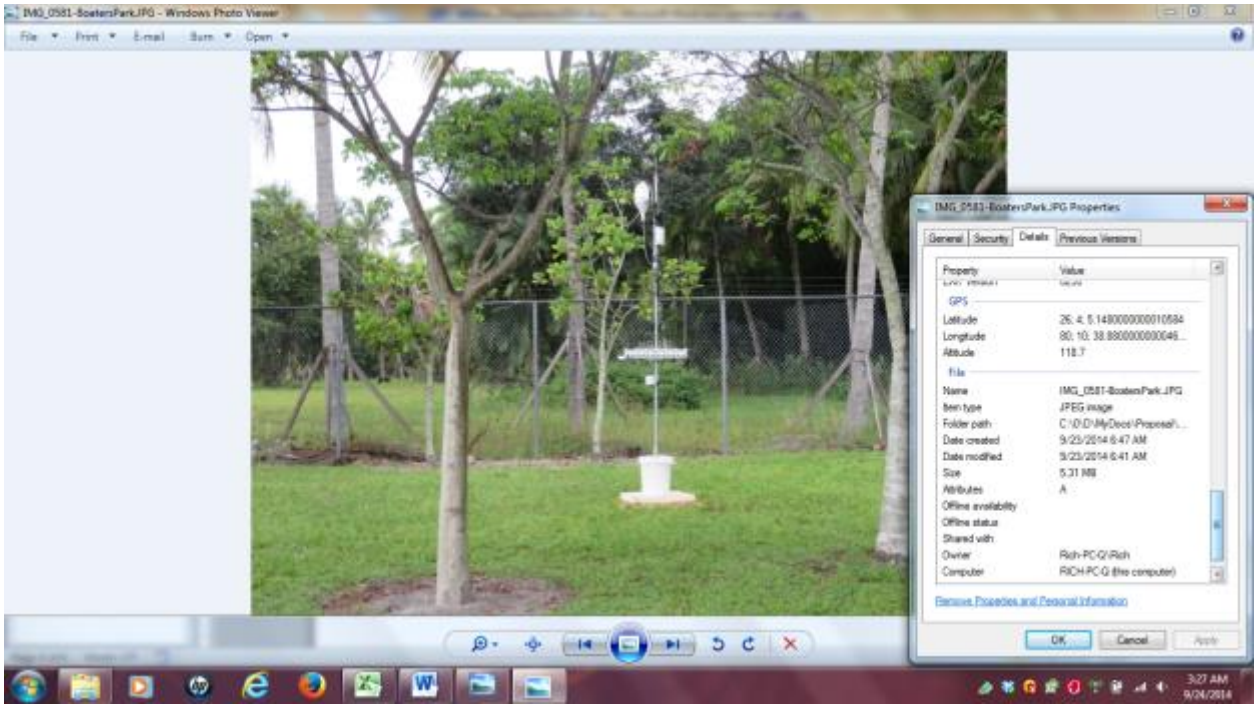

Figure A-24:Monitoring site 28 at Boaters park, Lat./Long.: 26.068398,-80.177624

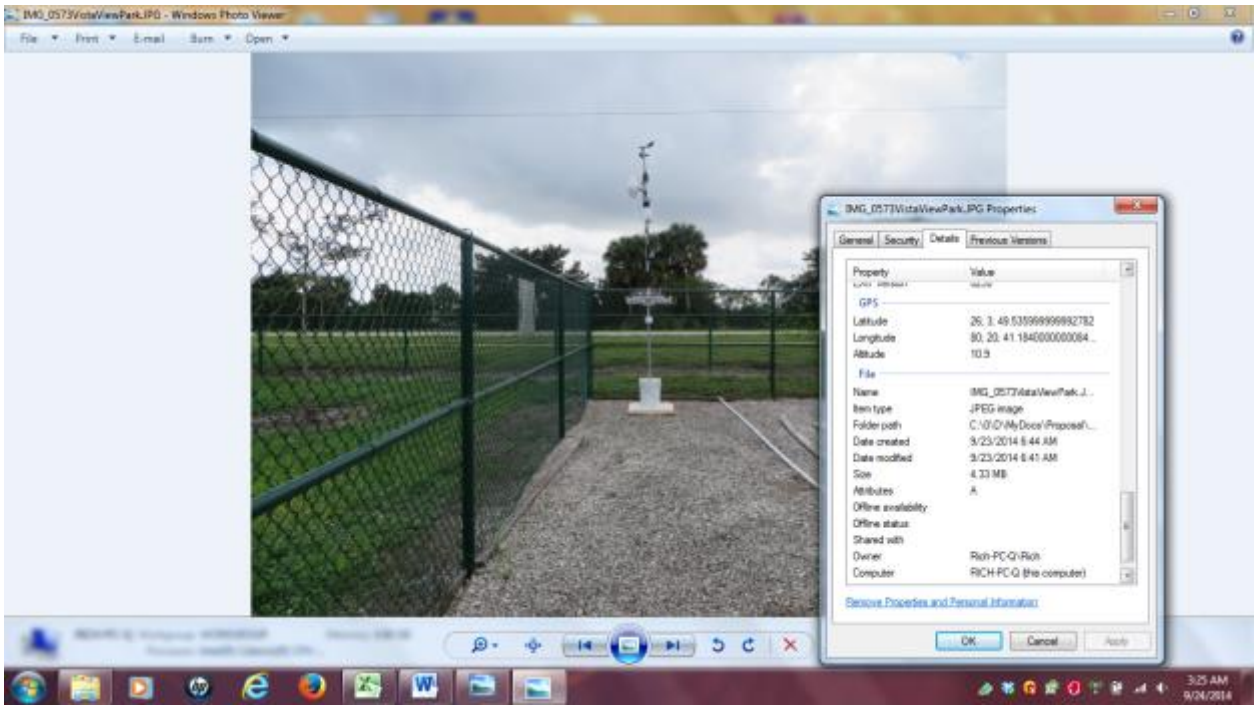

Figure A-25: Monitoring site 26 at Vista View park, Lat./Long.: 26.063695,-80.344783

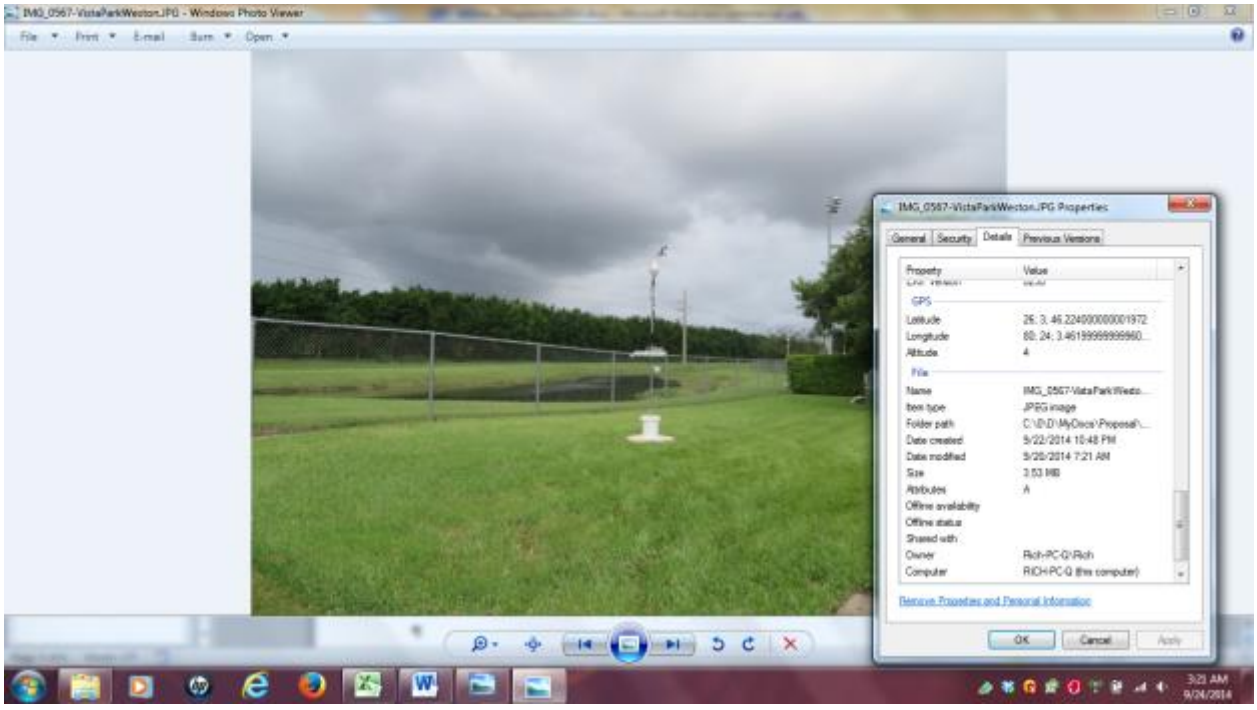

Figure A-26: Monitoring site 23 at Vista park, Lat./Long.: 26.062792, -80.400861

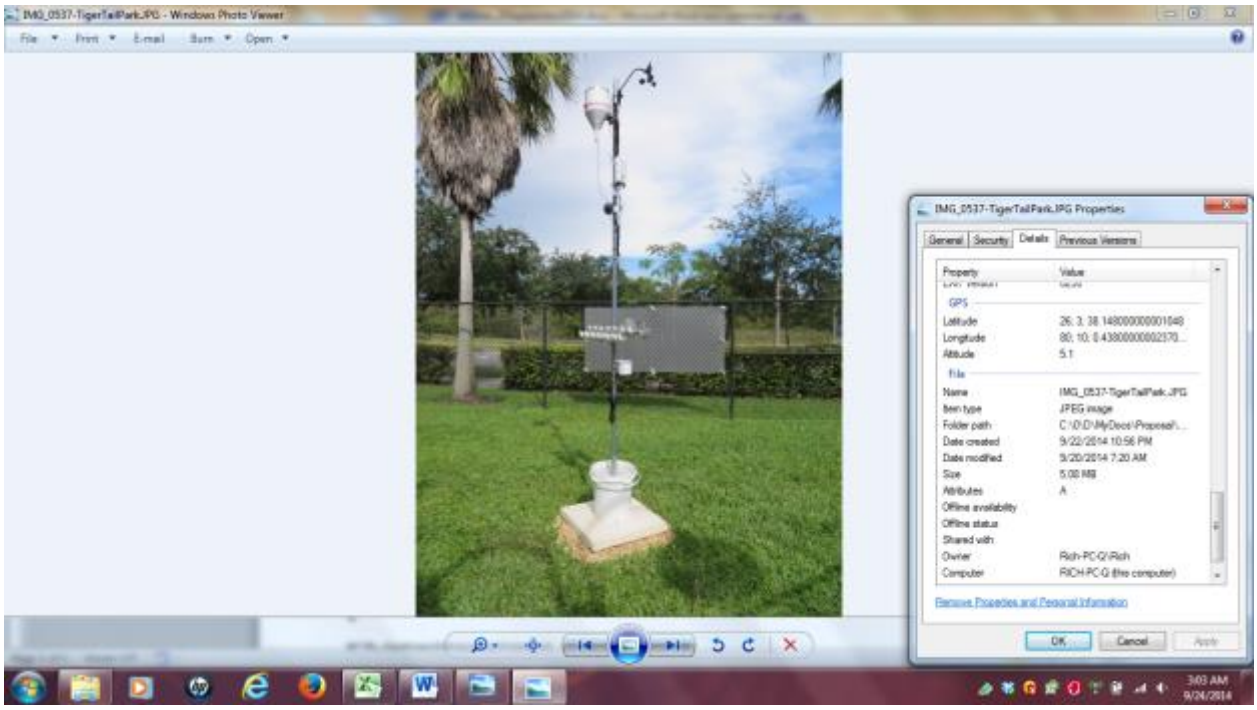

Figure A-27: Monitoring site 16 at Tigertail park, Lat./Long.: 26.060623, -80.16686

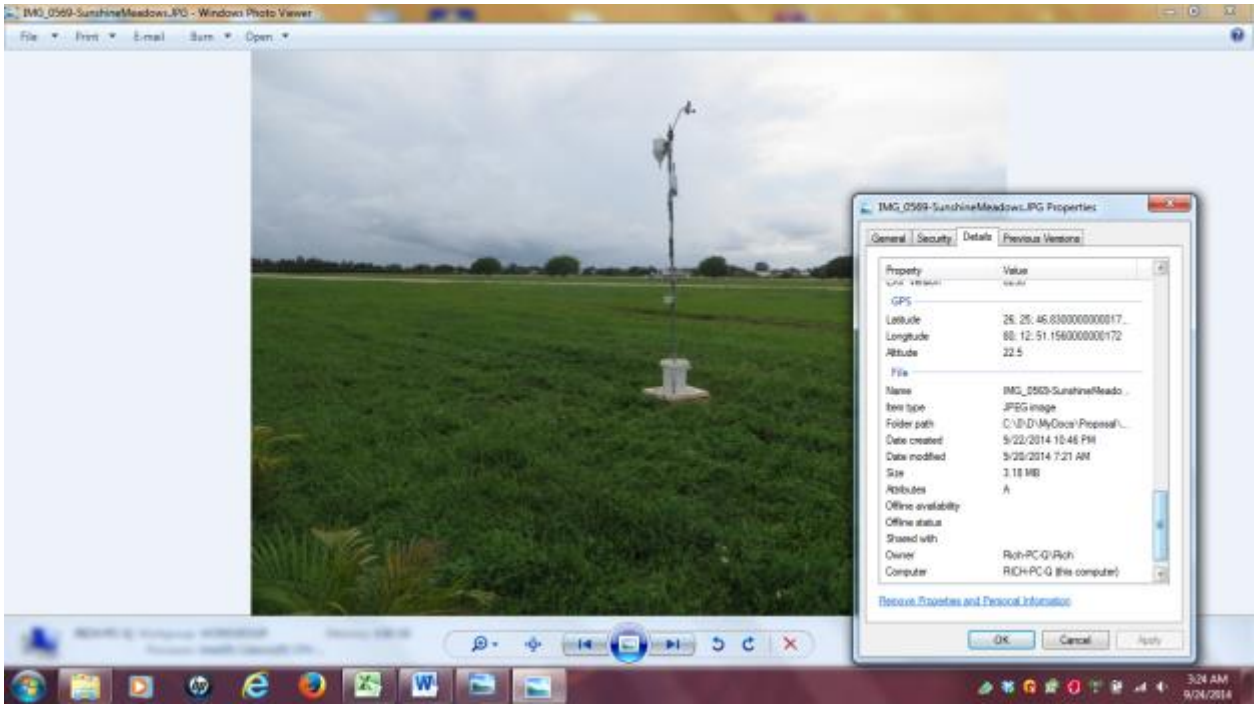

Figure A-28: Monitoring site 25 at Sunshine Meadows, Lat. Long.: 26.429712,-80.214247

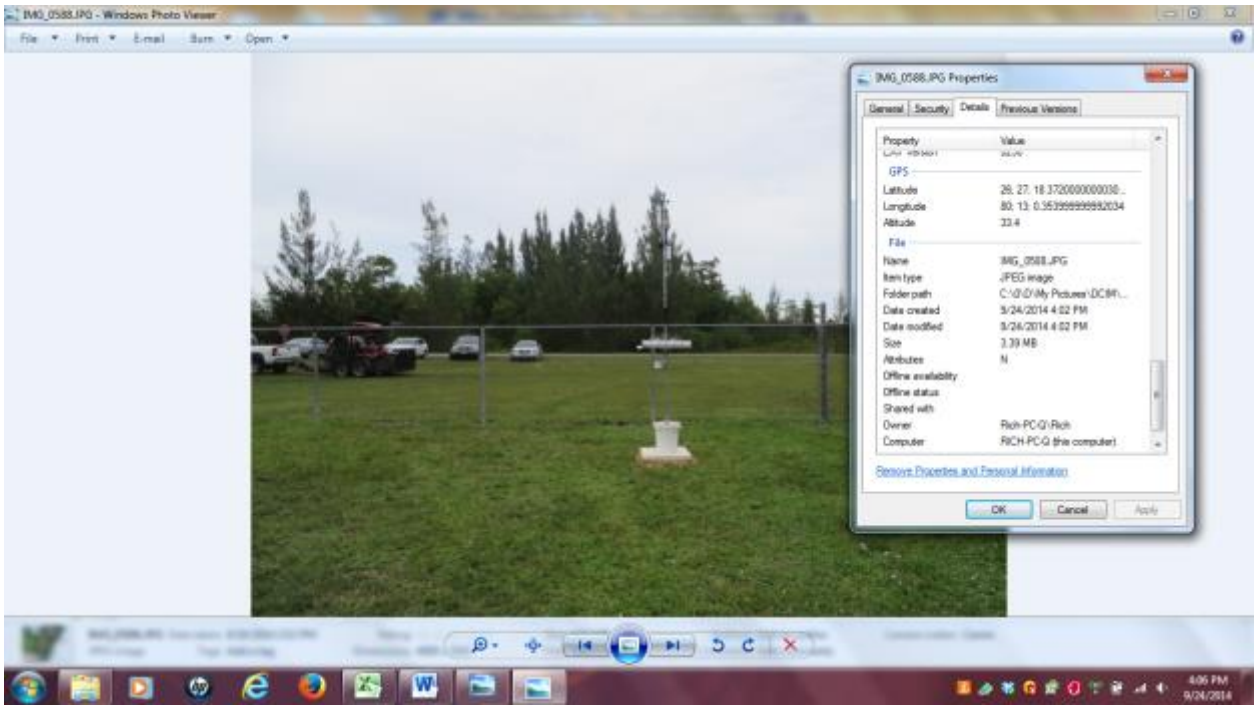

Figure A-29: Monitoring site 30 at West Delray Regional park, Lat/Long.: 26.455200, -80.216856

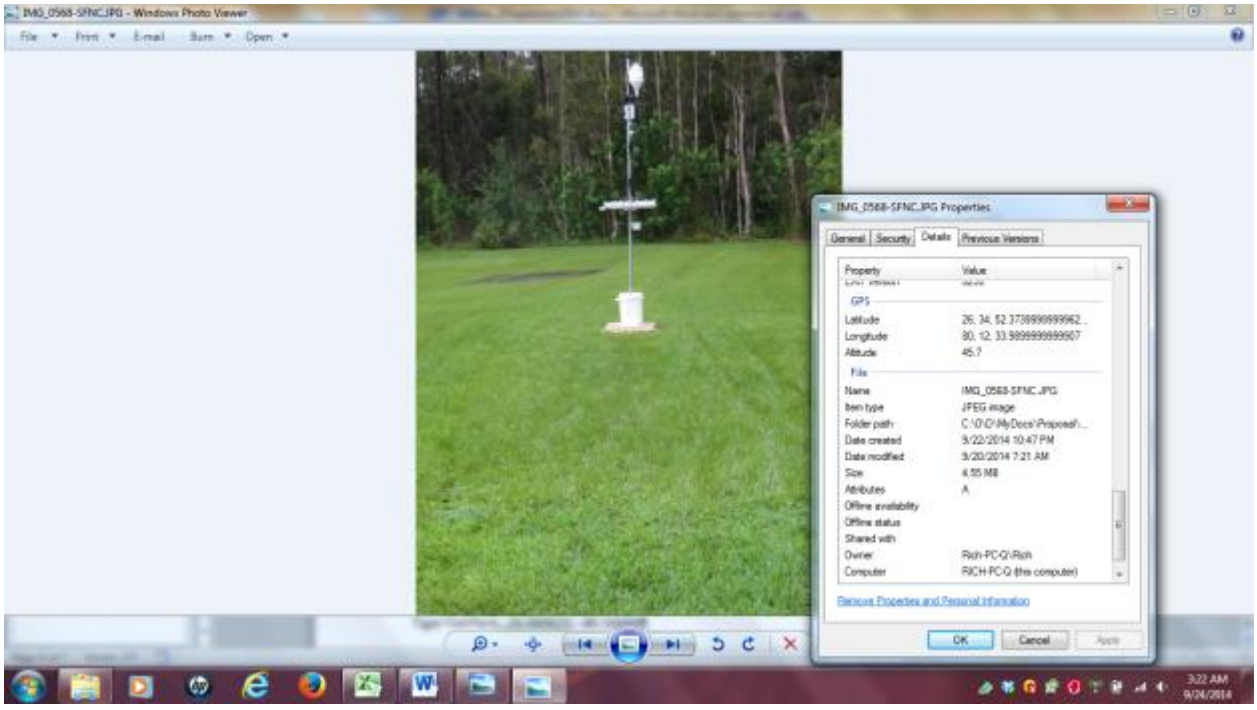

Figure A-30: Monitoring site 24 at South Florida Nat'l Cemetery, Lat./Long.: 26.58141,-80.2099

APPENDIX B: X-ray Diffraction Charts

The XRD charts are provided in the following pages. Each chart shows three XRD patterns. The patterns were grouped to present data obtained for each side of each plate: (a) the scraped off oxide powder (b) the plate before scraping off the oxide layer, and (c) the plate after scraping off the oxide layer. The horizontal axes are identical scales and units of 2θ degrees Co-Kα (cobalt anode source). The vertical axes are counts obtained.

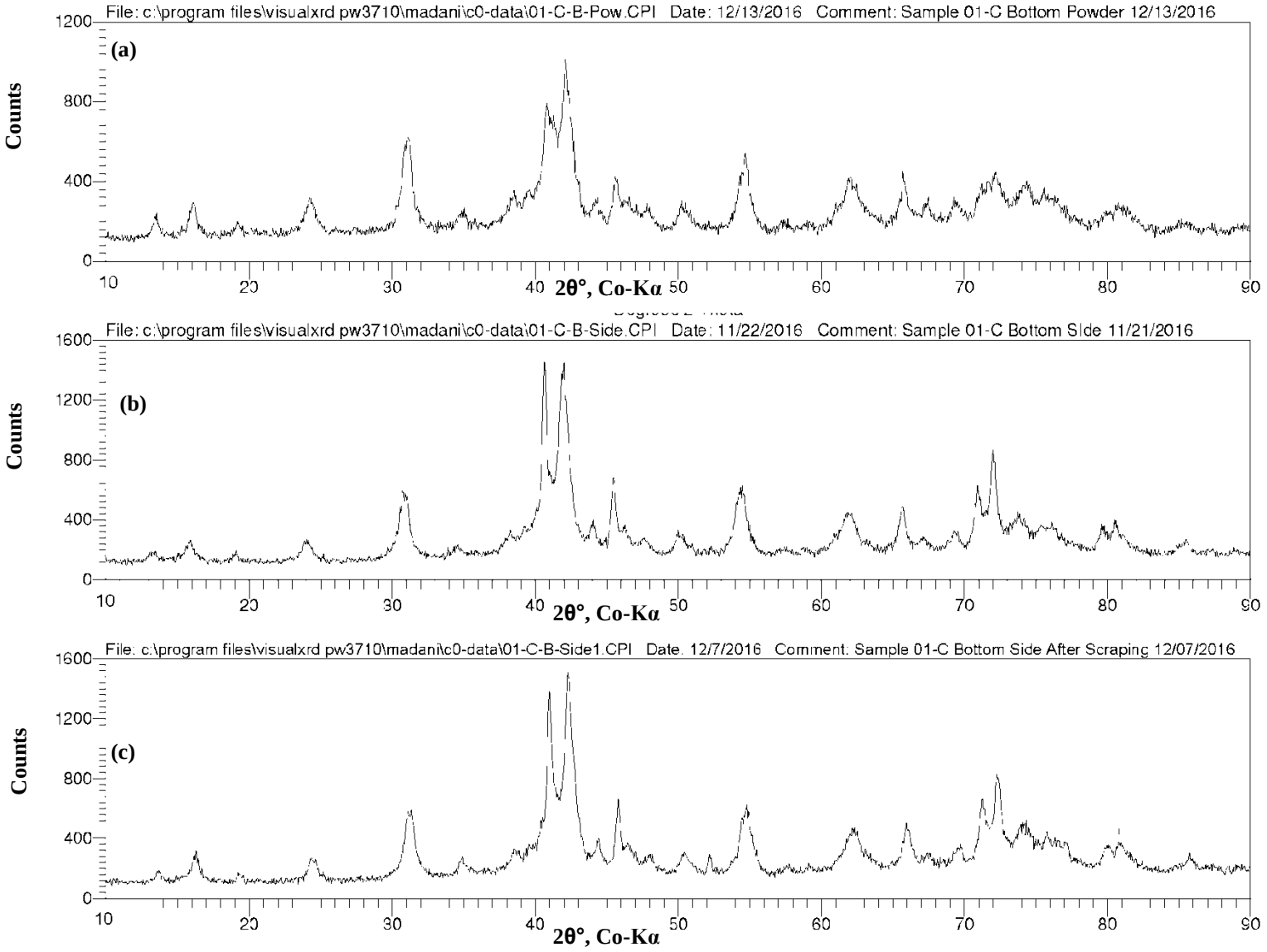

Figure B-1: XRD patterns, sample 01-C, (a) bottom side powder, (b) bottom before scraping, (c) bottom after scraping.

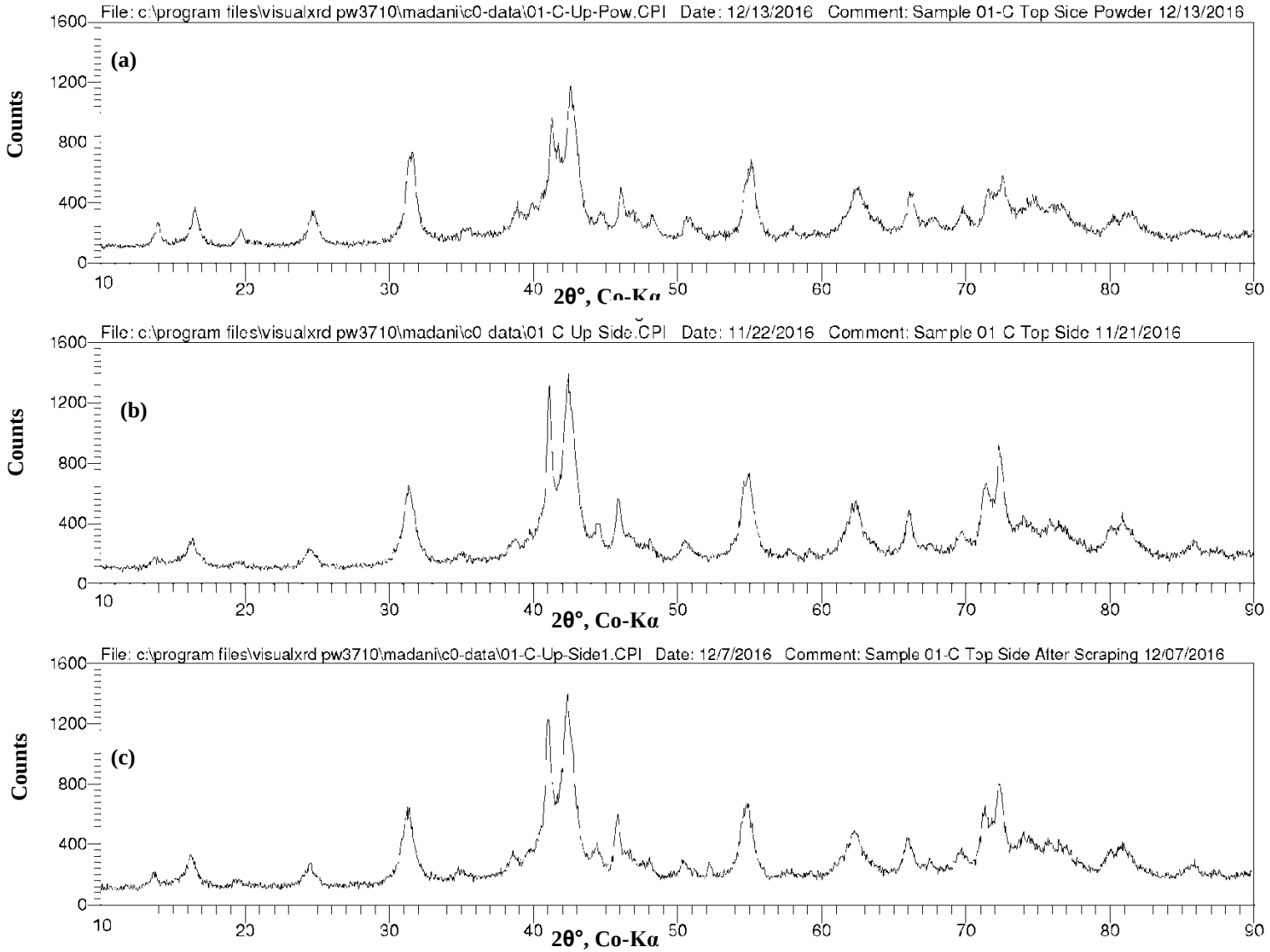

Figure B-2: XRD patterns, sample 01-C, (a) top side powder, (b) top before scraping, (c) top after scraping.

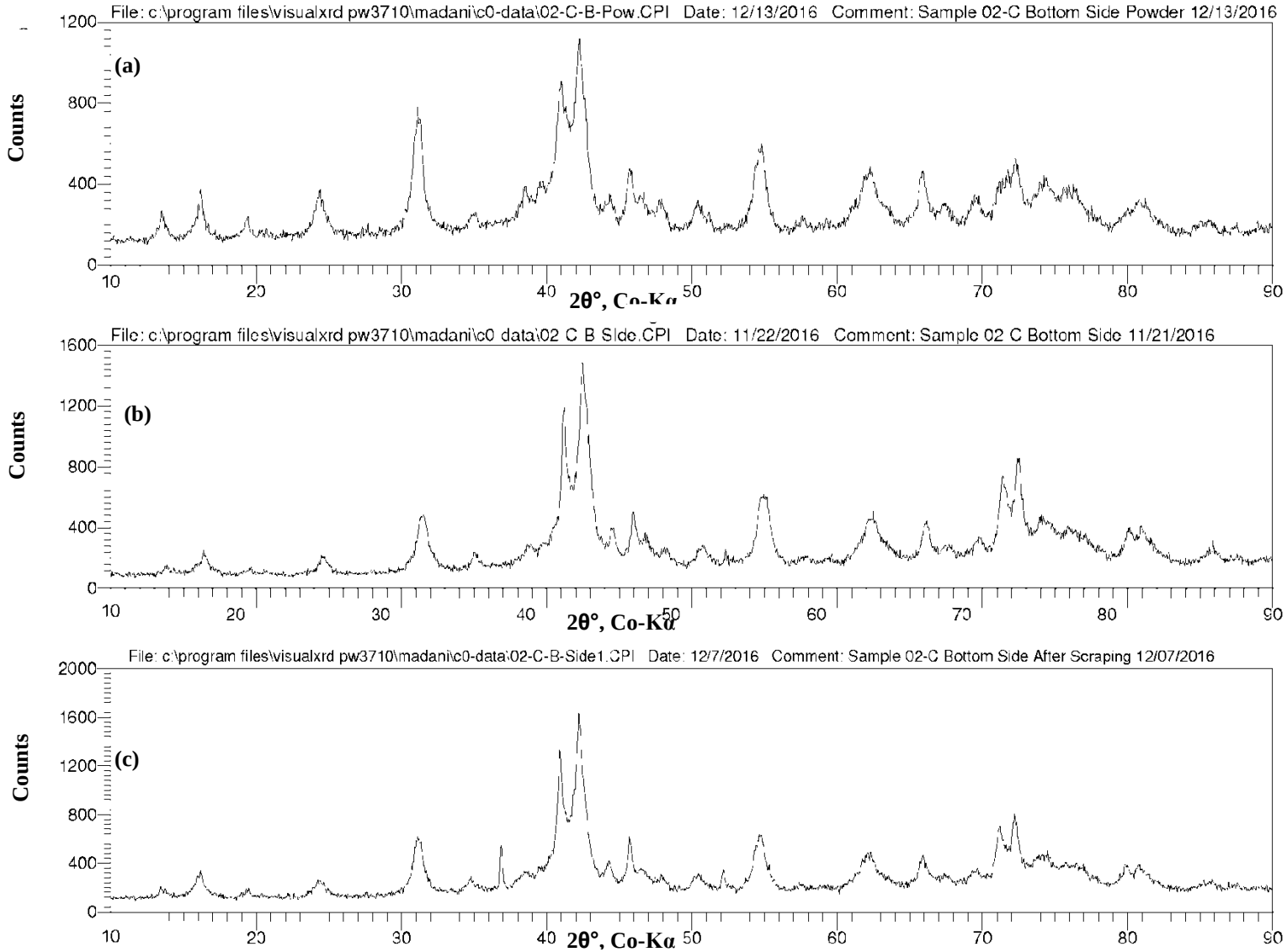

Figure B-3: XRD patterns, sample 02-C, (a) bottom side powder, (b) bottom before scraping, (c) bottom after scraping.

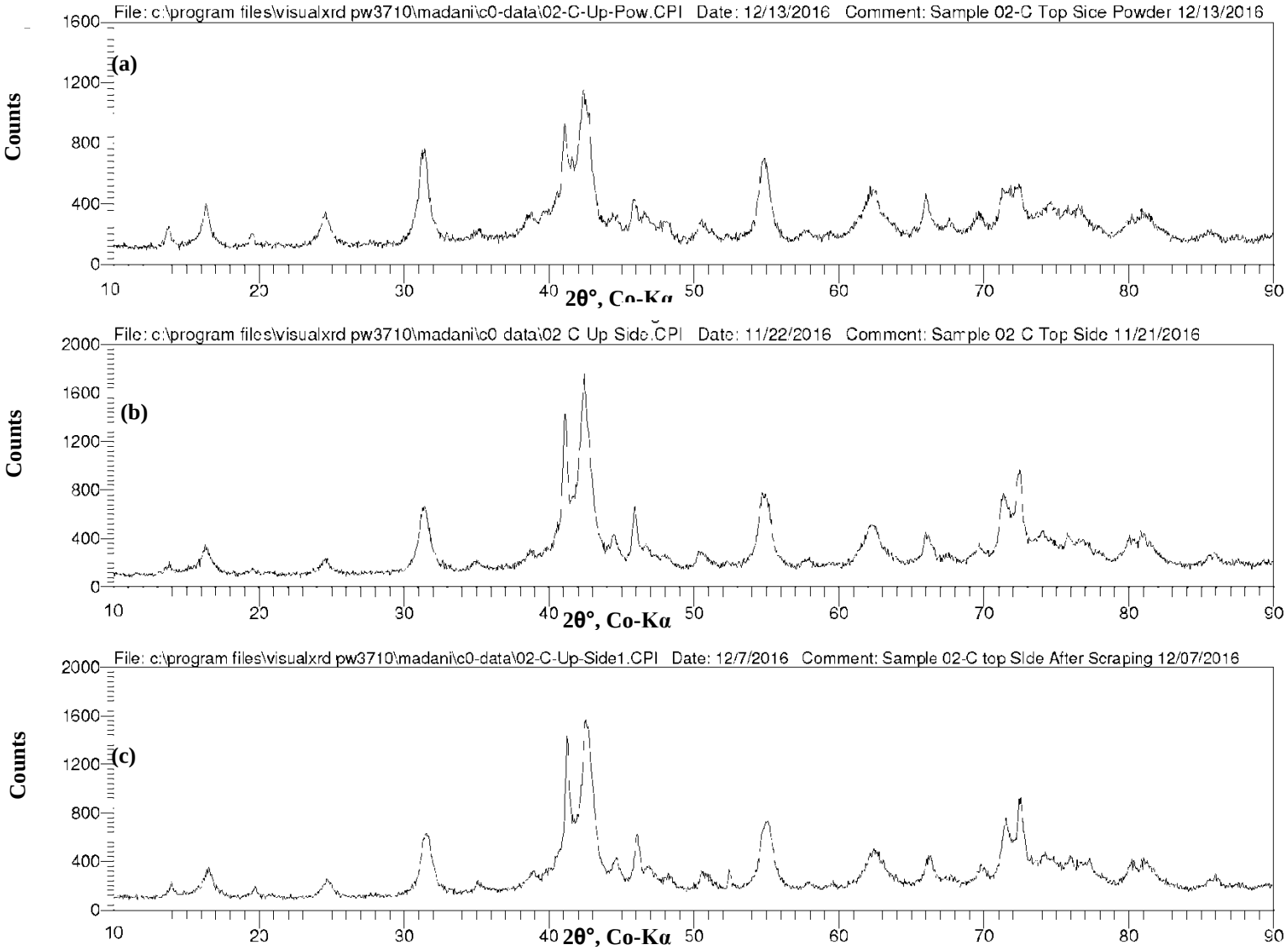

Figure B-4: XRD patterns, sample 02-C, (a) top side powder, (b) top before scraping, (c) top after scraping.

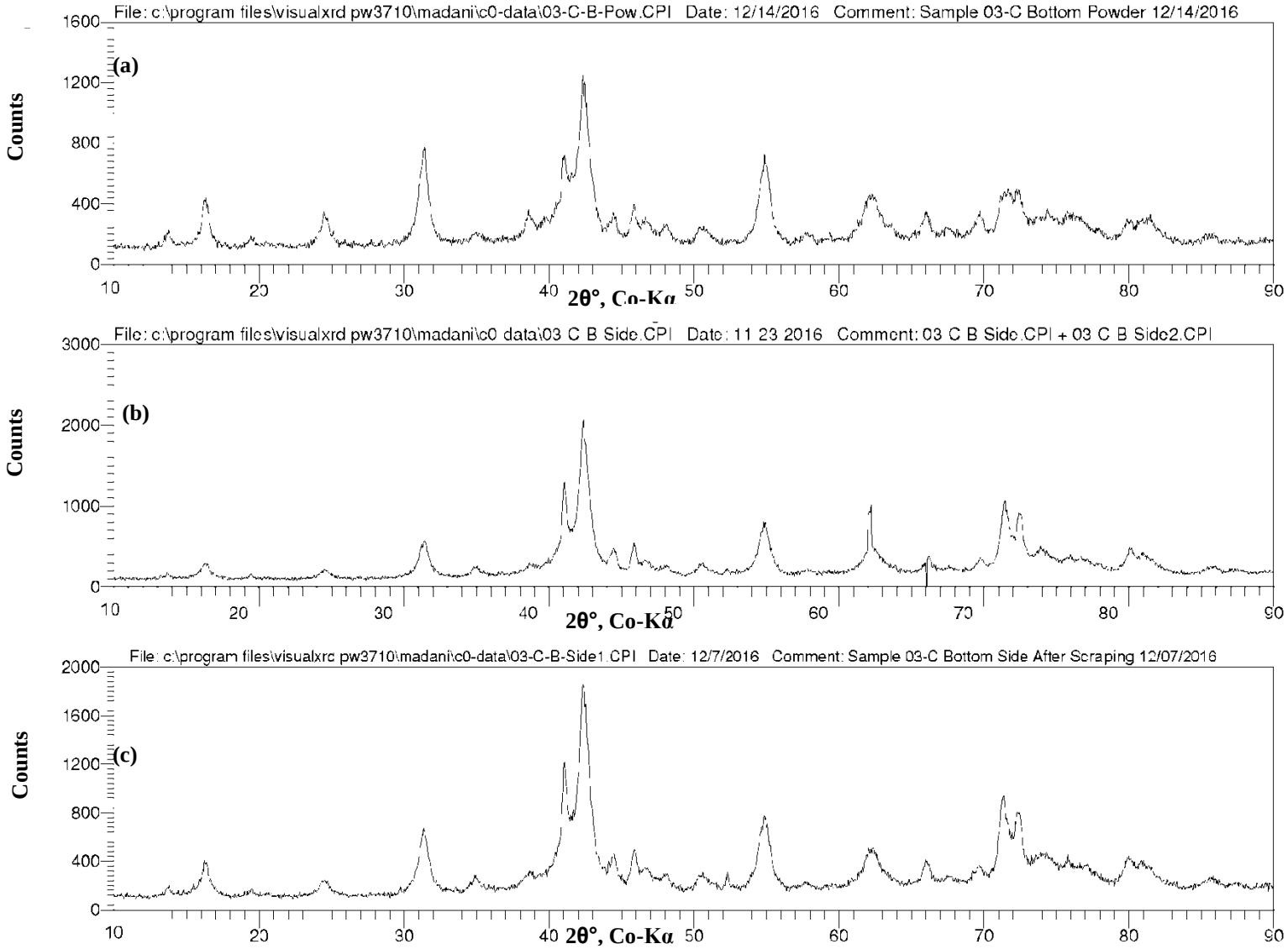

Figure B-5: XRD patterns, sample 03-C, (a) bottom side powder, (b) bottom before scraping, (c) bottom after scraping.

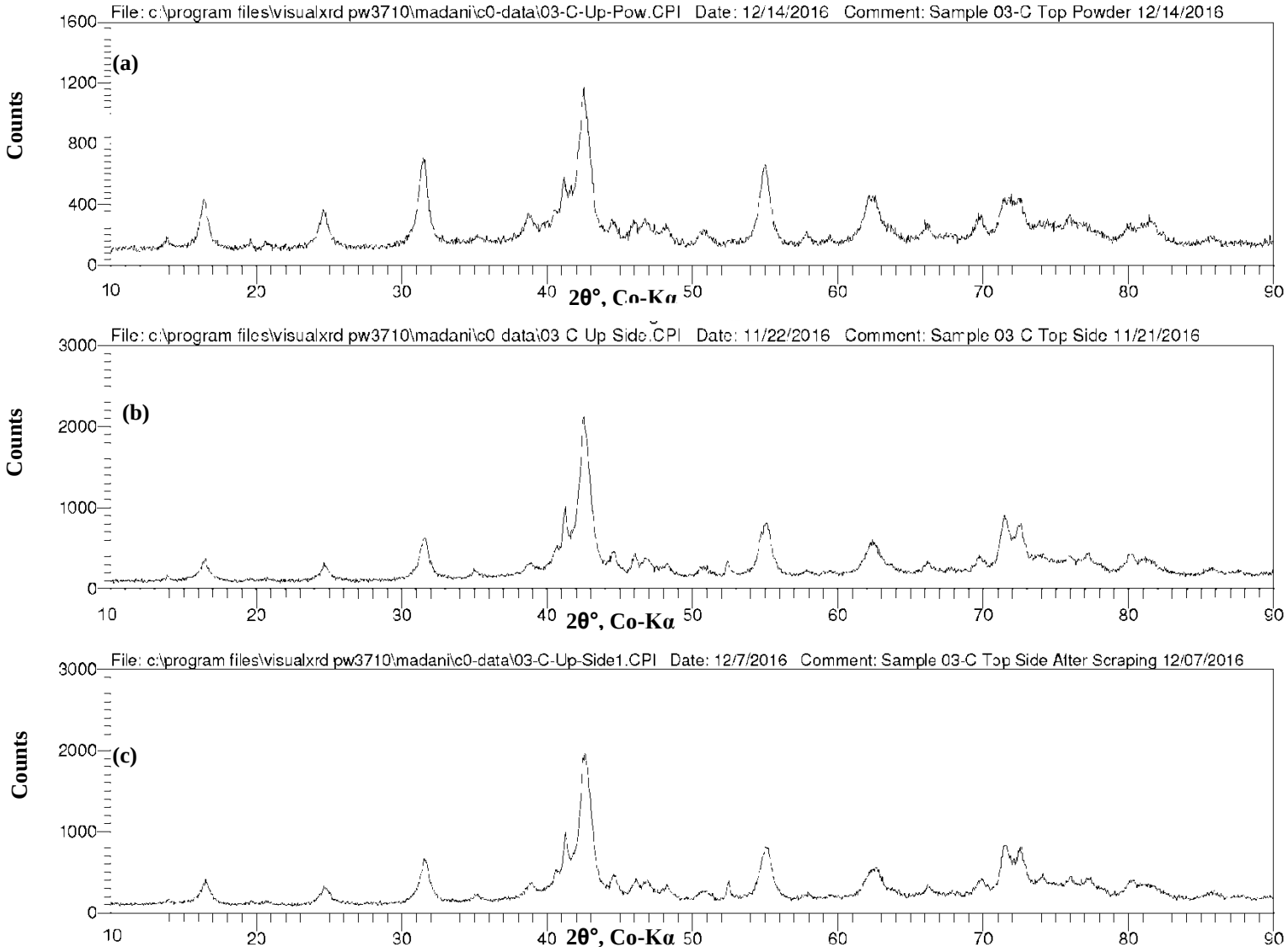

Figure B-6: XRD patterns, sample 03-C, (a) top side powder, (b) top before scraping, (c) top after scraping.

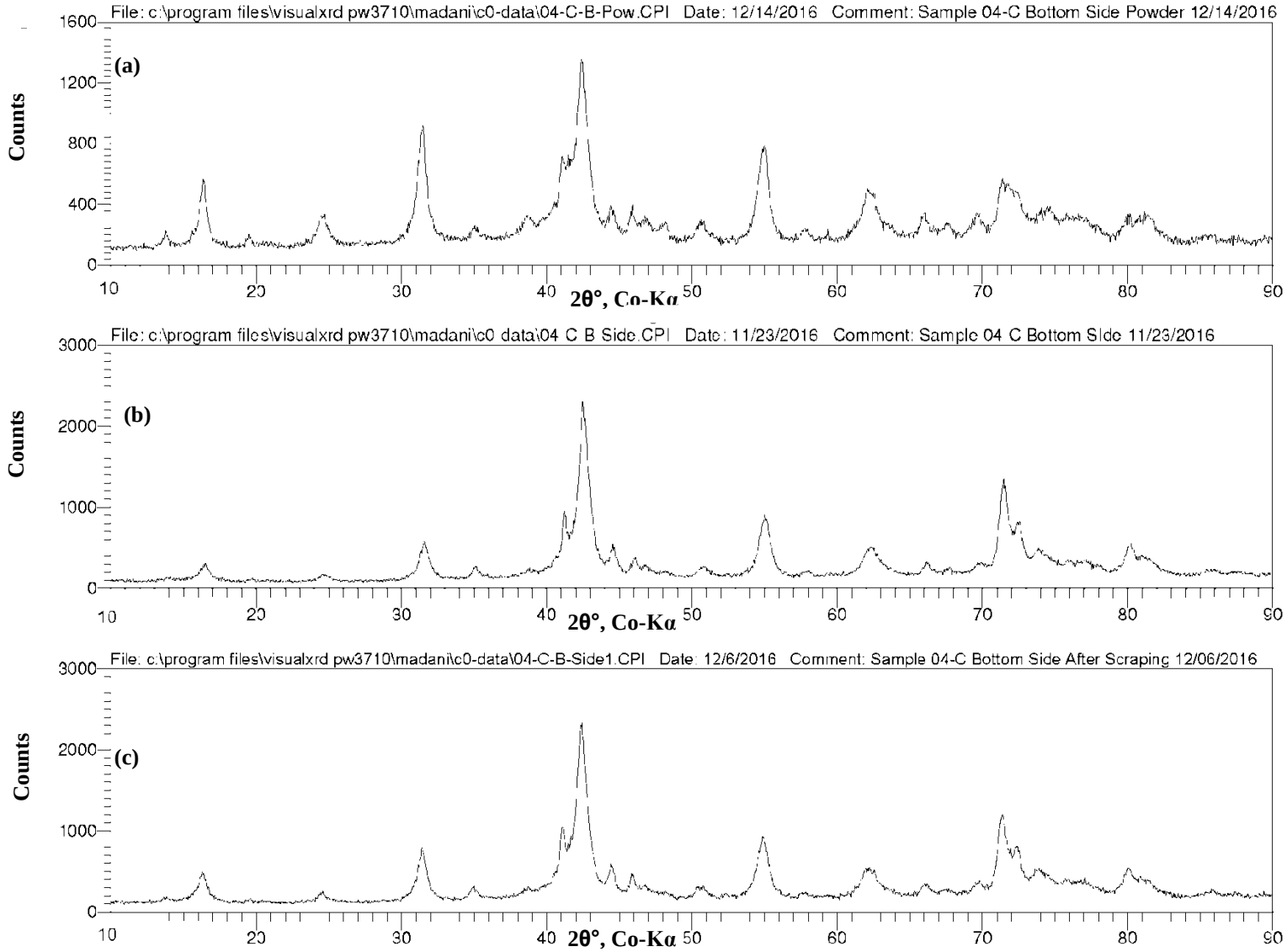

Figure B-7: XRD patterns, sample 04-C, (a) bottom side powder, (b) bottom before scraping, (c) bottom after scraping.

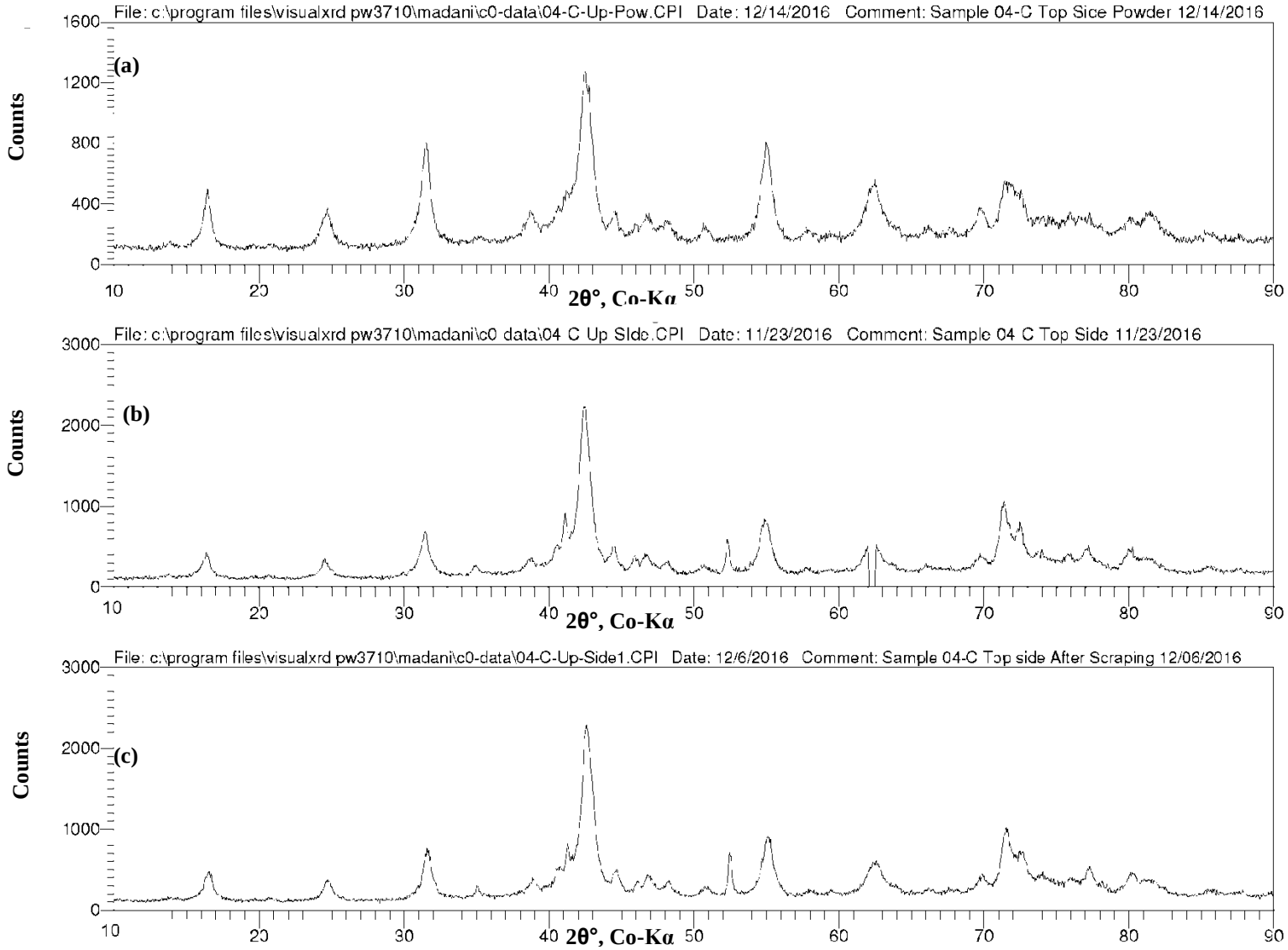

Figure B-8: XRD patterns, sample 04-C, (a) top side powder, (b) top before scraping, (c) top after scraping.

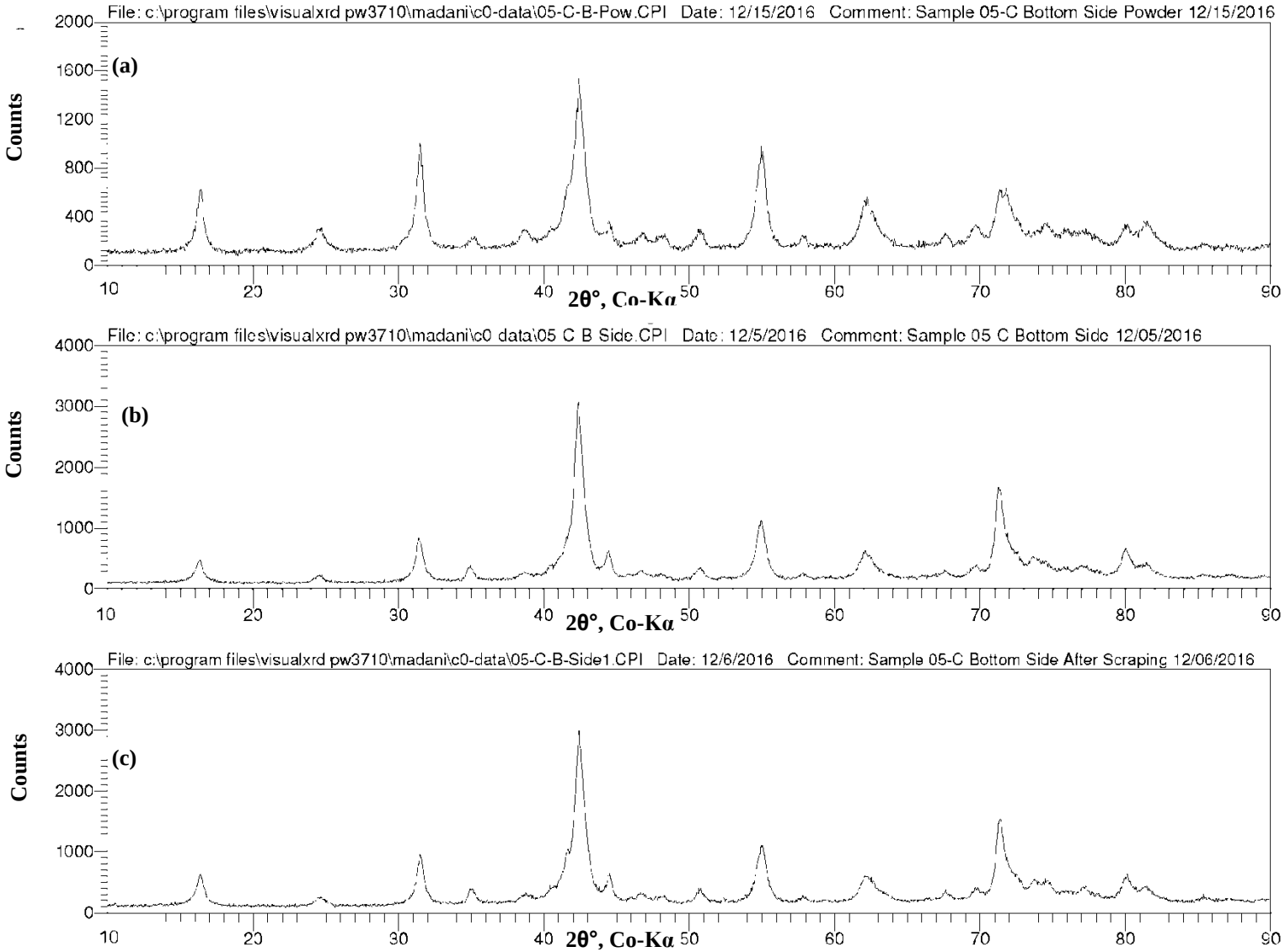

Figure B-9: XRD patterns, sample 05-C, (a) bottom side powder, (b) bottom before scraping, (c) bottom after scraping.

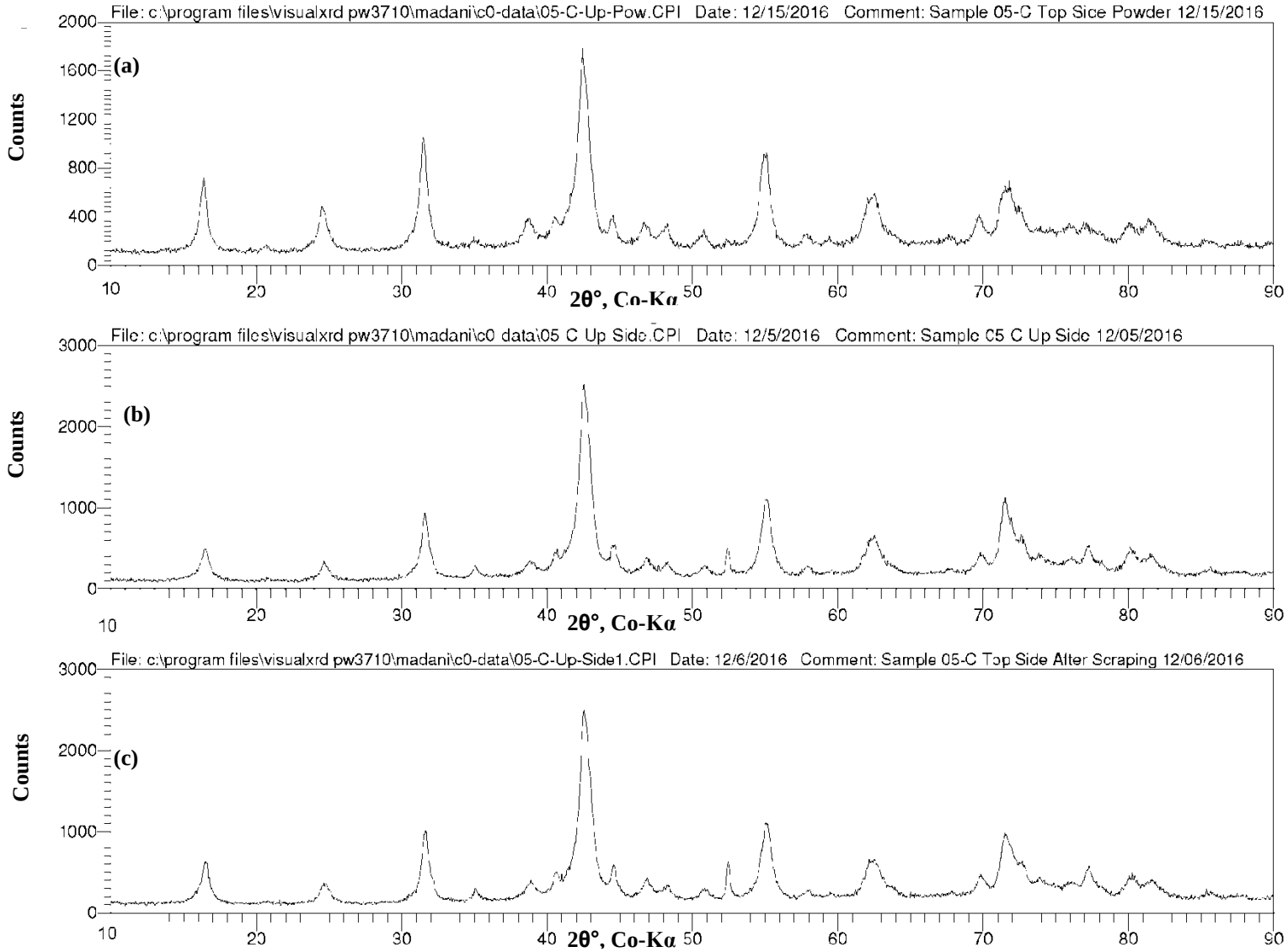

Figure B-10: XRD patterns, sample 05-C, (a) top side powder, (b) top before scraping, (c) top after scraping.

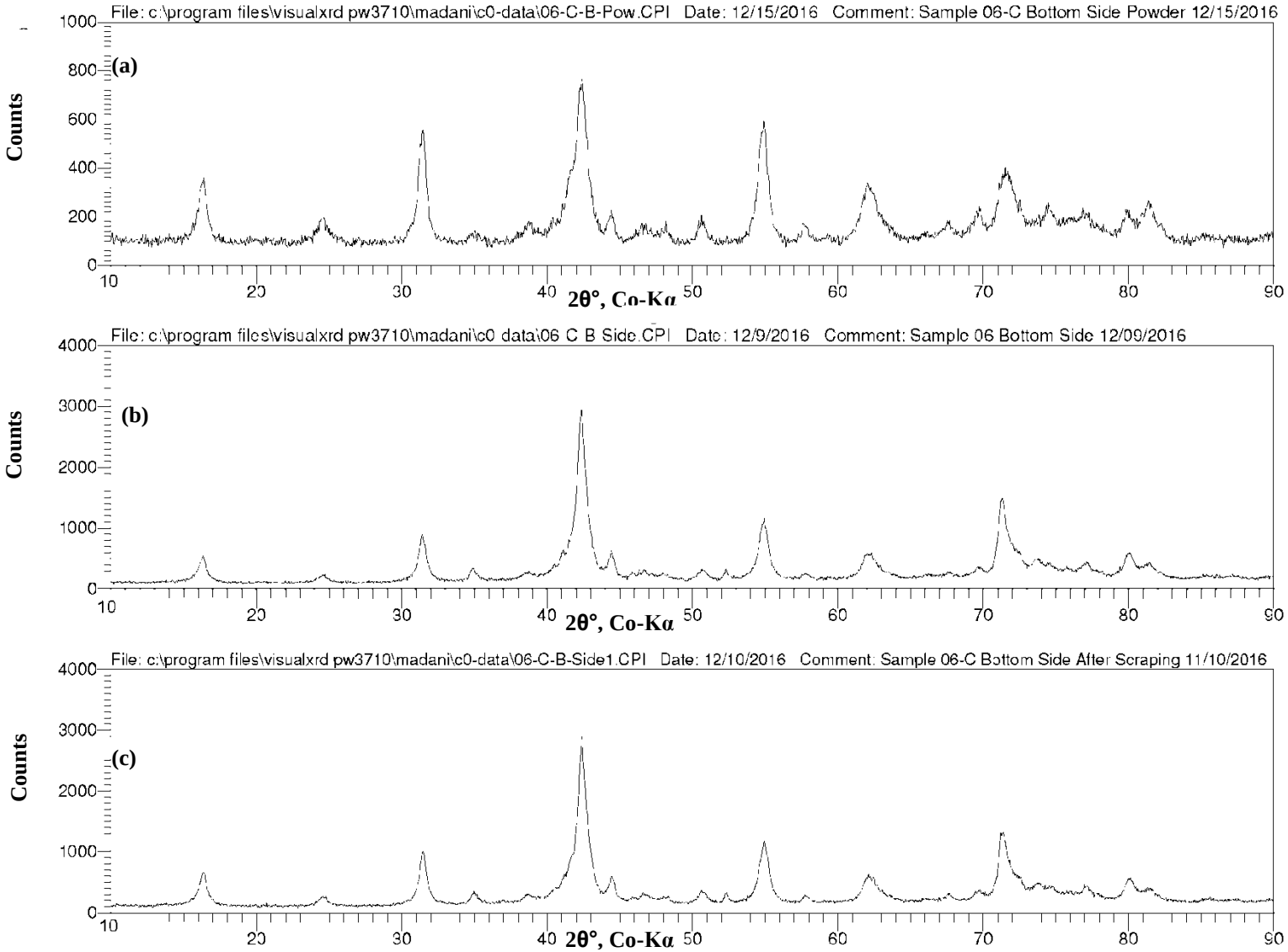

Figure B-11: XRD patterns, sample 06-C, (a) bottom side powder, (b) bottom before scraping, (c) bottom after scraping.

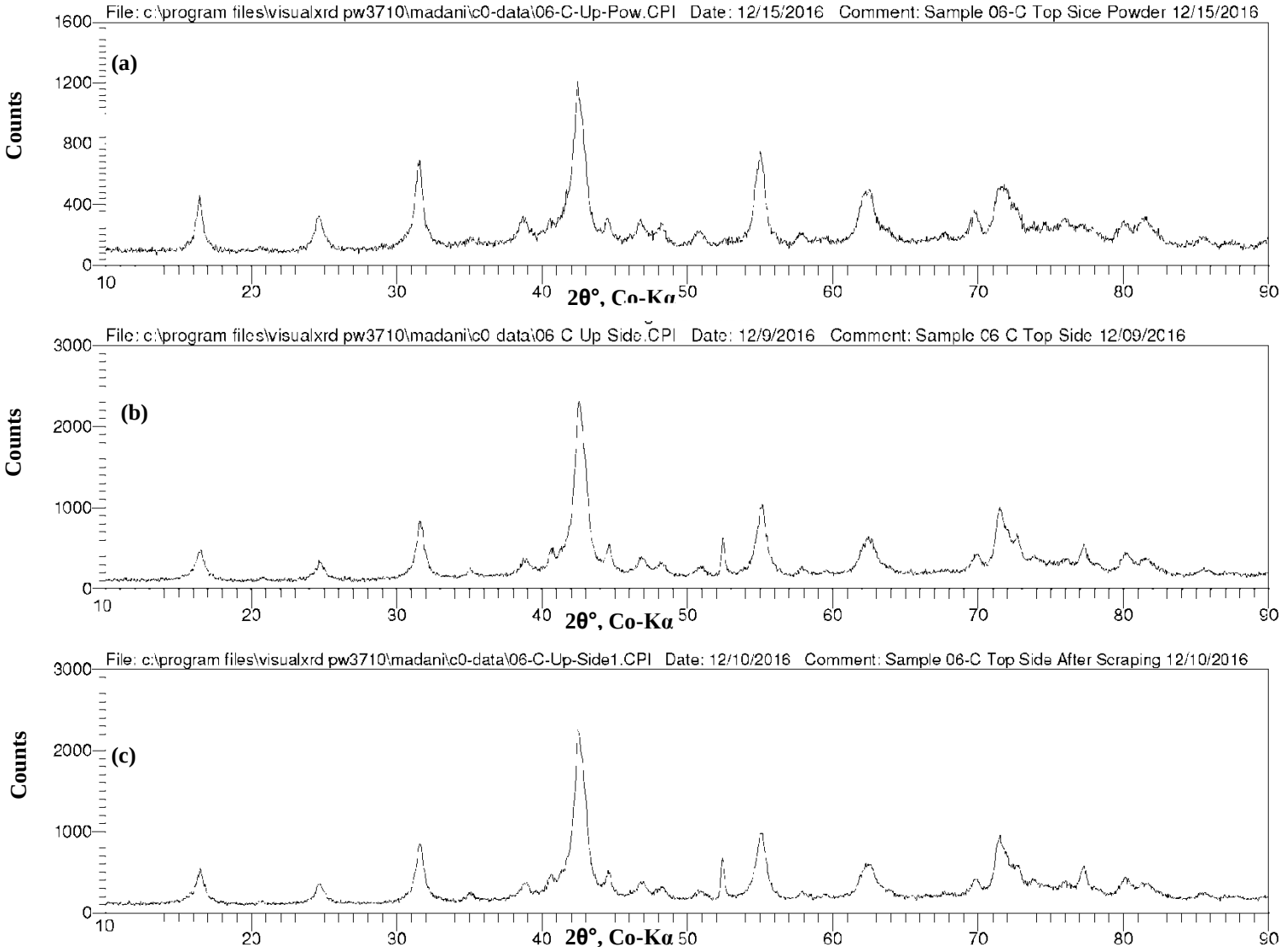

Figure B-12: XRD patterns, sample 06-C, (a) top side powder, (b) top before scraping, (c) top after scraping.

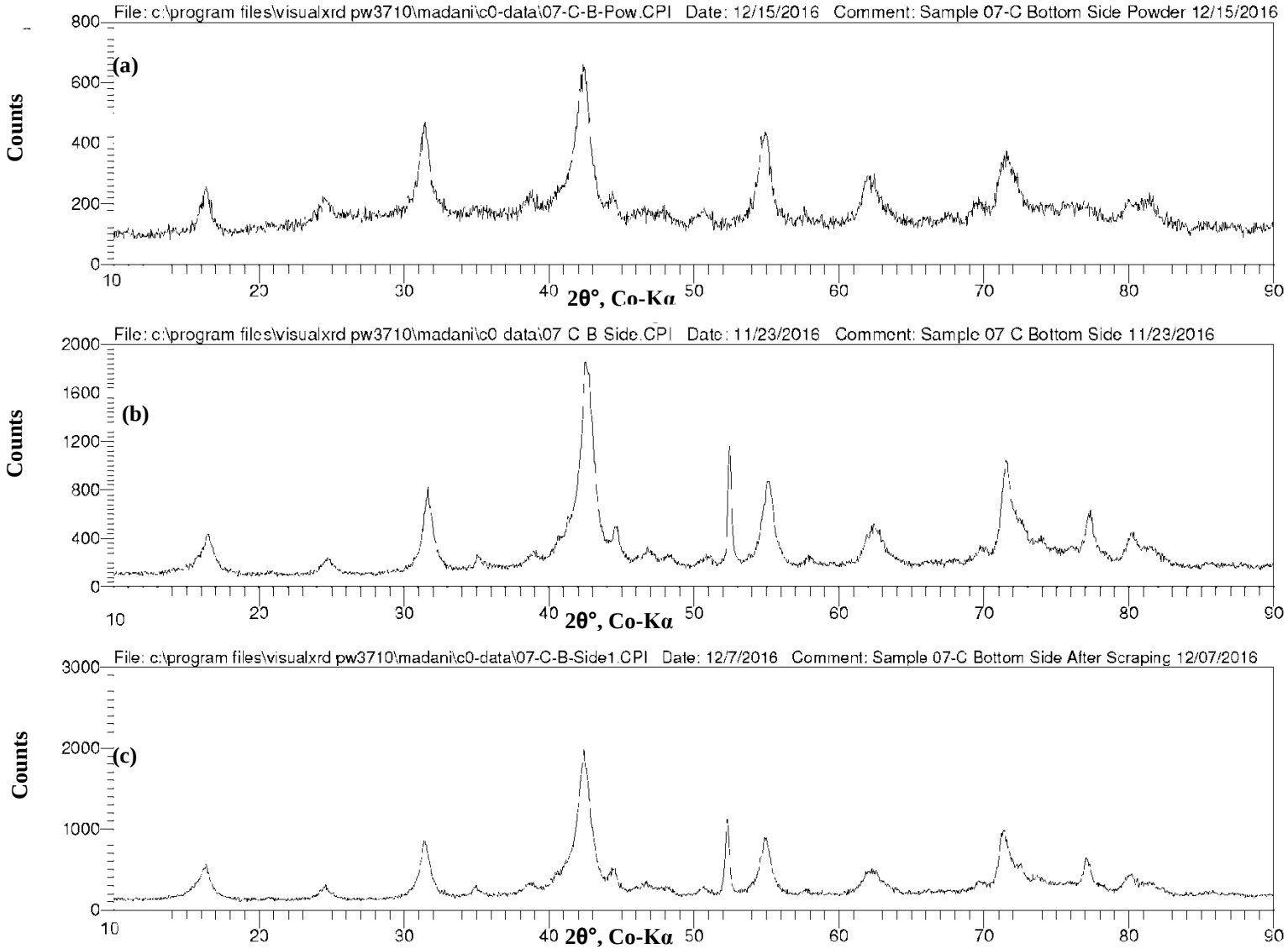

Figure B-13: XRD patterns, sample 07-C, (a) bottom side powder, (b) bottom before scraping, (c) bottom after scraping.

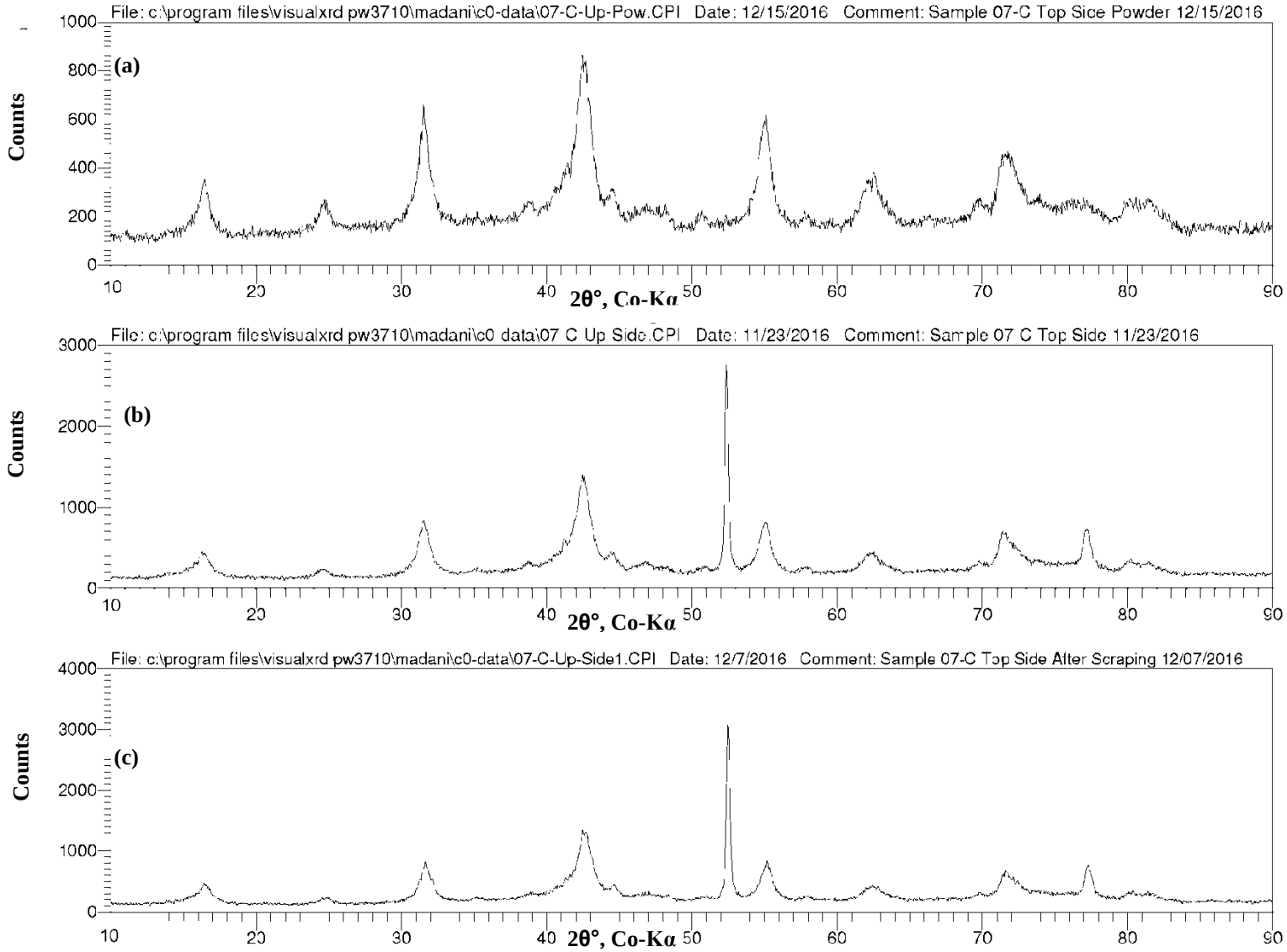

Figure B-14: XRD patterns, sample 07-C, (a) top side powder, (b) top before scraping, (c) top after scraping.

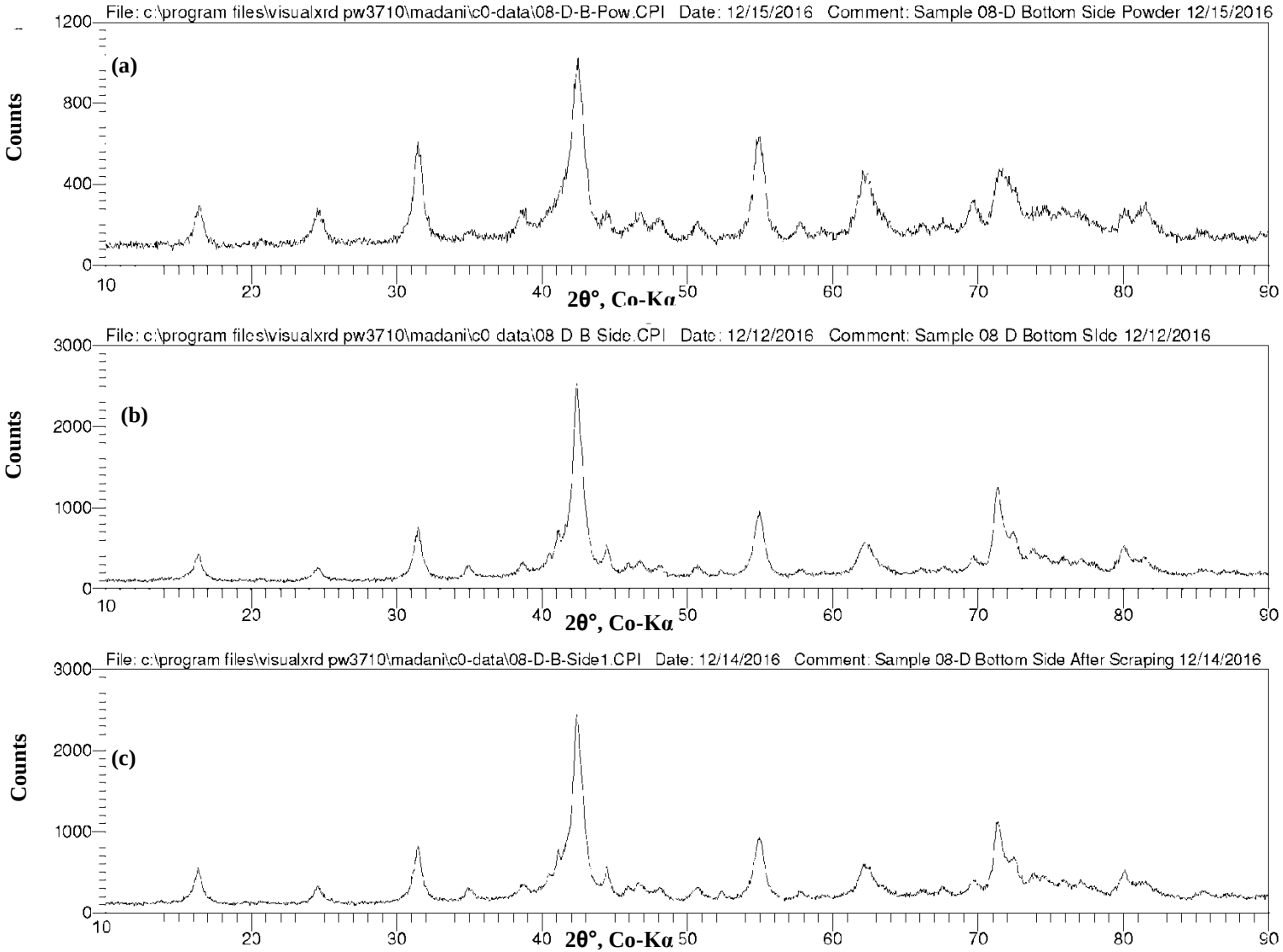

Figure B-15: XRD patterns, sample 08-D, (a) bottom side powder, (b) bottom before scraping, (c) bottom after scraping.

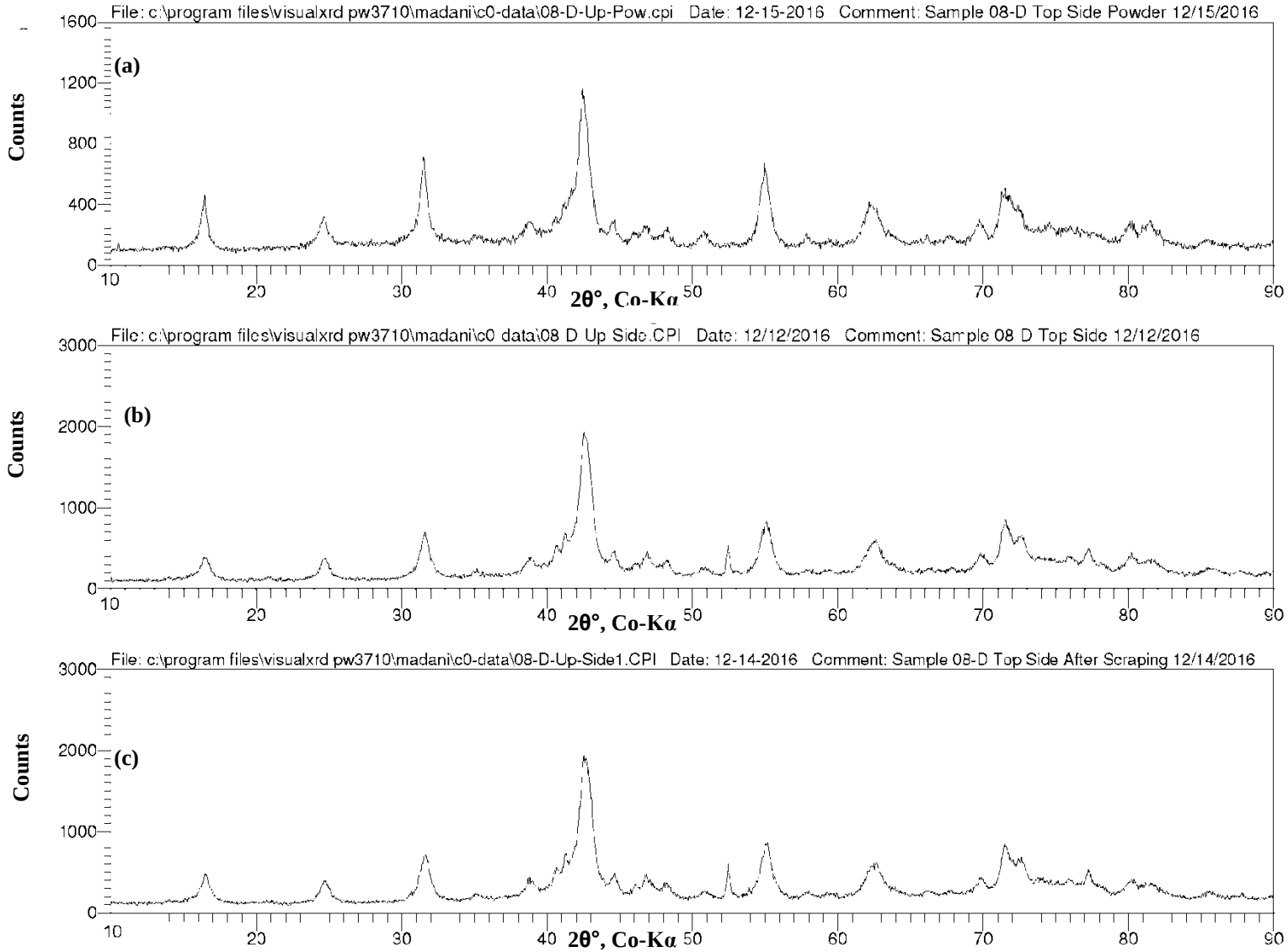

Figure B-16: XRD patterns, sample 08-D, (a) top side powder, (b) top before scraping, (c) top after scraping.

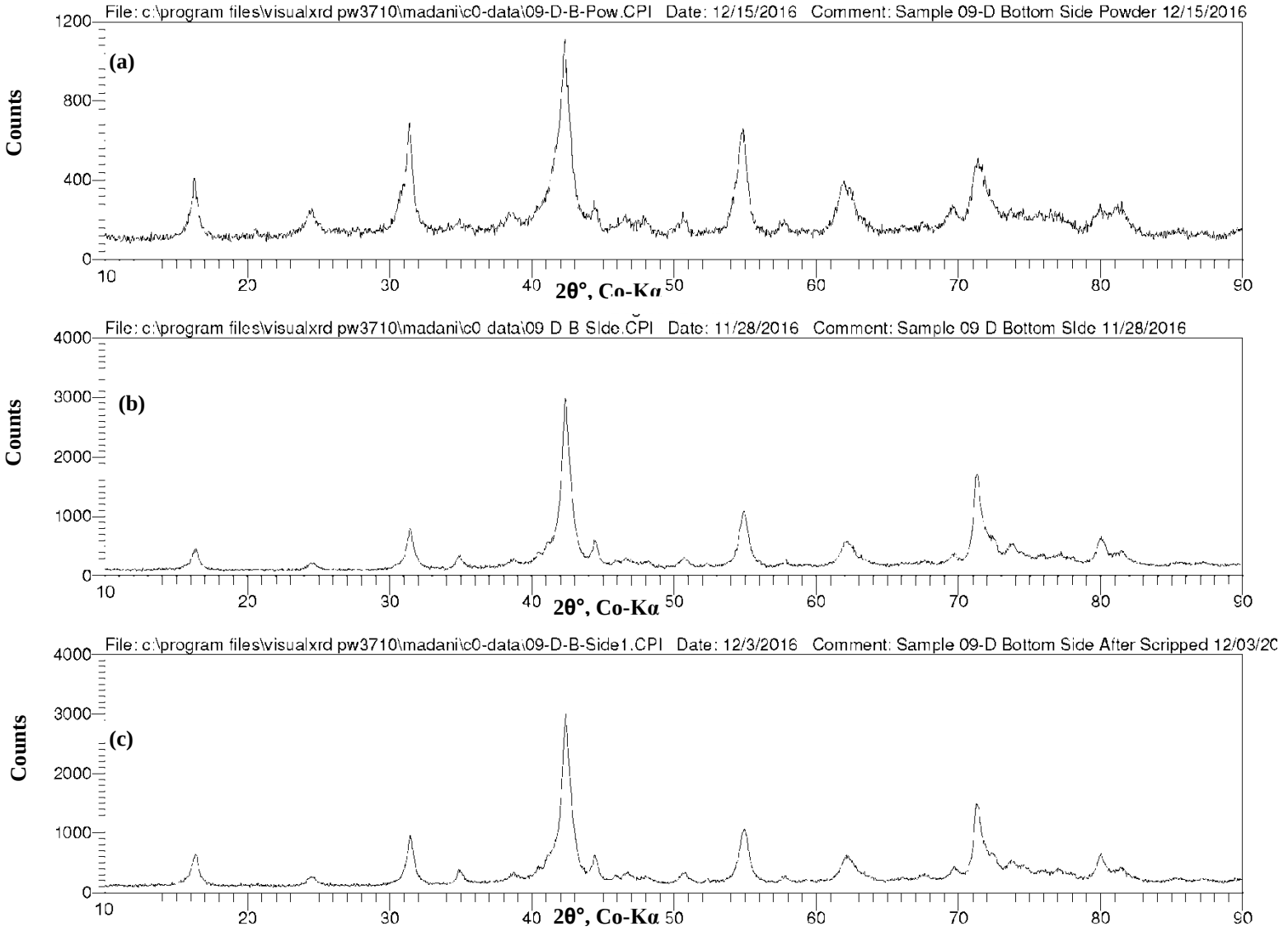

Figure B-17: XRD patterns, sample 09-D, (a) bottom side powder, (b) bottom before scraping, (c) bottom after scraping.

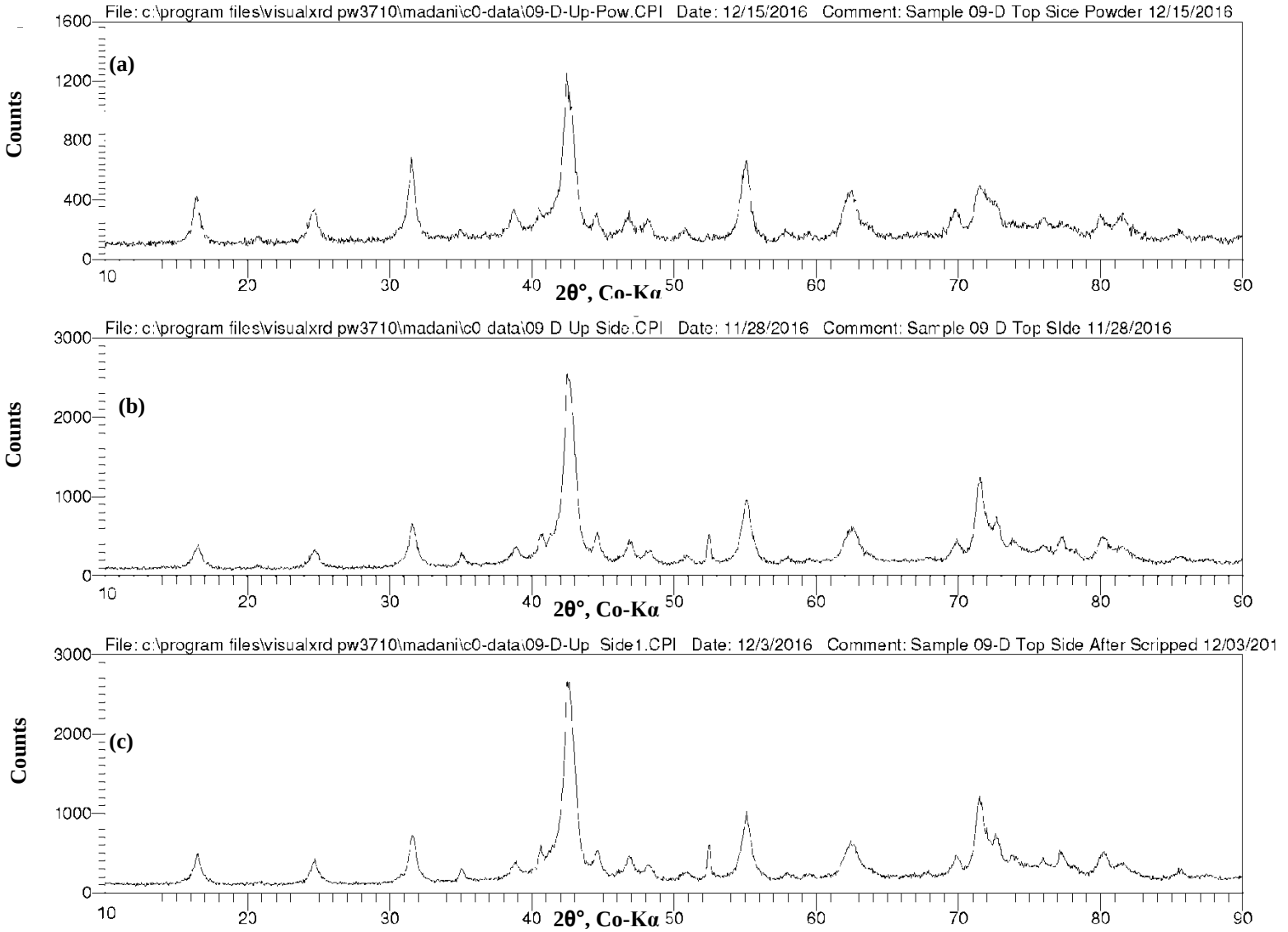

Figure B-18: XRD patterns, sample 09-D, (a) top side powder, (b) top before scraping, (c) top after scraping.

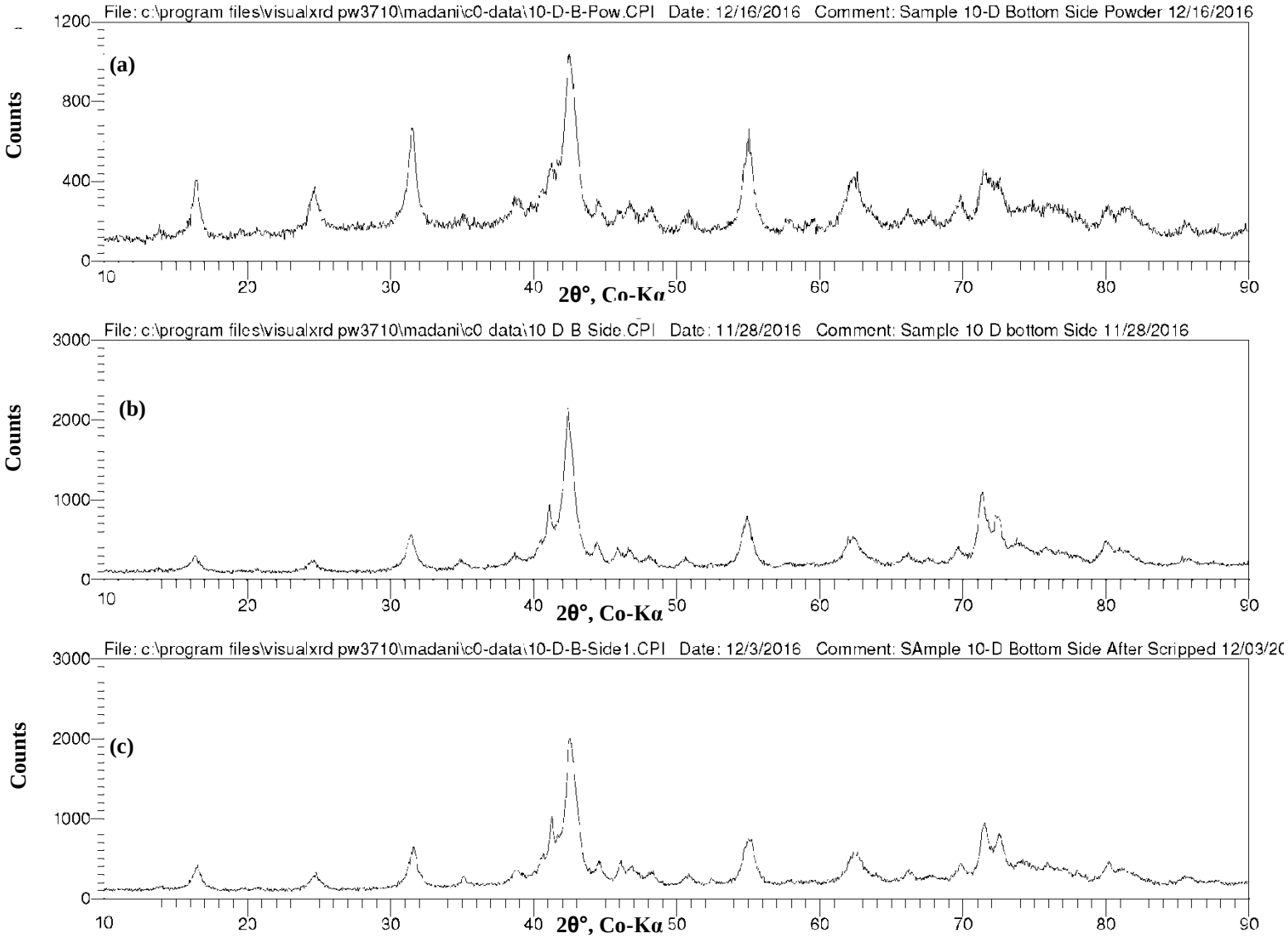

Figure B-19: XRD patterns, sample 10-D, (a) bottom side powder, (b) bottom before scraping, (c) bottom after scraping.

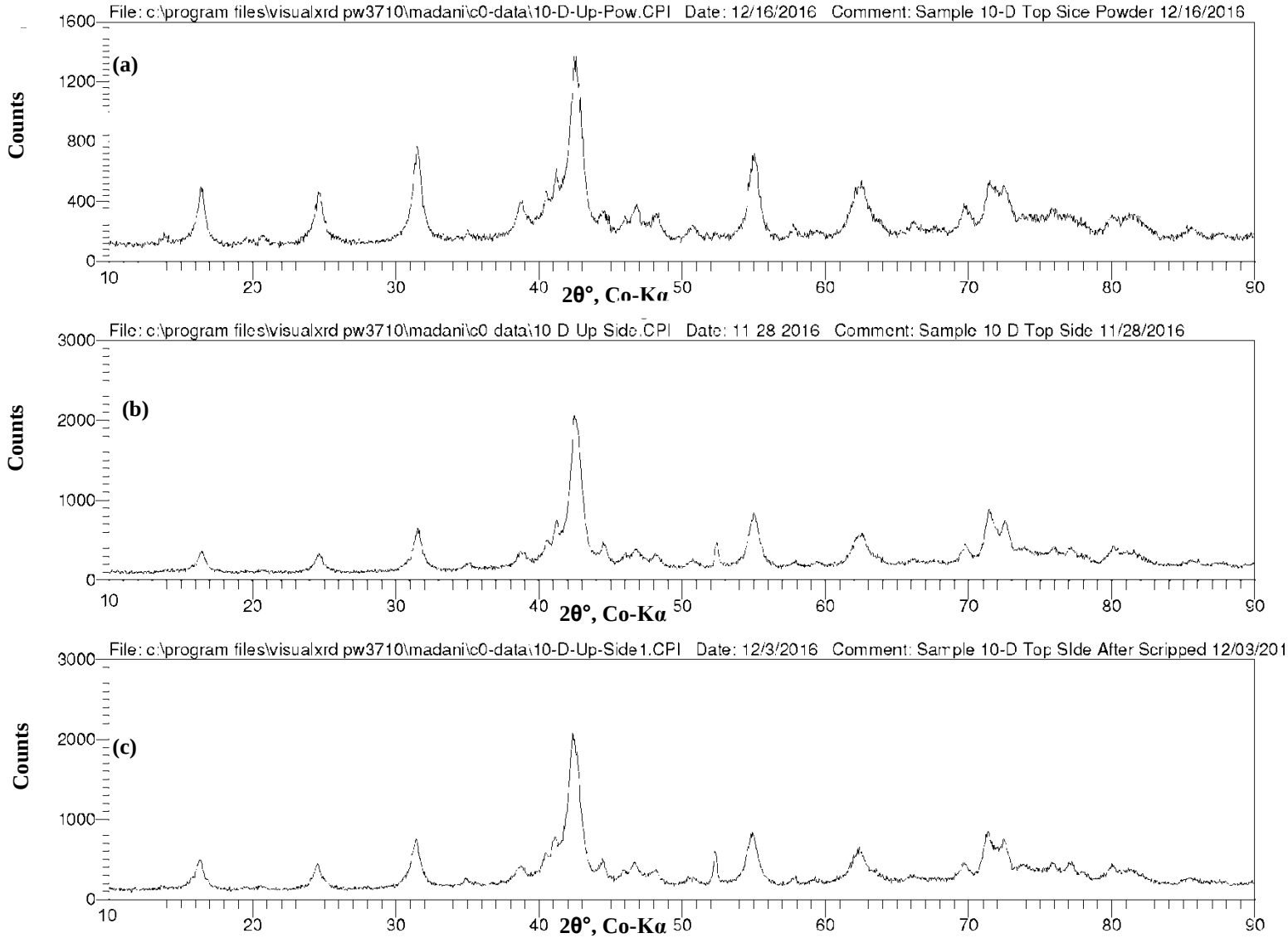

Figure B-20: XRD patterns, sample 10-D, (a) top side powder, (b) top before scraping, (c) top after scraping.

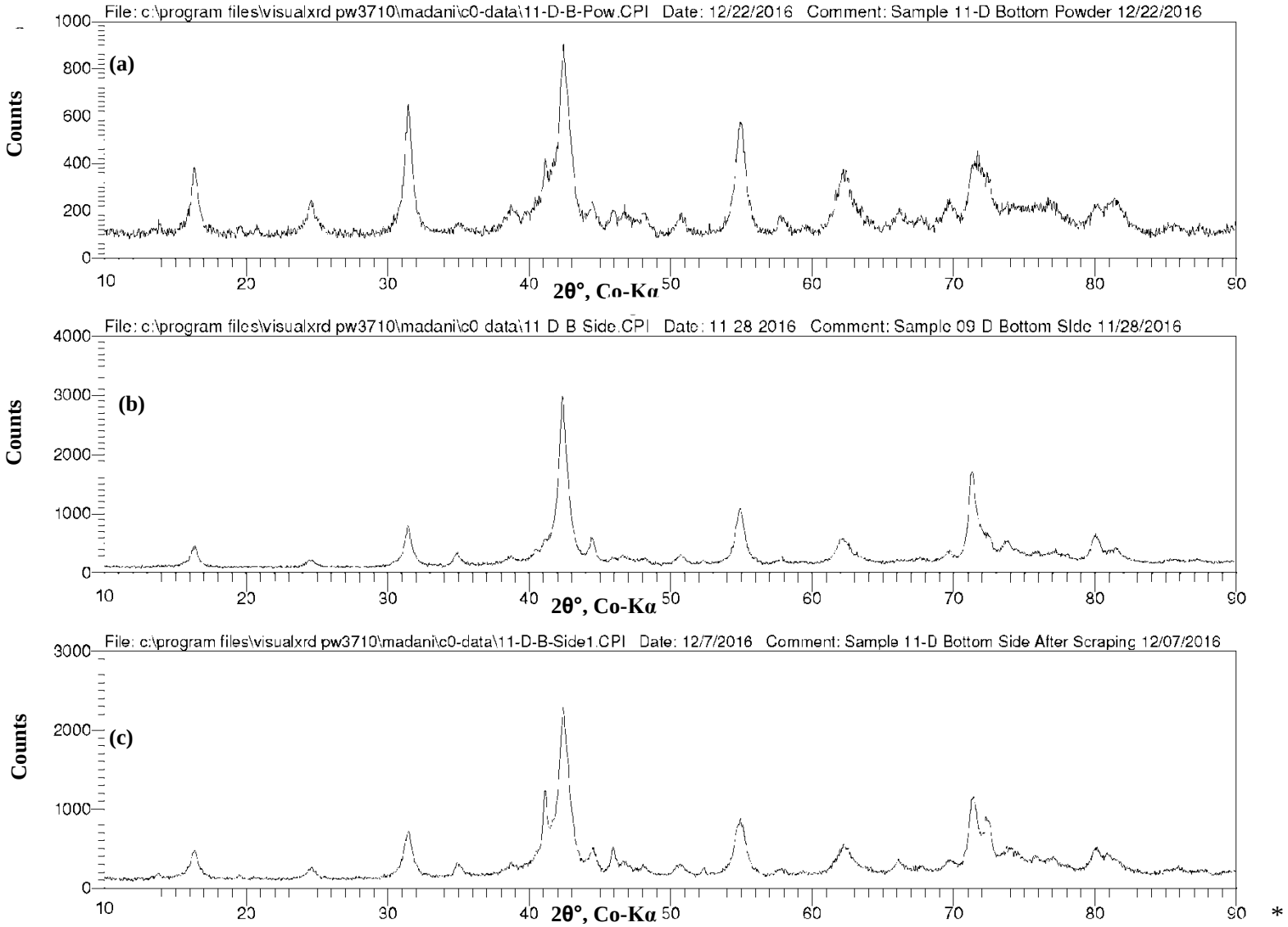

Figure B-21: XRD patterns, sample 11-D, (a) bottom side powder, (b) bottom before scraping, (c) bottom after scraping.

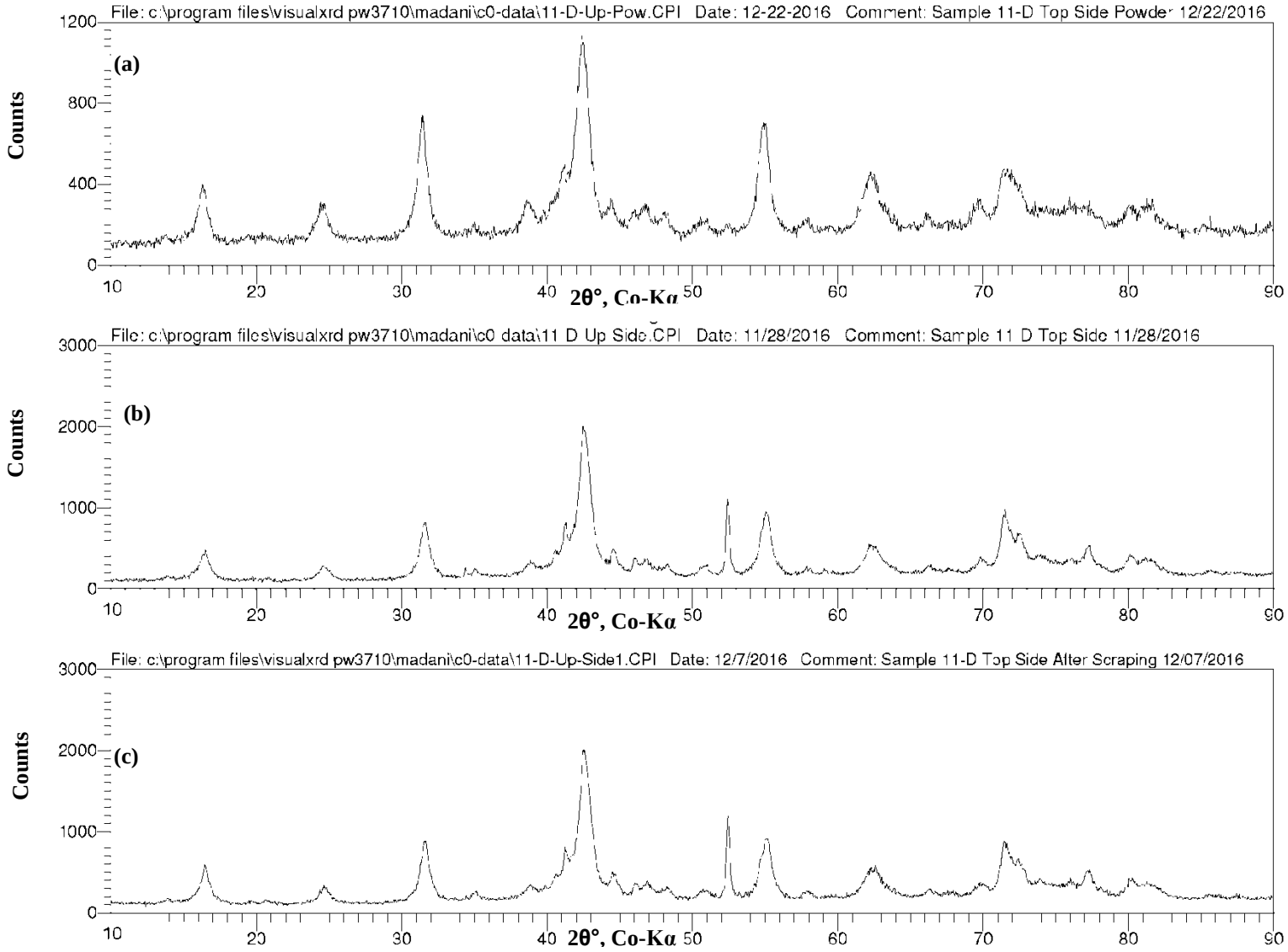

Figure B-22: XRD patterns, sample 11-D, (a) top side powder, (b) top before scraping, (c) top after scraping.

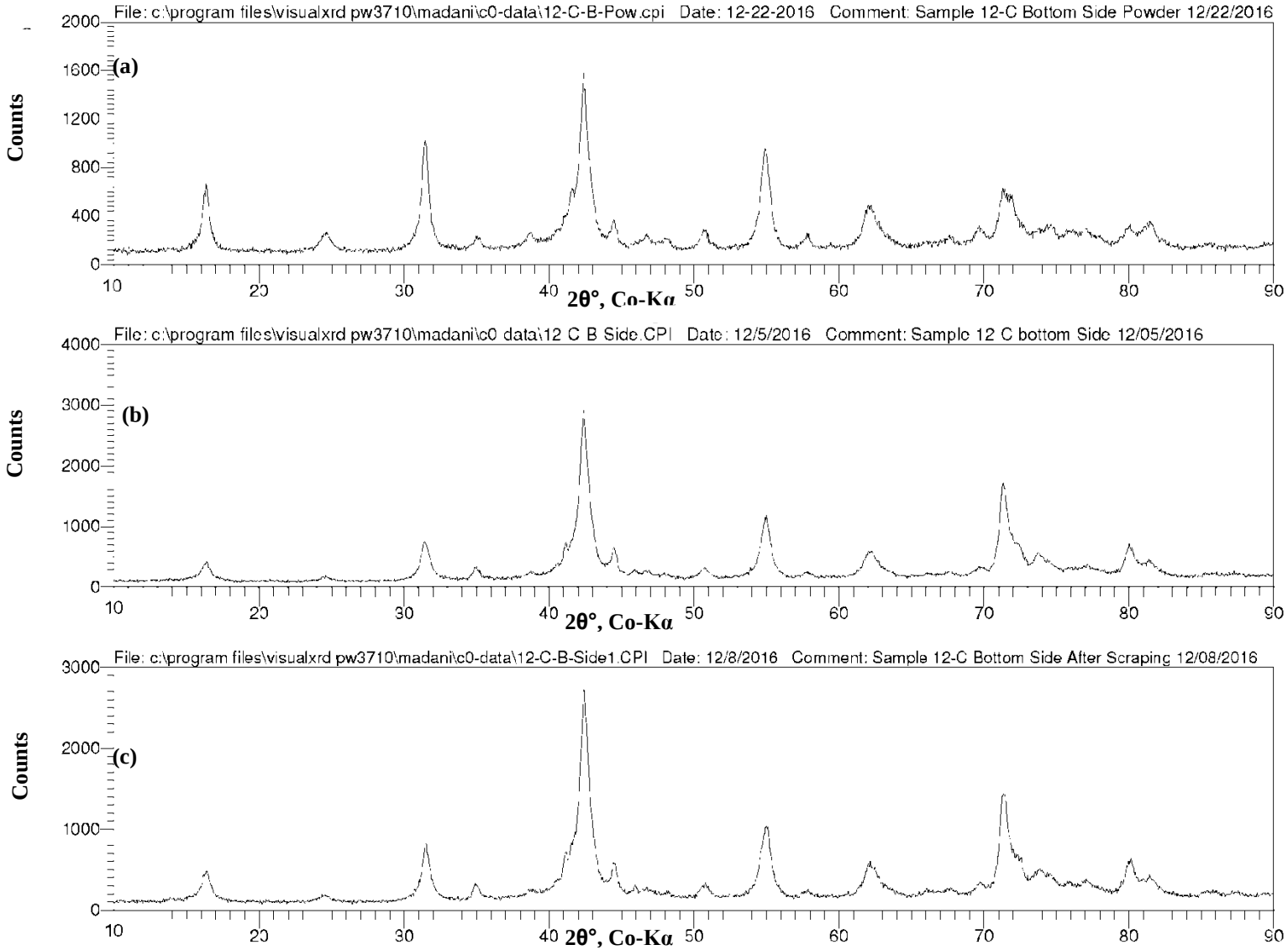

Figure B-23: XRD patterns, sample 12-C, (a) bottom side powder, (b) bottom before scraping, (c) bottom after scraping.

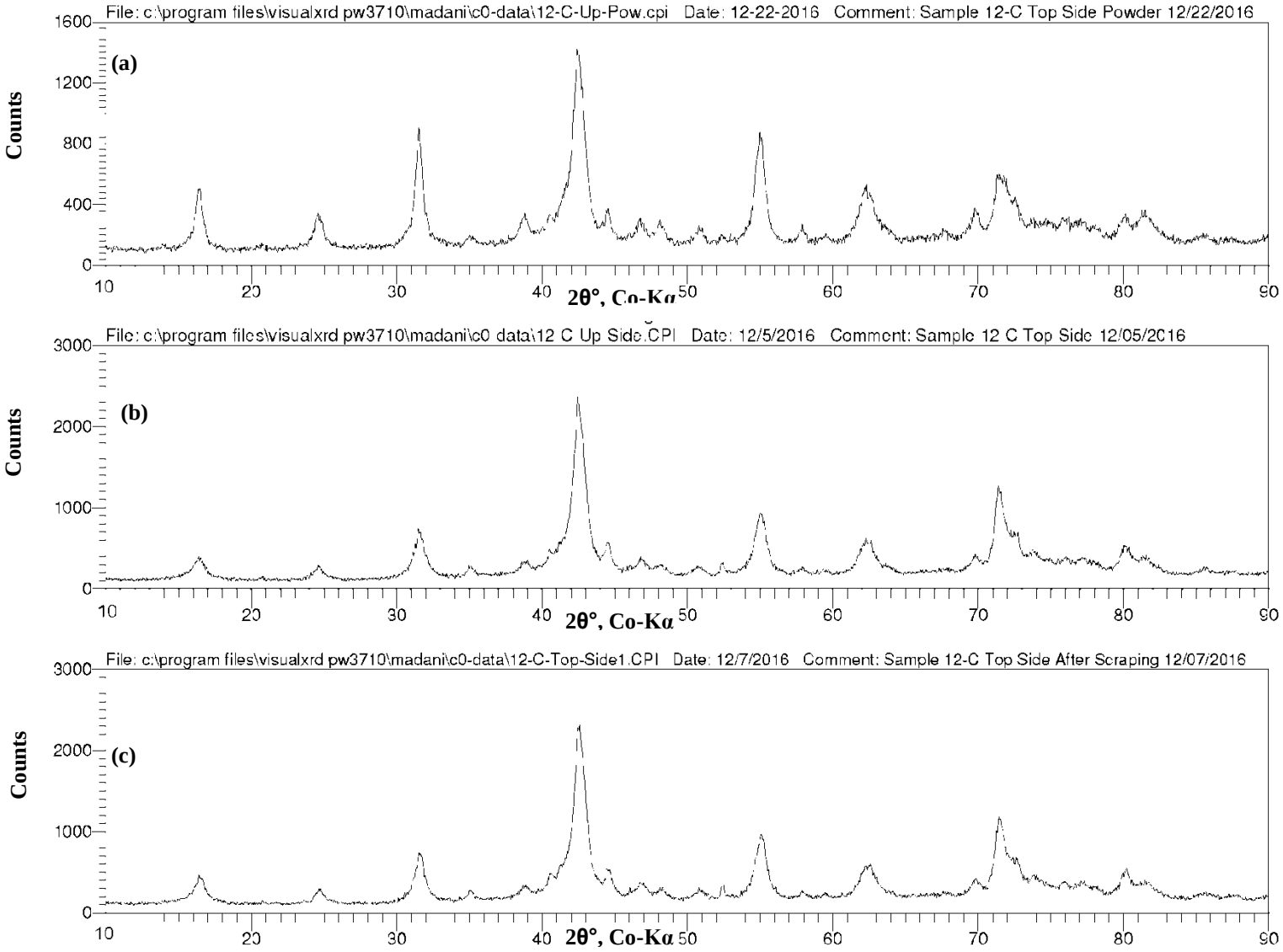

Figure B-24: XRD patterns, sample 12-C, (a) top side powder, (b) top before scraping, (c) top after scraping.

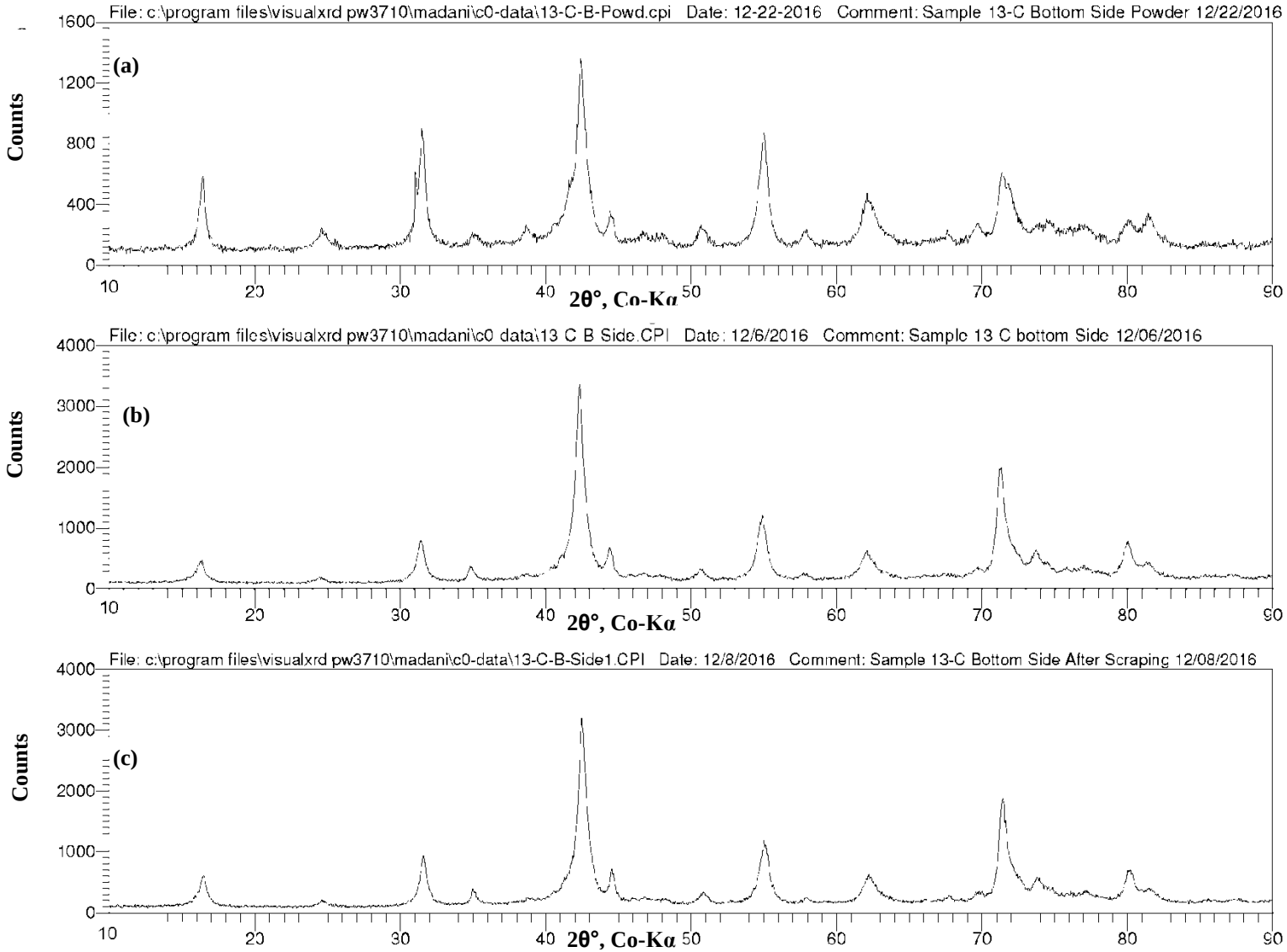

Figure B-25: XRD patterns, sample 13-C, (a) bottom side powder, (b) bottom before scraping, (c) bottom after scraping.

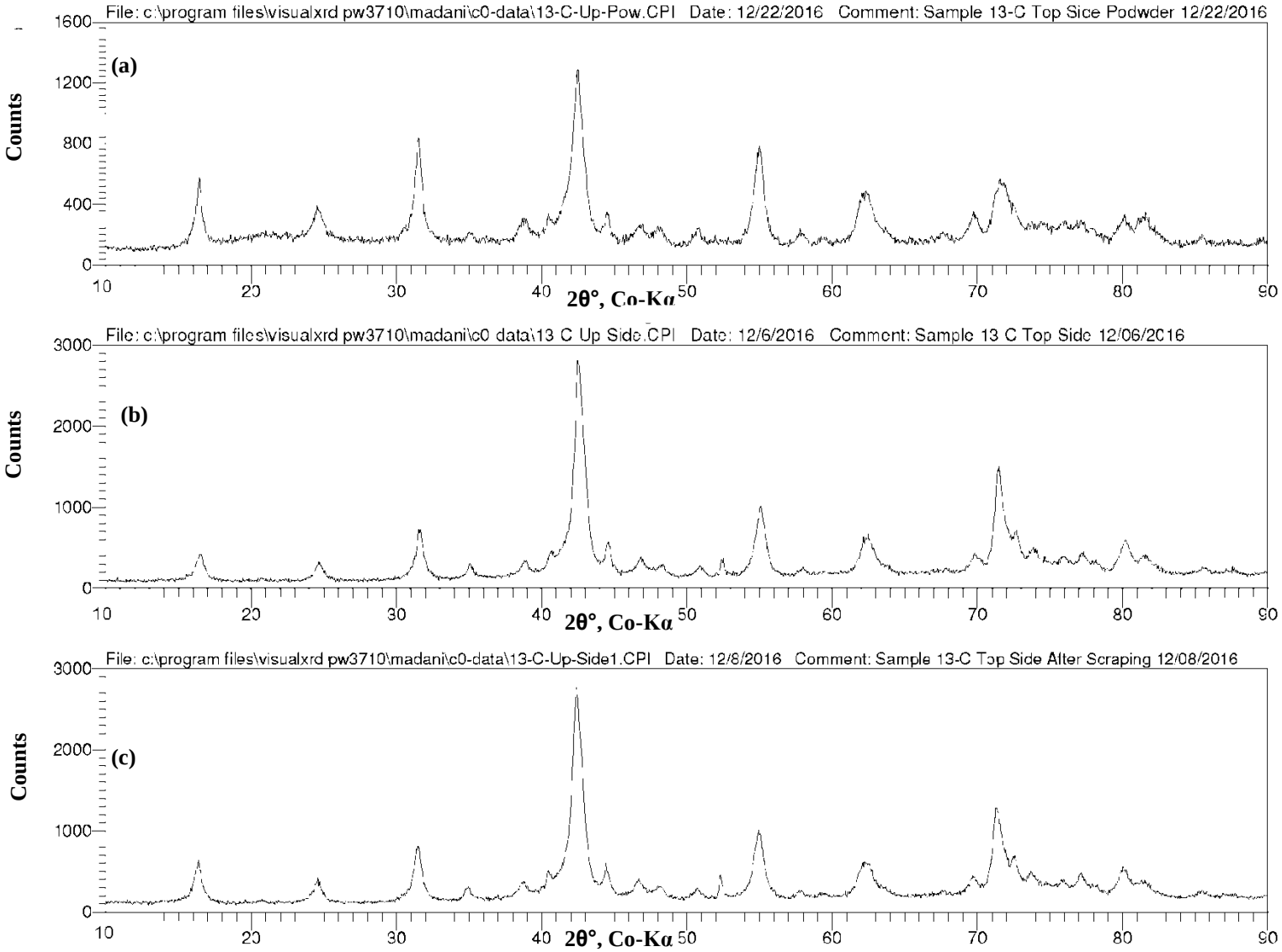

Figure B-26: XRD patterns, sample 13-C, (a) top side powder, (b) top before scraping, (c) top after scraping.

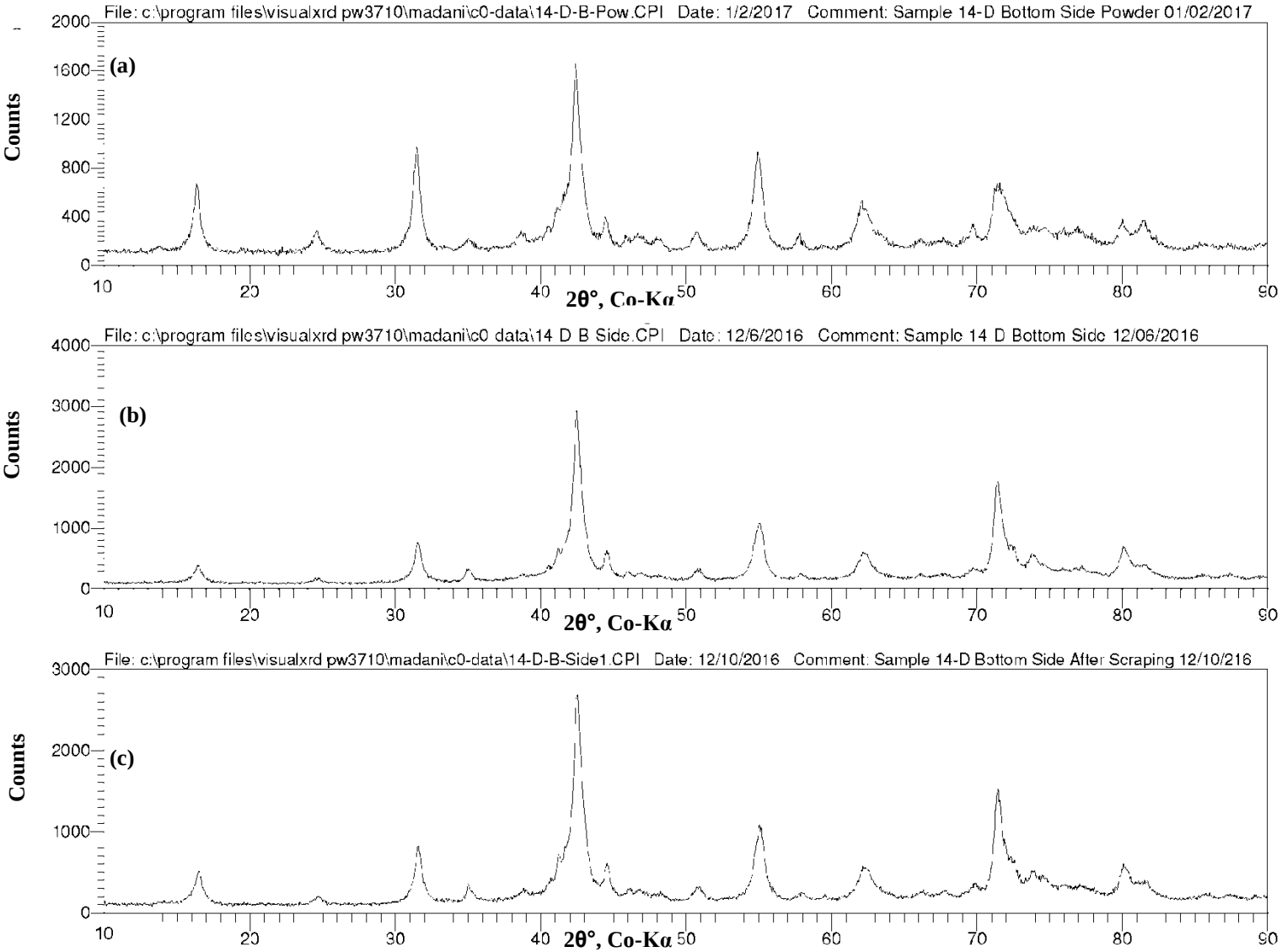

Figure B-27: XRD patterns, sample 14-D, (a) bottom side powder, (b) bottom before scraping, (c) bottom after scraping.

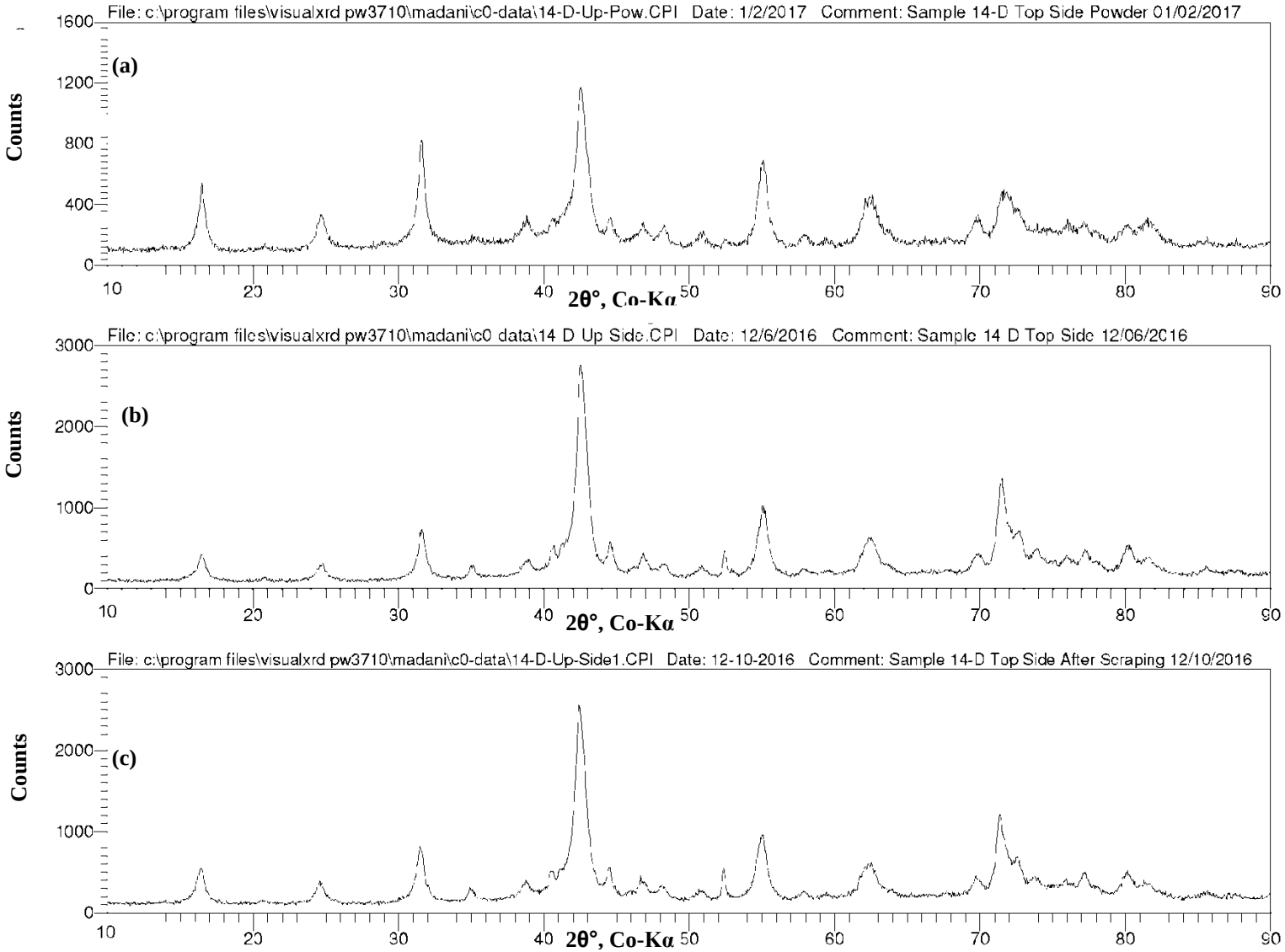

Figure B-28: XRD patterns, sample 14-D, (a) top side powder, (b) top before scraping, (c) top after scraping.

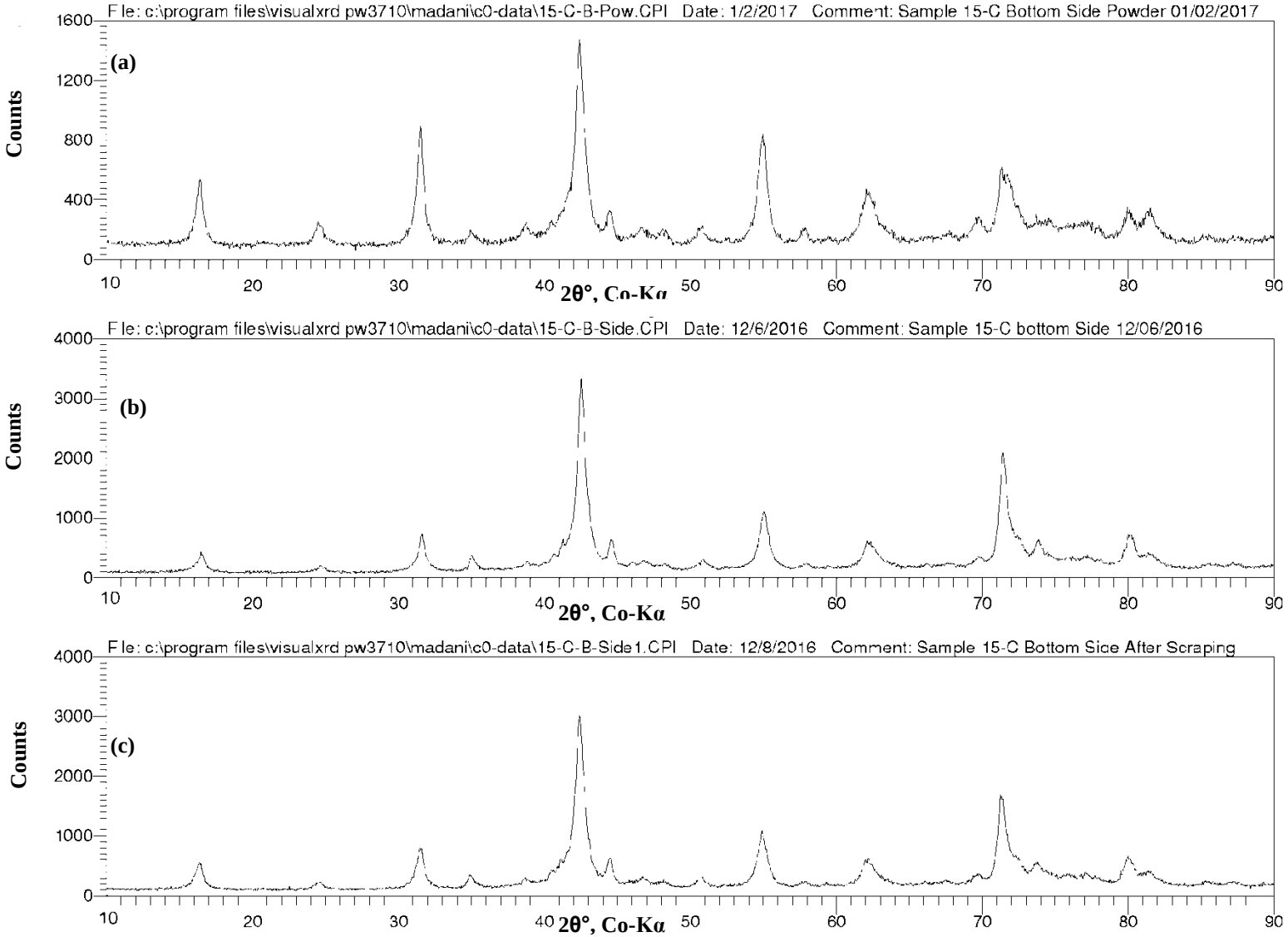

Figure B-29: XRD patterns, sample 15-C, (a) bottom side powder, (b) bottom before scraping, (c) bottom after scraping.

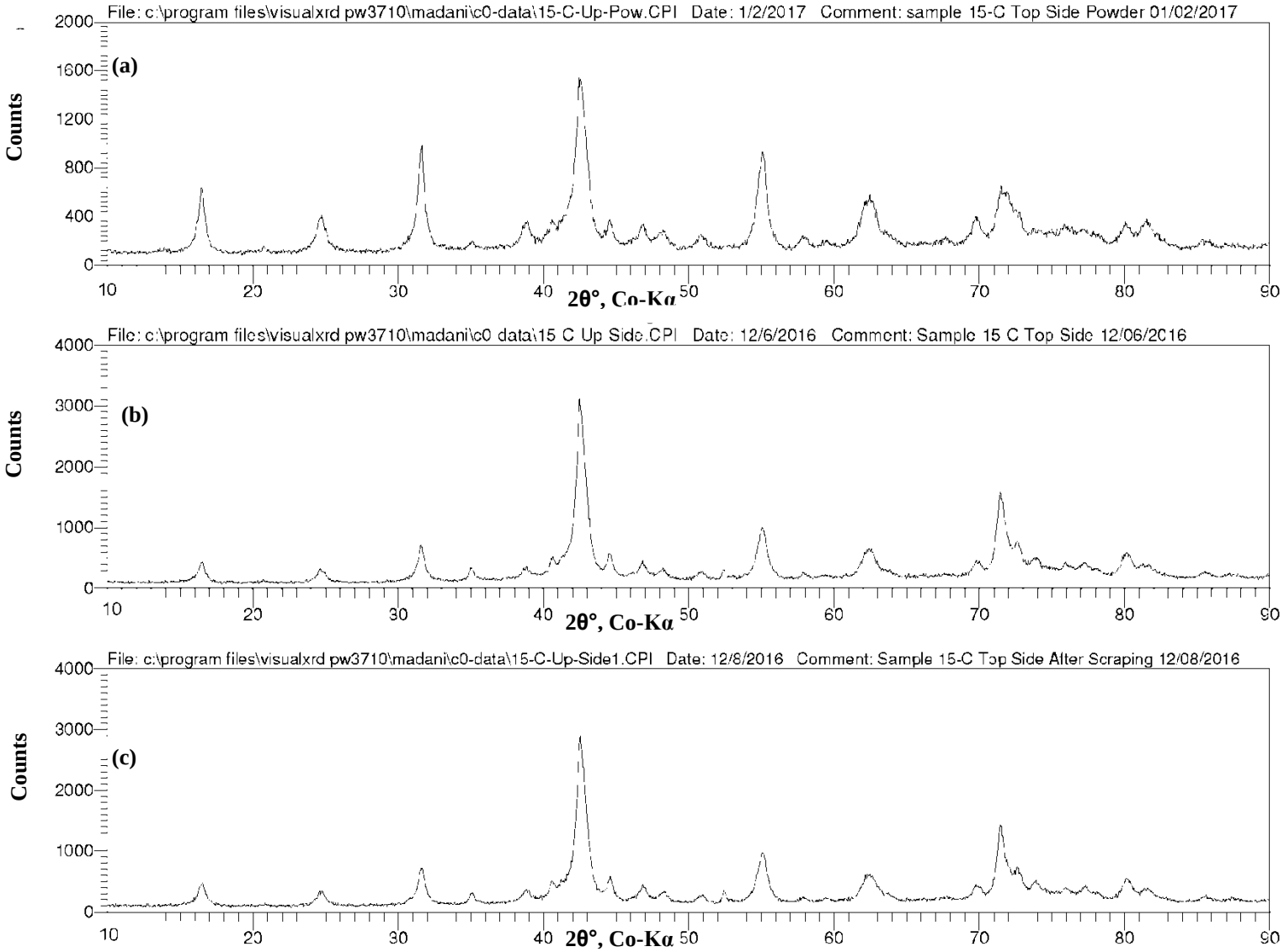

Figure B-30: XRD patterns, sample 15-C, (a) top side powder, (b) top before scraping, (c) top after scraping.

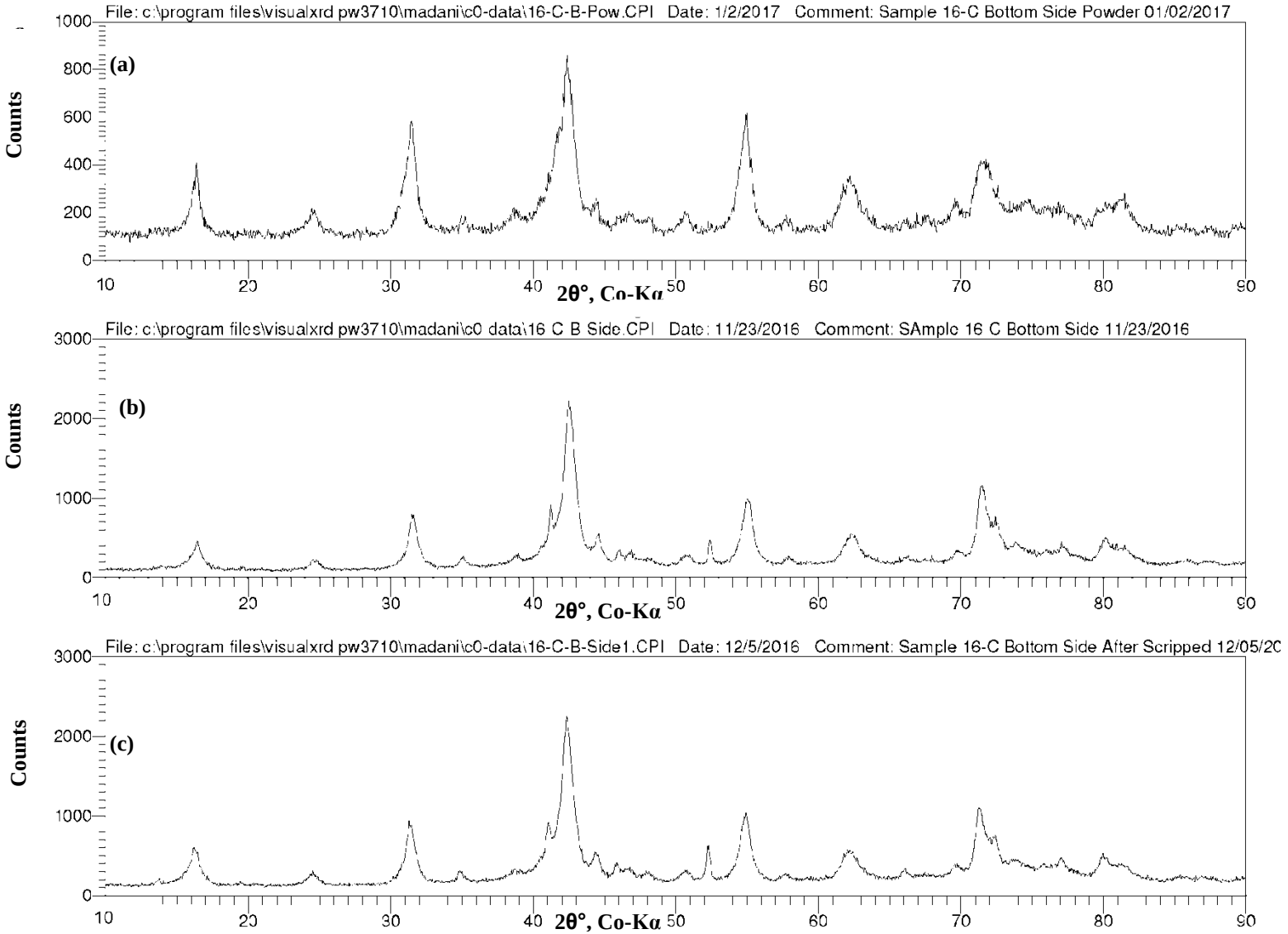

Figure B-31: XRD patterns, sample 16-C, (a) bottom side powder, (b) bottom before scraping, (c) bottom after scraping.

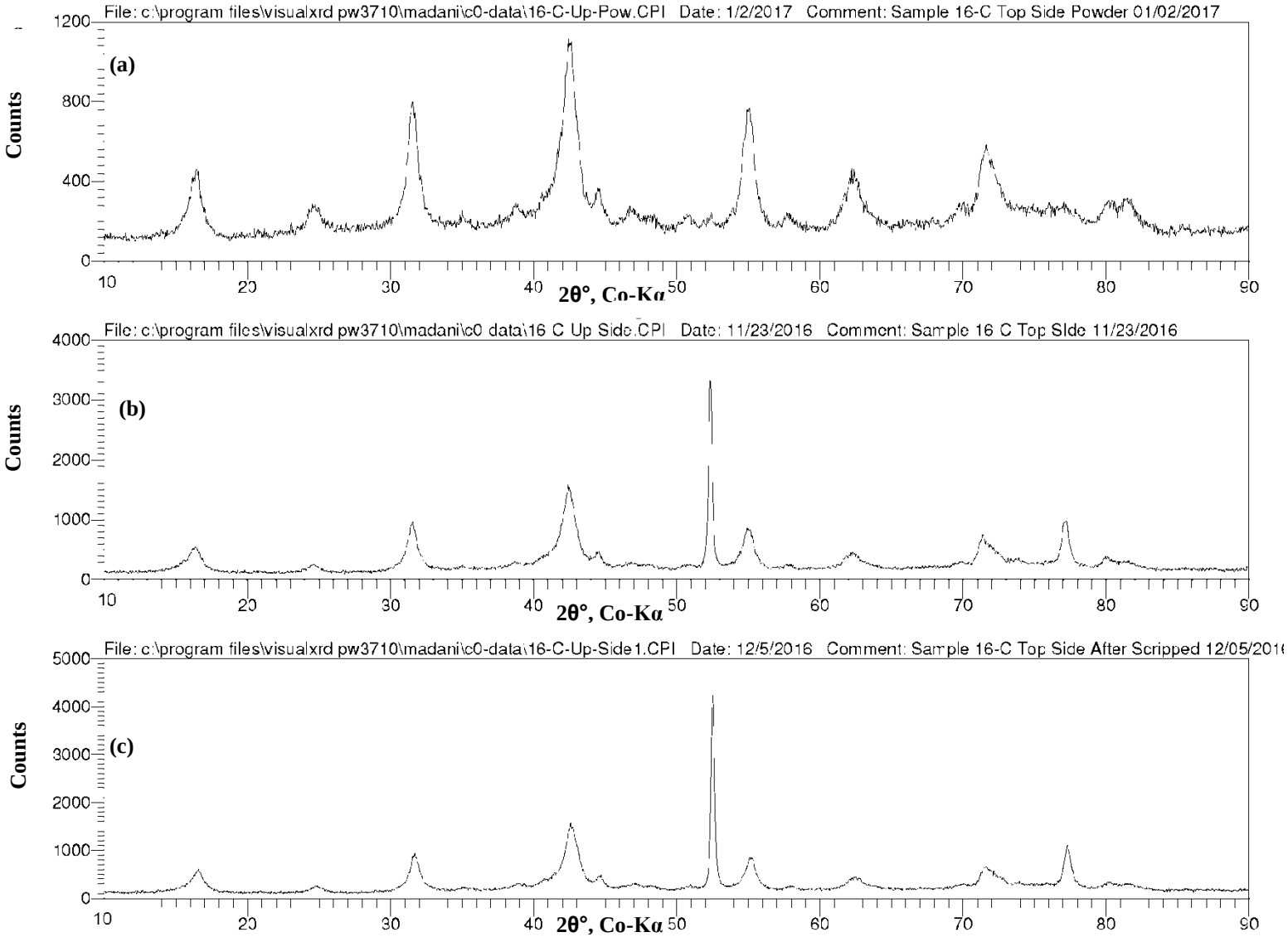

Figure B-32: XRD patterns, sample 16-C, (a) top side powder, (b) top before scraping, (c) top after scraping.

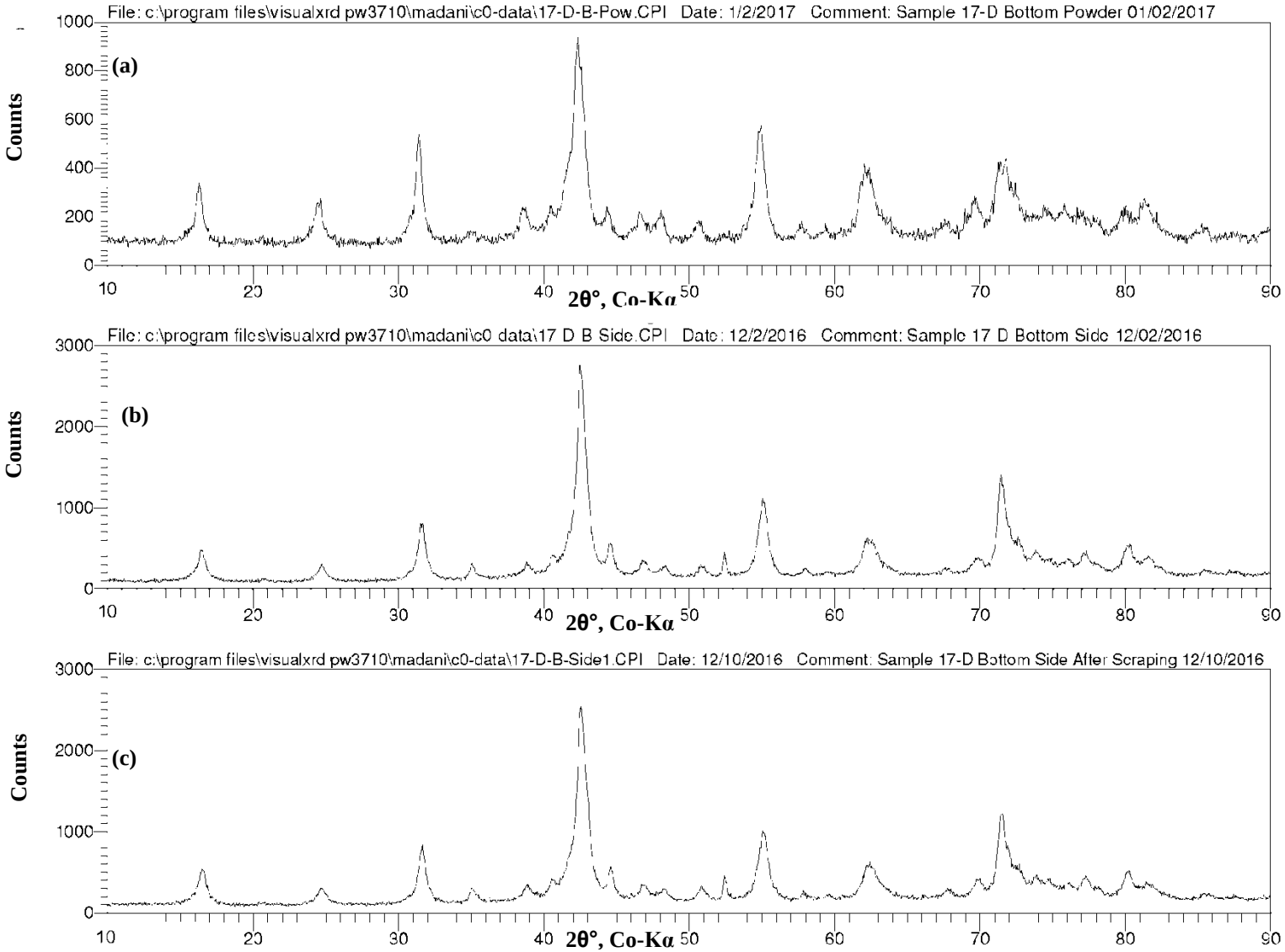

Figure B-33: XRD patterns, sample 17-D, (a) bottom side powder, (b) bottom before scraping, (c) bottom after scraping.

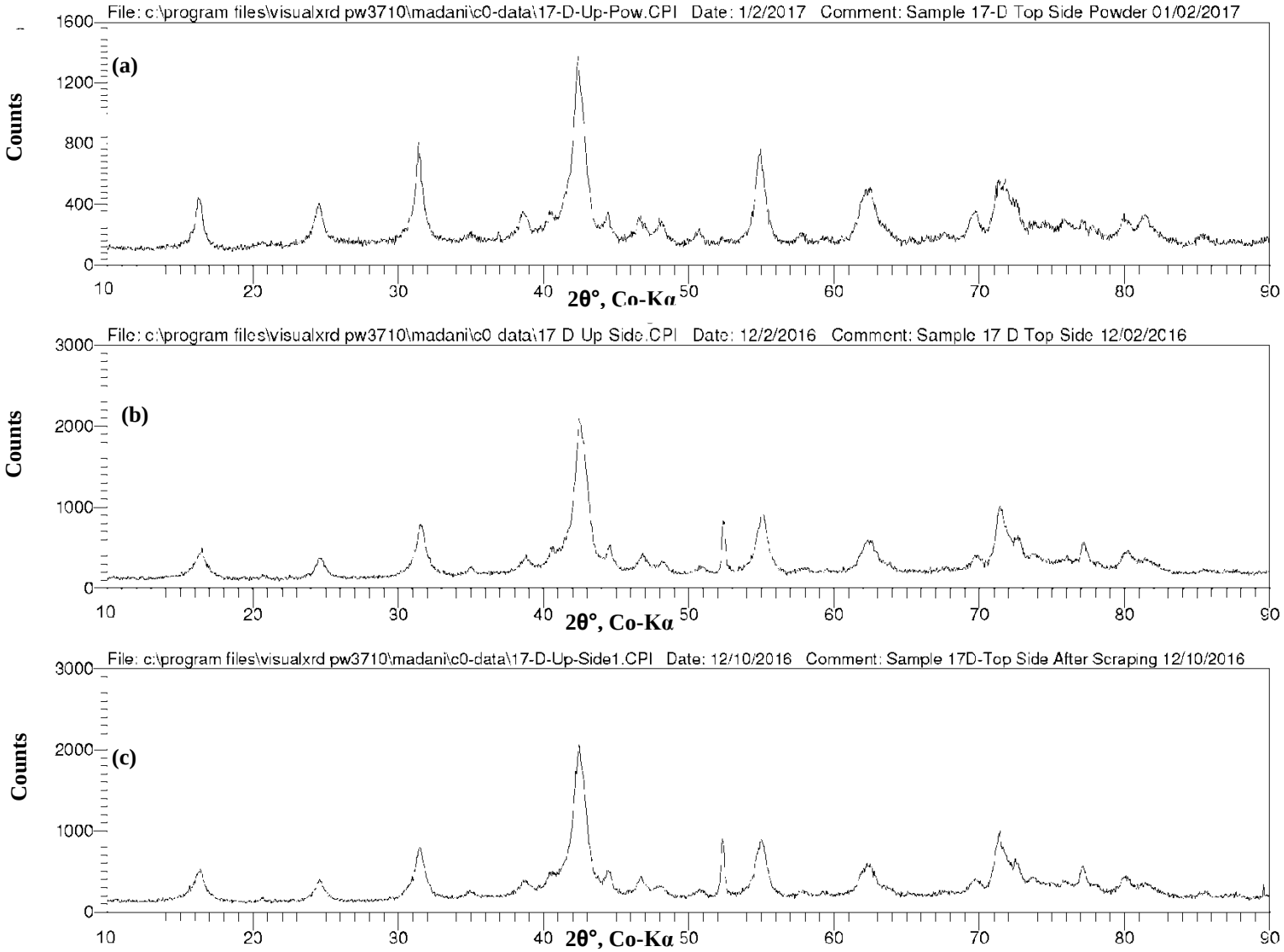

Figure B-34: XRD patterns, sample 17-D, (a) top side powder, (b) top before scraping, (c) top after scraping.

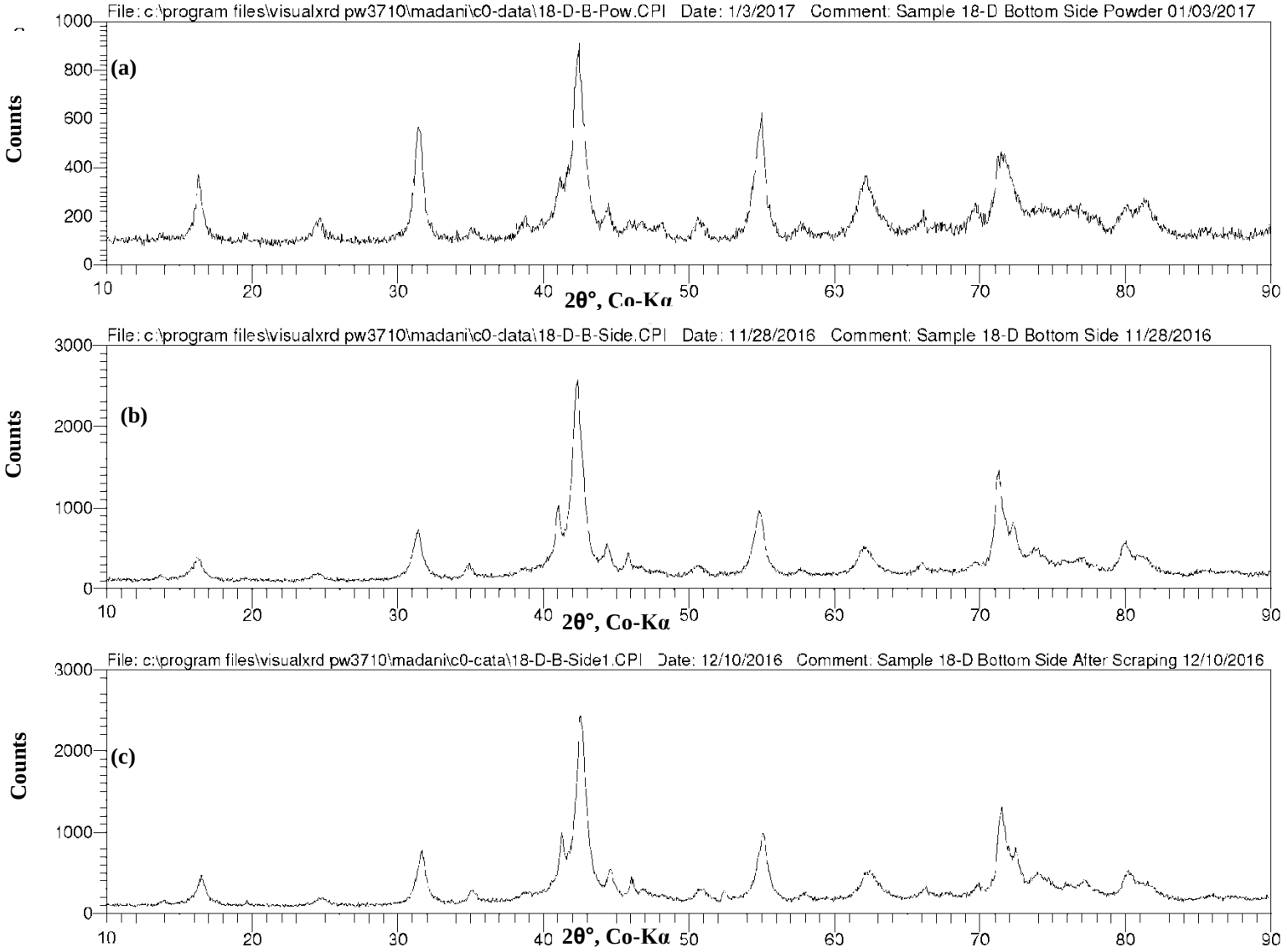

Figure B-35: XRD patterns, sample 18-D, (a) bottom side powder, (b) bottom before scraping, (c) bottom after scraping.

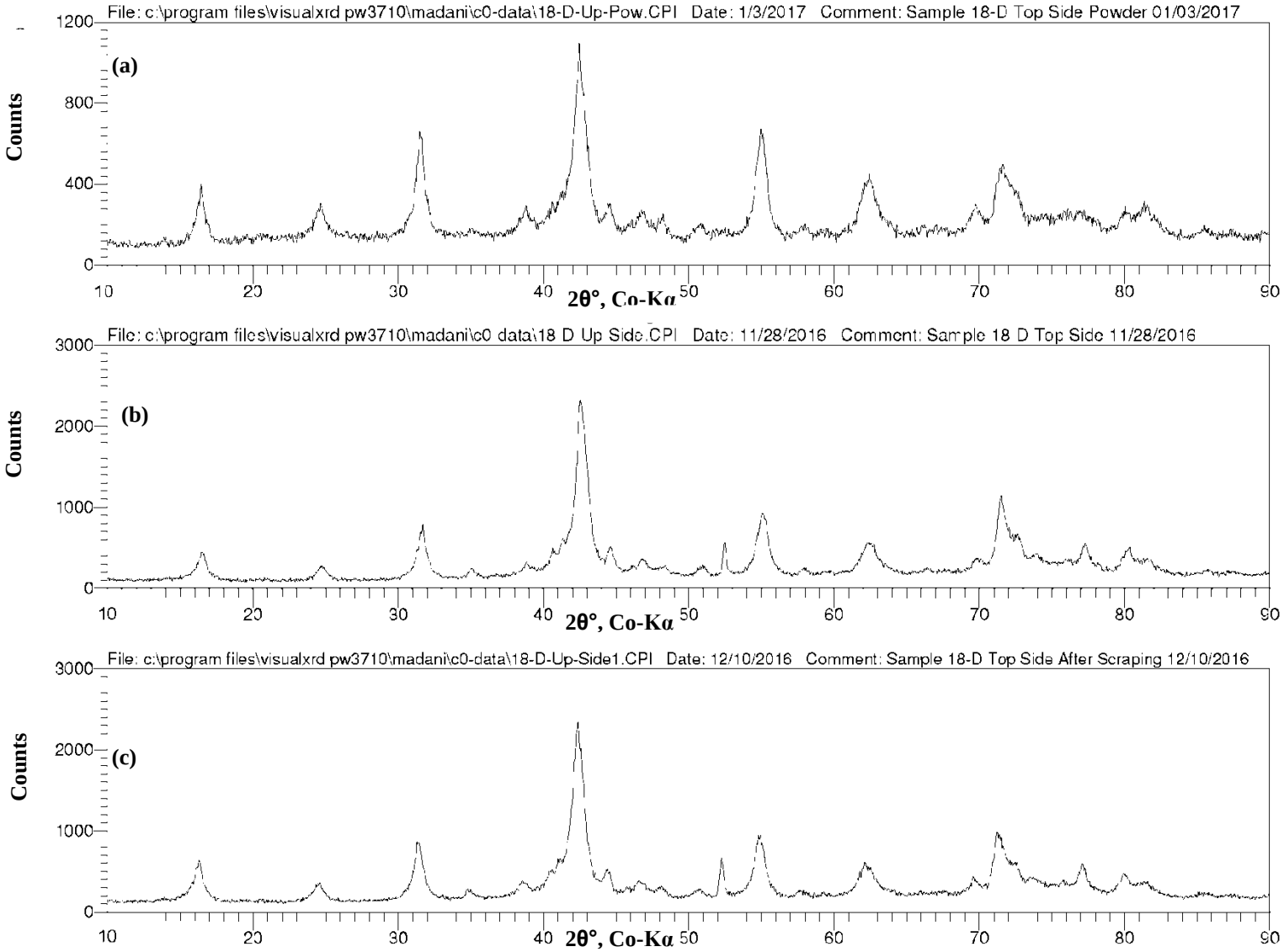

Figure B-36: XRD patterns, sample 18-D, (a) top side powder, (b) top before scraping, (c) top after scraping.

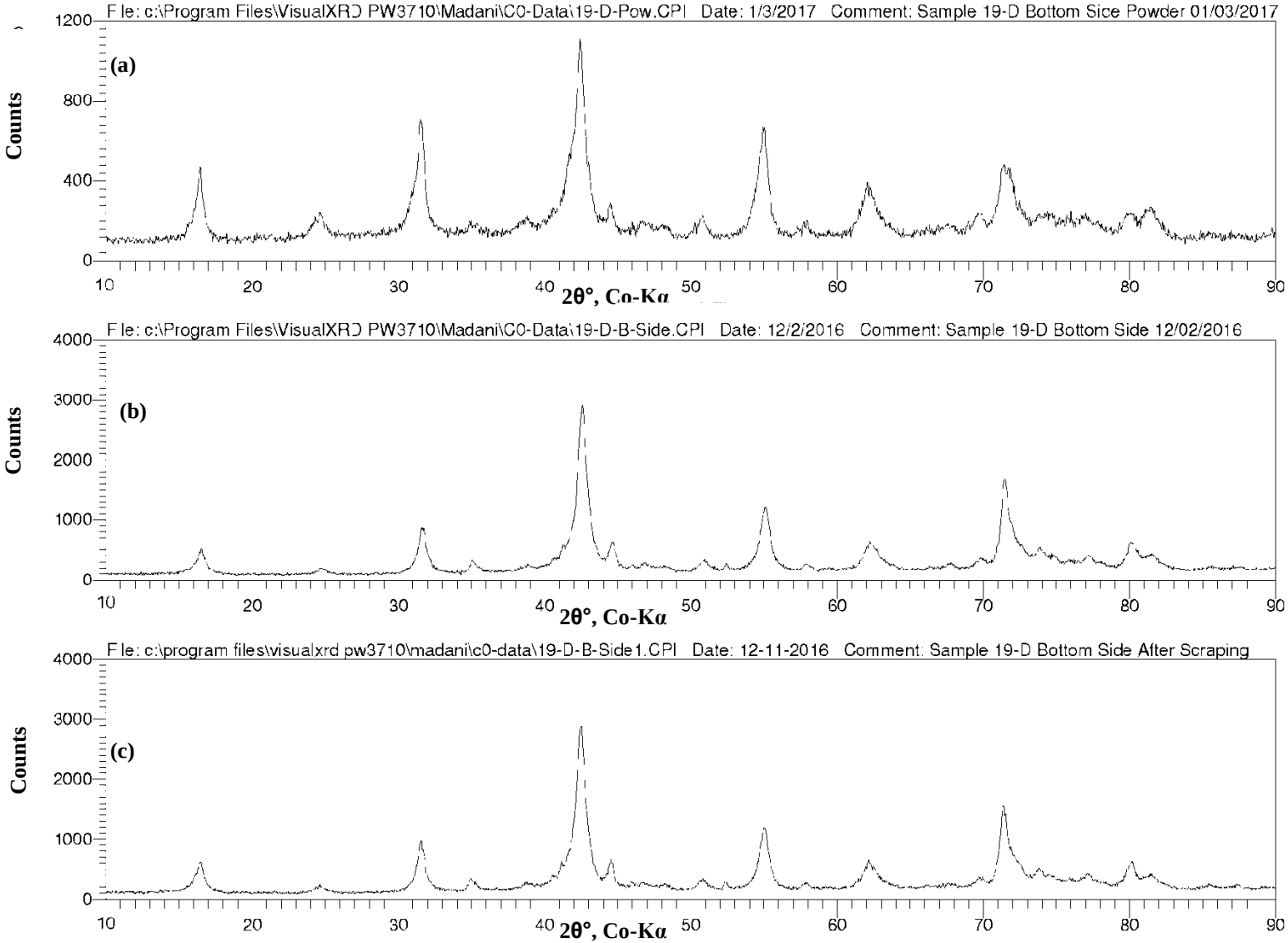

Figure B-37: XRD patterns, sample 19-D, (a) bottom side powder, (b) bottom before scraping, (c) bottom after scraping.

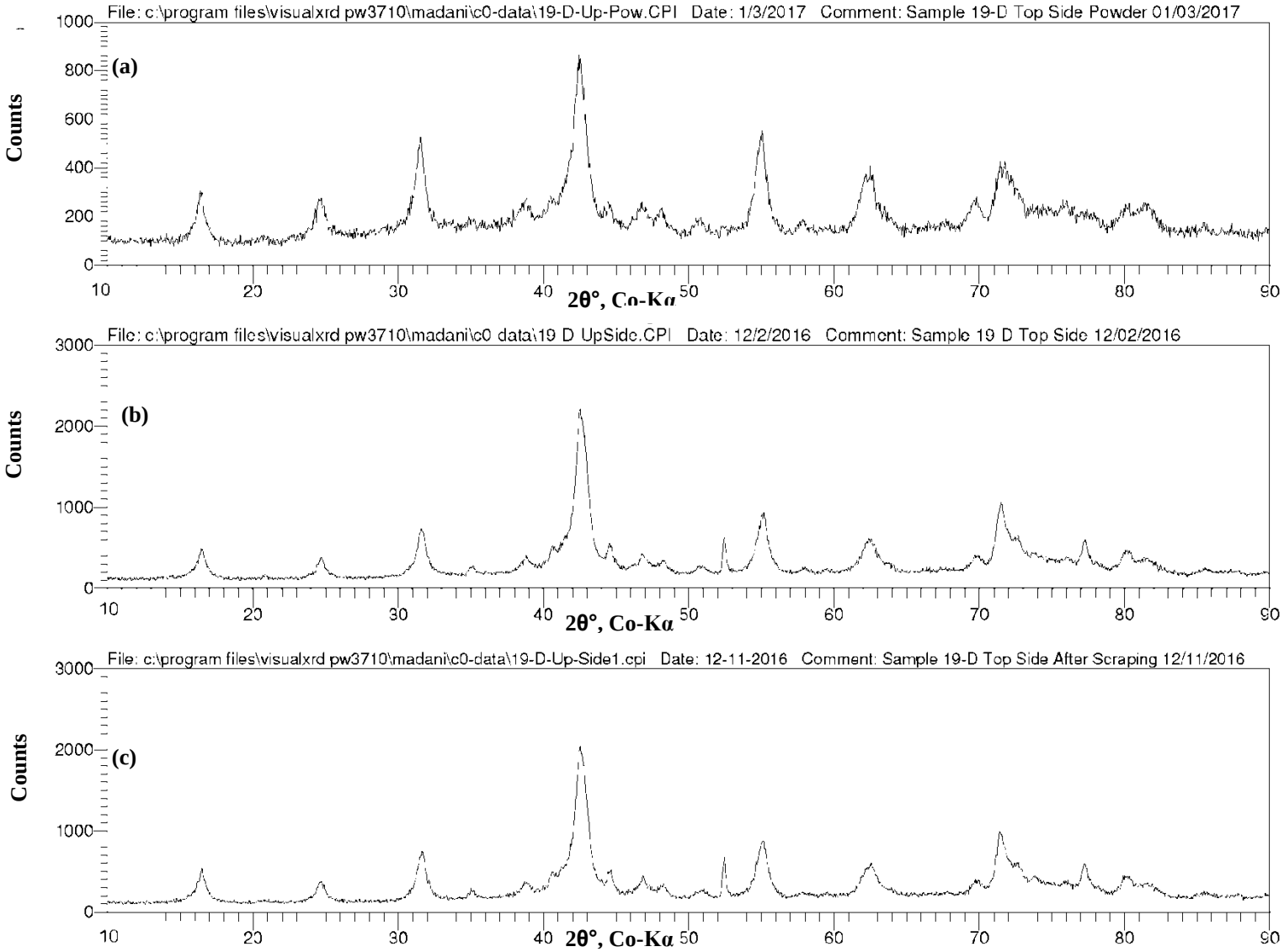

Figure B-38: XRD patterns, sample 19-D, (a) top side powder, (b) top before scraping, (c) top after scraping.

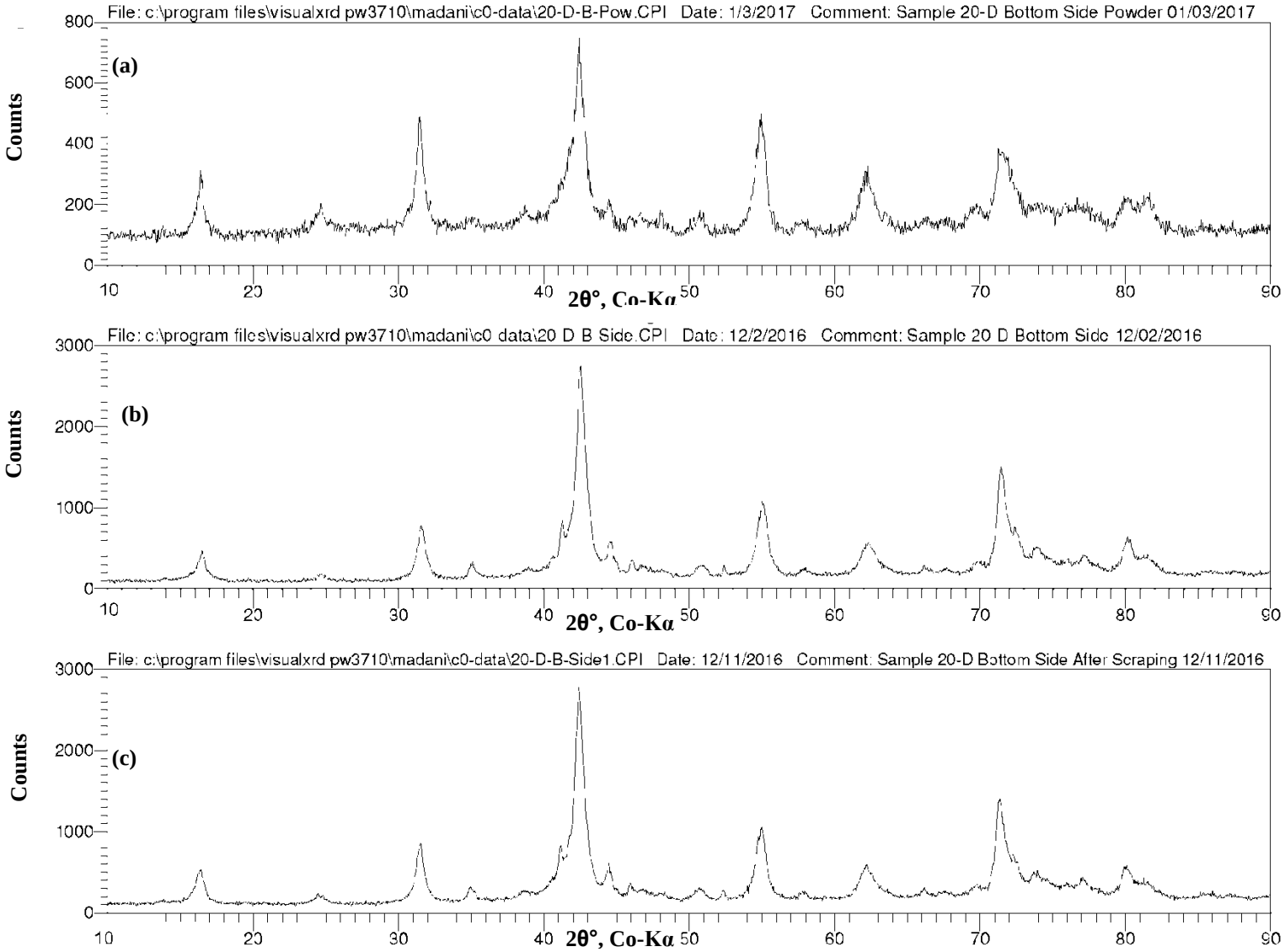

Figure B-39: XRD patterns, sample 20-D, (a) bottom side powder, (b) bottom before scraping, (c) bottom after scraping.

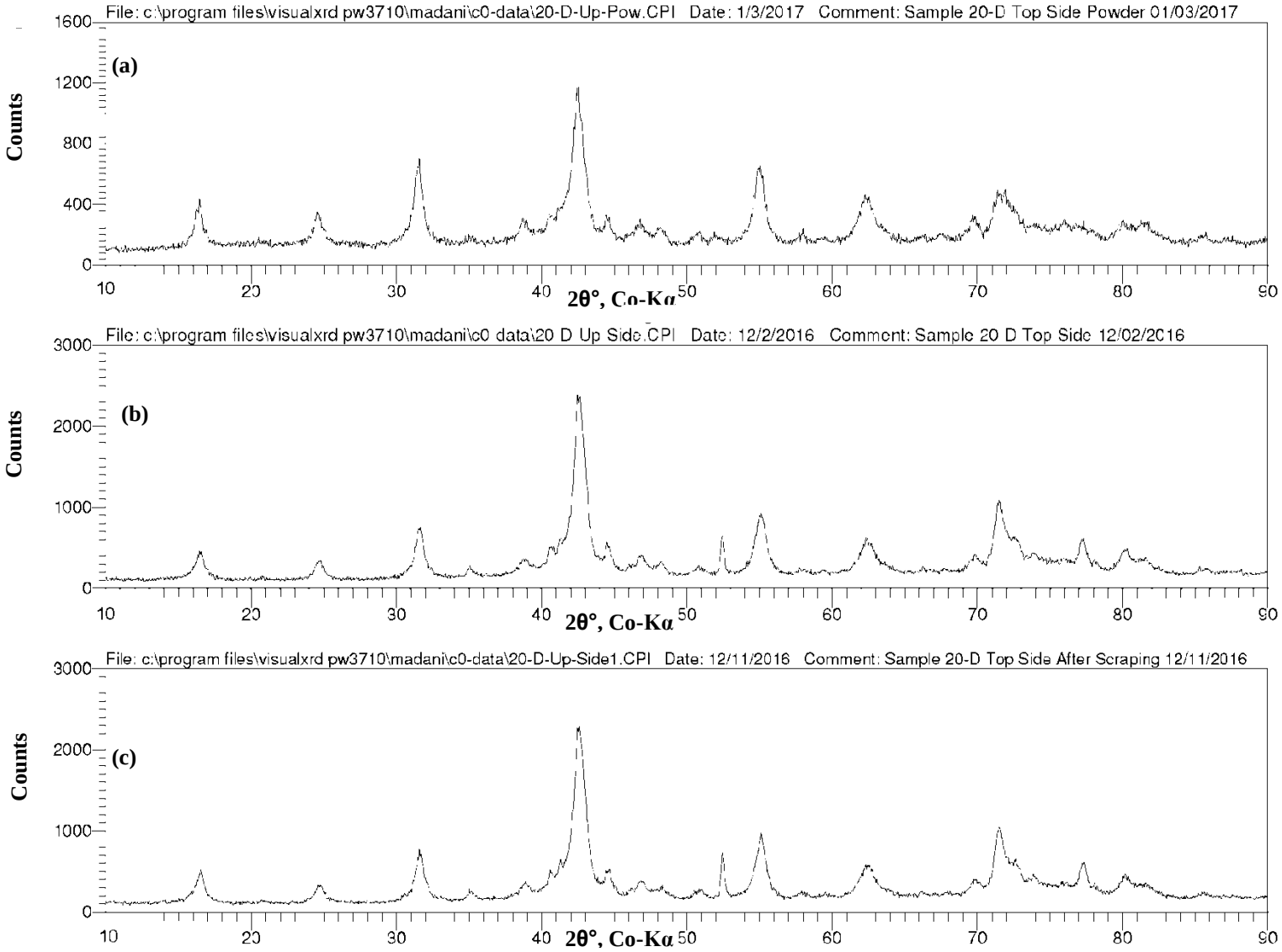

Figure B-40: XRD patterns, sample 20-D, (a) top side powder, (b) top before scraping, (c) top after scraping.

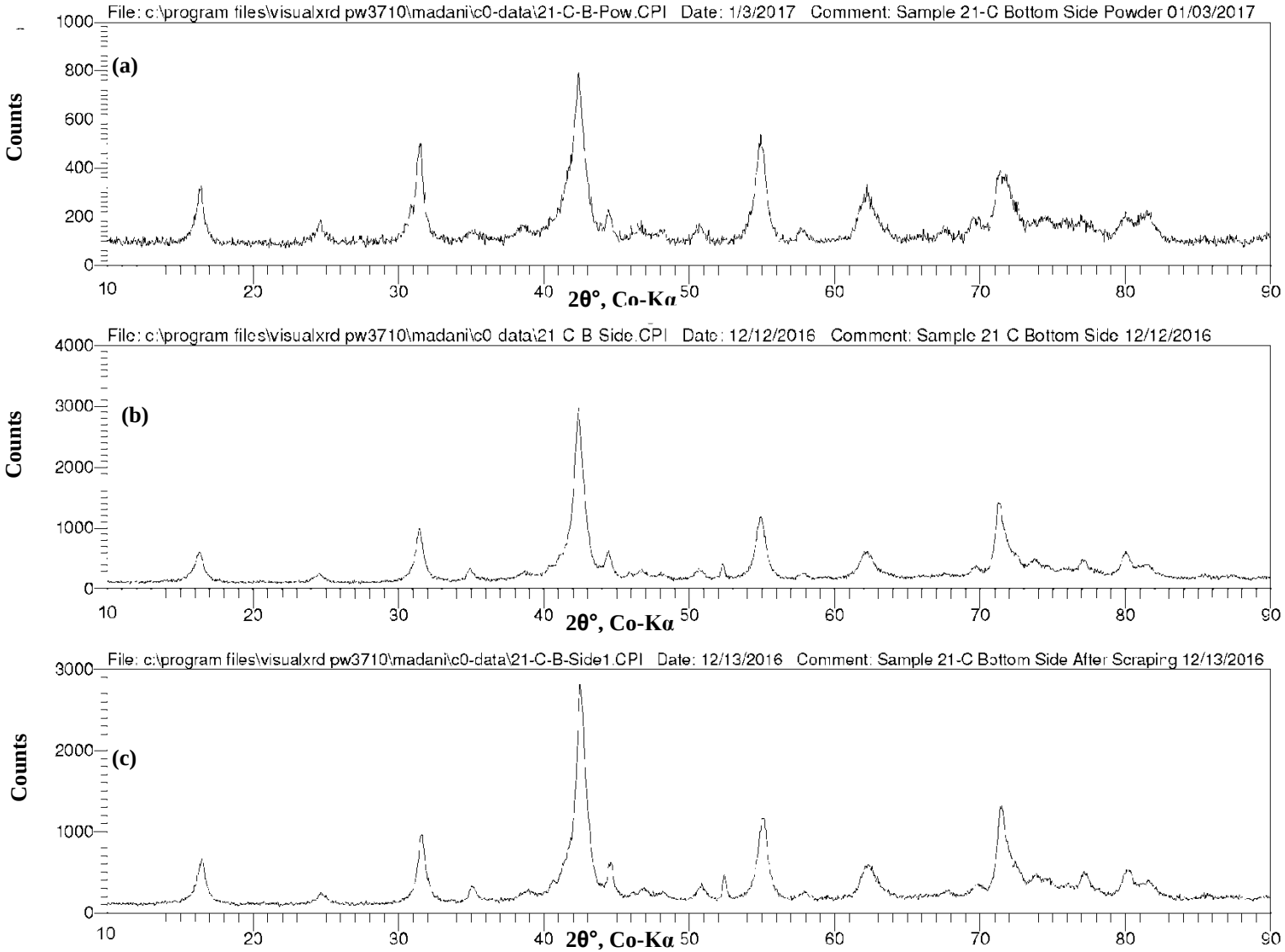

Figure B-41: XRD patterns, sample 21-C, (a) bottom side powder, (b) bottom before scraping, (c) bottom after scraping.

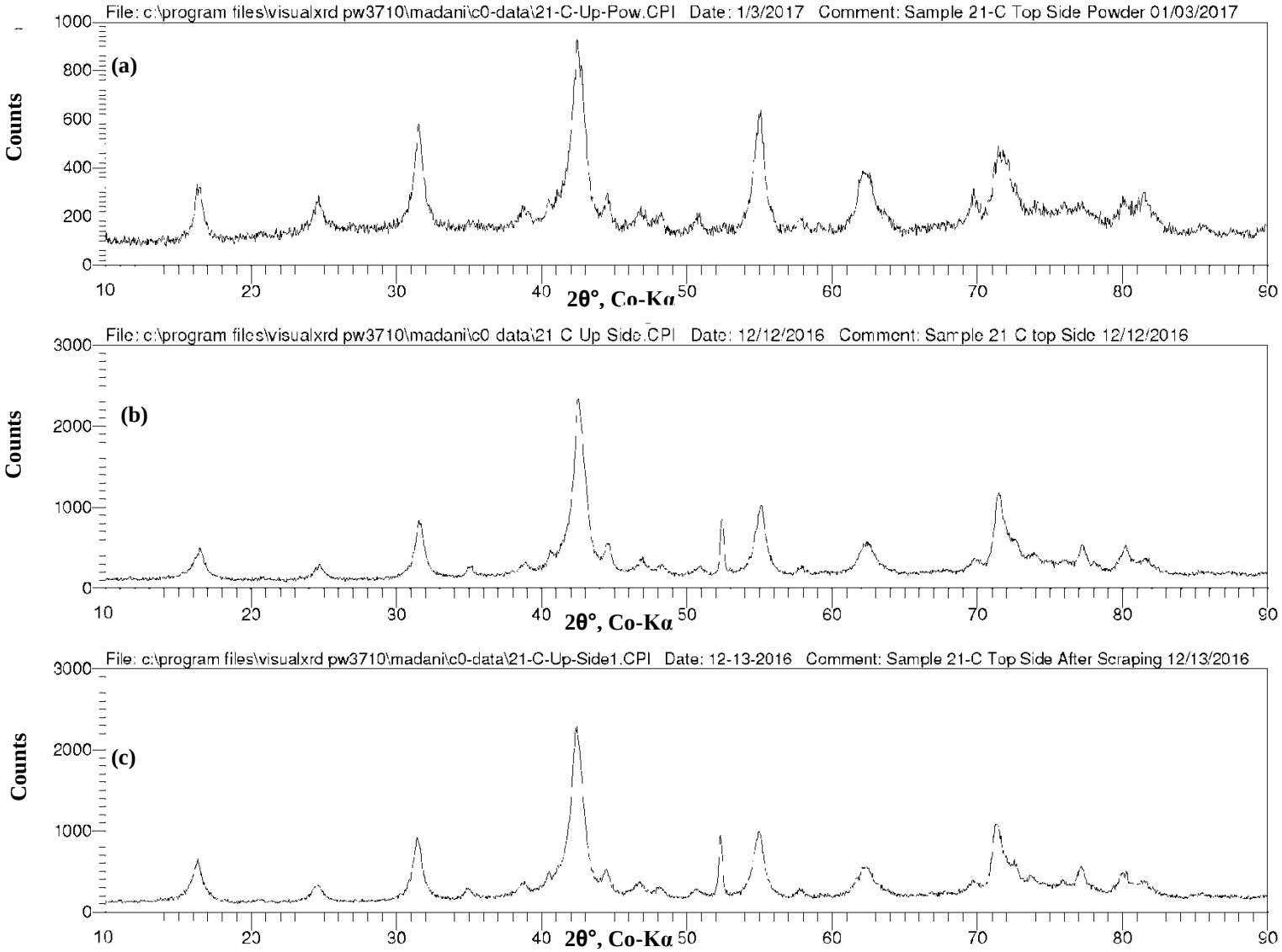

Figure B-42: XRD patterns, sample 21-C, (a) top side powder, (b) top before scraping, (c) top after scraping.

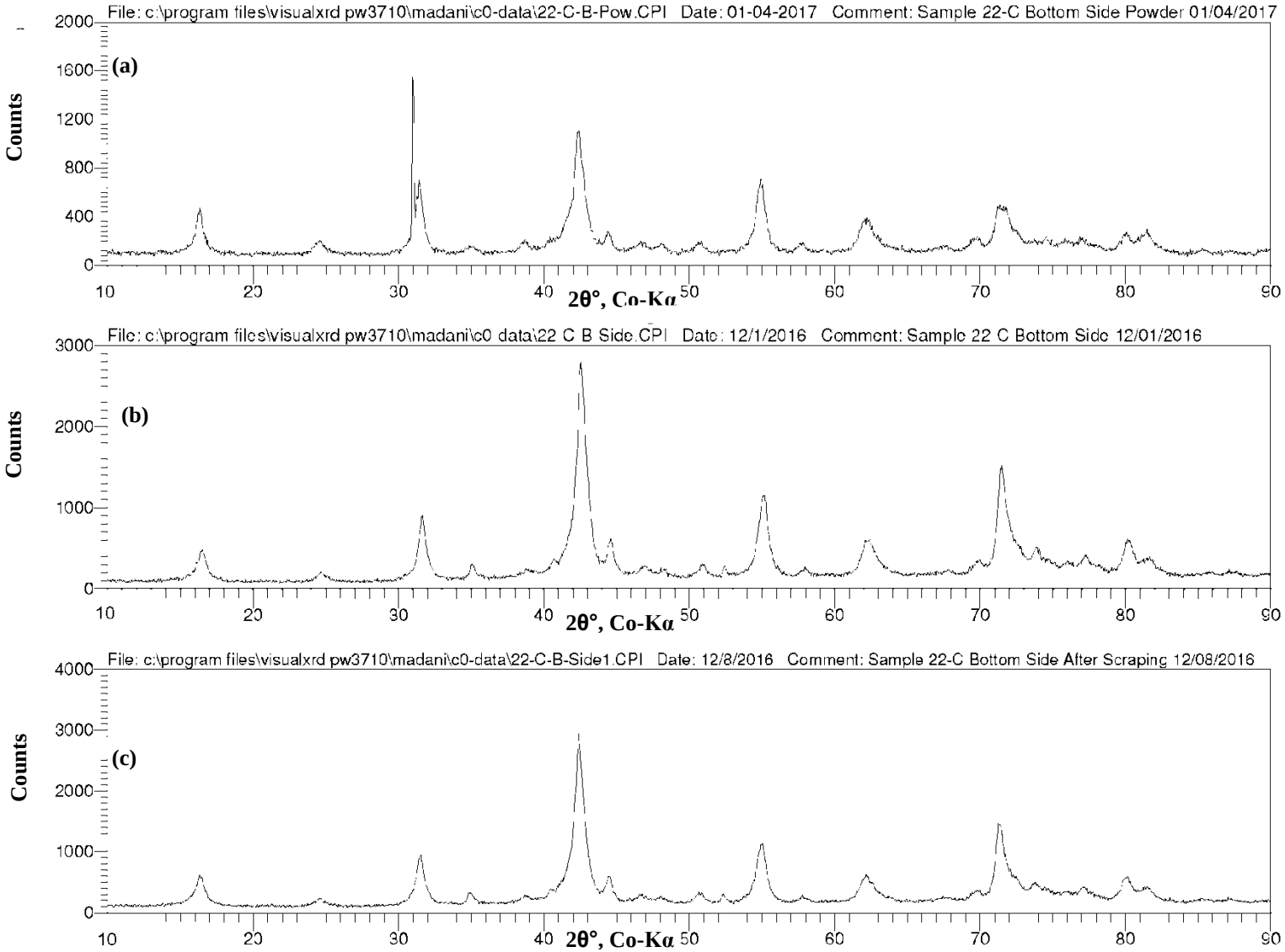

Figure B-43: XRD patterns, sample 22-C, (a) bottom side powder, (b) bottom before scraping, (c) bottom after scraping.

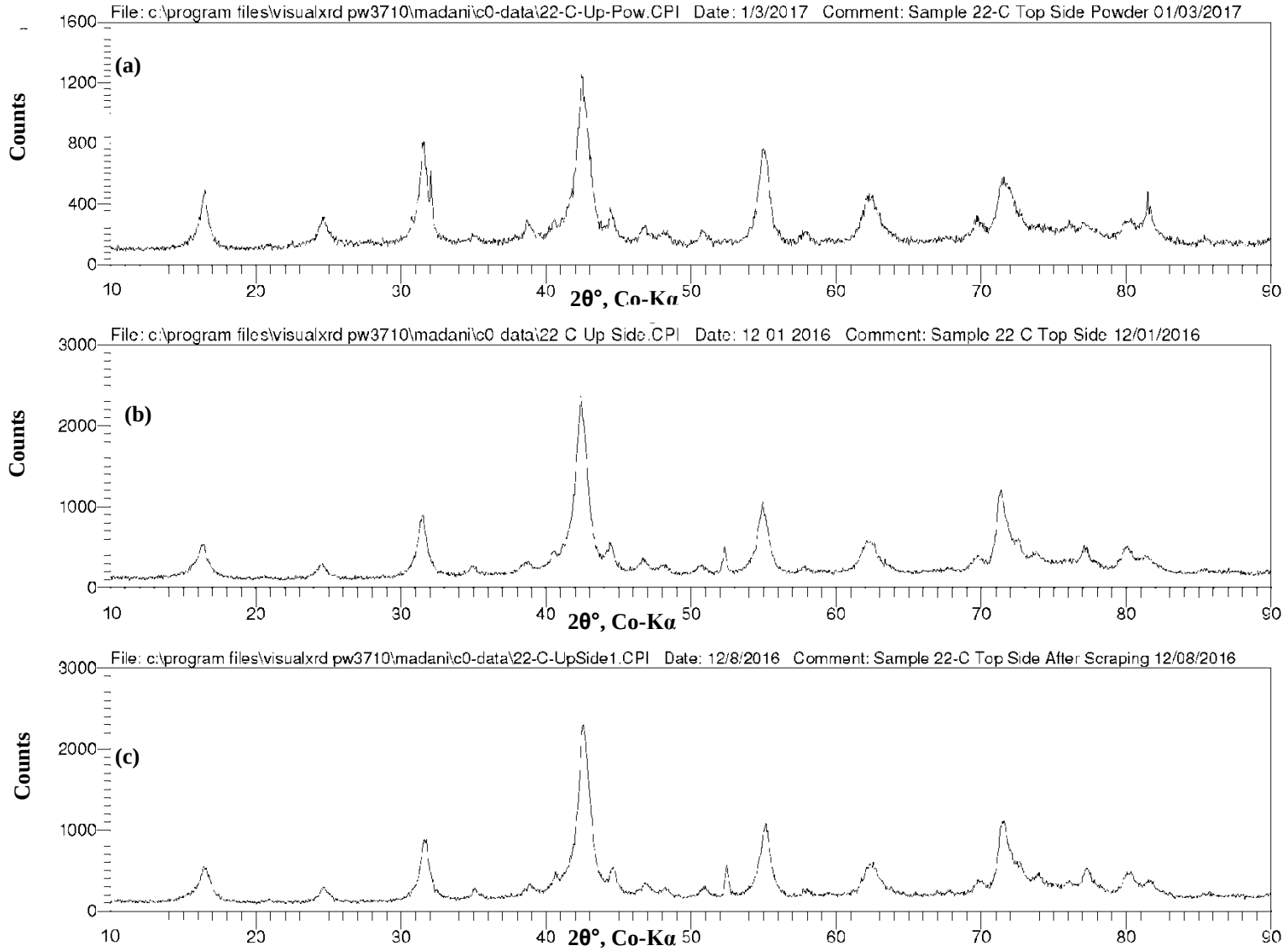

Figure B-44: XRD patterns, sample 22-C, (a) top side powder, (b) top before scraping, (c) top after scraping.

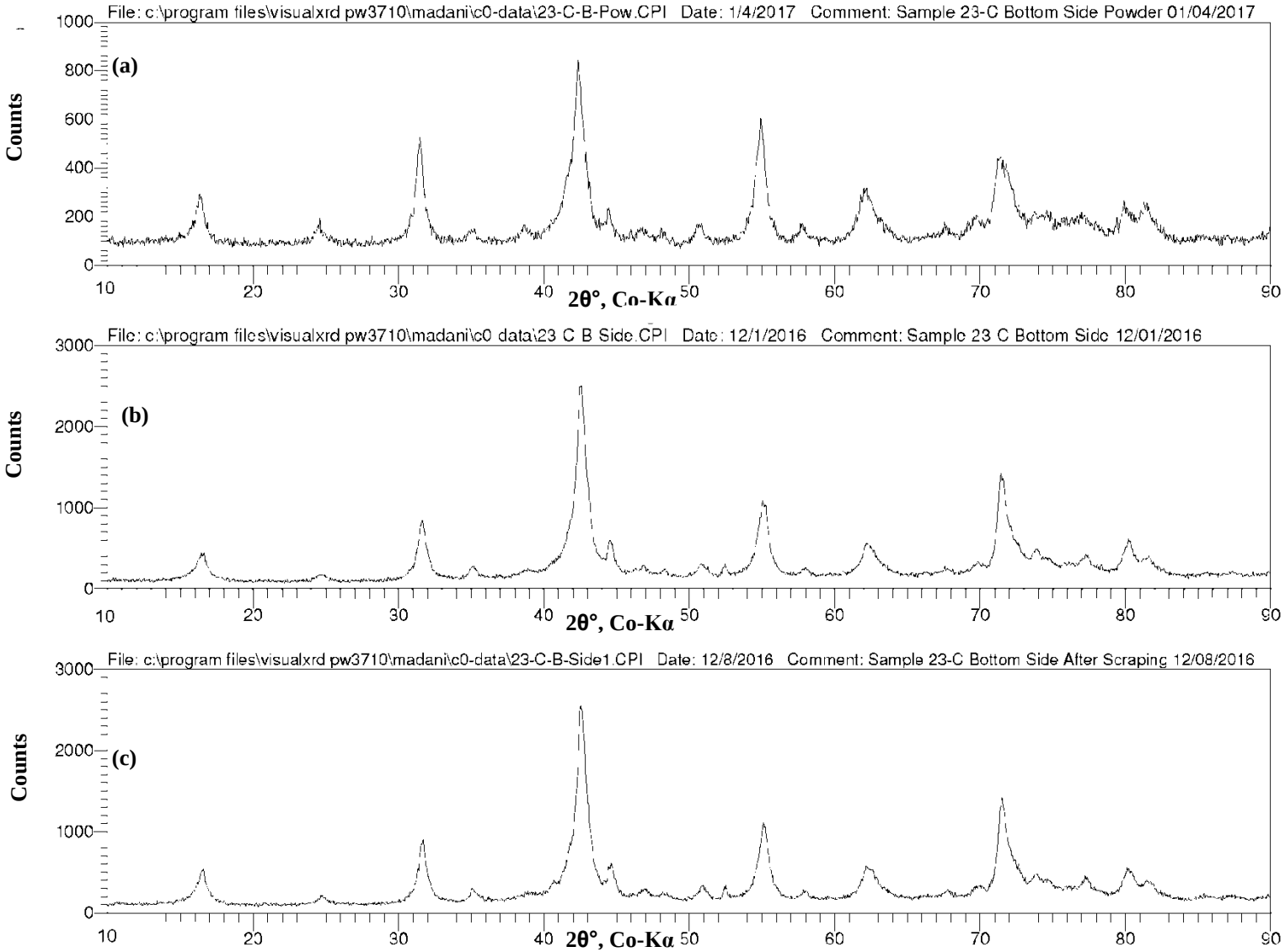

Figure B-45: XRD patterns, sample 23-C, (a) bottom side powder, (b) bottom before scraping, (c) bottom after scraping.

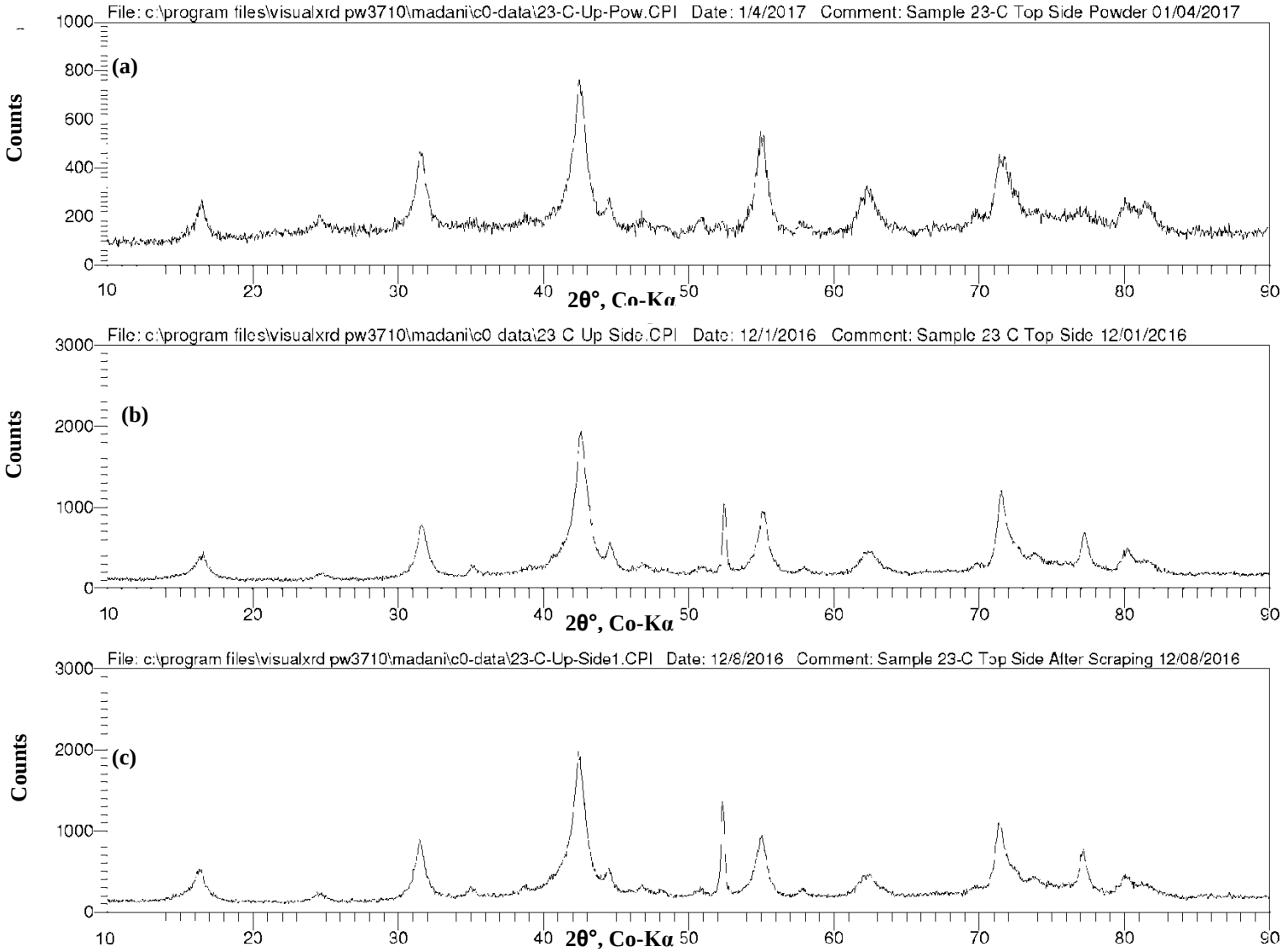

Figure B-46: XRD patterns, sample 23-C, (a) top side powder, (b) top before scraping, (c) top after scraping.

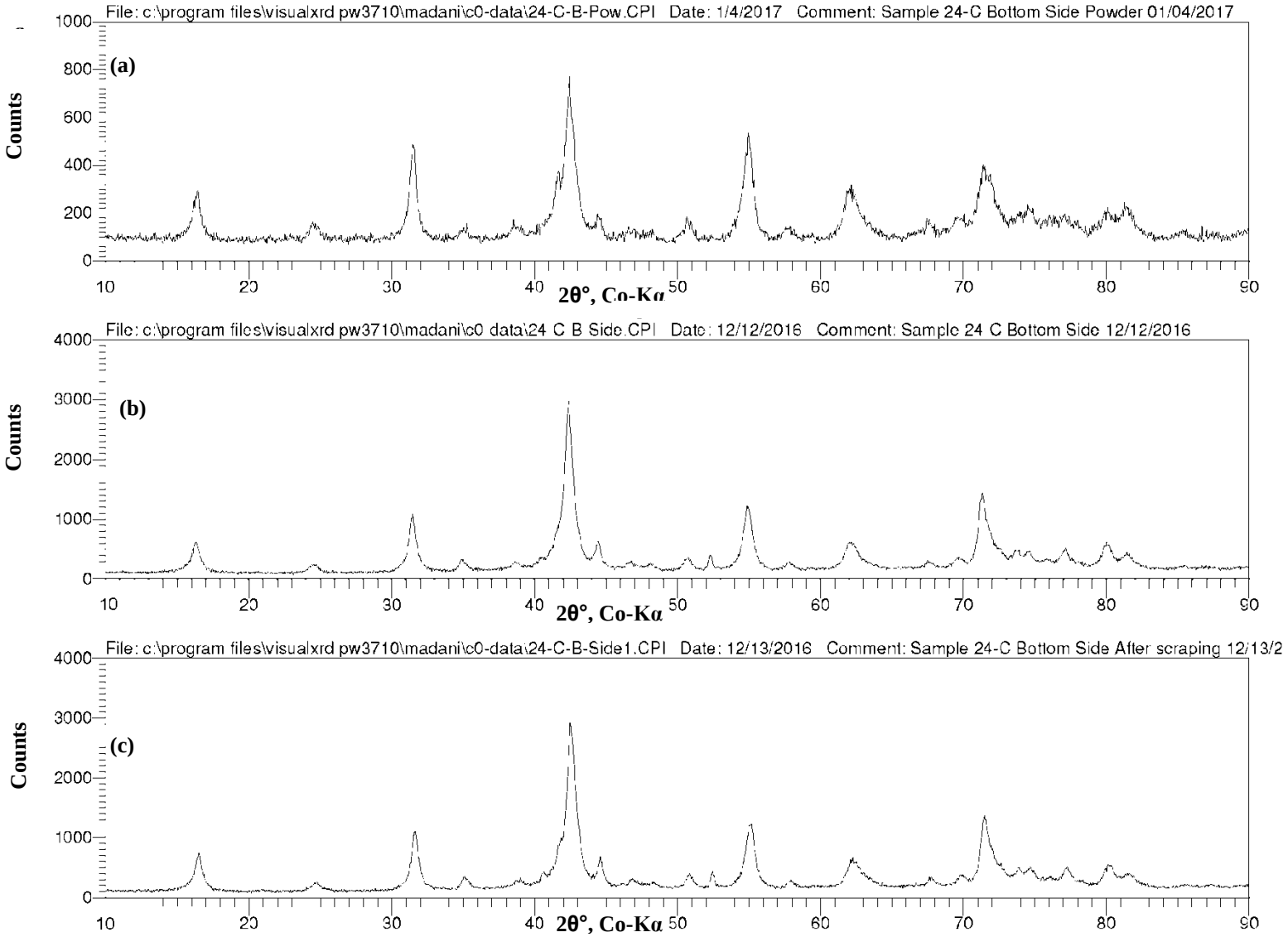

Figure B-47: XRD patterns, sample 24-C, (a) bottom side powder, (b) bottom before scraping, (c) bottom after scraping.

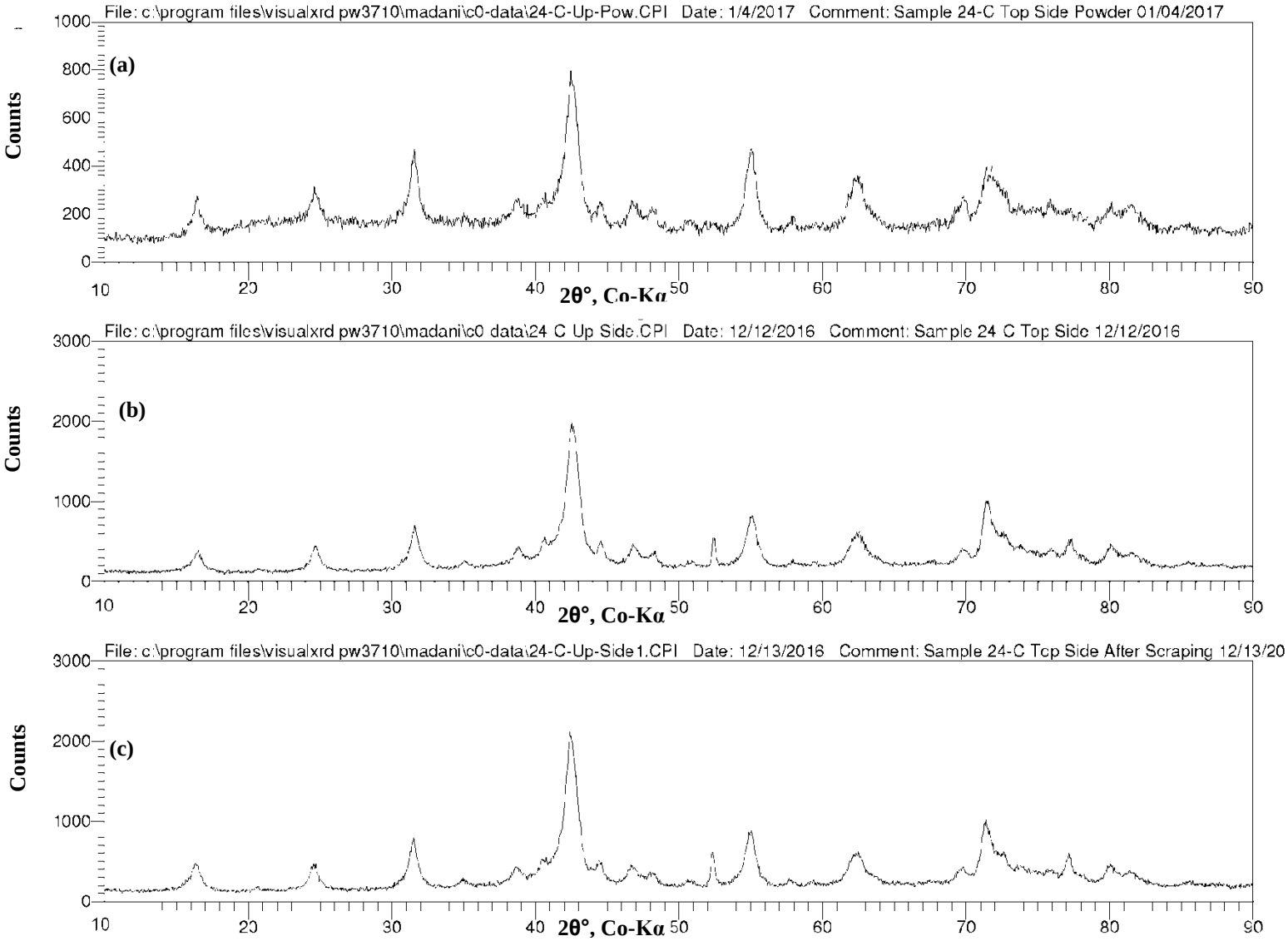

Figure B-48: XRD patterns, sample 24-C, (a) top side powder, (b) top before scraping, (c) top after scraping.

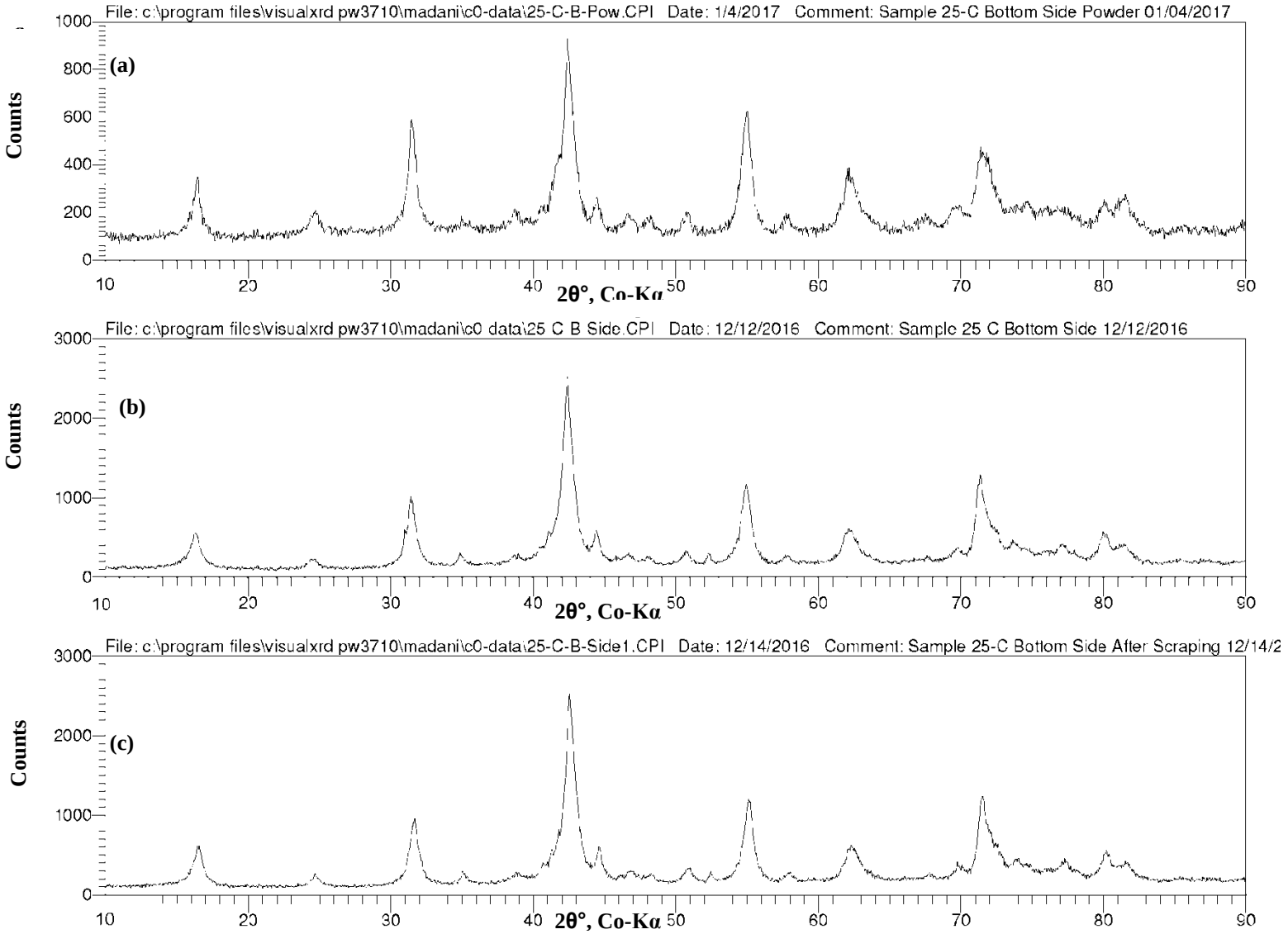

Figure B-49: XRD patterns, sample 25-C, (a) bottom side powder, (b) top before scraping, (c) bottom after scraping.

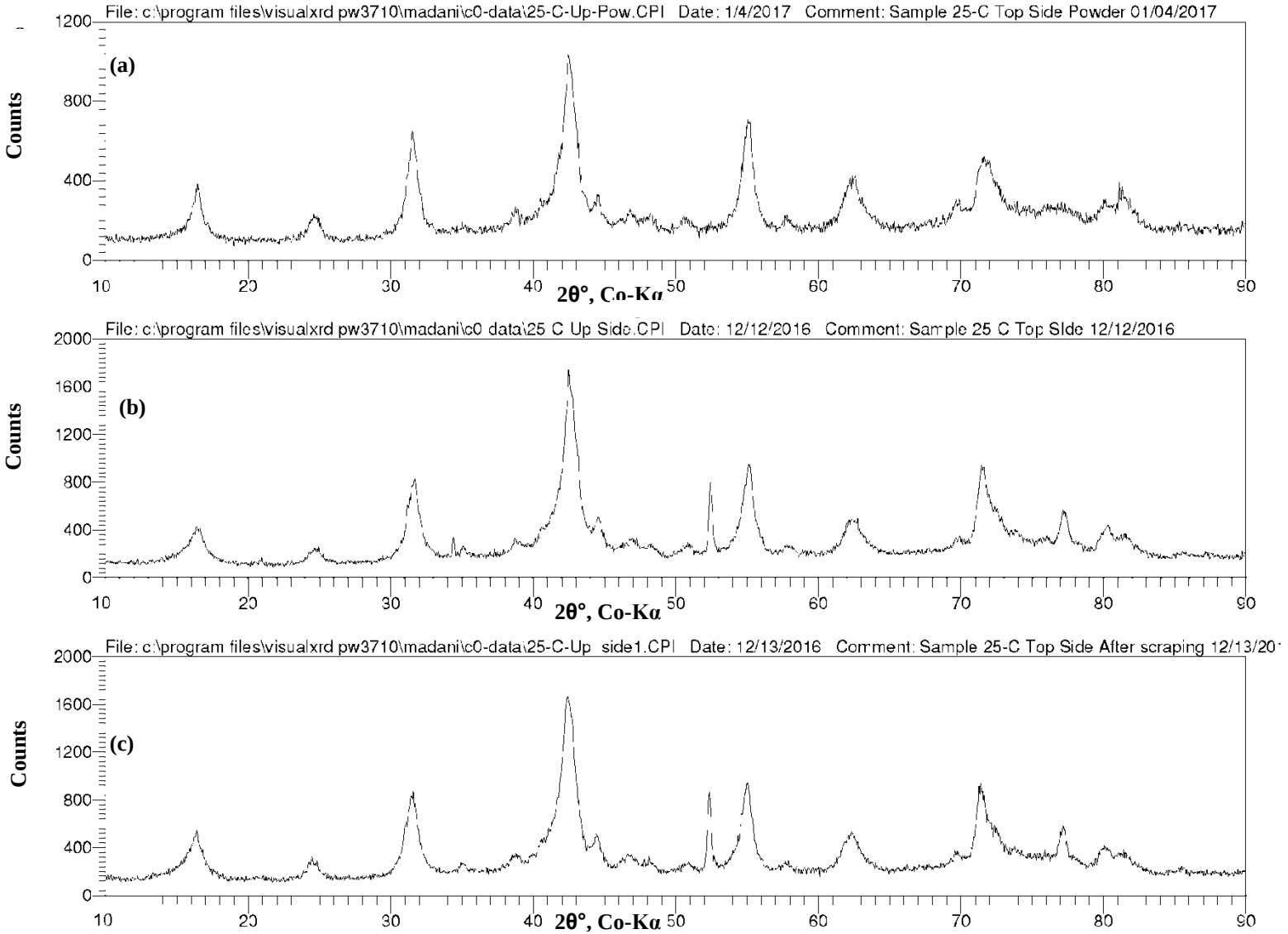

Figure B-50: XRD patterns, sample 25-C, (a) top side powder, (b) top before scraping, (c) top after scraping.

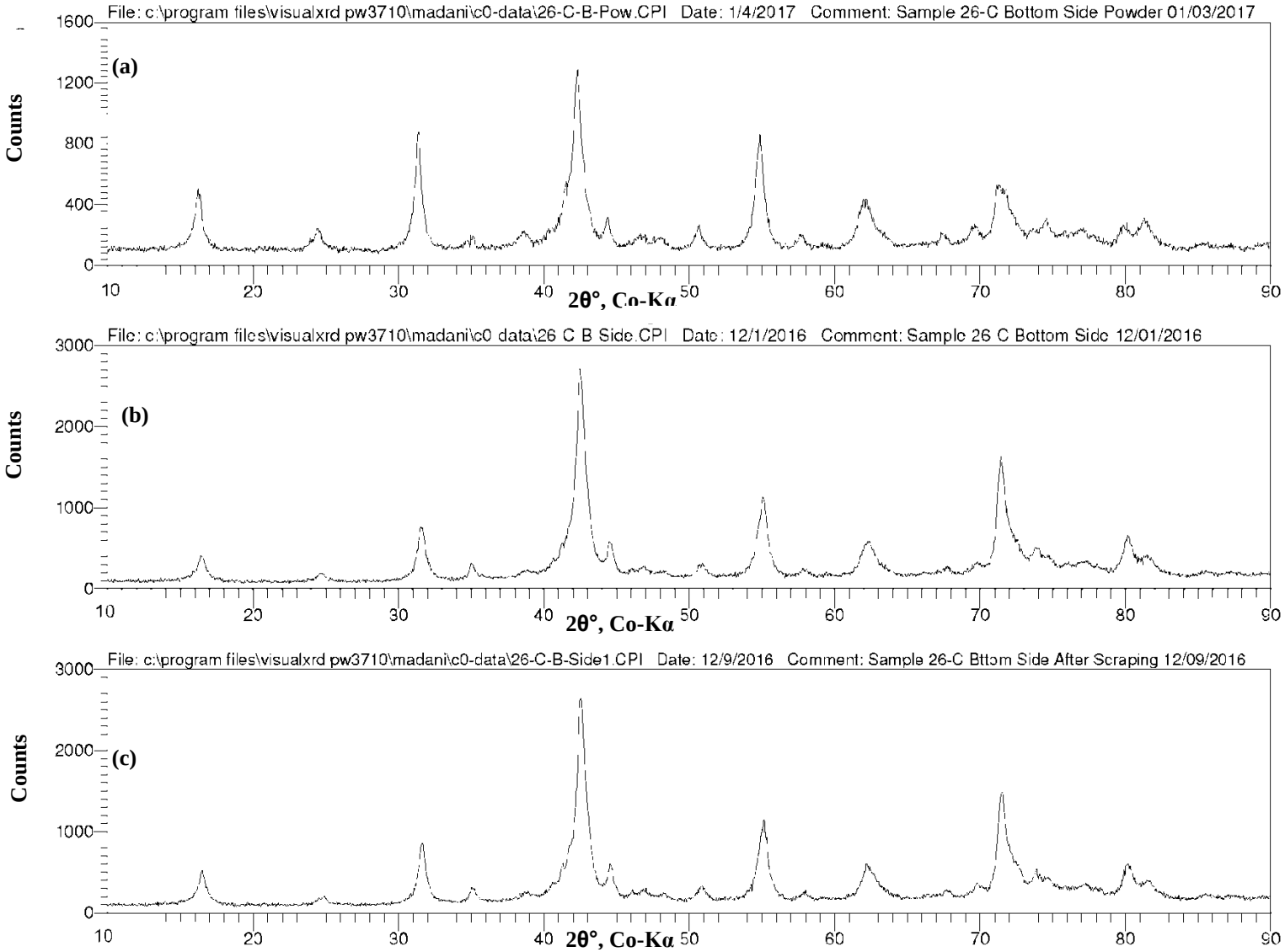

Figure B-51: XRD patterns, sample 26-C, (a) bottom side powder, (b) bottom before scraping, (c) bottom after scraping.

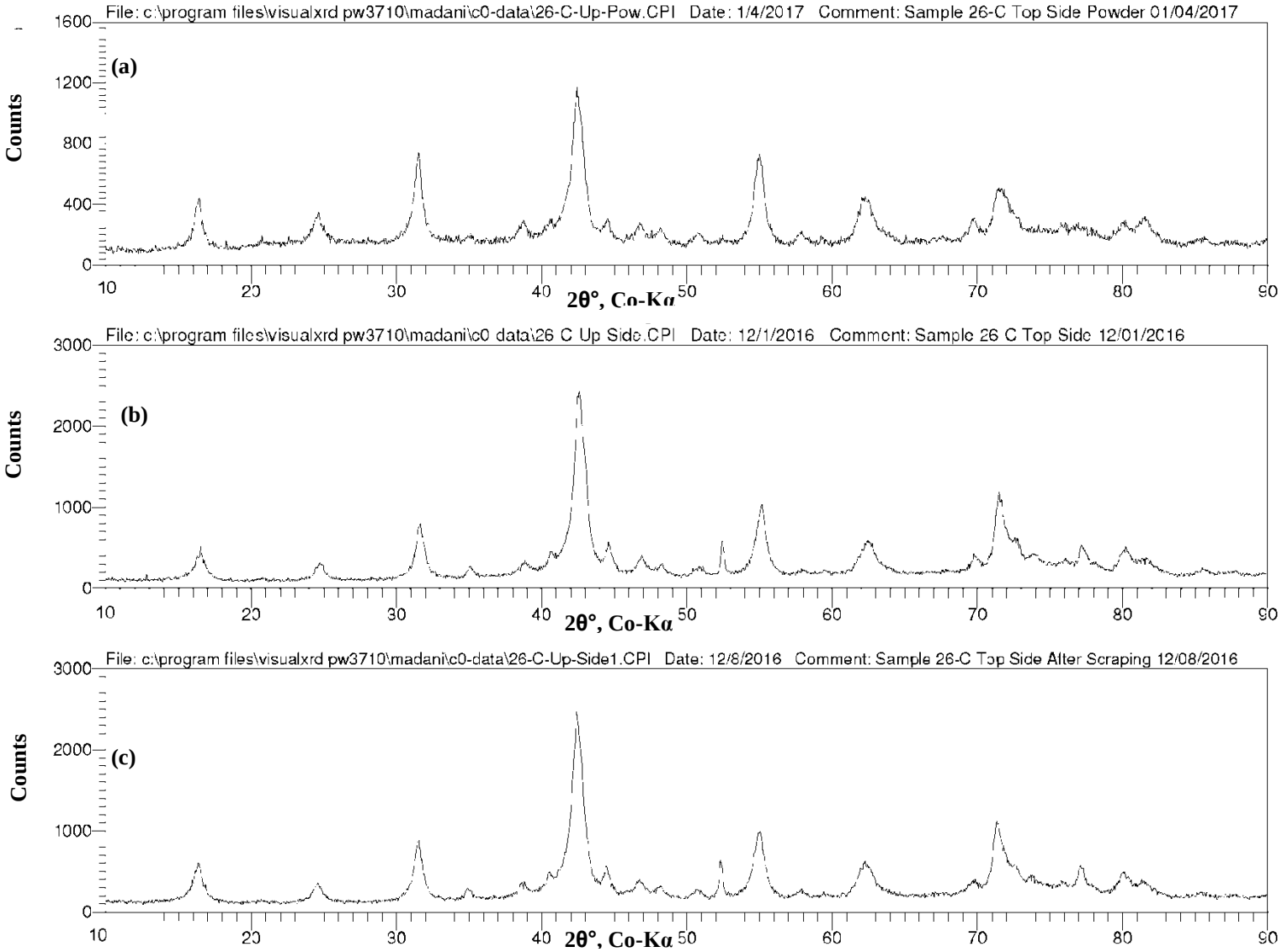

Figure B-52: XRD patterns, sample 26-C, (a) top side powder, (b) top before scraping, (c) top after scraping.

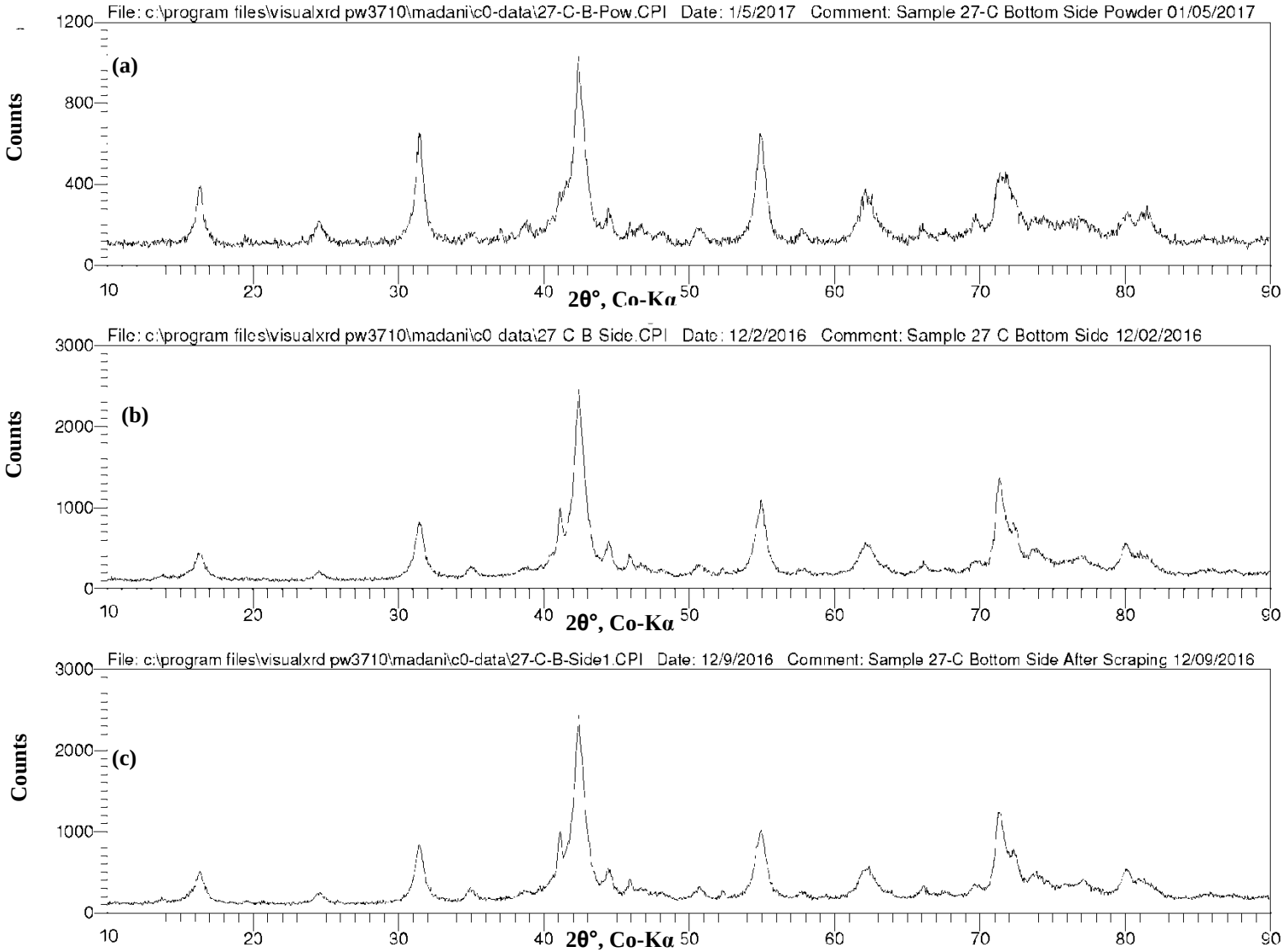

Figure B-53: XRD patterns, sample 27-C, (a) bottom side powder, (b) bottom before scraping, (c) bottom after scraping.

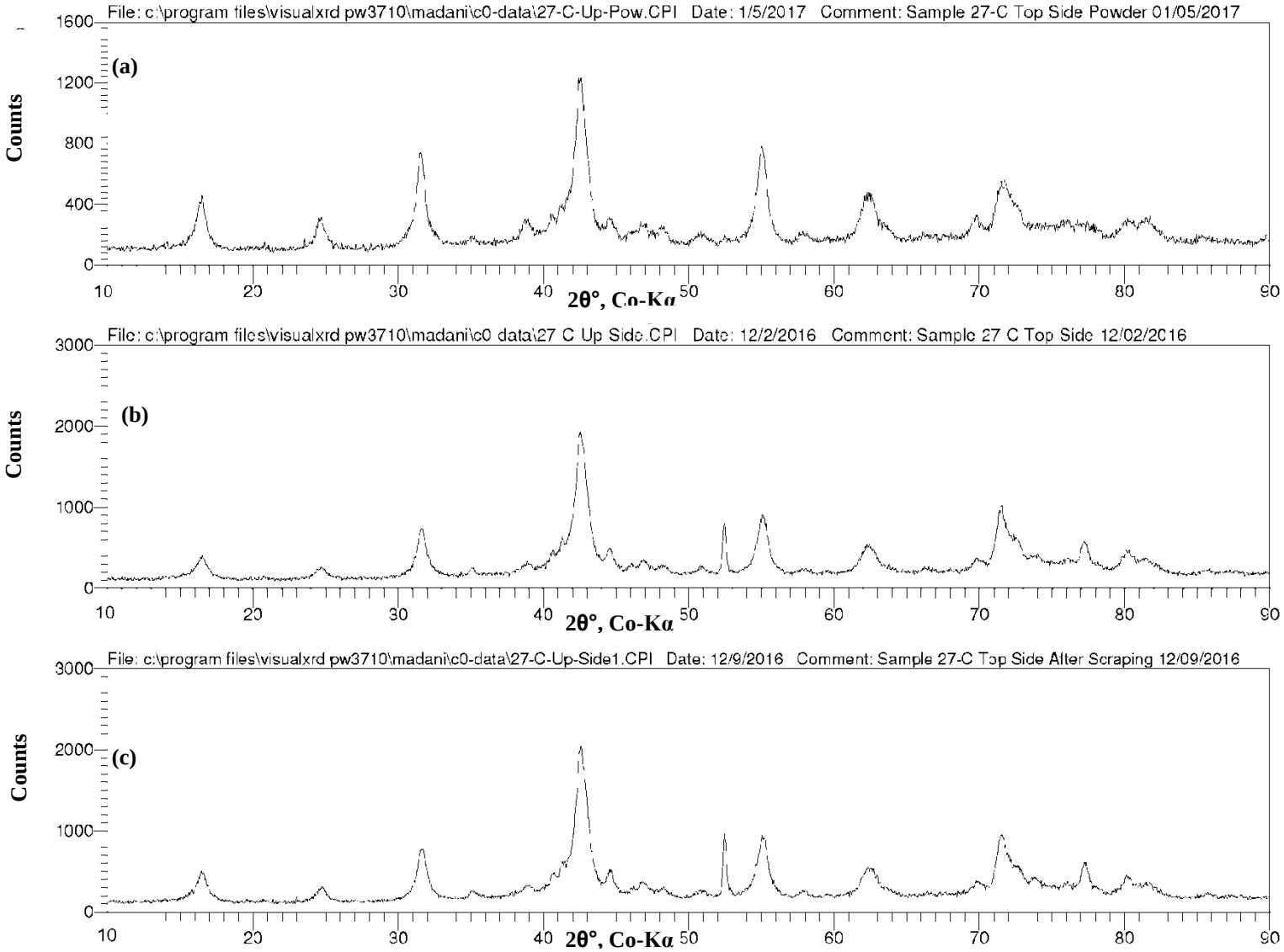

Figure B-54: XRD patterns, sample 27-C, (a) top side powder, (b) top before scraping, (c) top after scraping.

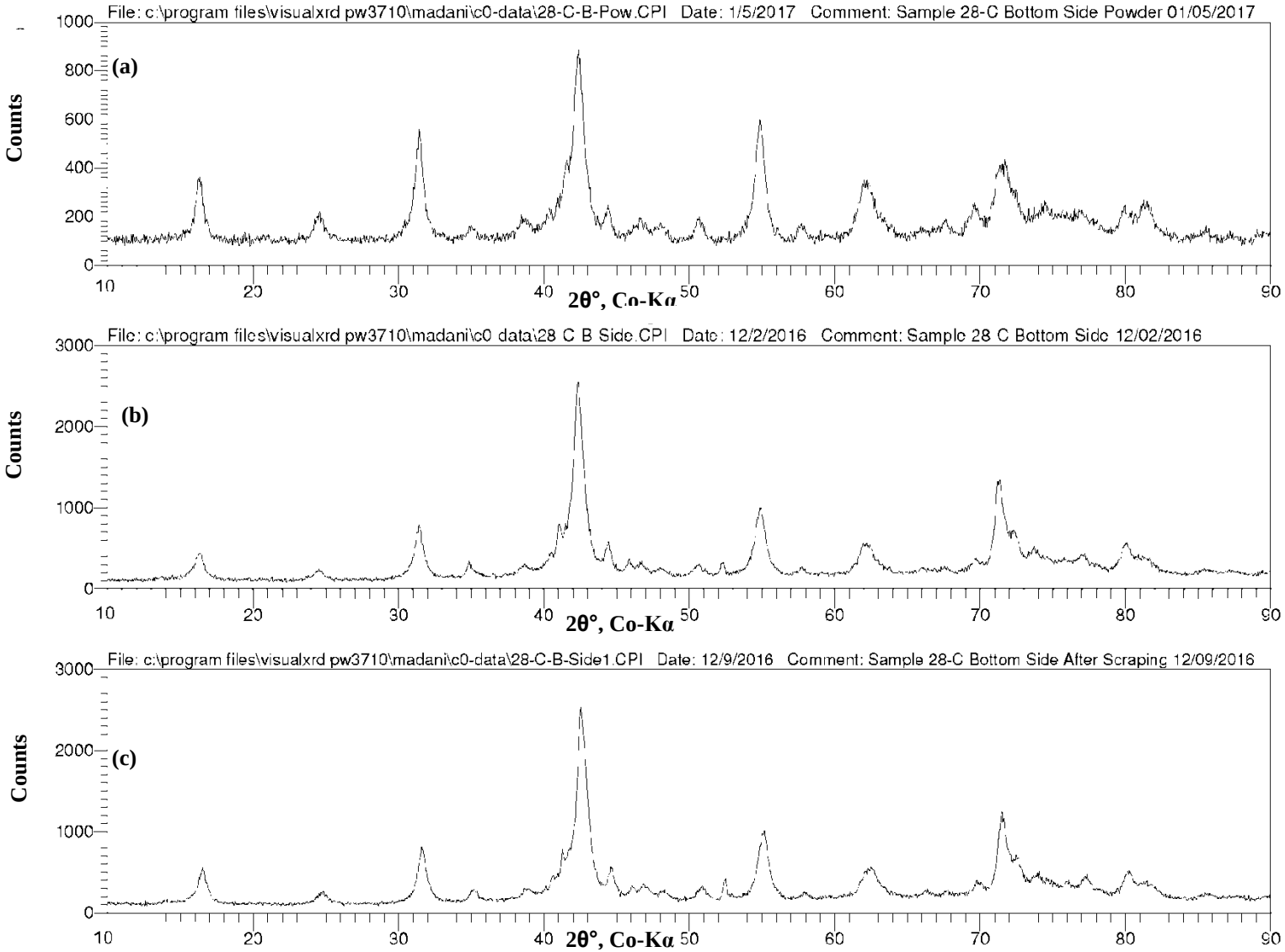

Figure B-55: XRD patterns, sample 28-C, (a) bottom side powder, (b) bottom before scraping, (c) bottom after scraping.

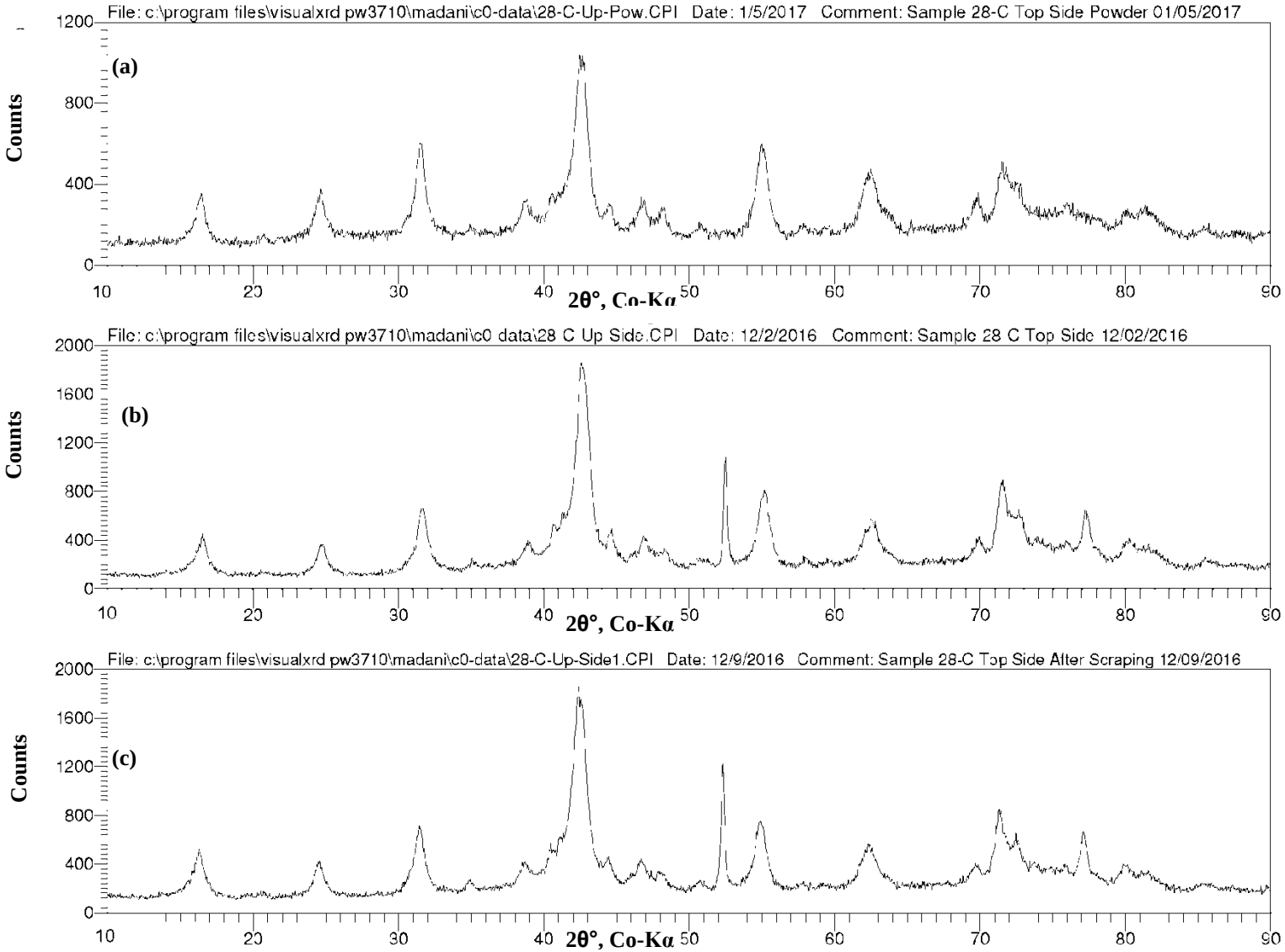

Figure B-56: XRD patterns, sample 28-C, (a) top side powder, (b) top before scraping, (c) top after scraping.

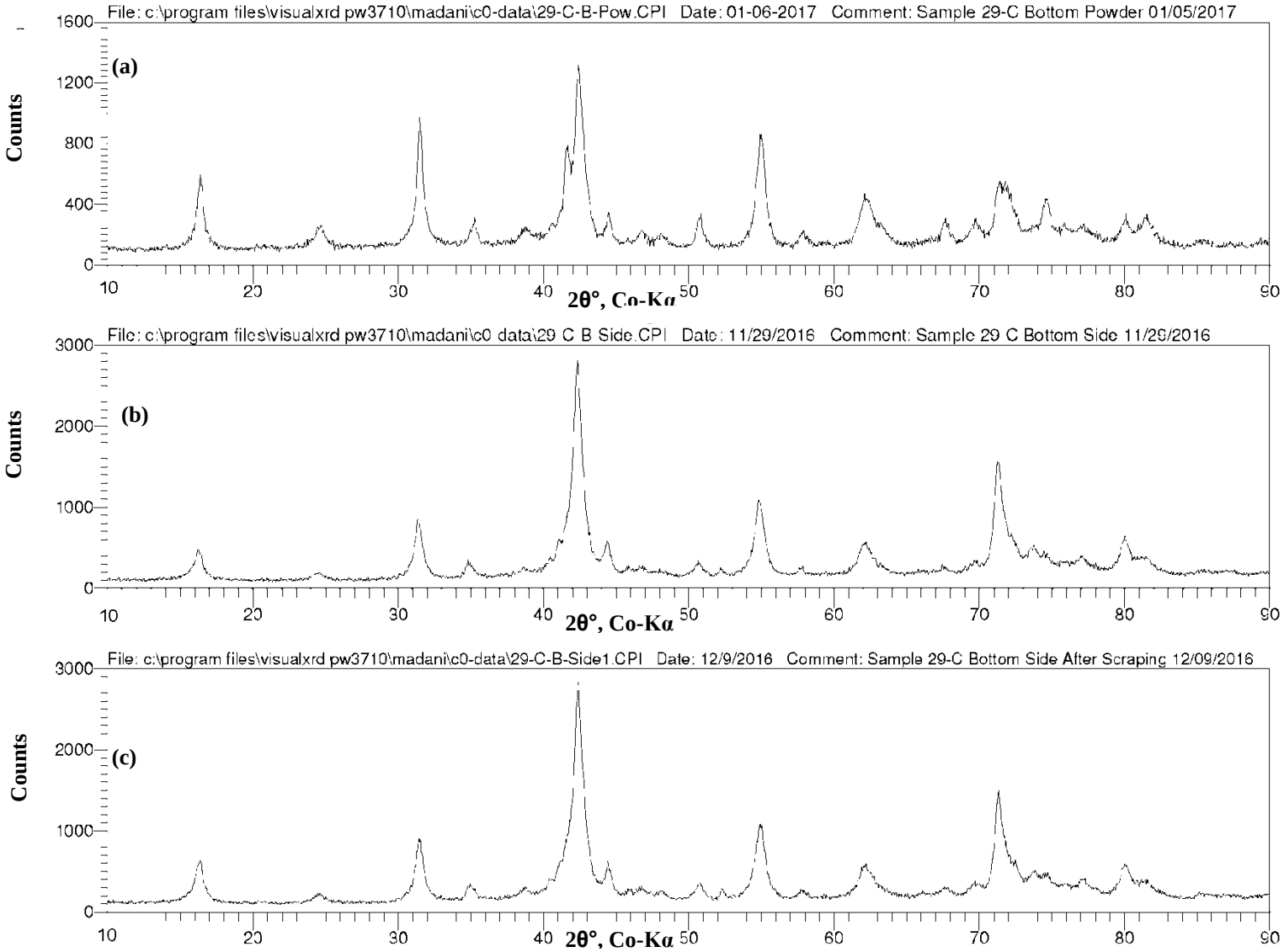

Figure B-57: XRD patterns, sample 29-C, (a) bottom side powder, (b) bottom before scraping, (c) bottom after scraping.

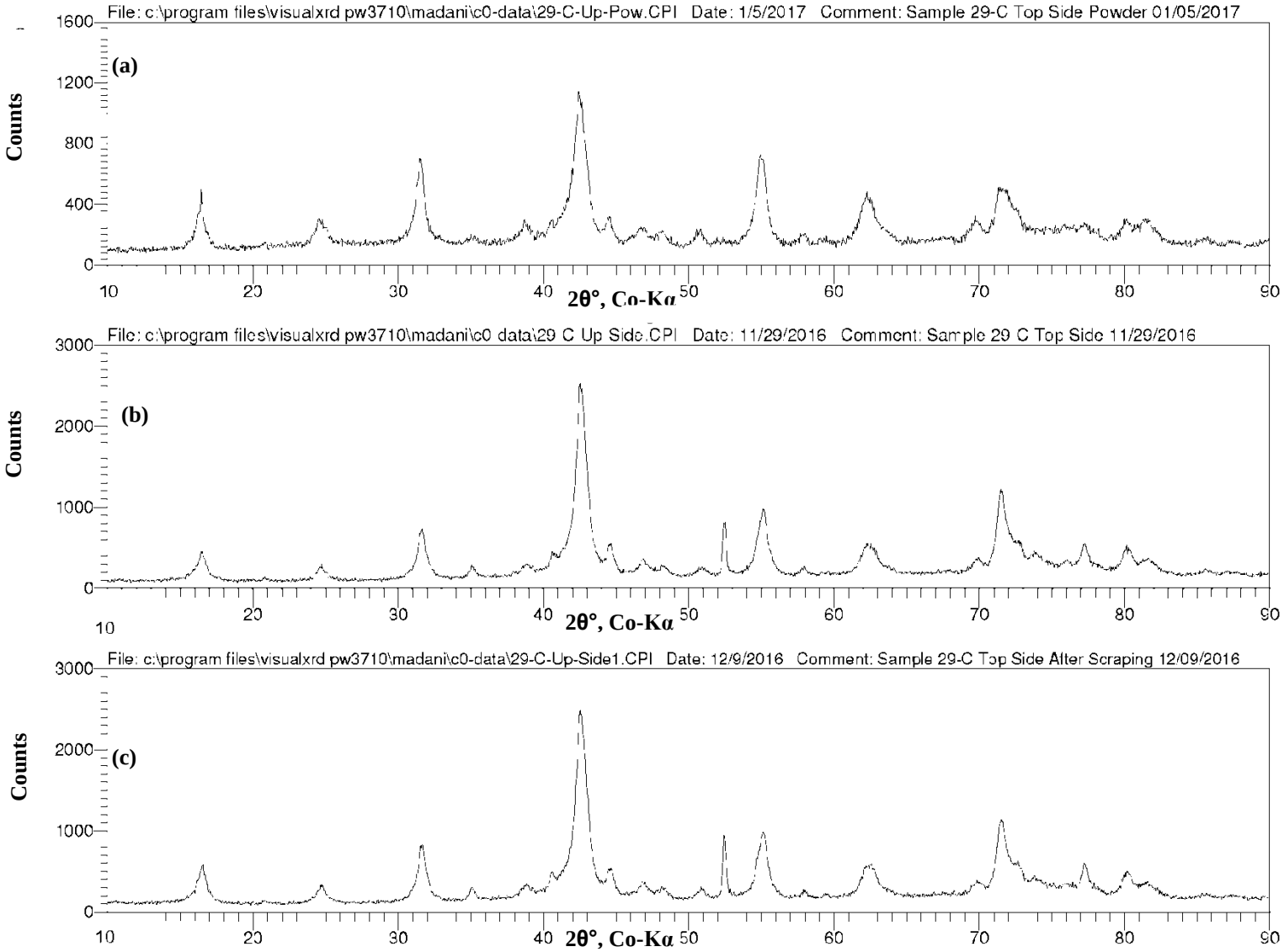

Figure B-58: XRD patterns, sample 29-C, (a) top side powder, (b) top before scraping, (c) top after scraping.

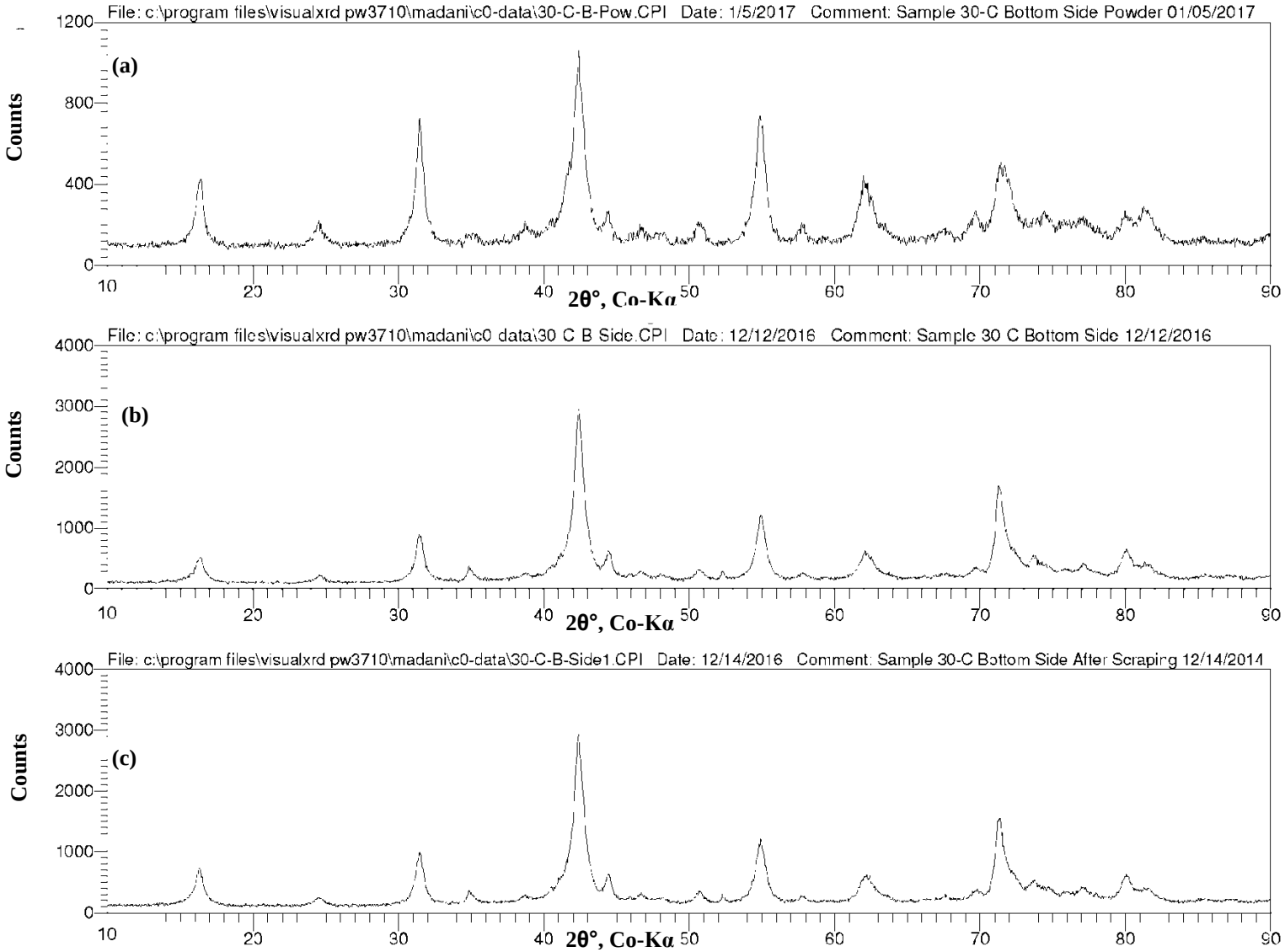

Figure B-59: XRD patterns, sample 30-C, (a) bottom side powder, (b) bottom before scraping, (c) bottom after scraping.

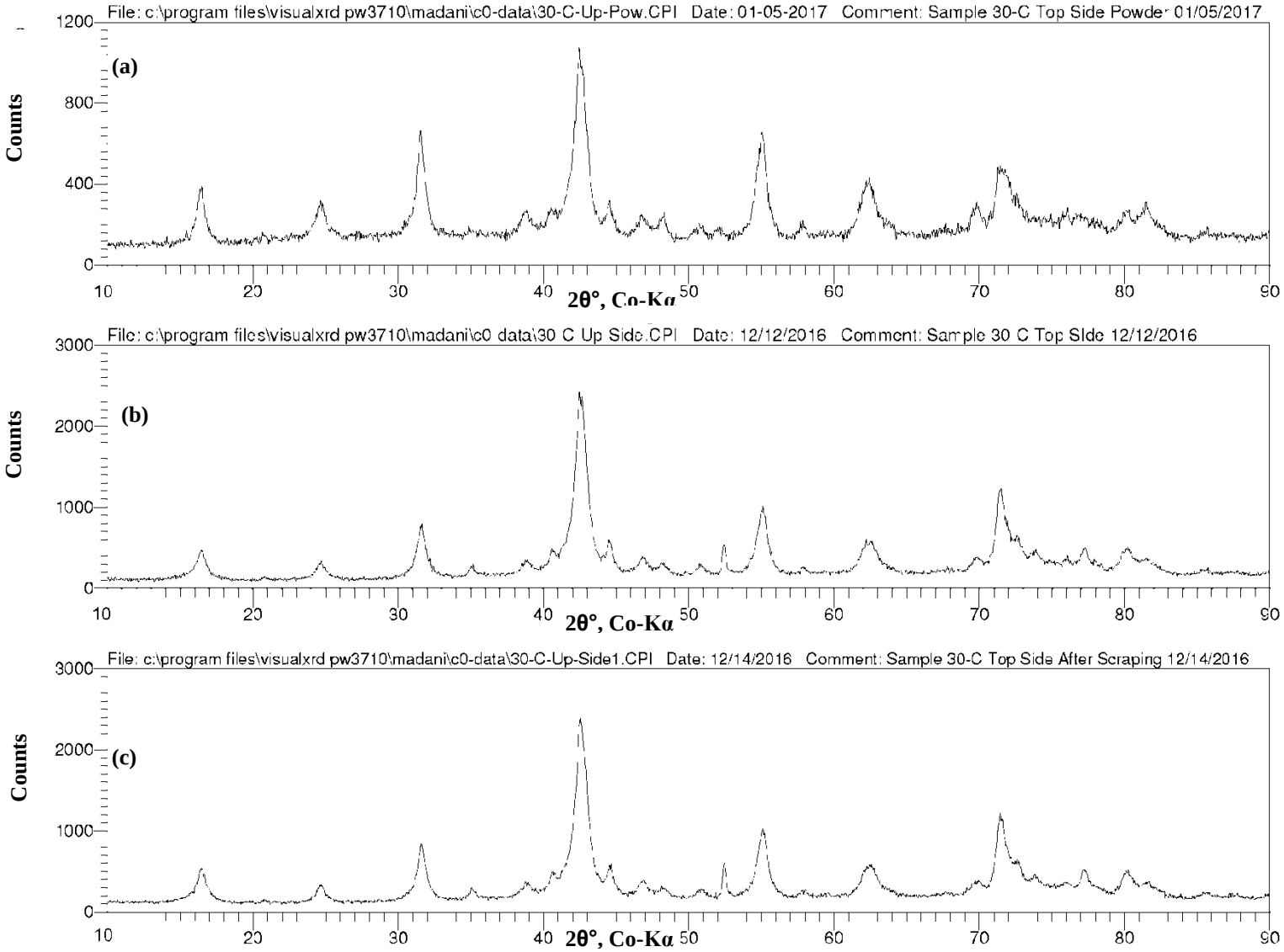

Figure B-60: XRD patterns, sample 30-C, (a) top side powder, (b) top before scraping, (c) top after scraping.